Table of contents

1 Introduction

1.1 The political scene in the field of magnetic fusion in 2003

In 2003, the siting of the ITER experiment (the next major step in fusion research) was at the forefront of the political scene in magnetic fusion. In parallel with the USA rejoining ITER negotiations, two new countries, China and South Korea, have joined. The participants in the negotiations are now: China, the EU, Japan, Russia, South Korea and the USA. At the end of November, a unanimous decision was made by the European Council of Ministers to propose Cadarache (near Marseilles) as the European site to host ITER, while Spain will host the European Legal Entity for ITER. This key move paves the way for decisions by the ITER Parties between the European site at Cadarache and the proposed Japanese site (Rokkasho, in the north of Honshu), on the project and management structure as well as the core team, and a final decision to go proceed with construction. It is anticipated that the site decision will be made in 2004.

The international commitment to ITER is now very strong, due to the recognition by governments that fusion represents an important energy option in a sustainable development policy. This was stressed for example by China when it joined the ITER negotiation process. Brazil and India have also expressed an interest in participating in ITER.

1.2 The CRPP in 2003

On the research front, 2003 has once again yielded exciting scientific results at the CRPP, in all our fields of activities, including:

- Using a combination of Electron Cyclotron Heating (ECH) and Electron cyclotron Current Drive (ECCD) on TCV, significant progress has been made in increasing the confinement enhancement factor of electron internal transport barriers in plasma discharges both driven non-inductively or with an inductive current component, in steady-state conditions. A clear linear relationship between the confinement improvement factor and the product of the barrier strength and enclosed volume has been found.
- The role of the current profile in achieving the improved regime has been clarified on TCV, not only by using combinations of on- and off- axis ECH and ECCD, but also acting on the ohmic current driven with power levels negligible compared to those of the injected ECH/ECCD power.
- The possibility of externally controlling Edge Localised Modes (ELMs) was demonstrated on TCV using coil perturbations that modulate the plasma edge current during single-null ELMy H-mode discharges. The ELM frequency is affected by the external drive frequency. The synchronisation between the external perturbation and the ELMs is influenced by sawteeth, which constitute a competing mechanism for triggering ELMs.
- The TORPEX team and device were completed with the first plasma created in March 2003, and the first measurements were made of linear and nonlinear drift wave characteristics, including the dispersion relation and turbulence statistical properties.

- The theory and modelling work on numerical simulations of low frequency instabilities and turbulence has made several substantial advances. In particular, using the Lagrangian approach, for which a fixed grid in phase space is used. This gives insight into the development of phase space structures in nonlinear electrostatic simulations with an unprecedented level of detail. As a milestone achievement, the development of a global linear gyrokinetic, fully electromagnetic code, which retains all finite β effects and both ion and electron dynamics has been completed.
- Materials research concentrated on modelling activities, including molecular dynamics simulations of damage accumulation in Cu, Ni, and Au, and of grain boundaries in face centred cubic Ni, and finite element calculations of ball punch deformation curves.
- Development and characterisation of nanocrystalline refractory materials for structural applications in fusion power reactors have also advanced well.
- In the field of superconductivity, a crucial experiment in SULTAN allowed us to quantify the degradation affecting the Nb3Sn cable-in-conduit conductors for TF coils, exposed to a transverse electromagnetic load.
- An experiment with an imposed current imbalance on NbTi conductors with different strand coating solved the issue of superconductor interstrand current sharing and its impact on conductor performance.
- The design of the 170GHz, 2MW gyrotron for ITER is completed and the contract for the production of the first prototype is ready for signature by the European Commission.
- The plasma processing group continued its close and fruitful collaboration with industry, the highlight being the exploration of the homogeneity of large area plasma deposition reactors, especially for solar cell production in Switzerland.

This wealth of results is reflected in a large number of overview, invited and contributed papers in international conferences on physics and technology, and in numerous papers appearing in refereed journals.

Collaborations play an important role in the activities of the CRPP. Scientific and technical links are maintained and strengthened with national and international research institutions and industries. In the latter field, of special importance are the issues of technology transfer and the involvement of industry in fusion activities.

Education and training of physicists and engineers are one of the missions of the CRPP. Besides its participation in the teaching of general physics, the CRPP has established a specialised course of the EPFL Doctoral School for all its PhD students, whose research fields covers all activities of the CRPP.

A major event this year for the CRPP was the nomination of its Director, Professor Minh Quang Tran, as the Leader of EFDA (European Fusion Development Agreement). In this additional role, he is responsible for the coordination and overall planning of the activities covered by this Agreement: the Technology Activities in the Associations and in European industry, the collective use of the JET facilities and the European contribution to international collaborations (including ITER).

A detailed description of all the results and activities can be found in the following pages. Some of these activities are carried out within the frame of the Euratom Contract of Association and some are funded outside this contract (as noted in the text). Finally, the CRPP wishes to thank all the funding bodies (listed in Appendix G) which support its long-term research goals.

1 Introduction

1.1 La fusion magnétique sur la scène politique en 2003

En 2003, le choix d'un site pour l'expérience ITER (International Tokamak Experimental Reactor) a occupé le devant de la scène de la politique de la fusion magnétique. En plus des Etats-Unis, deux nouveaux pays, la Chine et la Corée du Sud, ont rejoint le projet ITER. Les pays participant aux négociations finales sont donc maintenant la Chine, la Corée du Sud, les Etats-Unis, le Japon, la Russie et l'Union Européenne (UE). A la fin du mois de novembre, le Conseil des Ministres de l'Union Européenne a décidé, à l'unanimité, de proposer Cadarache, près de Marseille, comme le site européen pour construire ITER. L'Espagne sera le siège de l'autorité légale européenne pour ITER. Les négociateurs internationaux des pays participant au projet ITER vont donc devoir choisir entre le site européen de Cadarache et le site japonais de Rokkasho (au nord de Honshu). Ils devront également prendre des décisions sur la structure du projet et de sa direction, sur l'équipe de base, ainsi que donner le feu vert final pour la construction d'ITER. Il est escompté que la décision concernant le choix du site sera prise en 2004.

L'engagement international pour ITER est maintenant très fort, les gouvernements reconnaissant que la fusion représente une option énergétique importante dans une optique de développement durable. La Chine, en particulier, l'a mentionné lorsqu'elle s'est jointe au processus de négociations. Le Brésil et l'Inde ont également manifesté leur intérêt à participer à ITER.

1.2 Le CRPP en 2003

En ce qui concerne la recherche, l'année 2003 a de nouveau produit des résultats scientifiques passionnants, parmi lesquels on peut citer:

- En utilisant une combinaison de chauffage cyclotronique électronique (ECH) et de génération de courant (ECCD) sur TCV, des progrès significatifs ont été accomplis dans l'augmentation du facteur d'amélioration du confinement des barrières de transport électronique internes, dans des décharges de plasma maintenues totalement ou partiellement de façon non inductive, dans des conditions stationnaires. Une relation linéaire entre le facteur d'amélioration du confinement et le produit de la force de la barrière et du volume inclus a été trouvée.
- Le rôle du profil de courant dans ce régime de confinement amélioré a été clarifié dans TCV, non seulement en utilisant des combinaisons de chauffage et génération de courant (ECH-ECCD) ayant des profils centrés sur l'axe ou en périphérie, mais aussi en agissant sur le courant inductif (ohmique) avec des niveaux de puissance négligeables par rapport à la puissance ECH et ECCD injectée.
- La possibilité de contrôler les modes localisés au bord (ELMs) a été démontrée sur TCV en ajoutant des perturbations dans les bobines utilisées pour le contrôle de position verticale du plasma. Ces perturbations modulent le courant plasma au bord, dans des décharges à un point X en mode H (single-null ELMy H-mode). La fréquence de la perturbation a un effet sur celle des ELMs. La synchronisation des ELMs avec la perturbation est également influencée par les dents de scie, qui constituent un autre mécanisme actif dans le déclenchement des ELMs.
- La construction de la machine TORPEX a été terminée et l'équipe est maintenant au complet. Le premier plasma a été obtenu en mars 2003. Les

premières mesures des caractéristiques linéaires et non linéaires des ondes de dérive ont été faites, incluant leur relation de dispersion et les propriétés statistiques de la turbulence.

- Notre travail de théorie et de modélisation numérique des instabilités de basse fréquence et de la turbulence a fait plusieurs progrès substantiels. Mentionnons en particulier l'approche Lagrangienne, dans laquelle on utilise un réseau fixe dans l'espace de phase, et qui nous donne des informations sur le développement de structures dans cet espace avec un niveau de détail inégalé jusqu'ici, lors de l'évolution non linéaire de la turbulence électrostatique. Un succès majeur a été obtenu avec le développement d'un code global gyrocinétique linéaire complètement électromagnétique, dans lequel tous les effets de β ont été retenus, et qui inclut la dynamique à la fois des ions et des électrons.
- La recherche en matériaux s'est concentrée sur les activités de modélisation, notamment les simulations de dynamique moléculaire de l'accumulation des dégâts dans le Cu, le Ni et l'Au, et des frontières de grains dans le Ni cubique face centrée, ainsi que des calculs d'éléments finis de courbes de déformation « ball punch ».
- Le développement et la caractérisation de matériaux réfractaires nano-cristallins pour les structures des réacteurs de fusion ont également bien progressé.
- Dans le domaine de la supraconductivité, une expérience cruciale avec SULTAN nous a permis de quantifier la dégradation du conducteur Nb_3Sn des bobines toriques, lors de leur exposition à un champ électromagnétique transversal.
- Une expérience avec un déséquilibre de courant imposé sur des conducteurs NbTi dont les filaments sont pourvus de revêtements différents a résolu le problème du partage du courant entre les filaments et de son impact sur la performance du conducteur.
- La conception du gyrotron à 170 GHz et 2 MW pour ITER est terminée. Le contrat de production d'un premier prototype est prêt pour signature par l'UE.
- Le groupe des procédés plasmas a continué sa collaboration proche et fructueuse avec l'industrie. Un des points marquants est l'exploration de l'homogénéité des réacteurs de déposition de grande surface, notamment pour la production de cellules solaires en Suisse.

Cette richesse de résultats se reflète par un grand nombre de papiers présentés lors de conférences internationales de physique ou de technologie, que ce soit des papiers invités, de revue ou des contributions, ainsi que de nombreuses publications dans des revues avec arbitrage.

Les collaborations sont un élément important des activités du CRPP. Les liens scientifiques et techniques avec les institutions de recherche nationales et internationales et avec les industries sont maintenus et renforcés. Les questions du transfert de technologie et de l'implication de l'industrie dans les activités de la fusion sont particulièrement importantes.

La formation des physiciens et ingénieurs est une des missions du CRPP. En plus de participer à l'enseignement de la physique générale et d'assurer complètement celui de la physique des plasmas aux diplômants, le CRPP a mis sur pied un cours de l'Ecole Doctorale de l'EPFL, destiné à tous ses doctorants, actifs dans tous les domaines de recherche du CRPP.

Un événement majeur de l'année pour le CRPP a été la nomination de son Directeur, le Professeur Minh Quang Tran, comme pilote de l'accord EFDA (European Fusion Development Agreement). Dans ce rôle additionel, il est responsable de la coordination et de la planification globale des activités couvertes par cet accord : les activités de technologie dans les Associations et dans l'industrie

européenne, l'utlilisation collective des installations du JET (Joint European Torus), et la contribution européenne aux collaborations internationales (y compris ITER).

Une description détaillée de l'ensemble de nos résultats et de nos activités se trouve dans les pages suivantes. Plusieurs de ces activités sont entreprises dans le cadre du Contrat d'Association Euratom, alors que d'autres sont financées en dehors de ce contrat (indiqué dans le texte). Nos remerciements vont spécialement à toutes les institutions qui supportent financièrement nos objectifs de recherche à long terme, mentionnées dans l'Annexe G.

1 Einleitung

1.1 Die Kernfusion auf der politischen Szene im Jahr 2003

Im Hinblick auf die Kernfusion stand im Jahre 2003 auf der politischen Szene die Entscheidung über den Standort für den Internationalen Tokamak Experimental Reaktor (ITER) im Vordergrund. Ausser den USA, die sich inzwischen wieder an ITER beteiligen wollen, wurden mit China und Süd-Korea zwei neue Mitglieder ins Team aufgenommen. Letztlich werden also China, die EU, die Russische Federation, Süd-Korea und die USA an den nächsten Verhandlungsrunden teilnehmen. Mit seiner Entscheidung von Ende November unterstützt der Ministerrat der Europäischen Union (EU) nun einstimmig die Bewerbung von Cadarache (in Südfrankreich nördlich von Marseille) um den ITER-Standort. Der europäische Verwaltungssitz für das ITER-Projekt soll an Spanien gehen, das einen alternativen Vorschlag unterbreitet hatte. Damit ist der Weg bereitet für die nächsten Schritte auf internationaler Ebene. Es geht dabei um die prinzipielle Entscheidung über den Bau von ITER, den endgültigen Standort – Kandidaten sind Cadarache für Europa und Rokkasho für Japan - sowie um die Bildung einer Führungs- und Verwaltungsstruktur für das ITER-Projekt. Obwohl die Standortfrage auch Ende 2003 noch nicht endgültig geklärt sein wird, kann doch noch im Jahre 2004 mit einer prinzipiellen Entscheidung über die Durchführung des ITER-Projekts gerechnet werden. Brasilien und Indien haben ebenfalls Interesse bekundet, sich am ITER-Projekt aktiv zu beteiligen.

Es gibt also international eine breite Basis für ITER, da bei vielen Regierungen die Ueberzeugung besteht, dass die Kernfusion eine wichtige Option zur langfristigen Energieversorgung darstellt, die den Kriterien einer nachhaltigen Entwicklung entspricht. Dieser Aspekt wurde u.a. von der chinesischen Vertretung bei Ihrem Beitritt zum ITER-Projekt hervorgehoben.

1.2 Bedeutendes aus dem Jahr 2003 am CRPP

Im Bereich der wissenschaftlichen Forschung wurden am CRPP auch im Jahre 2003 in vielen Programmen interessante und bedeutende Ergebnisse erzielt. Hierzu eine kurze Uebersicht :

- Der gezielte Einsatz von Elektron-Zyklotronwellen für Heizung und Stromtrieb des Plasmas im TCV hat es ermöglicht, durch Erzeugung von internen Transportbarrieren, den Energieeinschluss wesentlich zu verbessern. Dies gelang sowohl im Betrieb mit vorwiegend induktiv getriebenem Plasmastrom als auch bei vollständig nicht-induktivem Stromtrieb. Die Untersuchungen ergaben einen linearen Zusammenhang zwischen verbesserter Energieeinschlusszeit und dem Produkt aus Volumen und Stärke der internen Transportbarriere.
- Durch Experimente mit lokalisierter Leistungseinkopplung für Heizung (ECH) und Stromtrieb (ECCD), sowie durch kontrollierte induktive Stromabsenkung bei konstanter Leistung, konnte die Bedeutung des Stromdichteprofils für die Erzeugung von Transportbarrieren herausgestellt werden.
- Die Modulation lokaler Ströme im Randbereich eines Plasmas in SN (single-null) Divertorkonfiguration mit Hilfe von Magnetfeldspulen hat Möglichkeiten der Kontrolle von so-genannten. ELMs (Edge Localised Modes) im H-mode Betriebsbereich aufgezeigt. Es ist gelungen, die Periodizität der ELMs mit der

externen Störung zu synchronisieren. Allerdings wird die ELM-Frequenz auch durch die internen Sägezahnoszillationen beeinflusst; daraus ergibt sich ein mit der externen Kontrolle konkurrierender Prozess.

- Im März 2003 konnte die neu gebildete Gruppe das TORPEX Experiment in Betrieb nehmen und ein erstes Plasma erzeugen. Erste Messungen zur Bestimmung der Dispersionsbeziehung von Driftwellen und deren Beitrag zur Plasmaturbulenz wurden durchgeführt.
- Im Bereich von Plasmatheorie und –modelisierung, mit einem Schwerpunkt auf dem Gebiet der Modelisierung von Instabilitäten niedriger Frequenz und Turbulenz, gab es bedeutende Fortschritte. Erwähnenswert ist insbesondere eine Methode mit festem Phasenraumgitter (Eulerian approach), die eine bis dahin unerreichte Auflösung bei der Untersuchung von dynamischen Strukturen im Phasenraum ermöglicht. Ein herausragendes Ergebnis ist die Fertigstellung eines numerischen Programms auf der Basis eines gyro-kinetischen und voll-elektromagnetischen Codes, der alle Effekte bei endlichem kinetischem Druck (finite β) und sowohl die Elektronen- als auch die Ionendynamik berücksichtigt.
- Die Aktivitäten auf dem Gebiet der Materialforschung waren auf numerische Simulation der Dynamik bei der Akkumulation von induzierten Defekten in Cu, Ni und Au sowie auf die Untersuchung von Korngrenzen in flächenzentrischen kubischen Ni-Kristallen ausgerichtet. Mit Hilfe von Simulationen nach der Methode der finiten Elemente wurden sogen. punch-ball Verformungsdiagramme berechnet.
- Auf dem Gebiet der Entwicklung und Charakterisierung von nano-kristallinen refraktiven Materialien für die Anwendung in Fusionsreaktoren wurden weitere Fortschritte erzielt.
- Experimente an Nb_3Sn “cable-in-conduit“ Supraleitern mit der SULTAN-Anlage haben es erlaubt, deren Verhalten in Gegenwart einer Belastung durch ein transversales elektromagnetisches Feld zu untersuchen. Daraus ergab sich eine Minderung der Eigenschaften für die toroidalen Feldspulen von ITER vorgesehenen Supraleiter.
- Weitere Experimente unter Bedingungen von unsymmetrischer Strombelastung in NbTi Supraleitern mit verschiedener Beschichtung der Leiterstränge lieferten die nötigen Kenntnisse zur Beurteilung des Problems der Stromverteilung. Dies hat wichtige Konsequenzen im Hinblick auf die Belastbarkeit dieser Supraleiter.
- Die Konstruktionspläne für ein Gyrotrons mit 2MW bei 170GHz für ITER liegen bereit und ein Vertrag mit der Kommission der EU über den Bau eines Prototyps kann demnächst zur Unterschrift vorgelegt werden.
- Die Plasmatechnologie-Gruppe (plasma processing) führt ihre enge und erfolgreiche Zusammenarbeit mit der Industrie fort. Ein Schwerpunkt der Forschung sind Untersuchungen zur Homogenität in Plasmareaktoren für grossflächige Beschichtungen, insbesonder im Hinblick auf die Herstellung von Solarzellen in der Schweiz.

Die Fülle der Forschungsergebnisse schlägt sich nieder in einer entsprechenden Zahl von Beiträgen an internationalen Konferenzen über Physik und Technologie, sowie in einer Reihe von Veröffentlichungen in renommierten wissenschaftlichen Zeitschriften.

Der Zusammenarbeit mit nationalen und internationalen Partnern in Wissenschaft und Industrie wurde am CRPP schon immer ein hoher Stellenwert eingeräumt. Diese Beziehungen wurden weiterhin aufrecht erhalten und vertieft. Dabei wurde berücksichtigt, dass dem Technologietransfer und der Einbindung von Industrieunternehmen in die Technologie der Fusion wachsende Bedeutung zukommen.

Als Bestandteil der EPFL hat das CRPP ebenfalls eine wichtige Aufgabe bei der Ausbildung und Weiterbildung von Physikern und Ingenieuren. Dazu gehört die

Beteiligung bei der Durchführung von Grundvorlesungen zur allgemeinen Physik. Darüber hinaus wurde vom CRPP ein weiterführender Kurszyklus für Doktoranden eingerichtet, der Themen aus allen am CRPP vertretenen Forschungsbereichen behandelt.

Ein herausragendes Ereignis für das CRPP war die Ernennung von Prof. M.Q. Tran zum EFDA-Leader (European Fusion Development Agreement). In dieser weiteren Verantwortung ist Prof. Tran zuständig für die Koordinierung und Gesamtplanung der Aktivitäten unter EFDA: die Technologieaktivitäten in den Assoziationen und der europäischen Industrie, die gemeinschaftliche Nutzung der JET Anlagen (Joint European Torus) und die europäischen Beiträge zu internationalen Zusammenarbeiten (einschließlich ITER.

Auf den folgenden Seiten finden Sie eine detailliertere Beschreibung der Forschungstätigkeit am CRPP und der daraus hervorgegangenen Resultate. Dieses Programm wurde zum Teil im Rahmen des EURATOM- Assoziationsvertrags durchgeführt. Einige Aktivitäten (siehe Anmerkungen im Text) wurden aus anderen Quellen finanziert. Wir wollen uns an dieser Stelle bei allen Förderern (siehe Liste im Anhang G) für die Unterstützung unserer langfristig angelegten Forschungsaufgaben bedanken.

1 Introduzione

1.1 Il panorama politico nel campo della fusione magnetica nel 2003

Nel 2003, il panorama politico della fusione magnetica è stato dominato dal dibattito sulla collocazione geografica del Reattore Internazionale Sperimentale di tipo Tokamak, ITER, che rappresenta il prossimo principale traguardo nella ricerca sulla fusione. Parallelamente al rientro degli Stati Uniti nei negoziati, due nuovi Paesi, la Cina e la Corea del Sud, si sono associati al progetto. Alle trattative finali partecipano ora la Cina, la Corea del Sud, il Giappone, gli Stati Uniti, la Russia e l'Unione Europea,. Alla fine di novembre, il Consiglio Europeo dei Ministri ha unanimemente scelto Cadarache (presso Marsiglia) come sito europeo candidato ad ospitare ITER. La Spagna sarà invece sede dell'Entità Giuridica Europea di ITER. Questo passo importante apre la strada ad una serie di decisioni da parte dei Paesi partecipanti: la scelta tra il sito europeo a Cadarache e il sito proposto dal Giappone (Rokkasho, nello Honshu settentrionale), la formazione della struttura progettuale e manageriale e la costituzione di un gruppo di lavoro ristretto, e infine la decisione definitiva di procedere alla costruzione del reattore. La decisione sul sito è prevista nel corso del 2004.

Si riscontra oggi un forte impegno internazionale nel perseguimento del progetto ITER, grazie al riconoscimento da parte dei diversi governi dell'importante opzione energetica offerta della fusione nel quadro di una politica di sviluppo sostenibile. Questo concetto è stato evidenziato per esempio dalla Cina in occasione del suo ingresso nelle trattative su ITER. Il Brasile e l'India hanno a loro volta espresso interesse a partecipare a ITER.

1.2 Il CRPP nel 2003

Sul piano della ricerca, nel 2003 il CRPP ha prodotto ancora una volta risultati scientifici di rilievo in tutti i suoi campi di attività, tra cui citiamo i seguenti:

- Impiegando una combinazione di riscaldamento e di generazione di corrente mediante onde di ciclotrone elettroniche (rispettivamente ECH e ECCD), sono stati compiuti importanti progressi nell'aumentare il fattore di miglioramento del confinamento dovuto a barriere interne di trasporto elettronico, in scariche puramente non induttive e in scariche contenenti una componente finita di corrente indotta. Una chiara relazione lineare è stata trovata tra il fattore di miglioramento del confinamento e il prodotto dell'altezza della barriera e del volume in essa contenuto.
- È stato messo in luce su TCV il ruolo del profilo di corrente nell'ottenimento del regime a confinamento migliorato, non solo impiegando una combinazione di ECH ed ECCD centrali e periferici, ma anche intervenendo sulla corrente ohmica, indotta con una potenza immessa trascurabile rispetto alla potenza ECH/ECCD.
- E' stata esplorata la possibilità di un controllo esterno dei Modi Localizzati al Bordo (ELMs) su TCV grazie a perturbazioni nelle correnti delle bobine esterne che permettono di modulare la corrente nel bordo del plasma in scariche in modo H con ELMs (in una configurazione caratterizzata da un solo punto di azzeramento del campo magnetico poloidale). La frequenza degli ELMs è condizionata dalla frequenza di questa perturbazione esterna. La

sincronizzazione tra la perturbazione e gli ELMs è a sua volta influenzata dai denti di sega, che rappresentano un meccanismo concorrenziale di eccitazione degli ELMs.

- L'installazione di TORPEX è stata completata, con il primo plasma creato nel marzo 2003, da un gruppo scientifico ormai a sua volta al completo. Durante il resto dell'anno sono state effettuate le prime misure delle caratteristiche lineari e non lineari delle onde di deriva, e in particolare della loro relazione di dispersione e delle proprietà statistiche della turbolenza risultante.
- Il lavoro teorico e di modellizzazione numerica sulle instabilità e turbolenza a bassa frequenza ha conosciuto progressi fondamentali su molti fronti, usando in particolare l'approccio lagrangiano che utilizza un reticolo fisso nello spazio delle fasi: questo permette di visualizzare l'evoluzione di strutture in tale spazio, in simulazioni elettrostatiche non lineari, con una finezza di dettaglio senza precedenti. Inoltre, il completamento di un programma di simulazione girocinetico globale lineare, completamente elettromagnetico, in grado di riprodurre tutti gli effetti legati ad un β finito e la dinamica degli ioni e degli elettroni, ha rappresentato una pietra miliare importante.
- La ricerca sui materiali si è concentrata su attività di modellizzazione, tra cui simulazioni di dinamica molecolare dell'accumulo del danno in Cu, Ni e Au e dei bordi di grano in Ni a struttura cubica a facce centrate, e calcoli agli elementi finiti della funzione di deformazione da carico indotto da punzone sferico.
- Si sono riscontrati buoni progressi nello sviluppo e nella caratterizzazione di materiali rifrangenti nanocristallini per applicazioni strutturali in centrali a fusione nucleare.
- Nel campo della superconduttività, un esperimento cruciale su SULTAN ci ha permesso di quantificare la degradazione subita dai cavi superconduttori di Nb3Sn in guaina (previsti per le bobine del campo magnetico toroidale di ITER), allorché sono sottoposti ad un carico elettromagnetico trasversale.
- Un esperimento condotto con uno squilibrio di corrente imposto tra conduttori di NbTi con diversi rivestimenti di cavo ha risolto la questione della ripartizione di corrente tra cavi superconduttori e del suo impatto sulle prestazioni dei conduttori stessi.
- Il progetto di girotrone di 2 MW a 170GHz per ITER è stato completato e il contratto per la fabbricazione del primo prototipo è pronto per essere firmato dalla Commissione Europea.
- Il gruppo specializzato nei processi al plasma ha continuato la sua stretta e fruttuosa collaborazione con l'industria; merita un risalto particolare il lavoro di esplorazione dell'omogeneità dei reattori per deposizione con plasma a grande area, specialmente per la produzione di celle solari in Svizzera.

La ricchezza di questi risultati si riflette in un numero elevato di relazioni di compendio e invitate o ancora di contributi spontanei a congressi internazionali di fisica e tecnologia, e in numerosi articoli apparsi in riviste scientifiche internazionali.

Le collaborazioni esterne costituiscono un elemento importante delle attività del CRPP, che mantiene e rafforza costantemente legami scientifici e tecnici con vari istituti di ricerca e industrie, sia nell'ambito nazionale che in quello internazionale. Nelle collaborazioni con l'industria rivestono particolare importanza la problematica del trasferimento tecnologico e la partecipazione dell'industria stessa alle attività della fusione.

L'istruzione e la formazione di fisici e ingegneri costituisce una delle missioni del CRPP. In parallelo alla sua partecipazione all'insegnamento della fisica generale, il CRPP ha istituito una serie di corsi specialistici nell'ambito del programma di dottorato di ricerca dell'EPFL, destinati in particolare a tutti gli studenti di dottorato del CRPP, e i cui campi di ricerca spaziano attraverso tutte le attività del Centro.

Un evento importante al CRPP durante il 2003 è stata la nomina del suo Direttore, il Professor Minh Quang Tran, alla guida dell'EFDA (European Fusion Development Agreement, ovvero Accordo Europeo per lo Sviluppo della Fusione). In tale ruolo aggiuntivo, il Prof. Tran è responsabile della coordinazione e pianificazione generale delle attività contemplate da questo Accordo: le attività tecnologiche nelle Associazioni e nell'industria europea, l'utilizzo collettivo del JET e il contributo europeo alle collaborazioni internazionali (tra cui ITER).

La descrizione dettagliata di tutti i nostri risultati e delle nostre attività è contenuta nelle pagine che seguono (solo in inglese). Alcune di queste attività si svolgono nel quadro del Contratto di Associazione Euratom e alcune sono finanziate da fonti esterne a tale contratto (come indicato nel testo). In conclusione, il CRPP tiene a ringraziare in modo particolare tutti gli organi (elencati nell'appendice G) da cui riceve finanziamenti per il loro sostegno dei suoi obiettivi di ricerca a lungo termine.

2 Research achievements of the CRPP in 2003

2.1 The TCV tokamak

2.1.1 Overview of the experimental programme

Magnetic fusion physics is investigated experimentally at CRPP primarily on the *Tokamak à Configuration Variable*, TCV, characterised by a major radius R=0.88m, a minor radius a<0.255m, a toroidal magnetic field B_t<1.54T and a vessel elongation of three. A large degree of flexibility in its configuration, control and auxiliary heating systems makes the TCV tokamak a unique tool worldwide to contribute to a number of crucial areas of research, of interest both for the next generation of burning plasma experiments, such as ITER, and for longer term developments towards the development of magnetic fusion reactors. Among the common goals for ITER and the tokamak concept improvement are the achievement and control of high performance plasma regimes, with large core plasma pressure, good energy and particle confinement, and exempt from macroscopic plasma instabilities. These regimes require optimisation of the plasma geometry and the ability to control the profile of a number of plasma parameters such as the plasma pressure or the electrical current.

TCV pursues these studies using its recently completed systems for electron cyclotron heating and current drive (ECH and ECCD). The total power available is 4.5MW, 3MW at the second harmonic (X2) and 1.5MW at the third harmonic (X3) of the electron-cyclotron frequency. 3.5MW have been already injected into the plasma at the same time, which is a world record. The TCV installation exploits the timing and geometrical flexibility, the ease of control of the deposition location and the very narrow spatial localisation of the absorption which are unique properties of ECW systems.

The 2003 experimental campaign resumed in mid-January after a 10 week shutdown for minor diagnostic upgrades and repairs. TCV operated, as planned, through three separate periods of five, seven and ten weeks, until the end of October. Investigations were conducted in ohmic and ECH-ECCD plasmas (both with X2 and/or X3), including Helium plasmas and forward and reversed field scenarios.

The 2003 TCV experimental results are grouped into four sections. The first (2.1.2) is devoted to the physics developments toward the achievement of high β plasmas and the study of plasmas close to the β limits. The second (2.1.3) focuses on the physics experiments on current drive and superthermal particles (β is the ratio between plasma pressure and magnetic field pressure) using combined X2 and X3 ECH-ECCD. The third section (2.1.4) illustrates the progress achieved on TCV towards the realisation and the understanding of advanced regimes of operation, building on the knowledge of the ECH and ECCD effects on the plasma profiles. The fourth section (2.1.5) encompasses a number of physics topics addressed in the unique TCV plasma conditions, including the triggering of ELMs (Edge Localised Modes) using an externally driven perturbation, transport of bulk plasma particles and plasma impurities in highly shaped plasmas, edge and divertor physics studies and the sawtooth stability as a function of plasma shape. This overview highlights the most salient progress made on TCV during 2003, while the details are discussed in the individual sections which follow.

The achievement of high β plasmas in TCV requires a certain number of developments, from the avoidance of deleterious macroscopic plasma instabilities, to optimising the bulk plasma transport, understanding how to achieve high confinement modes and their edge stability properties, and how to efficiently heat plasmas whose high density is inaccessible to the second, or even the third, EC harmonic waves.

Generally, present tokamaks have identified the limits imposed by ideal Magneto-Hydro-Dynamics (MHD). However, TCV is among the few devices that study ideal limits in previously unexplored regions of parameter space, being so highly shaped. Broadening of the plasma current profile is necessary to reduce the vertical instability at high plasma elongation and low current, and is provided on TCV by off-axis EC power injected in a current drive configuration, with a finite component of the electric field in either toroidal direction.

Off-axis ECH is also used for fundamental transport studies. The high power density available in TCV allows us to extend the range of one of the key physics parameters, the normalised electron temperature gradient, by a factor of four compared to other tokamaks. MHD instabilities that can limit plasma performance are investigated. A rotating mode localised at the q=1 resonant surface (q is the helicity of the field lines) is observed to replace sawteeth for high density, high elongation plasmas, and to lead to a similar flattening of the temperature profile.

The effect of plasma density on the transition from low (L-) to high (H-) confinement mode is assessed in EC heated plasmas: a threshold density value is found, below which no H-mode is obtained. The threshold power for L-H transition increases with increasing density. Third harmonic ECH has been applied to H-mode discharges. For high ECH powers the plasma tends towards an ELM-free phase, a density rise and to a subsequent loss of EC absorption. For low ECH power, the ELM frequency is observed to decrease and reach a stationary value, at which ELMs and sawteeth are synchronised.

In order to heat plasmas that are overdense even to the third ECH harmonic, investigations of possible schemes for mode conversion of the electromagnetic wave into electrostatic waves that propagate irrespectively of the plasma density are being conducted. The most promising scheme for TCV is based on conversion of the O-mode into the X-mode, then into an electrostatic Bernstein wave in the presence of a strong density gradient at the upper hybrid resonance layer. This method is, however, delicate and presents a considerable experimental challenge.

Further progress has been made in investigating the superthermal electron dynamics and the related fundamental properties of ECCD. Fully ECCD sustained discharges using no transformer flux to drive the plasma current were operated with wave-particle interaction occurring predominantly on the high field side of the tokamak, where fast electrons are less trapped by the ripple of the toroïdal magnetic field, in principle enhancing the ECCD efficiency. The operational margin for controlling ECCD sustained discharges was investigated experimentally by imposing temporary power loss of variable duration. Perturbative experiments have been performed to determine the distribution of suprathermal electrons at birth and its temporal evolution due to transport. These transport phenomena were also investigated comparing the data with quasi-linear computer simulations. It was concluded that different values of radial diffusion coefficient act on different energy classes of suprathermal electrons. The influence of the suprathermal population on the interpretation of Thomson scattering measurements of the electron temperature was investigated to obtain a quantitative correction factor for the electron temperature. Measurements of the ion energies from a neutral particle analyser during ECCD injection indicate the presence of a suprathermal ion tail that carries a significant fraction of the total ion energy.

Relativistic effects giving rise to wave absorption by higher harmonics (third harmonic with X2 and fourth with X3) were studied both experimentally and numerically. A way to selectively drive specific energy classes of suprathermal electrons using X3 radiation launched vertically, parallel to the resonant surface, was demonstrated. Through iterated comparisons between models and data, an electron distribution function was reconstructed that gives rise to the observed strong (~100%) absorption of perpendicularly launched X3 radiation and is compatible with all available experimental measurements.

Putting into play our increased understanding of the effect of ECH and ECCD on the current profile, and of transport, significant progress was achieved in enhanced confinement regimes. The properties of the electron internal transport barriers on TCV which lead to record temperature have been quantified. A clear linear relationship between the confinement improvement factor and the product of the barrier strength and enclosed volume has been found.

Significant progress has been made in increasing the confinement enhancement factor of electron internal transport barriers in plasma discharges both driven non-inductively or with an inductive current component, in steady-state conditions. The confinement enhancement over the TCV L-mode energy confinement time, which is well described by the Rebut-Lallia-Watkins scaling, has reached H_{RLW}=5. Note that these advanced scenarios are achieved in TCV by acting on the fully diffused current profile during the flat top portion of the discharge. The role of the current profile in achieving the improved regime has been clarified, not only by using combinations of on- and off- axis ECH and ECCD, but also acting on the ohmic current driven with power levels negligible compared to those of the injected ECH/ECCD power.

The MHD activity which limits the performance in advanced regimes has been investigated. In the improved core electron confinement regime, performance is limited by the appearance of a neo-classical tearing mode close to the maximum pressure gradient location. Fast relaxations of ideal MHD character, identified as global ideal kink modes, act to flatten the soft X-ray emission profile in cases with relatively low plasma current.

The possibility of externally controlling ELMs was explored using control coil perturbations that modulate the plasma edge current during single-null diverted ELMy H-mode discharges. The ELM frequency is affected by the external drive frequency. The synchronisation between the external perturbation and the ELMs is influenced by sawteeth, which constitute a competing mechanism for triggering ELMs.

The existence of an anomalous particle for bulk plasma particles pinch driving particles into the plasma core was confirmed experimentally even in stationary, fully relaxed and fully ECCD driven discharges. Impurity transport was also investigated in ECH and ECCD plasmas using Argon puff and laser ablation techniques. Although some confinement degradation was observed for impurities, it is an order of magnitude lower than for the bulk electron population.

Edge physics research on TCV has concentrated on anomalous "detachment" of the energy flow from the plasma to the wall on the outer of the two diverted plasma "legs" and on new edge turbulence measurements. The role of molecular recombination of D_2 is ruled out in the detachment process. Among the other possible explanations of the observed detachment characteristics, the data suggest an important role played by molecular assisted recombination of hydrocarbon and by edge plasma drifts.

The edge turbulence database has been extended in ohmic discharges with measurements of poloidal phase velocities of the turbulent structures and of the magnitude and direction of the ExB driven flux. The probability distribution function of the ion flux flowing along the field lines indicates an increasing occurrence of large outgoing events as the distance from the confined plasma is increased. The first parallel flow measurements on TCV confirm the importance of MHD ballooning mode transport on the low magnetic field side in driving the anomalous parallel flows observed at the edge of most tokamak plasmas.

Sawtooth dependence on plasma triangularity (the plasma cross-sectional shape) have been measured and compared with a numerical model based on the ideal internal kink mode. The data and the model agree, indicating that both positive and negative triangularities lead to sawtooth stabilisation, of importance for the destabilising of neo-classical MHD tearing modes.

2.1.2 Enhancement of plasma β using a combination of second and third harmonic extraordinary launch for electron cyclotron heating and current drive

This section describes the TCV studies aimed at understanding the conditions for improving the plasma β using electron cyclotron heating and current drive (ECH and ECCD), in second and third harmonic extra-ordinary mode (X2 and X3). These include adjusting the plasma current profile to avoid instabilities at high plasma elongation, characterisation of electron profiles and transport with off-axis heating, MHD instabilities that can limit plasma performance, the L- to H-mode transition, and the effect of edge Localised Modes (ELMs). The prospective use of Electron Bernstein Waves to heat plasmas with densities above the second harmonic cut-off is also discussed.

Use of off-axis electron cyclotron heating to broaden the current profile to reduce the vertical instability at high elongation

The vertical instability of highly elongated low current plasmas is reduced by a broad current profile. EC power in the off-axis ECCD scenario, with a deposition location vertically above the plasma axis, has been shown to be more effective at broadening the current profile than ECH. Injecting the EC beam at a toroidal angle of typically $\varphi=\pm 15^{o}$ improves effectiveness by 15-20% over ECH conditions ($\varphi=0^{o}$). Calculations using the CQL3D code indicate that the increased drop in internal inductance is not due to the EC driven current, since the interaction occurs totally in the trapped electron region of phase space. Instead, it is due to the fast electrons generated by EC power, which decrease the loop voltage for both signs of the injection angle also increasing P_{EC}/P_{OH}. The presence of these fast electrons is confirmed by high field side EC emission data.

Further improvements are expected in the future with the implementation of the digital control system, in particular to keep the optimal EC power deposition location in discharges with evolving elongation. Using the four upper lateral launchers, it should be possible to extend extremely high elongation operation to normalised current values $I_N=I_p/aB$ closer to 2, corresponding to the highest β limits from ideal MHD. The remaining X2 power from the equatorial launchers together with X3 power will then be used to heat the core in standard or improved confinement regimes.

Off-axis heating and electron heat transport

The plasma response to ECH power deposition at two different radial positions, in the centre and off-axis, was investigated. Substantially different electron temperature gradients are obtained (Fig. 2.1.1).

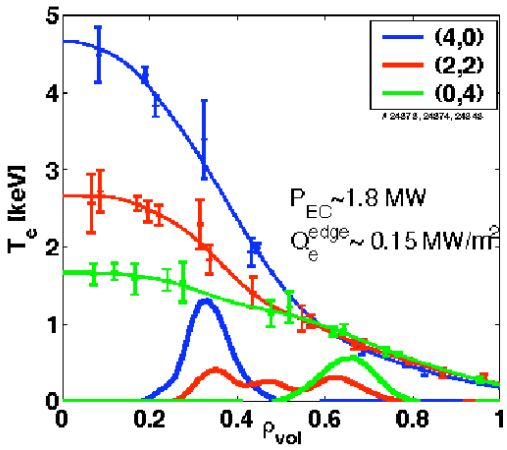

Fig. 2.1.1 *Variation of the electron temperature gradient at constant edge heat flux obtained by varying the EC power deposition indicated in the lower part of the figure.*

To detect a possible dependence of the radial electron heat diffusivity on plasma triangularity, the experiments were performed at two different values of triangularity, δ~0.2 and δ~0.4. The electron temperature gradient ∇T_e and its normalised value $R\nabla T_e/T_e=R/L_{Te}$ were varied at constant edge heat flux by changing the radial distribution of the EC power deposition at constant total EC power. The comparison with data from ASDEX-Upgrade shown in Fig. 2.1.2 provides an example of how the high EC power density in TCV has allowed us to extend the range of R/L_{Te} by a factor of four. The electron thermal diffusivity χ_e exhibits the previously observed threshold behaviour at low gradients, an increase with R/L_{Te} for medium $R/L_{Te}<15$, but also an unexpected decrease for the highest temperature gradients ($15< R/L_{Te}<25$).

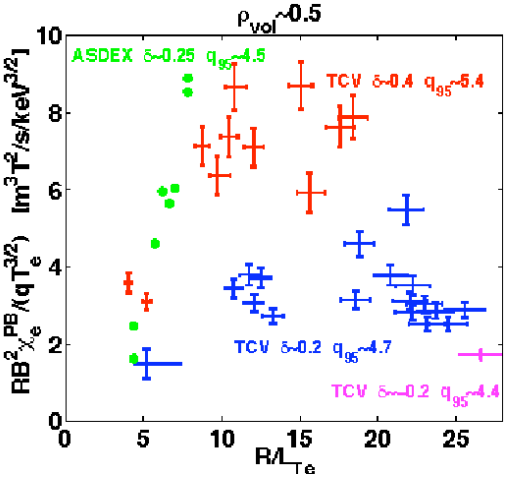

Fig. 2.1.2 *Comparison of $\chi_{e\ norm}(R/L_{Te})$ for TCV and ASDEX-Upgrade, showing a stronger stiffness of the electron temperature profile in ASDEX-Upgrade at $R/L_{Te}<10$ and the roll-over at higher values of R/L_{Te} obtained at the high power densities available in TCV. Higher χ_e are observed at higher triangularities in TCV..*

The reduction of transport at high R/L_{Te} appears more pronounced at δ~0.2 than at δ~0.4. It is not clear at present whether the difference observed with triangularity is intrinsic to the plasma shape or depends on another plasma parameter, like the ion temperature. Resolution of this question is important in relation to the possibility of easing the access to internal transport barriers by plasma shaping. In these experiments control of the elongation is mandatory to compensate for the effect of changing the current profile.

High performance and mode activity with central third harmonic and off-axis second harmonic launch

In high density, highly elongated discharges with strong off-axis heating, sawtooth activity is replaced by a continuous rotating mode. Magnetic and soft X-ray measurements show a mode structure with several poloidal/toroidal harmonics (m/n=1/1, 2/2, 3/3), all resonant on the q=1 surface. This is in contrast with standard sawtooth precursors, for which multiple harmonics are generally not observed. The mode activity appears at fixed l_i=0.89±0.02, independent of current and elongation, similar to the previously observed ohmic discharges at much higher elongation. It is preceded by an increasing level of precursor oscillations and reduced sawtooth crash amplitude. Moreover, the mode can exist in stationary conditions as long as X2 is applied. In the presence of off-axis heating, the T_e and j_ϕ profiles are flattened, l_i decreases and the elongation κ increases, while the q=1 surface is observed to shrink on a resistive diffusion time scale. This leads to a region of decreased current density and low magnetic shear around q=1 and could lead to the destabilisation of a magnetic island.

If central X3 heating is added, the current density peaks again and κ decreases. The continuous mode first decreases in amplitude, then disappears while sawtooth activity restarts on a time scale compatible with the local resistive diffusion time. At the onset and offset of the mode the plasma conditions are very similar, in particular the value of l_i.

Comparison with theory shows an increased linear stability of the ideal kink mode due to the smaller size of the q=1 surface that largely compensates the destabilising effect of the increased elongation. Plasma resistivity is then believed to play a major role in triggering and sustaining this multi-harmonic mode activity.

L- to H-mode transitions

A series of experiments was devoted to identifying the minimum H-mode threshold power in TCV, both in ohmic and additionally heated discharges. This is particularly important in view of the application of third harmonic EC power to enhance the TCV plasma β in discharges that are overdense to second harmonic ECH. In ohmic discharges, the power ramp was produced by a plasma current ramp applied after the formation of the separatrix, while in additionally heated discharges it was simply produced by increasing the ECH power. The plasma density was scanned from pulse to pulse and experiments were performed for both directions of magnetic field to assess the effect of the ion grad-B drift.

Figure 2.1.3 shows the measured threshold power as a function of the plasma density. The circles represent ohmic LH transitions with favourable ion grad-B drift direction. The threshold power increases with increasing density. Below $0.4\times10^{20}m^{-3}$, discharges remain in L-mode even if the plasma current is increased up to the value imposed by the q_{95}=2 limit. This reveals the presence of a threshold density below which no LH transition is observed in ohmic plasmas. The threshold power is larger when the magnetic field is reversed (triangles) and confirms the influence of the ion grad-B drift direction on the LH transition.

The threshold power obtained with X3, indicated by a single square on the graph, corresponds to that of ohmic discharges with similar density. LH transitions were also obtained at low density with X2 (stars). In this case, the threshold density is lower than in the ohmic case but the threshold power is higher. Since the threshold power decreases with decreasing density at higher densities, a minimum is located between the X2 and ohmic data. The threshold power values found at the lowest

density in ohmic discharges correspond to the minimum power necessary to access the H-mode in TCV with the favourable ion grad-B drift direction.

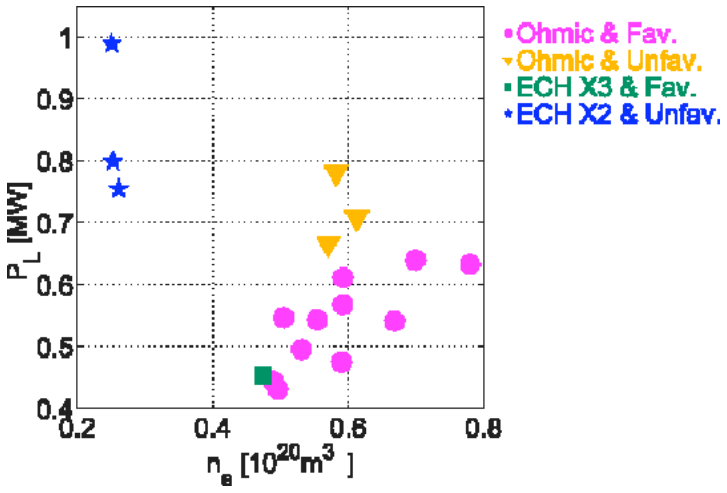

Fig. 2.1.3 *Loss power (Ohmic + ECH power - variation of plasma energy content) as a function of the plasma line averaged density for ohmically and ECH heated discharges in plasma with favourable and unfavourable ion grad-B drift directions.*

Access to the H-mode was also studied in Helium plasmas. A few LH transitions were obtained in both ohmic and ECH plasmas with the ion grad-B drift directed towards the X-point, while to date none have been obtained in the reversed magnetic configuration.

Effect of third harmonic power on ELMy H-modes: Synchronisation of Edge Localised Modes with sawteeth

The X3 ECH system was used to heat ELMy H-mode discharges. The injected power was varied from 0 to 960kW, giving rise to an absorbed power, calculated by the TORAY-GA code, between 0 and 625kW. The direct measurement from the DML response is problematic in H-mode, Section 3.2.1.

At absorbed power values >400kW, the ELM frequency strongly decreases, the discharge becomes ELM free and the X3 power has no more effect as the uncontrolled increase of the density causes a strong refraction of the X3 beams. At lower power, the ELM frequency decreases at the beginning of the heating phase and then reaches a stationary value. At very low power the ELM frequency is not modified, Fig. 2.1.4. This figure presents the ELM and sawtooth frequencies for three discharges in which different levels of ECH X3 power were injected. In the first case the ELM frequency slightly varies when the ECH power is applied, while the modification of the ELM frequency in both other cases is important. The sawteeth frequency remains constant when the X3 power is applied.

Before the ECH pulse, the ELM frequency coincides with the sawtooth frequency. In pulse #23344, ELMs and sawteeth are synchronised, with an ELM occurring at every sawtooth crash. This synchronisation is lost when ECH power is applied. In #23351, the ELM frequency decreases to approximately 2/3 of the sawteeth frequency and synchronisation is again lost. In #23347, the ELM frequency decreases to approximately half of the sawteeth frequency and synchronisation occurs, with the ELMs synchronous with every second sawtooth, Fig. 2.1.5.

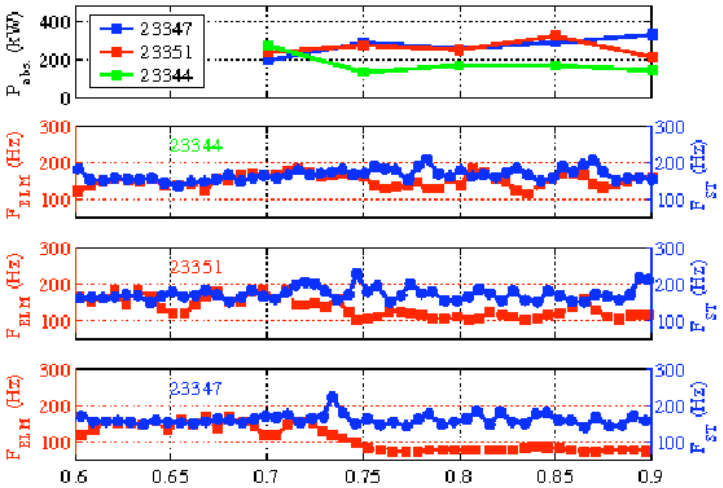

Fig. 2.1.4 *Evolution of the ELM and sawtooth frequency for three discharges with different X3 heating powers, starting at t=0.7s*

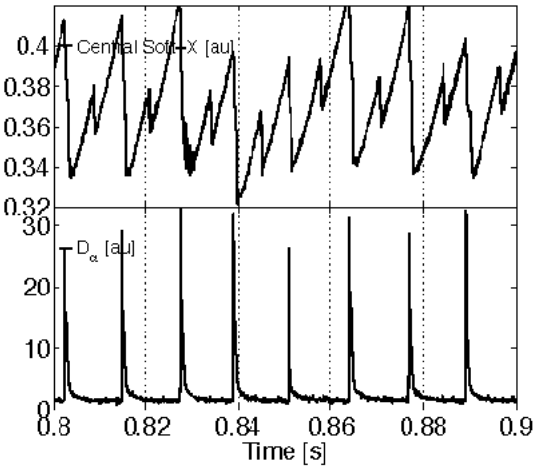

Fig. 2.1.5 *Detail of the evolution of the central X-ray emission and the D_α emission for discharge #23347 (Fig. 2.1.4, lowest box) showing synchronisation between sawteeth and ELMs. The ELM frequency locks at half the sawtooth frequency*

Electron Bernstein wave studies

At electron densities larger than $4.2\times10^{19}m^{-3}$, electromagnetic waves at the second cyclotron harmonic in the extraordinary mode do not propagate. Heating of overdense plasmas should be possible by mode converting these electromagnetic waves to electrostatic waves that can propagate irrespective of density, such as Electron Bernstein Waves (EBWs). With a view to extending the operational space of additionally heated plasmas on TCV, efforts are being made to develop EBW heating of overdense plasmas.

For direct mode conversion, fast X-mode to Bernstein wave (XB) there must be a very large density gradient ($>10^{22}m^{-4}$) in a region of the plasma where the extraordinary mode at the first cyclotron harmonic is evanescent. For Ordinary to slow X-mode to Bernstein wave (OXB) conversion to occur, the plasma frequency and the upper hybrid frequency must coincide in a region of the plasma where there exists a substantial density gradient ($>10^{21}m^{-4}$).

Preliminary studies revealed that the direct XB conversion scheme is extremely difficult on TCV but that the OXB scheme may be possible in high density H-mode. Attempts have been made to produce plasmas that will allow mode conversion. It has been possible to produce discharges suitable for mode conversion studies in ELM-free H-mode, although the conditions to allow OXB conversion have been attained only briefly for less than 100msec.

2.1.3 Physics of current drive and suprathermal particles using combined second and third harmonic extraordinary mode launch for electron cyclotron heating and current drive

During 2003, further progress has been made in investigating the fundamental properties of ECCD, in particular by extending the database of fully sustained discharges to scenarios with the wave-particle interaction occurring predominantly on the high field side of the torus. A study of the tolerance of ECCD-sustained discharges to a temporary RF power loss has also been carried out, with practical implications for plasma control. Investigations into the dynamics of suprathermal electrons have continued, with perturbative experiments aimed at determining their distribution at birth as well as their temporal evolution under the effect of transport processes. In parallel, additional quasi-linear simulations have been performed in an attempt to shed light on the underlying causes of their transport. The influence of the suprathermal population on electron temperature measurements by Thomson scattering has been investigated in detail. A suprathermal ion tail is also known to exist in the presence of ECCD and has now been studied systematically by means of a neutral particle analyser.

Particular emphasis was placed on higher harmonic absorption, both in experimental and numerical work. Selective absorption of X3 radiation launched parallel to the resonant surface by suprathermal electrons of specific energy has been demonstrated. Fully relativistic calculations have revealed the potential for significant higher harmonic absorption (third harmonic with X2 and fourth with X3) in the presence of a sizable suprathermal population. Through an iterative heuristic process, we have succeeded in constructing an electron distribution function that leads to nearly 100% absorption of perpendicularly launched X3 radiation, as observed in earlier experiments, and also matches all experimental measurements.

Electron cyclotron current drive physics and control

During the past four years we have assembled an extensive database of fully non-inductive TCV discharges driven by a combination of ECCD and bootstrap current. As the stationary phase of these discharges has strictly no Ohmic current component, the global current drive efficiency can be accurately determined. The database has recently been completed with a series of discharges at reduced toroidal magnetic field, in which the X2 ECH resonance is located on the high field side of the magnetic axis. The lower fraction of trapped electrons in this region is theoretically predicted to lead to higher ECCD efficiency. We have slightly increased our previous records of fully non-inductive current drive (210kA with 5 instead of 6 gyrotrons, 180 vs. 160kA with 3 gyrotrons), although this increase is partly attributable to different densities and temperatures. The parametric dependence of the local efficiency will have to be determined by a broad statistical analysis of the entire database. The previously discovered effects of the radial transport of fast electrons were confirmed in far off-axis heating configurations: one 120kA discharge was driven by EC waves deposited by 5 gyrotrons at a normalised minor radius of ~0.6-0.7 (see Fig. 2.1.6), while linear efficiency calculations predicted a current 6 to 10 times smaller.

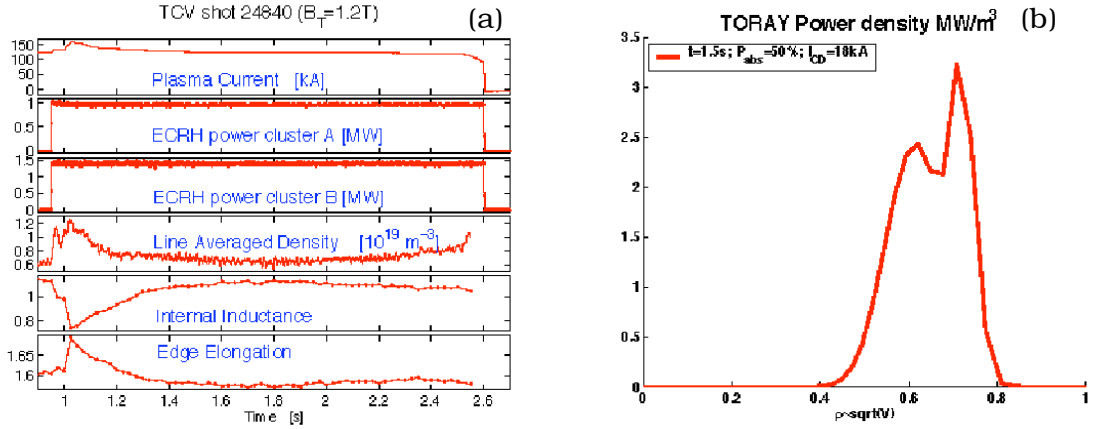

Fig. 2.1.6 *(a) Fully ECCD-sustained TCV discharge; (b) EC power density calculated by TORAY-GA ray tracing*

For the practical applications of ECCD, it is important to assess the sensitivity of the plasma discharge to beam alignment and to temporary cuts in the delivered microwave power. A new study has started to answer these questions, using non-inductive discharges in which one cluster of X2 gyrotrons is replaced by a second symmetrical one, with either a time delay or a shift in the deposition location. The time delay part of the study has been completed and the discharge survived EC power cuts up to 70ms, but not longer. This time corresponds to approximately 25% of the natural plasma current decay time in the Ohmic phase.

Experimental measurements of suprathermal electron dynamics

A perturbation technique has been developed to investigate the dynamics of suprathermal electrons without significantly affecting the properties of the plasma bulk. Short, localised, periodic ECCD pulses with low duty cycle are applied to the plasma with one or two 450kW sources (with identical aiming). The response of electron cyclotron emission (ECE) on the high field side (HFS) is analysed by coherent averaging throughout the steady-state phase of the discharge, comprising up to 200 ECCD pulses. The pulse length of 0.25ms was empirically adjusted to be well below the time for quasi-linear saturation and to permit observation of the spatial propagation of the pulse after turn-off. The suprathermal origin of the signal is confirmed by direct comparison with the signal detected by a new 65-100GHz radiometer placed symmetrically on the low field side (LFS). The two are in excellent agreement before the pulse, whereas the HFS radiative temperature increase during the pulse is over 5 times larger than its LFS counterpart at all locations.

To characterise the suprathermal population, we assume a bi-Maxwellian energy distribution. The characteristic temperature of the suprathermal component can be estimated from the relativistic downshift of the radiation, as well as by equating the pulse decay time with the collisional slowing-down time. The suprathermal density can then be derived from the measured radiative temperature.

A simple measure of the radial propagation of the pulse is the time to peak, which is plotted in Fig. 2.1.7 for four different centrally heated pulses with the ECE observation chord located at different distances from the magnetic axis. The overlapping data are in satisfactory agreement, with most of the scatter attributed to density variations. The ray tracing code TORAY-GA places the EC deposition in

the region ρ=0-0.2, which is confirmed by the measurements to be a region of zero delay, within the ECE time resolution of 0.05ms.

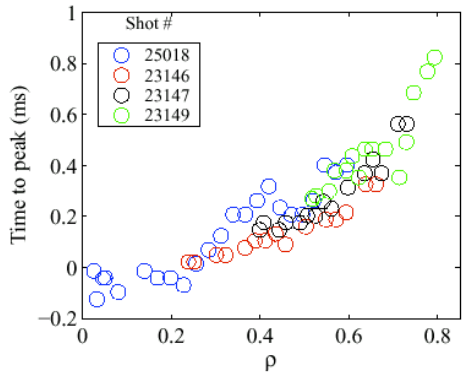

Fig. 2.1.7 *Time lag from the end of a central ECCD pulse to the ECE peak, as a function of the deposition location, normalised to the minor radius, ρ, calculated by taking into account the estimated relativistic downshift, for four different pulses (I_p=230kA, n_e=1.5-2.1×10^{19}m^{-3}, T_e=1.5keV, κ=1.6, power =0.45-0.9MW)*

The transfer function of the system is determined using a system identification method. A calculation based on two or three common poles for all ECE channels yields optimal results. No further improvement in the fitting is obtained using more than three poles. Results for two discharges are shown in Fig. 2.1.8. The eigenmodes are normalised such that their sum (also shown) represents an estimate of the source function. The two cases are identical except for the addition of 0.45MW continuous central pre-heating in Fig. 2.1.8(b), which increases the suprathermal temperature from 11 to 20keV. In the latter discharge the source function is seen to be anomalously broad. Work is currently in progress to apply this analysis method to more pulses.

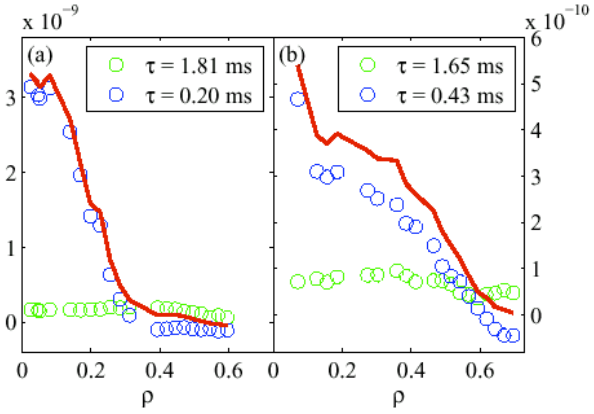

Fig. 2.1.8 *Two-pole eigenmodes (circles) of the system transfer function (EC power to suprathermal density) and corresponding source functions (solid lines), for (a) #25018, (b) #25032 (similar except for 0.45MW central EC power, T_b~2keV). The time constant is given for each eigenmode.*

Modelling of suprathermal electron diffusion

The Fokker-Planck quasi-linear code CQL3D is our main tool for modelling current drive and suprathermal electron dynamics. In our simulations the radial electron diffusion coefficient is adjusted to reproduce the global current drive efficiency measured in the experiment, which is intermediate between the linear (low power) value and the quasi-linear value in the absence of transport. The code also calculates the bremsstrahlung radiation incident on the TCV multi-channel hard X-ray (HXR) camera. The spectrum of the calculated and measured radiation are

generally in good agreement, although discrepancies of up to an order of magnitude are observed in both the intensity and in its spatial variation.

The diffusion coefficient can have an arbitrary dependence on the radial position and on the parallel velocity. We have studied the sensitivity of the simulation to these functional dependences for a conventional L-mode discharge fully sustained by ECCD. A uniform diffusivity profile was compared with a monotonically increasing profile, and the case of no velocity dependence was compared with that of the linear dependence that might arise from magnetic turbulence. The spatial profile is taken to be representative of L-mode, $D \propto [1+(3\rho)^2]/n_e$. The results are only weakly affected by these dependences, provided the value of the diffusivity is similar in the relatively narrow regions in the physical and velocity spaces in which most of the wave-particle interaction takes place. Therefore this method is incapable of leading to a definite conclusion on the underlying nature of suprathermal transport in these types of discharges.

Electron internal transport barriers (eITBs) are formed in fully non-inductive discharges by sustaining the current with off-axis co-ECCD and applying further heating or moderate counter-ECCD in the centre (Section 2.1.4). The synergy with the bootstrap current generated in the steep pressure gradient region results in high confinement with up to 80% bootstrap fraction. These discharges pose an additional challenge to electron distribution modelling, since thermal energy transport is strongly suppressed in the barrier region while suprathermal electron transport must still be sufficiently large to be compatible with the measured total driven current. In this case the assumption of a uniform and velocity-independent diffusivity profile would result in a smooth electron pressure profile that is incompatible with the transport barrier observed in the experiment (Fig. 2.1.9).

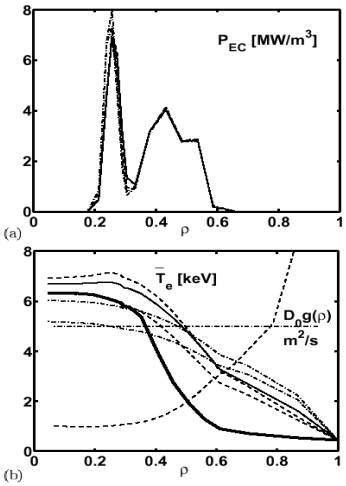

Fig. 2.1.9 *(a) Power deposition profiles calculated with three diffusion models: flat g(ρ) with D_0=3-5m^2/s (dash-dotted lines); L-mode g(ρ) with D_0=0.4-1m^2/s (dashed lines); g(ρ) with D=0.5m^2/s below 25keV and 5m^2/s above; (b) Average energy profiles for the three cases and maximum values of D for the first two cases; the thick solid line represents the Thomson scattering temperature.*

An adhoc energy dependence was then introduced, with a stepwise diffusivity with different values below and above 25keV. The pressure profile is primarily sensitive to the low-energy diffusivity, whereas the total driven current is mostly dependent on the high-energy diffusivity. The best match to the experimental measurements is obtained with diffusivities of 0.5m^2/s and 5m^2/s, respectively. This model succeeds in generating a steeper electron pressure gradient at mid-radius, although the high gradient region is still not as narrow as measured, Fig. 2.1.9. Because most of the current is sustained by off-axis beams while the high confinement region is in the plasma centre, it can be expected that a monotonically increasing radial diffusivity profile may also reproduce the experimental results satisfactorily, without any energy dependence. Indeed, the L-mode-like spatial dependence described earlier yields a similar pressure profile to the uniform case with a stepwise energy dependence.

Influence of suprathermal electrons on Thomson scattering measurements

The signal analysis of the incoherent Thomson scattering at 25 radial points (analysed on TCV by a spectrometer with 3 to 4 wide-band filters) is generally performed assuming a Maxwellian electron distribution. Since the distribution cannot be Maxwellian in the presence of high power ECCD, the error in the Thomson scattering estimate of the electron temperature and energy needs to be assessed under these conditions. The signals measured by the spectrometer for selected spatial channels were simulated using the electron distribution function calculated by CQL3D, then processed similarly to the experimental ones. The electron energy determined this way is compared with the energy contained in the model distribution function. In Ohmic plasmas as well as in plasmas heated with ECH with no current drive (perpendicular injection), the deviation from a Maxwellian is negligible, and a maximum 5% discrepancy is found between the energies calculated with different filter ratios, which lies within the typical experimental uncertainty. The stronger suprathermal component generated by ECCD leads to a larger scatter. The simulated signal ratios are in good agreement with the experimental values for the same discharge In this case the Maxwellian assumption leads to a 20-30% underestimation of the total electron energy.

Suprathermal ion studies

Charge-exchange spectra measured by a neutral particle analyser (NPA) reveal the presence of a suprathermal ion tail during ECH and, more strongly, ECCD. The NPA views the plasma centre along a vertical chord. Spectral analysis is performed by electrostatic discrimination into five energy bins, with the voltage swept to measure neutral particle energies in the energy range 0.6-6.5keV, with a time resolution of 13ms. During X2 power injection, two distinct ion populations are clearly observed, a thermal bulk (~500eV) and a suprathermal component with an effective temperature up to 2.5keV (Fig. 2.1.10). The measured neutral flux indicates that the density of suprathermal ions is up to 10% of the thermal ion density and the energy content of suprathermal ions is up to 50% of the bulk ion energy.

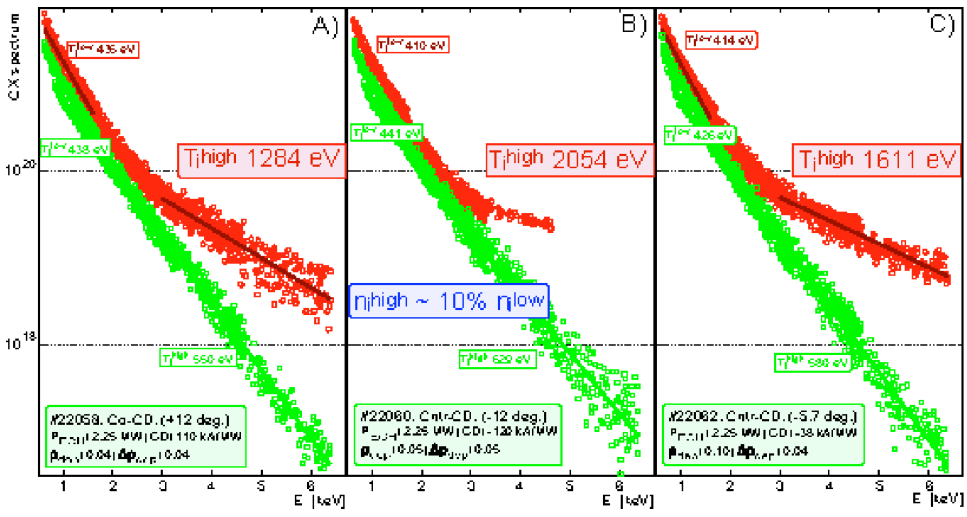

Fig. 2.1.10 *NPA charge exchange spectra for X2 on and off phases, with 2.25MW power: A) co-ECCD, toroidal angle +12°; B) counter-ECCD, angle -12°; C) counter-ECCD, angle -5.7°.*

This suprathermal feature has been studied systematically in one set of discharges with central X2 deposition and varying X2 toroidal injection angle and in a second set with varying deposition location and constant injection angle. The angle scan shows that the suprathermal feature is stronger with ECCD than with pure ECH, and is more prominent with counter- than with co-ECCD. The suprathermal ion temperature is well correlated with the bulk electron temperature. The density and temperature of the ion tail also increase with EC power. The radial deposition scan shows that the hot ion feature is not observed when the deposition location is placed outside the sawtooth inversion radius. A dependence on plasma shape is also observed: the suprathermal ion temperature decreases with plasma elongation and increases with plasma triangularity; both dependences are opposite to those of bulk ions and carbon impurities.

The formation of the hot ion tail occurs within 10ms of X2 switch-on (shown in Fig. 2.1.11). Although the time evolution cannot be determined more precisely due to the limited time resolution of the measurement (~13ms), this response time is considerably shorter than the Coulomb thermal electron-ion equilibration time (typically 30-150ms). The variation of the bulk ion temperature, by contrast, is in good agreement with a classical model based on thermal equilibration of multi-component plasmas. This temporal dynamics rules out a collisional mechanism for the ion tail creation by the thermal or fast electrons and points instead to anomalous electron-wave-ion energy exchange, also suggested by the observed correlation with the electron temperature.

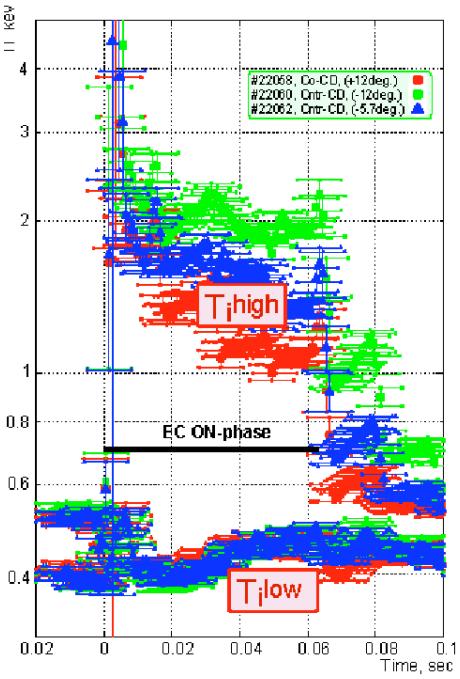

Fig. 2.1.11 *Time histories of the temperatures of the high and low energy components of the ion distribution, after X2 switch-on, for three values of the toroidal injection angle*

Third and fourth harmonic electron cyclotron wave absorption: Comparison of fully and weakly relativistic cyclotron damping

The physics of ECH and ECCD includes relativistic effects. In view of the strong suprathermal features of the electron distribution function in TCV under high power ECCD, we have developed a numerical, fully relativistic dispersion relation solver and compared its results with those obtained with the weakly relativistic approximation. It was found that the latter, although adequate in many cases, can be significantly inaccurate when multiple microwave frequencies, multiple harmonics and non-Maxwellian features are at play. An important result is that when there is a significant high-energy electron component, the wave is subject to significant damping before reaching the desired harmonic layer, due to the

relativistically downshifted next higher harmonic. These calculations have been performed by assuming a bi-Maxwellian distribution, an approximation that is qualitatively supported by CQL3D results.

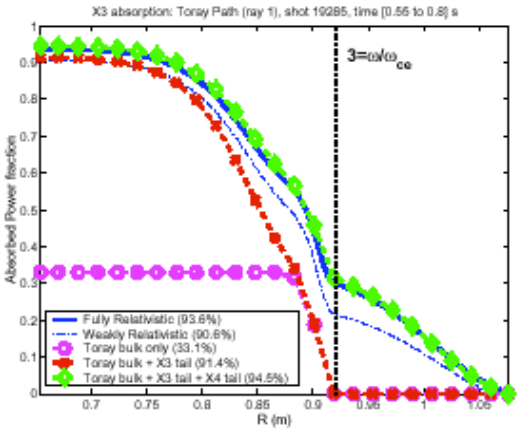

Fig. 2.1.12 *X3 power absorption as a function of major radius for a beam entering from the low-field side. The solid line is from the fully relativistic calculation, the thin dot-dashed line is from the weakly relativistic calculation, and the symbols are from multiple TORAY-GA runs.*

Figure 2.1.12 shows the case of a suprathermal component that accounts for 20% of the total density and is characterised by a 25keV temperature (flat temperature profile), for LFS X3 heating. Nearly 30% of the power is absorbed on the downshifted 4th harmonic resonance (at 118GHz) before reaching the 3rd harmonic. It is found that a linear superposition of multiple separate calculations with TORAY-GA (a cold plasma ray-tracing code with fully relativistic damping calculations) for the different harmonics and Maxwellian components is in agreement with the full solution of the dispersion relation.

Top launched third harmonic extraordinary mode as a suprathermal electron diagnostic

Strong coupling of third harmonic radiation launched from the top of the vessel with suprathermal electrons, resulting in enhanced absorption, was observed in previous experiments. This suggests the use of top-launched X3 as a way of creating a particular suprathermal electron energy class, for example for diagnostic purposes. When the injection is exactly vertical, the radial separation between the X3 launcher and the cold resonance, ΔR, is directly linked to the energy of the coupled electrons through the relativistic downshift of the cyclotron frequency. Preliminary experiments have been performed in which the radial position of the X3 mirror, was scanned from shot to shot. The suprathermal population was generated by 1MW X2 co-ECCD and was monitored by the HFS ECE radiometer.

With R=0.87m, as shown in Figure 2.1.13(a), the ray tracing code TORAY-GA, assuming a Maxwellian distribution function, predicts no X3 absorption. On the other hand, about 25% absorption is experimentally measured by a diamagnetic loop (DML) during modulated ECH. The anomalous X3 power absorption is attributed to a suprathermal population with a characteristic temperature 26±12keV, corresponding to the resonant energy at this spatial location. At R=0.89m, both TORAY-GA and the DML measurement give 45% absorption, consistent with coupling with the thermal bulk. Future experiments are planned to explore this selective coupling more systematically.

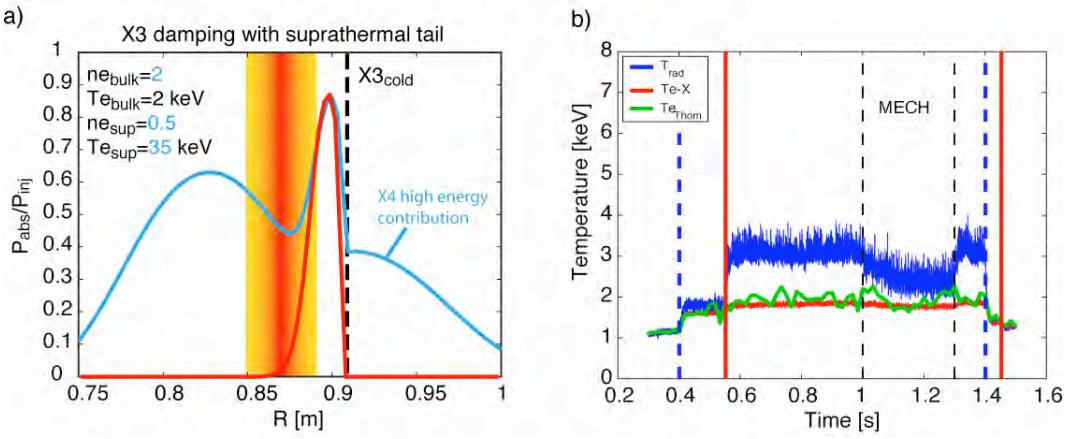

Fig. 2.1.13 *a) X3 absorption as a function of the radial position of the single ray vertical path, calculated with a weakly relativistic code assuming a bi-Maxwellian model (blue curve) or a simple Maxwellian (red). The beam path is schematically drawn for R=0.87m whereas the cold resonance is at R=0.91m; b) Bulk temperature (measured by Thomson scattering and soft X-ray emission) and HFS ECE radiative temperature during the X2 co-ECCD phase and during the X3+X2 phase.*

Feedback control of the third harmonic extraordinary mode launcher

Previous experiments using X3 top-launch have shown the strong dependence of the X3 absorption on the poloidal injection angle. Therefore feedback control on the X3 launcher is required in order to maintain the maximum absorption with time-varying plasma parameters. The feedback control, based on a synchronous demodulation method using a PID controller, has been constructed and is now able to generate in real time an angle error signal shown in Fig. 2.1.14e). In order to improve the signal to noise ratio, a narrow band-pass filter will be implemented. The feedback loop will be tested in the 2004 experimental campaign.

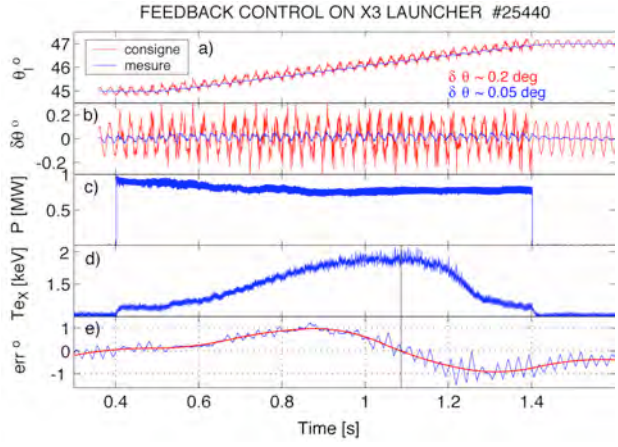

Fig. 2.1.14 *The launcher angle is swept from 45° to 47° with a 0.2° sinusoidal modulation at 40 Hz a) & b). The sweep range passes through the maximum absorption as observed on the temperature measured with soft X-ray emission d). The error signal is zero at the maximum absorption e).*

Modelling of laterally launched third harmonic extraordinary mode with second harmonic extraordinary mode pre-heating

The initial X3 experiments were performed using a lateral launcher injecting waves perpendicular to the magnetic field. In the presence of X2 ECCD, anomalously high X3 absorption up to 100% was measured while the absorption predicted by linear calculations never exceeded 45%. This discrepancy was attributed to the suprathermal population generated by X2 ECCD. Recently, CQL3D simulations have been carried out to test this hypothesis. A maximum absorption of 70% was observed, but these simulations are not yet conclusive, as they do not fully converge due to an insufficient mesh size.

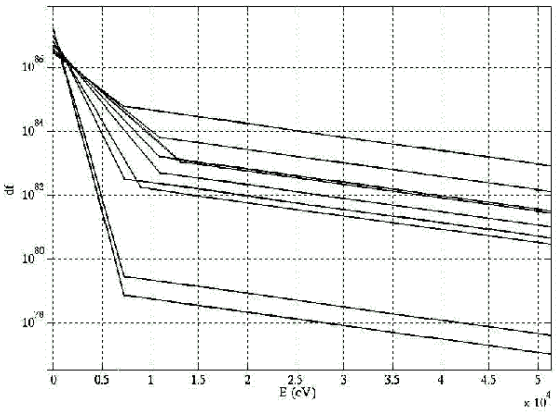

Fig. 2.1.15 *Model electron distribution function at different spatial locations, as a function of energy, in logarithmic scale.*

Simpler modelling was employed recently, starting from an *ad hoc* electron distribution function, and proceeding through a weakly or fully relativistic wave absorption calculation and simulations of the HFS ECE and Thomson scattering measurements. The process is iterated until a satisfactory match with all the available information is reached. Better results are obtained with a two-slope distribution function, featuring a sharp transition between the two energy regions at approximately 7 to 13keV (depending on the spatial location, Fig. 2.1.15), than with a bi-Maxwellian with a continuous first derivative. Total absorption of perpendicular X3 radiation was successfully reproduced with a suprathermal density locally equal to approximately 20% of the bulk density, but concentrated in a relatively narrow central region. The calculated HFS ECE (Fig. 2.1.16) and Thomson scattering signals are in good agreement with experimental data, and the postulated suprathermal density profile is qualitatively consistent with the HXR emissivity profile.

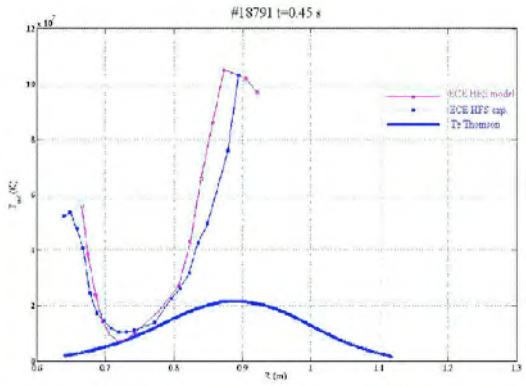

Fig. 2.1.16 *Comparison of measured HFS ECE radiative temperature (blue) with the simulated temperature (magenta) from the model distribution function of the previous figure. The Thomson scattering temperature profile is also shown for comparison (thick blue line).*

2.1.4 Enhanced confinement regimes

Progress has been made in increasing the confinement enhancement factor of electron internal transport barriers (eITB) in plasma discharges both driven non-inductively ($eITB_{NI}$) or with a finite inductive current component ($eITB_{OH}$), in steady-state conditions. The confinement enhancement over the TCV L-mode energy confinement time, which is well described by the Rebut-Lallia-Watkins scaling, has reached H_{RLW}=5.

Characterisation of electron internal transport barrier properties

All scenarios with electron internal transport barriers (eITB) on TCV are believed to be associated with a reversed magnetic shear. Thus, the confinement enhancement and the barrier properties both in the non-inductive and in the inductive regime should be characterised by quantities related to the current profile. We have employed in particular a definition of shear reversal given by the depth of the hollow current profile, or $\Lambda - j_0/j_{max}$. Similarly, the volume enclosed by the barrier is equivalent to that contained inside the location of j_{max}. However, the current density profile is not measured directly in TCV, rather it is inferred from the sum of j_{CD}, calculated from CQL3D, and j_{BS}, bootstrap current calculated from the pressure profile measured by Thomson scattering. In the presence of an inductively driven current component, this technique suffers from large uncertainties in the current profile, originating from experimental uncertainties in T_e and Z_{eff}. Thus, in order to compare inductive and non-inductive cases we adopt a more direct definition of barrier strength, given by ρ^*_{max}, the maximum value of the parameter $\rho^*_T = \rho_s/L_T$. Here ρ_s is the ion sound gyroradius and L_T the electron temperature gradient scale length (Fig. 2.1.17). This parameter is proportional to $grad(T_e)/T_e^{0.5}$. The volume of the enhanced confinement region can then be obtained directly from the location of this maximum. Experimentally, a strong correlation was established between the two alternative heuristic definitions of barrier strength in non-inductive eITB discharges.

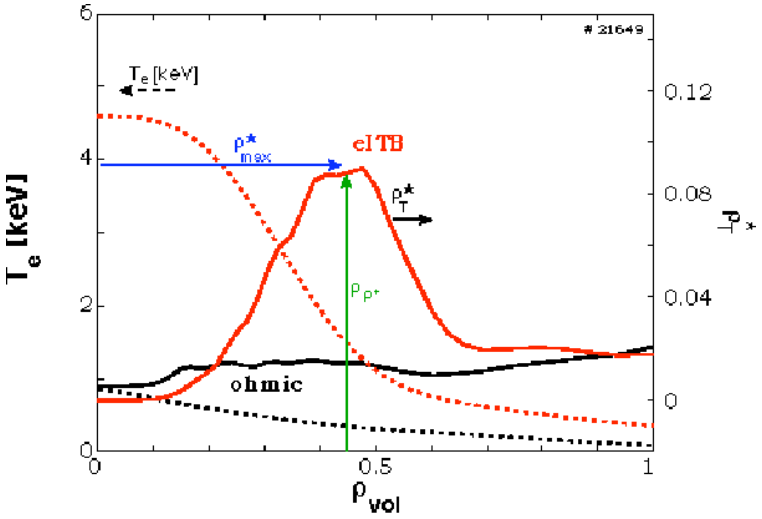

Fig. 2.1.17 *The averaged T_e (dashed) and ρ^*_T (solid) profiles for the ohmic (black) and eITB (red) phases with the barrier strength (ρ^*_{max}) and volume (ρ_{ρ^*}) defined.*

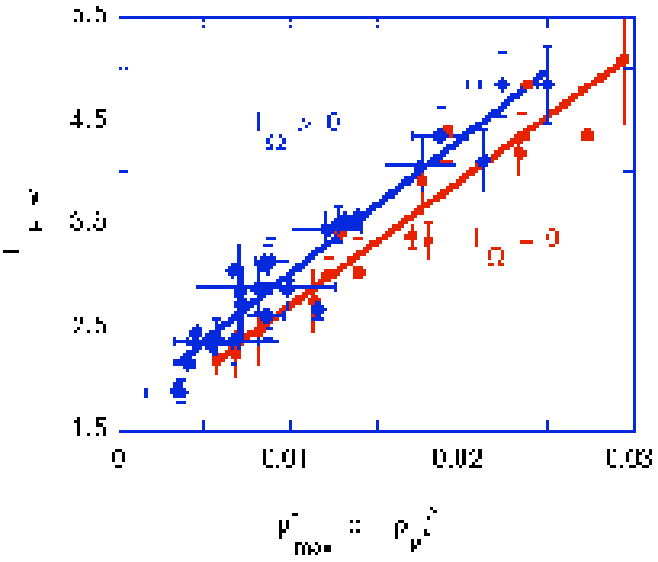

Fig. 2.1.18 *A confinement enhancement figure of merit for the $eITB_{OH}$ (blue) and $eITB_{NI}$ (red) is the product of the barrier strength and volume*

The observed linear dependence of H_{RLW} on the product of the barrier's volume and strength (Figure 2.1.18) led to the choice of the latter as a general figure of merit for the potential confinement enhancement in TCV. The $eITB_{OH}$ (blue points) seems to have slightly improved confinement over the $eITB_{NI}$ (red points), which may be attributed to an increased ratio of power deposited inside and outside the high confinement region (up to 3.0, vs. 0.5 in $eITB_{NI}$). In both the $eITB_{OH}$ and $eITB_{NI}$ enhancement factors up to 5 have been achieved in steady state with bootstrap current fractions of up to 80%. In the following, the subscript 0 refers to ECH power deposited in the centre, whereas the subscript *co* refers to the off-axis co-ECCD beams.

Inductively driven electron Internal Transport Barrier discharges

Previously, the $eITB_{OH}$ volume was limited to a very small central region of the plasma, and the deposition location of both central counter-ECCD and off-axis ECH had to be accurately controlled to avoid peaking of the T_e and P_e profiles leading to terminal MHD modes. The barrier volume has now been increased with an improved balance of power in the off-axis heating and central counter-ECCD. This is seen from the wider T_e and ρ^*_T profiles in Fig. 2.1.19, and results in an increase of H_{RLW} from ~2.9 to 4.4 in steady-state conditions.

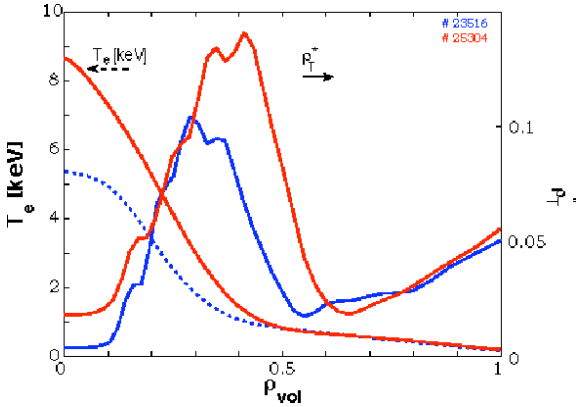

Fig. 2.1.19 *The averaged T_e (dashed) and ρ^*_T (solid) profiles which show a noticeable increase in barrier strength and volume from an earlier $eITB_{OH}$ (blue) and more recent, optimised $eITB_{OH}$ (red)*

In this scenario, the barrier position can be controlled by varying the plasma current and/or the power deposited in the plasma centre. Results from experiments at two values of I_p are shown in Fig. 2.1.20. In both cases the central power is ramped up slowly to reach its maximumof 1MW, at 1.5s. The radius of the $eITB_{OH}$ expands during the power ramp. By reducing I_p from 200 to 120kA for the same heating conditions, the eITB location moves from $\rho \approx 0.2$ to 0.3, widening the high confinement region.

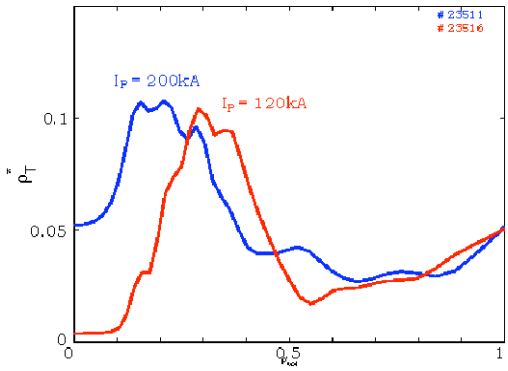

Fig. 2.1.20 *Comparison of two cases at I_p=200kA (blue curve) & 120kA (red curve) and identical parameters for ECH and ECCD, the barrier volume increases with decreasing plasma current*

Experiments with higher κ have been undertaken to avoid peaking of the central current density and shrinking of the $eITB_{OH}$ volume as I_p is increased. The effect of simultaneous variations of I_p and ρ^* is illustrated in Fig. 2.1.21. Since the additional inductive current component has to be compensated to maintain a hollow current profile, the counter-ECCD power is increased at the same time as I_p. The sequence of temperature profiles shows a clear broadening of the eITB radius during the I_p ramp-up phase. Figure 2.1.22 confirms that, in spite of the increase in additional power, the confinement time and the value of H_{RLW} keep rising. So far, these record values with H_{RLW}>5 could only be achieved during a transient phase terminated by MHD activity. Future experiments will have to show whether or not optimisation of the counter-ECCD power density in the centre can keep the pressure gradient below criticality and achieve steady-state conditions.

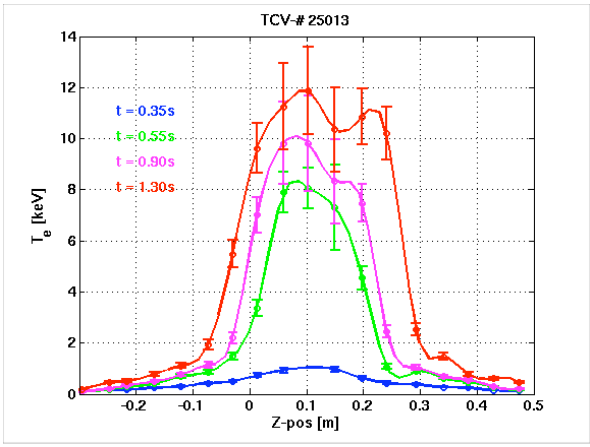

Fig. 2.1.21 *T_e profiles from Thomson scattering for #25013 for simultaneous increase of Ip, kappa and central ECCD power. Time steps: 0.3s ohmic phase (blue), 0.55s formation of ITB (green), 0.8s (magenta) & 1.3s (red) expansion of ITB during ramp phase.*

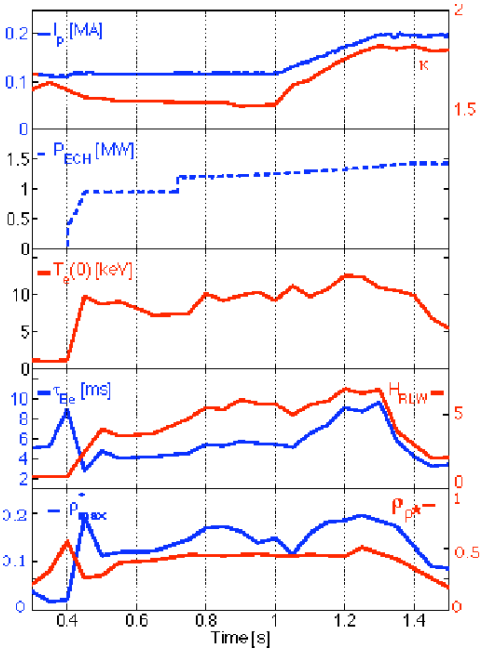

Fig. 2.1.22 *Evolution of plasma parameters, ITB_{OH} position and global confinement quantities during #25013. During the ramp phase the volume expands and τ_{eE} increases in spite of the additional power input. High performance phase with H_{RLW}~5.5 and T_{e0}>10keV terminated by mode activity after t=1.3s.*

Non-inductive electron Internal Transport Barrier discharges

Scans of the toroidal injection angle of the centrally deposited beams, ϕ_0, and of the off-axis deposition radius, ρ_{co}, on a shot-to-shot basis (with P_0=0.5MW and P_{co}=0.9MW) have led to potential independent control of the $eITB_{NL}$ barrier strength and volume.

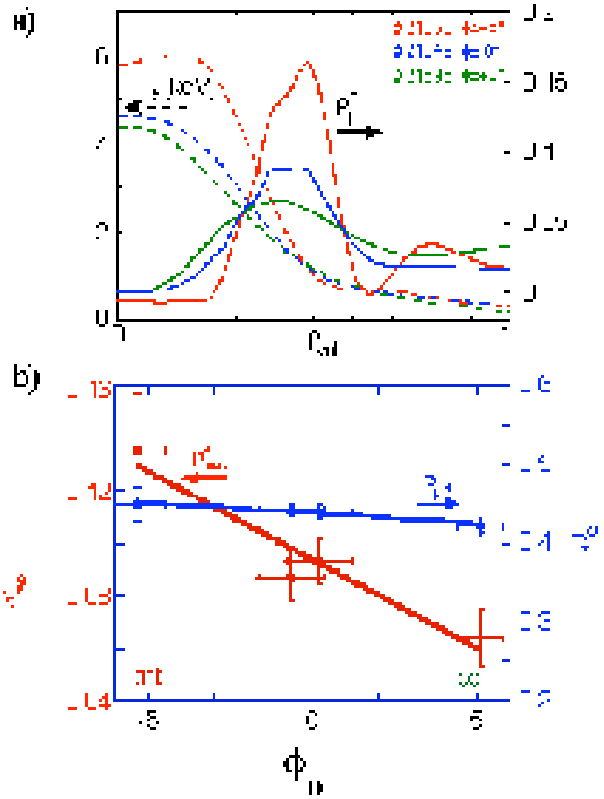

Fig. 2.1.23 *The $eITB_{NI}$ performance during a scan of the toroidal injection angle, ϕ_0, as observed on (a) the T_e (dashed) and ρ^*_T (solid) profiles and (b) the barrier strength and volume*

As ϕ_0 approaches the values used for counter-ECCD (Fig. 2.1.23), a noticeable increase in T_e (dashed) and ρ^*_T (solid) is observed, while the volume enclosed by the barrier remains nearly constant. The injection of counter-ECCD on-axis provides a negative current source in the plasma centre, which increases the hollowness of the current profile, which in turn is presumed to strengthen the eITB. Thus φ_0 offers external control of the barrier strength while maintaining a nearly constant volume. Similarly, a scan of ρ_{co} from ~0 to 0.45 was performed while keeping $\varphi_0 \sim 0^0$. As shown in Fig. 2.1.24, the T_e and ρ^*_T profiles increase in amplitude and broaden as ρ_{co}increases. Thus ρ_{co}affects both the barrier strength and volume. In conclusion, the externally selected parameters ρ_{co} and φ_0 offer separate control of the barrier volume and strength.

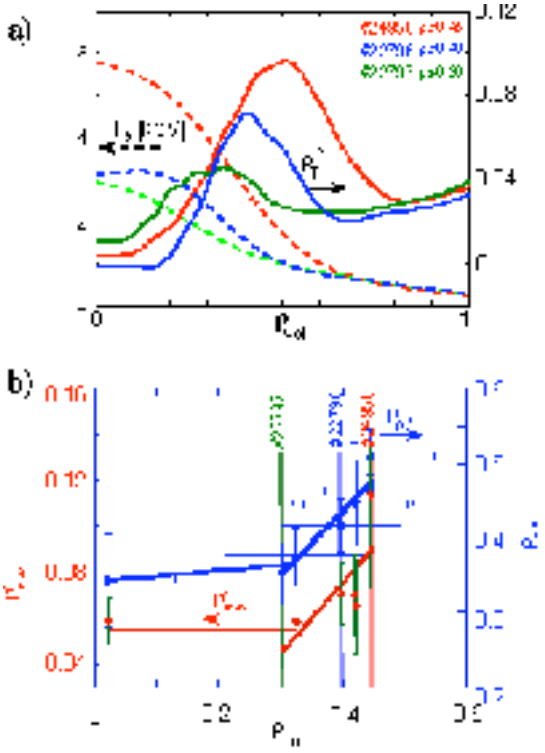

Fig. 2.1.24 *The $eITB_{NI}$ performance during a scan of the radial position, ρ_{co}, as observed on (a) the T_e (dashed) and ρ^*_T (solid) profile; and (b) the barrier strength and volume*

Inductive perturbation of non-inductive electron Internal Transport Barriers

In $eITB_{NI}$ discharges, the inductive current is removed by holding the transformer coil current constant, $dI_{OH}/dt=0$, resulting in zero loop voltage. The influence of the inductive current on the eITB was investigated by introducing a pre-programmed ramp of I_{OH} after the formation of the barrier. Since $j_\Omega \propto T_e^{3/2}$, the majority of the inductive current is driven within the barrier, partially filling in and narrowing the hollow j_p profile. The barrier strength and volume decrease, resulting in degradation of the confinement, as demonstrated in Fig. 2.1.25. Conversely, central counter-ECCD removes this degradation, causing the depth and volume of the hollow current profile to increase again (Fig. 2.1.26). These results confirm the crucial role played by the current profile in the advanced plasma scenarios with internal transport barriers.

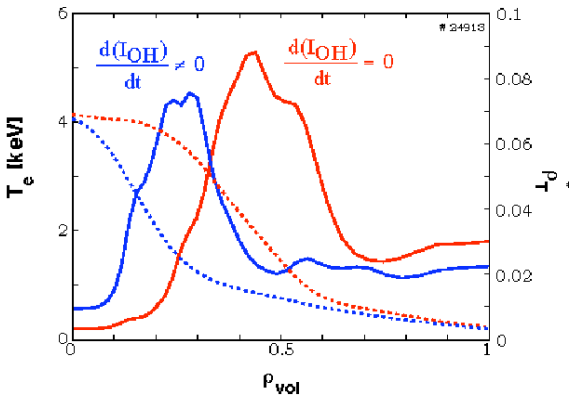

Fig. 2.1.25 *The T_e (dashed) and ρ^*_T (solid) profiles during a non-inductively driven phase of an $eITB_{NI}$ (red) and in the same discharge a pre-programmed inductive current contribution (blue)*

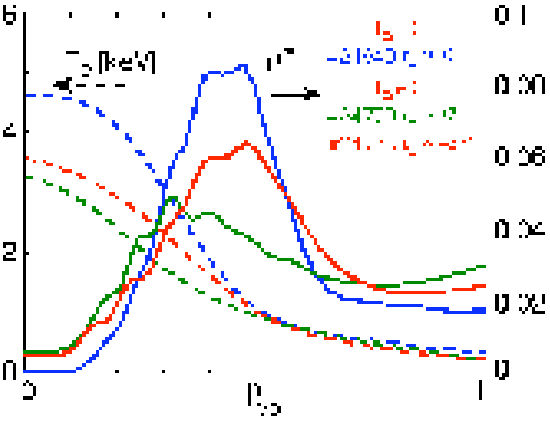

Fig. 2.1.26 *The T_e (dashed) and ρ^*_T (solid) profiles of three similar discharges, #21649 is a standard $eITB_{NI}$ with central heating (blue), which is repeated in #24770 but with an ohmic current contribution (green). The inductive current can be partially negated by replacing the central ECH with counter-ECCD nearly re-establishing the eITB strength and volume of #21649*

β-limiting activity in reversed shear scenarios

Different MHD modes can limit the achievable β in TCV advanced scenarios. During the so-called Improved Core Electron Energy Confinement (ICEC) mode with low to moderate reversed shear, a 2/1 Neo-classical Tearing Mode (NTM) located close to maximum pressure gradient is observed to degrade the confinement. Sporadic soft X-ray crashes are associated with this mode, and the crashes become periodic (τ~20ms) with sawtooth-like shape when the resonant q=2 surface is shifted inward, typically at ρ~0.5-0.6. In this case 2/1 oscillations appear on the soft X-ray crashes, similar to those observed on ASDEX-Upgrade in a reversed shear scenario. In contrast to the case of flat pressure profiles, a low value of the internal inductance l_i seems to have a beneficial effect in reducing MHD activity in the presence of internal electron transport barriers.

In discharges with low plasma current (~120kA) fast relaxations flatten the soft X-ray profile over a large fraction of the minor radius. These are preceded by a mode that grows on a very fast time scale, τ<20μs, suggesting an ideal instability. The post-cursor oscillations have a n=1, m=3 structure and are strongly localised poloidally on the low field side. This mode is de-stabilised when the plasma is close to the ideal β-limit. In the fully non-inductive reversed shear scenario, similar MHD activity has been recently recognised as n=1 global ideal kink instability through comparisons with the ideal code KINX.

2.1.5 Underlying tokamak physics on TCV

Magnetic triggering of Edge Localised Modes

Fast voltage perturbations applied to the radial field control coils on TCV have been used to modify the ELM frequency during single null ELMy H-mode discharges. The input signal for the perturbation was added to the vertical stabilisation feedback loop, consisting of a series of square pulses, which produced spike like pulse trains in the radial field coil current. These spikes cause rapid deviations in the plasma vertical position. The ELM cycle and the external perturbation become locked in phase, and the ELM frequency f_{elm} follows the variations in the external driver frequency f_D over a frequency range that increased with the amplitude of the perturbation. Figure 2.1.27 shows a discharge in which three bursts of perturbations at 200Hz are injected during an ELMy H-mode phase. With the exception of a short ELM-free phase starting at 0.57s, f_{elm} clearly tracks f_D most of the time during each burst, and its value doubles compared with the value between bursts. Intermittent interruptions in the phase lock have been observed during perturbation bursts. DINA code simulations confirm that the effect of our perturbation is to modulate the edge current, thereby acting to either delay or precipitate ELM events.

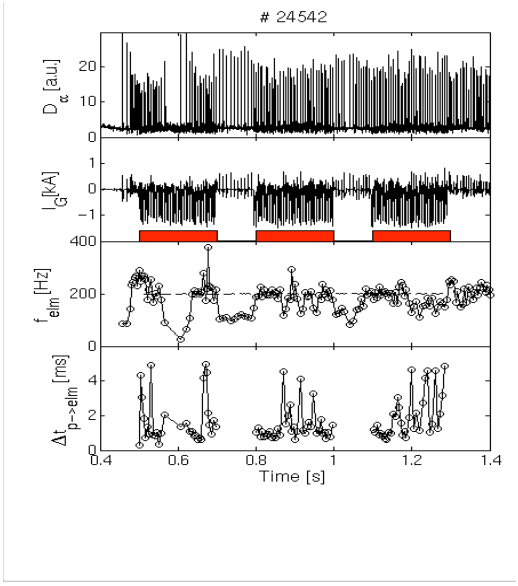

Fig. 2.1.27 *(a) D_a emission showing ELMs; (b) Current in the internal radial field coil, red bars indicate bursts; (c)f_{elm} (circles) and f_D (dashed line); (d) Time delay from the perturbation to the next ELM.*

Over most conditions these interruptions cause a momentary shift in f_{elm} towards its unperturbed value. Over most conditions, in ELMy H-modes on TCV, the ELM and the sawtooth cycles are dynamically coupled, with f_{elm} corresponding to the fundamental sawtooth frequency f_{st} or one of its harmonics. This coupling between ELMs and sawteeth is also apparent in externally driven discharges. In Fig. 2.1.28 a detail of discharge #24542 shows f_{elm}, f_{st}, $2f_{st}$ and f_D before and during the second perturbation burst. Before the burst, f_{elm} is clearly locked to f_{st}. The driver frequency roughly coincides with $2f_{st}$ between 0.8 and 0.85s, and synchronisation of ELMs with the driver is found over this period. After about 0.85s, $2f_{st}$ slowly drifts away from f_D, and three interruptions in the frequency entrainment occur. The mutual coupling between the external driver, the ELMs and sawteeth may be illustrated by considering the ELM phase in the driver cycle and sawtooth cycle (ϕ_D and ϕ_{st} respectively). These results are interesting from the point of view of understanding ELMs and of possibly affecting them. Work is underway on the question of extrapolating the results to larger tokamaks.

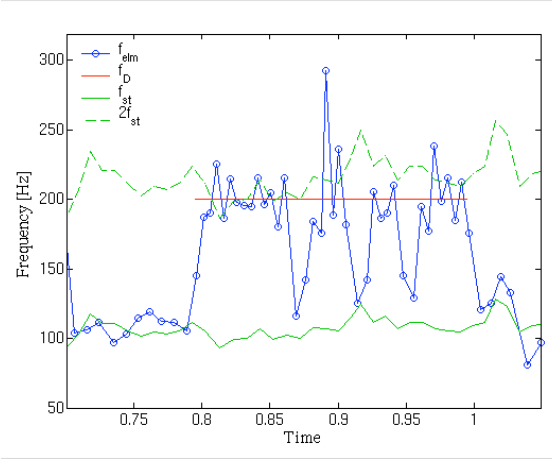

Fig. 2.1.28 *Detail of #24542 showing f_{elm}, f_D, f_{st} and $2f_{st}$.*

Figure 2.1.29 presents a contour plot of the number of ELMs per bin in ϕ_D and ϕ_{st} (using 30 bins from 0 to 2π in each case), for a set of 24 discharges in which a positive top hat perturbation was used with various driver frequencies. A vertical feature is clearly visible for $\phi_D/2\pi \sim 0.2$, which corresponds to the occurrence of ELMs in response to the increase in edge current provided by the perturbation. In these discharges, f_D was generally closer to $2f_{st}$ than f_{st}. The splitting of this vertical feature into two peaks reflects partial synchronisation with $2f_{st}$ during periods when the ELMs were also synchronised with the driver.

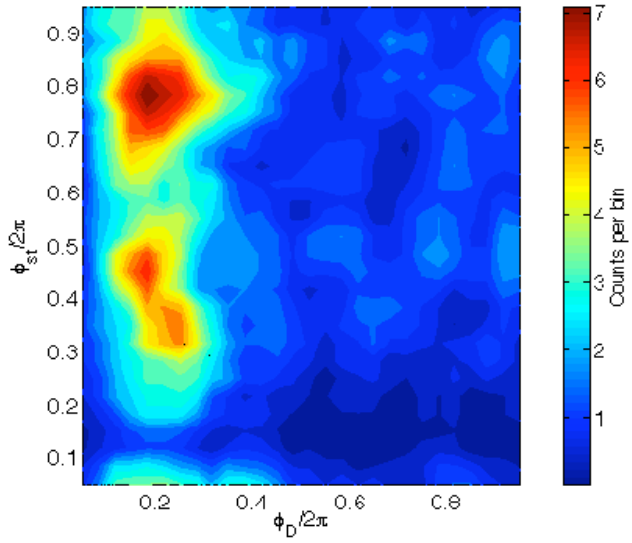

Fig. 2.1.29 *Contour plot of the number of ELMs per bin in ϕ_D and ϕ_{st}. 30 bins are used in both cases, and a 3x3 box-car smoothing kernel is applied.*

Observation and modelling of the anomalous particle pinch

Moderately peaked electron density profiles are observed in virtually all plasma conditions in TCV. The behaviour of the density profiles from a database of 300 Ohmic L- and H-mode, as well as ECH and ECCD discharges, is compared with predictions of empirical models based on the Ware pinch, the anomalous curvature pinch (or turbulent equipartition) and anomalous thermo-diffusion. The database covers a wide range of plasma conditions: $1<\kappa_a<2.6$, $0.5<\delta_a<0.7$, $2<q_{95}<7$, $1.2\times10^{19}m^{-3}<n_e<12\times10^{19}m^{-3}$, $0.02<\nu^*_{75}<10$, $0.8>T_i/T_e>0.1$, where κ_a and δ_a refer to the LCFS and ν^*_{75} is the normalised electron collisionality at 75% of the poloidal flux. The edge particle source was modelled using the KN1D code provided by PSFC, MIT. It shows that the particle source is insignificant in the bulk of the plasma and cannot explain the peaking of the density profile. The behaviour of stationary Ohmic plasmas, where the density profile width $\langle n_e\rangle/n_e(0)$ scales with that of the

current profile, $\langle j \rangle/(j_0 q_0) \sim 1/q_{95}$, and can be modelled by one of the three above convective processes. With high power ECH ($P_{ECH} >> P_{OH}$) the peaking of the density profiles is reduced, especially at low values of $\langle j \rangle/(j_0 q_0)$. This behaviour cannot be modelled if the Ware pinch is assumed to be the only convective mechanism. The existence of an anomalous pinch is in fact unambiguously demonstrated by the observation of peaked density profiles in stationary, fully relaxed, fully ECCD driven discharges. The best overall agreement throughout the database is obtained by combining an anomalous pinch mechanism, such as the curvature pinch, with the Ware pinch, shown in Fig. 2.1.30. Since most of the samples in the database have relaxed current profiles, a strong correlation exists between the temperature and current profile. This prevents us from singling out the anomalous pinch as either thermo-diffusion or the curvature pinch and calls for an extension of the database to include a wider variety of current driven discharges.

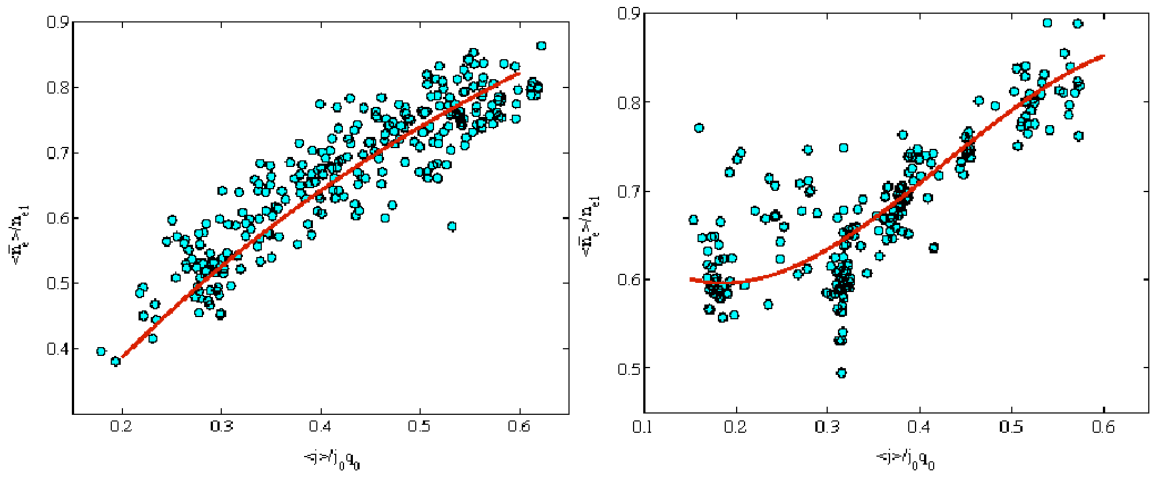

Fig. 2.1.30 *Density profile peaking factor $\langle n_e \rangle / n_e(0)$ versus $\langle j \rangle/(q_0 j_0)$ in Ohmic (left) and ECH (right) discharges. Data points: experiments. Lines: average predictions of a profile model, assuming a combination of Ware pinch and curvature pinch.*

Impurity transport including the effect of equilibrium shape

The TCV tokamak is equipped with a laser ablation system, exploited jointly with KFKI, Budapest. Extensive studies in previous years have shown that the confinement time of injected silicon impurities may exceed the electron energy confinement time in Ohmic plasmas by a factor of three, depending on discharge parameters, such as plasma elongation and current. In some low current cases, above a threshold density, the impurities are seen to accumulate in the plasma core, despite the presence of sawteeth. In 2003 systematic investigations of ECH and ECCD plasmas using laser ablation and short puffs of Argon have been undertaken. Although these experiments are still being analysed, some intriguing observations can already be made. Additional ECH power causes a reduction of the energy confinement time, consistently with the usual power scaling, but has little effect on the Silicon impurity confinement time, summarised in Fig. 2.1.31. Although both confinement times are about the same in ohmic plasmas (P_{ECRH}=0), the impurity confinement time decreases only by 20% when 1MW of ECH is added in L-mode, whilst the electron energy confinement time drops by a factor of 2. We link the effect to the delivered power, rather than to an EC wave particle interaction.

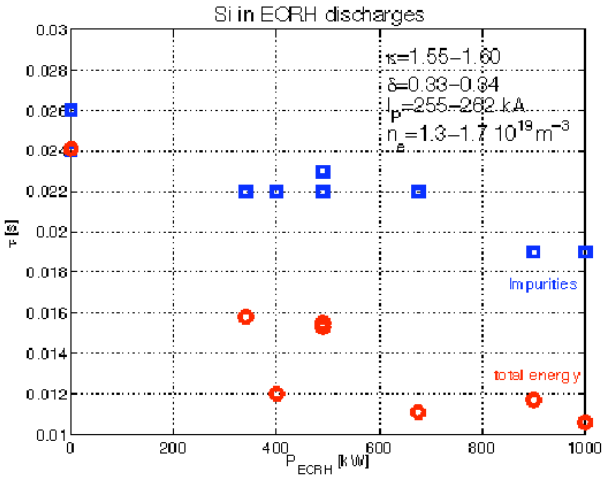

Fig. 2.1.31 *Effect of additional ECH power on electron energy (dots) and impurity confinement times from laser ablation (squares)*

Impurity transport coefficients can also be obtained from a measurement of the ionisation equilibrium, which departs from coronal when transport effects are significant. A proof-of-principle experiment has been conducted using the multi-layer ultra-soft X-ray spectrometer on TCV, operated jointly with IPP Prague. This measures the spatial distribution of hydrogen-like and helium-like intrinsic carbon impurities. Transport coefficients are clearly anomalous for carbon and silicon. We believe that simultaneous measurements of the transport coefficients for heat, electrons (overall density) and different impurities may shed light onto the underlying transport processes and provide constraints for the development and validation of transport models and theories.

Edge and divertor physics

Edge physics research on TCV during 2003 has continued with the development of two of the principle themes described in the previous report: the explanation, via code simulations and new experimental data, of the anomalous outer target detachment observed in ohmic, deuterium only fuelled discharges and the study of edge turbulence.

Divertor detachment at the outer target of L-mode deuterium discharges is regularly observed on TCV, even though measured divertor densities are much lower than those found in detaching plasmas on larger tokamaks. For some time, modelling efforts using the B2.5-Eirene (SOLPS5.0) code package have been underway in an attempt to elucidate the mechanism controlling this detachment. The degree of sophistication of these simulations has been increased in 2003 by upgrading to a new version of the Eirene neutrals code and by using a collisional radiative model for atomic and molecular ionisation, recombination and dissociation rate coefficients and an improved treatment of molecular vibrationally excited states. In addition a more realistic three dimensional representation of the toroidal geometry has been included.

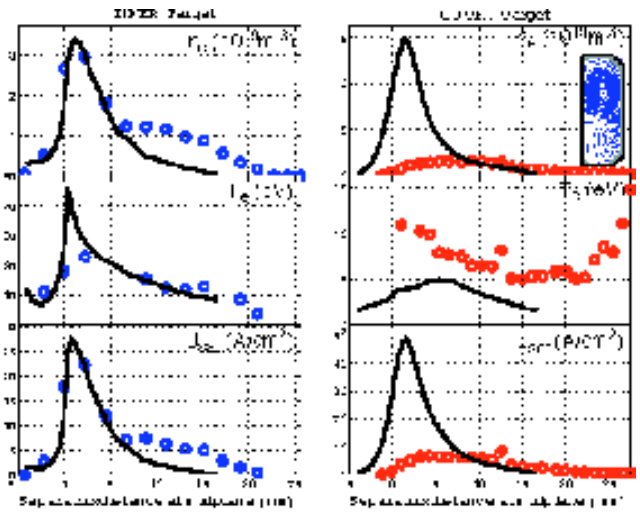

Fig. 2.1.32 *Comparison of experimental data (points, TCV pulse #17823) and SOLPS5.0 simulations (full lines) of TCV ohmic SNL divertor target ion flux, T_e and n_e profiles mapped to the outside mid-plane for a line average density, $\bar{n}_e$~6.0x10^{19}m^{-3} at the onset of the "anomalous" detachment at the outer target. Despite the inclusion of refinements in the Eirene neutral model, the outer target ion fluxes cannot yet be matched*

Figure 2.1.32 shows the latest simulation results compared with target profile data. New main chamber profile data from an edge Thomson scattering system have been used in constraining these most recent code predictions. Whilst agreement at the inner target is now excellent, the more refined code simulations still fail, by a considerable margin, to match the outer target ion fluxes, though the outer divertor T_e is now more closely approximated and the predicted ion flux (and hence density) is somewhat reduced compared with earlier results. It would thus appear that a strong role for D_2 molecules, long suspected (via molecular assisted recombination (MAR) processes) as being the most likely candidate to explain the detachment, has now been ruled out. Of those remaining, hydrocarbon driven MAR has the potential to drive significant recombination under the TCV divertor plasma conditions (TCV is an all-graphite machine). New simulations are underway, in which a number of hydrocarbon species have been included in the Eirene package. A possible strong role for edge plasma drifts is also under investigation using experimental detachment data obtained in a recent TCV campaign with negative toroidal field direction.

Following some very preliminary first measurements in late 2002, the database of edge turbulence data has been significantly extended in 2003. These results are obtained with a fast reciprocating probe installed at the outside tokamak mid-plane, which places the probe just under the magnetic axis of SNL divertor configurations. A new probe head shaped to match the poloidal curvature of these standard diverted equilibria has been used throughout most of the 2003 experiments but very recently a further improvement, offering Mach probe capability, has been successfully deployed.

Measurements to date have been made exclusively in ohmic discharges with the aim of characterising the turbulence under simple conditions and in particular with varying density and distance from the magnetic separatrix. The probe measures radial profiles of the turbulence in ion flux and in poloidal electric field, assuming negligible fluctuations in T_e, providing measurements of poloidal phase velocity and the magnitude and direction of the turbulent, cross-field ExB driven flux. The

composite Fig. 2.1.32 illustrates some typical experimental data showing, for $\bar{n}_e$~6.0x10^{19}m^{-3}, the radial profiles of poloidal phase velocity and skewness of the probability distribution function, or PDF, describing the relative size of fluctuations in the parallel ion flux (a measure of the degree of departure from Gaussian statistics). Examples of PDFs near the nominal separatrix location (as determined by the shear in the poloidal phase velocity) and in the far scrape-off layer (SOL) are also included. The data demonstrate clearly the tendency, with increasing distance from the confined plasma, for an increase in the number of large, positive (i.e. outgoing) events. This is a manifestation of the non-diffusive or "bursty" transport often seen in the tokamak SOL and now being discussed within the framework of "main chamber recycling" providing for increased transport in the far SOL and hence a weaker sink for particles due to divertor action. Data have also been obtained during ELMing ohmic H-mode, in matched forward and reversed field discharges and in helium plasmas.

Very recent measurements with the new Mach probe referred to above have provided the first ever parallel flow measurements in TCV. Strong flow near the separatrix in the direction from inner to outer target for discharges with the VB drift direction away from the X-point has been observed, offering further support to the importance of ballooning transport on the low field side in driving the anomalous parallel flows seen in the SOL of most tokamaks. Analysis is now underway to determine the link, recently identified on JET, between the cross-field turbulent driven flux and the magnitude of the parallel flow.

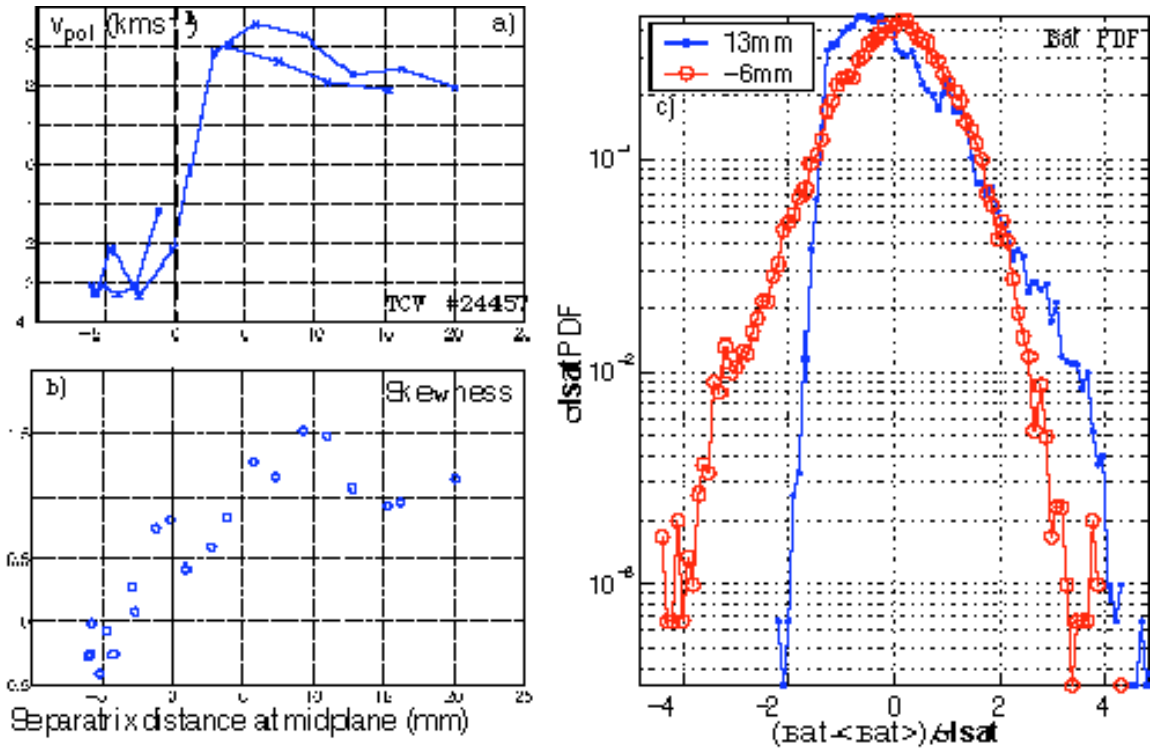

Fig. 2.1.33 *Radial profiles of a) poloidal velocity of potential fluctuations showing the shear near the nominal separatrix position and b) skewedness of the PDF of parallel ion flux to one of the fast probe pins. The normalised PDFs in c) for radii just inside (-6mm) and far outside (+13 mm) the nominal separatrix position demonstrate an increase of positive, "intermittent" transport events in the SOL.*

Sawtooth stability variation with plasma shape

Recent systematic calculations on the effect of triangularity on the stability of the ideal internal kink mode, which can be responsible for the sawtooth activity observed in tokamaks, have shown a maximum growth rate at slightly negative triangularity $\delta \approx -0.2$. Therefore not only positive triangularity but also very negative values can lead to sawtooth stabilisation. This non-monotonic behaviour has motivated a series of experiments with plasma of various triangularity values, from –0.6 to +0.3. Plasmas with and without additional heating (ECH) at different plasma currents have been investigated. These plasmas have an elongation of about 1.5, densities around $10^{19}m^{-3}$ and plasma current of about 300kA. In ohmic plasmas, the sawtooth period normalised by the electron density, as it scales with density, shows a clear minimum at small negative triangularity (see Fig. 2.1.34) as expected from theoretical predictions. The results with additional heating are under study. Further studies should also check which regime is relevant with respect to resistive and ideal internal kinks.

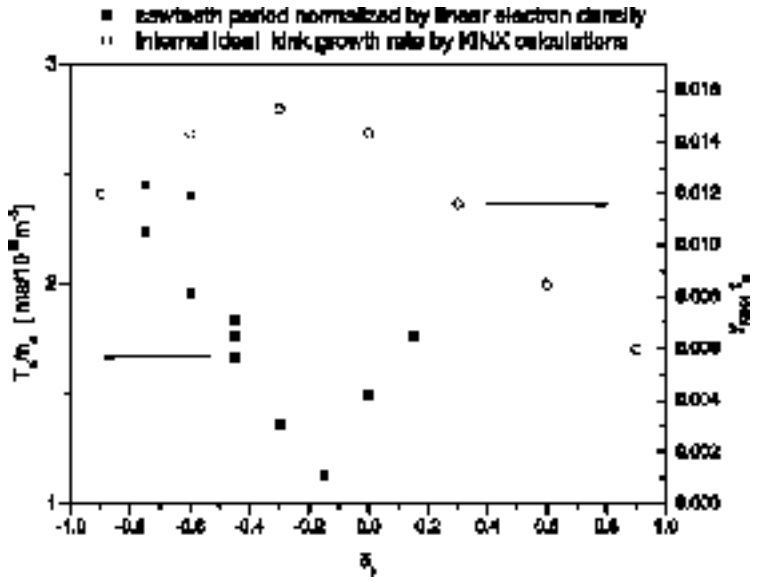

Fig. 2.1.34 *Sawtooth period normalised by the line-averaged electron density (solid squares) vs triangularity, compared to the ideal internal kink growth rate. The short sawtooth periods correspond to the most unstable cases*

2.2 Theory and numerical simulation

2.2.1 Physics underlying anomalous transport

Nonlinear global gyrokinetic simulations

The nonlinear evolution of ion temperature gradient (ITG) modes is characterised by the generation of an axisymmetric component of the perturbation, called the zonal ExB flow, which in turn contributes to suppress ITG turbulence. Last year, numerical simulations had shown that the zonal flows establish long-lived radial structures. The development of refined numerical tools is a necessity in order to capture this nonlinear physics accurately. A revised algorithm of nonlinear gyrokinetic Particle-In-Cell (PIC) simulations has been developed. An equation for the time evolution for the perturbed part of the distribution function, δf, was shown

to be redundant. The new scheme is simpler, it requires fewer computations, and it opens the way for new techniques that have the potential to reduce further the numerical noise inherent to the PIC method.

An alternative to the PIC schemes, which consists of solving for the full distribution function on a fixed grid in phase space, has the advantage of avoiding the numerical noise problem. The present version of the code for nonlinear drift-kinetic electrostatic ITG modes is now able to explore the nonlinear regime deeper into the saturation phase with a good control of the conserved quantities: relative errors are 10^{-7} in particle number, 10^{-5} in entropy, and 6% in total energy. These results have been achieved using a Bulirsch-Stoer algorithm for the calculation of the characteristics instead of a parabolic approximation and a logarithmic interpolation to avoid the problem of the appearance of negative values in the distribution function. We have shown how finer and finer structures develop in phase space (Fig. 2.2.1).

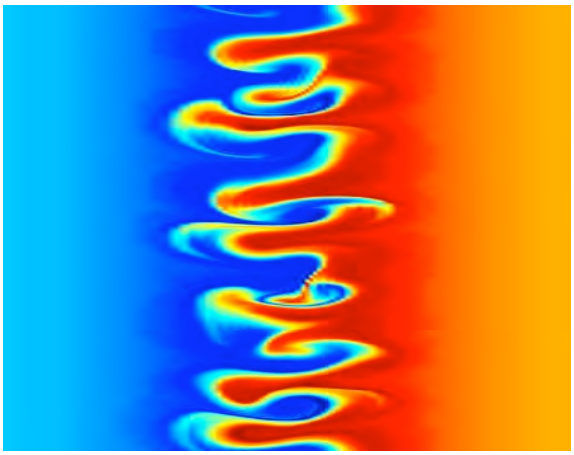

Fig. 2.2.1 *Contour plot of the distribution function in the nonlinear stage (cross-section in r, horizontal axis, and θ, vertical axis).*

Linear gyrokinetic simulations

The global spectral gyrokinetic electromagnetic numerical code, EM-GLOGYSTO, aims at studying finite plasma β effects on microinstabilities. It has been improved with new physics and numerical optimisation, with a more efficient parallelisation of the code which has led to a reduction in the execution time by an order of magnitude. For the first time, the behaviour of electromagnetic microinstabilities (Alfvén-ITG, AITG) has been investigated in the presence of radial electric fields (ExB flows). First results show that the stabilising effect of ExB flows on AITG is weaker than for the electrostatic toroidal-ITG. The physics of the parallel component of the fluctuating B-field and Shafranov shift effects have been included. Two equilibria have been analysed differing in their magnetic shear profile and the major results obtained are : (i) the parallel B-field fluctuation is effective only at relatively large shear values; (ii) there is a stabilisation of AITG modes at high β (above about 7%) due to parallel B-field; (iii) for the first time, full radius (global) eigenmode structures of high frequency modes such as AITG's including parallel B-fluctuations are obtained (Fig. 2.2.2); (iv) the Shafranov shift is shown to be in general stabilising but is not sufficient to bring about complete stabilisation. (vi) The existence of multiple modes with competing growth rates is demonstrated (Fig. 2.2.3). The AITG is likely to limit β at slightly less than the ideal MHD limit, for large or small tokamaks.

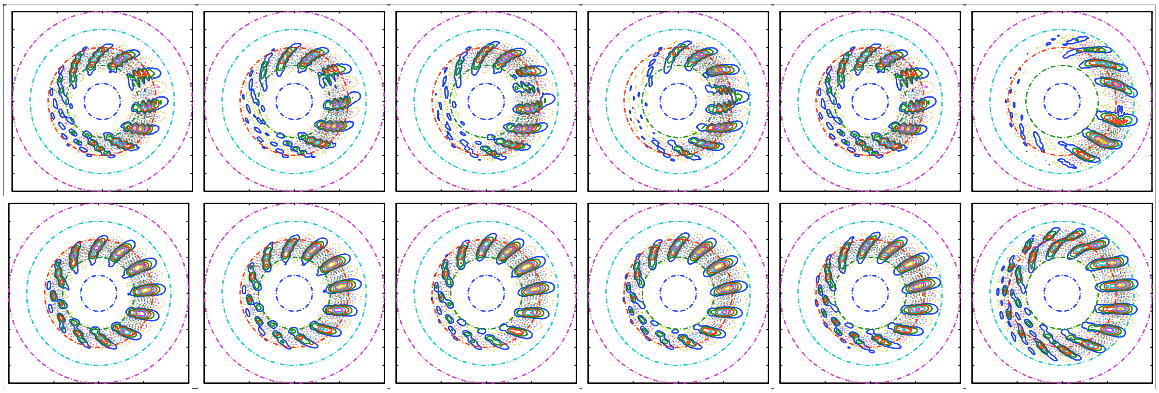

Fig. 2.2.2 *Eigenmodes from a 3-potential full radius model. The top row is the parallel vector potential and the bottom row is the perpendicular vector potential. Plasma β increases from left to right (4, 6, 8, 10, 12 and 15 %, respectively).*

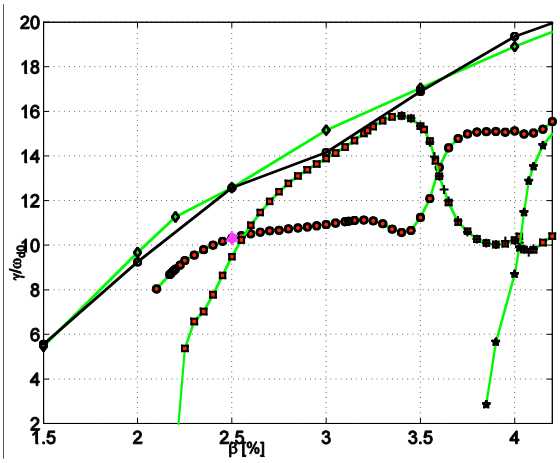

Fig. 2.2.3 *Growth rates of Alfvén-ITG modes vs plasma β. Open circles (open diamonds) are 3(2)-potential full radius results without Shafranov shift effects. Filled circles, diamonds and stars are 3 eigenmodes with Shafranov shift effects.*

For electrostatic microinstabilities, we have adapted the global linear gyrokinetic code LORB5 to be run for experimental tokamak equilibria and it has been benchmarked against the local code GLF23. Results for ASDEX-Upgrade, JET and TCV discharges show good qualitative and quantitative agreement between the two codes in the case of monotonic q profiles. In reverse shear discharges, GLF23 shows that the most unstable mode is localised around the null shear region while for LORB5 the absolute maximum in the mode amplitude is in the positive shear region. Preliminary LORB5 results for TCV internal transport barrier discharges show that trapped electron effects dominate the instability.

2.2.2 RF waves

Electron cyclotron heating and current drive

The modelling of specific TCV experiments with dominant EC heating and current drive has continued. New simulations of the X3 heating scenarios have started with the Fokker-Planck CQL3D code. The comparison with TORAY-GA results in the

linear regime show good agreement with both horizontal and vertical launch geometry. Simulations with both X2 and X3 waves have started.

Alfvén Waves in 3D plasma configurations

A new 3D solver for electromagnetic wave propagation has been developed. This code computes the full wave field in stellarator configurations in the Alfvén frequency range. An optimised algorithm for equilibrium coefficient evaluation in Fourier space significantly reduces the matrix construction time and global power balance is easily satisfied even with low mesh resolution. Several spectra in the Alfvén gap region have been analysed for various equilibria with different symmetries. In a 3D quasi-axisymmetric system the analysis is complicated by the coupling of m and n mode components, but a comparison with the corresponding cylindrical branches still proves useful and helps to distinguish the main modes and mode conversion surfaces (Fig. 2.2.4).

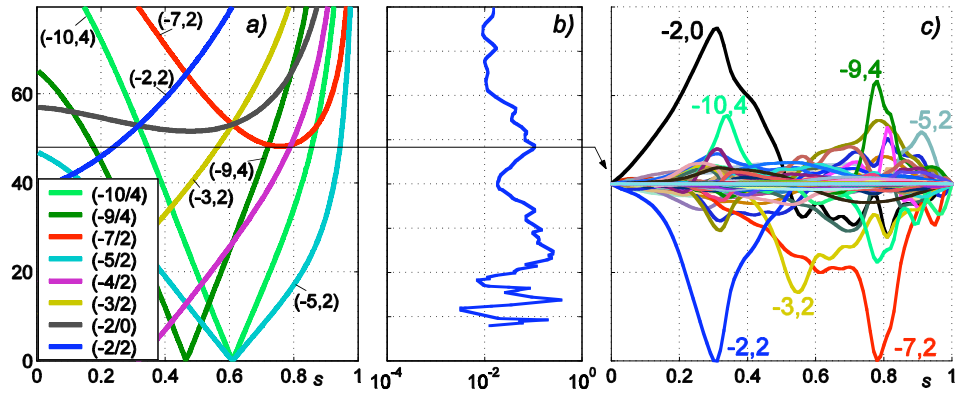

Fig. 2.2.4 *a) Mode structure for a cylinder with the same q-profile as the QAS. b) Normalised plasma response. c) Wavefields $A_{||}$ (au) at f=48.5kHz. Only the dominant Fourier harmonics are shown.*

Alfvén Waves in tokamaks

For the new antenna planned for JET-EP, computations of Alfvén eigenmode coupling at intermediate toroidal mode numbers, n=5 and 10, were performed with the global code LION. Different proposed antenna configurations have been studied. The computations have contributed to the new antenna design in that they have shown a coupling to the TAEs and EAEs of comparable strength to the n=0,1 and 2 Alfvén eigenmodes by the large saddle coils used in previous experiments. This increases confidence that the planned experiments will permit the investigation of Alfvén eigenmodes of intermediate mode numbers, which are supposed to be the most easily destabilised by fast ions.

2.2.3 Operational limits and comparison with experiments

Sawtooth behaviour and internal kink mode

The scaling of the growth rate of the internal kink with plasma profile and shape parameters has been linked to the change of sawteeth behaviour observed at high elongation. The scaling shows that the time at which sawteeth "vanish" is consistent with the growth rate being above a certain threshold value of the order of the ion diamagnetic drift frequency.

Studies continue into mechanisms that stabilise sawteeth in tokamaks. The internal kink mode, which manifests itself as a rigid shift of the toroidal equilibrium inside the q=1 surface, has frustrated and surprised theoretical researchers for many years. This is particularly highlighted by the well established result that effects which are purely due to toroidicity completely cancel out contributions that arise in the cylindrical limit, so that even in a torus with an infinite aspect ratio, the internal kink mode is a purely toroidal mode.

A similarly unexpected result has been observed in recent studies into the effect of energetic circulating ions on the internal kink mode. Energetic particles which are asymmetrically distributed in velocity parallel to the magnetic field give rise to a non-adiabatic contribution to internal kink stability which is stabilising for positive velocity asymmetry and destabilising for negative velocity asymmetry. This mechanism has been used to explain the stabilisation of sawteeth in recent experiments with unbalanced negative-ion-based neutral beam injection (NNBI). However, on self-consistently accounting for the radial orbit width of these energetic particles, the non-adiabatic term found earlier is cancelled by an adiabatic contribution. Due to the rigid shift property of the mode and radial excursion of energetic ions, circulating ions close to the q=1 surface contribute to destabilising the mode in the region of poor curvature when the velocity asymmetry is positive. Such ions yield a destabilising adiabatic contribution, thereby cancelling the stabilising non-adiabatic response. In contrast, where there is negative skew in the parallel velocity distribution, the circulating particles contribute predominantly in the region of good curvature, thereby cancelling the destabilising non-adiabatic response. Studies continue into the search for a new mechanism which can explain sawtooth stabilisation with NNBI and thus assist predictions of sawteeth in ITER.

High-n edge kink/ballooning modes

Edge localised MHD instabilities are thought to be the trigger mechanism for ELM bursts often observed in tokamak H-mode discharges. The KINX stability code, which consistently takes into account the plasma configuration up to the separatrix, was employed for high-n ideal external mode stability analysis using reconstructed TCV equilibria as a starting point. In the presence of a separatrix at the plasma boundary, robust edge current density stability limits were found. The stability boundaries were found to scale well with the product of the pedestal width times the toroidal wave number.

Current hole

A wide range of tokamak equilibria with current density reversal in the plasma core was numerically studied using a new equilibrium problem formulation and computational algorithm not assuming nested magnetic surfaces. Examples of hollow current density equilibria with a current hole like the JET experiments were calculated with and without current density reversal in the low current density region. Sequences of equilibria corresponding to total current reversal and magnetic surface structure similar to the AC tokamak operation experiments were obtained.

MHD limits in electron Internal Transport Barrier reversed shear discharges

TCV discharges with strong eITB and reversed shear are sometimes terminated by a fast MHD mode. Sometimes the transport barrier is removed during a fast event similar to an internal ideal MHD mode. The analysis of these cases has started, considering the influence of reversed shear as well as strong localised pressure gradients. These should help TCV experiments avoid these modes. The equilibrium

code CHEASE is being extended to allow for the specification of the safety factor profile as input. This should facilitate the study of MHD and gyrokinetic simulations of reversed shear cases.

2.2.4 Optimisation of 3D magnetic configurations

Optimisation of stellarator systems requires varying the plasma shape to achieve desired physics objectives. The boundary obtained therefore constitutes a single point in the phase space of the physics objectives targeted. Using a reverse engineering procedure, a coil system is devised by discretising the distributed current on a control surface that would generate the optimal plasma boundary surface. The physics properties with the discrete coils must be then verified and the sensitivity to variations of plasma pressures, currents and profiles must be ascertained.

The impact of a self-consistent bootstrap current (BC) in the collisionless $1/\nu$ regime is examined on the equilibrium and global ideal MHD stability properties of a 2-period quasi-axisymmetric stellarator (QAS) reactor under free boundary conditions. Finite β causes the plasma column to shift outward from the major axis. Adding finite BC causes the column to become more elongated on all cross-sections and becomes distorted on the horizontally elongated up-down symmetric cross section (Fig. 2.2.5). The BC also causes the rotational transform to exceed the critical resonant value $\iota=1/2$ for $\beta\sim2\%$ destabilising a $m/n=2/1$ global external kink. Unlike fixed boundary conditions, the BC fails to converge for $\beta>4\%$ because not only the current profile varies during the iterations, but the plasma shape changes also (Fig. 2.2.6). A modest vertical field can restore the vacuum plasma shape at the expense of a mirror term in the magnetic field spectrum.

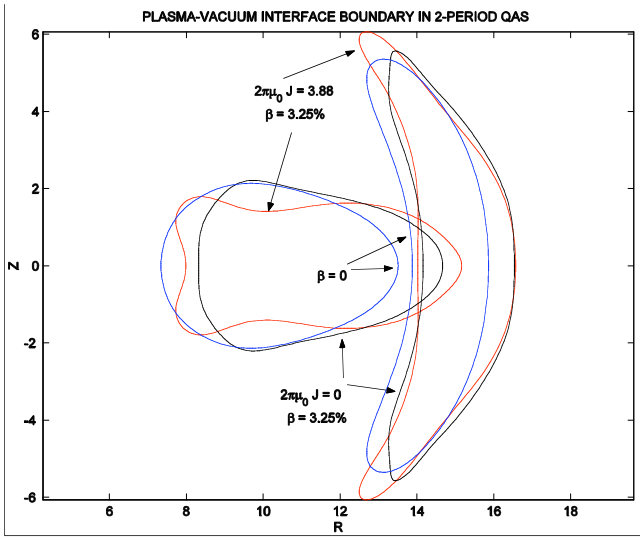

Fig. 2.2.5 *The plasma-vacuum interface boundary in the vacuum state and at β=3.25% with and without the BC effect.*

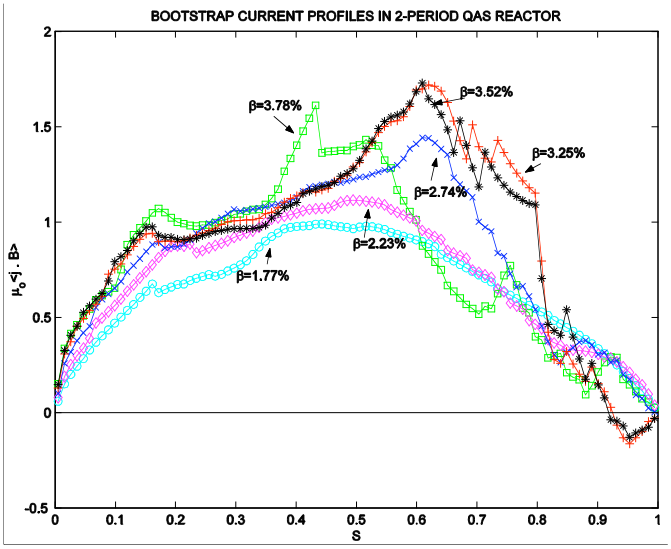

Fig. 2.2.6 *The bootstrap current profiles for different values of β*

The optimisation of a 2-period QAS device with respect to reduced Pfirsh-Schlueter currents has been achieved. However, the magnetic field strength spectrum is noticeably deteriorated by the appearance of large amplitude symmetry breaking components.

Configurations with 6 and 9 field periods have been optimised to have poloidally closed contours of the second adiabatic invariant for deeply, moderately and barely trapped particles, simultaneously. These configurations also satisfy conditions of pseudo-symmetry which manifests itself through almost constant mod-B lines closing poloidally, thus satisfying poloidal quasi-symmetry. Another important characteristic of these optimised systems is that both the regions of maximum and minimum magnetic field strength B display vanishing magnetic field line curvature. The Pfirsh-Schlueter currents thus localise within one period of the system vanishing around maximum B. The N=9 configuration can achieve stable β values in excess of 10% and further possible improvements could enhance its potential as a viable reactor. An N=3 configuration with β=5% that is optimised with respect to quasi-isodynamicity has also been obtained.

2.2.5 Integrated tokamak modelling using the DINA 1.5D simulation code

In 2002 we presented successful modelling of TCV discharges from the point of view of poloidal field coil voltage perturbations, VDEs in the inhomogeneous vertical field decay index and the application of additional EC heating and current drive. In order to extend the use of the DINA code beyond the version developed for TCV, we have continued developing the new, open architecture version of DINA, known as DINA-CH, in collaboration with the RRC Kurchatov Institute and the TRINITI institute, both in Moscow.

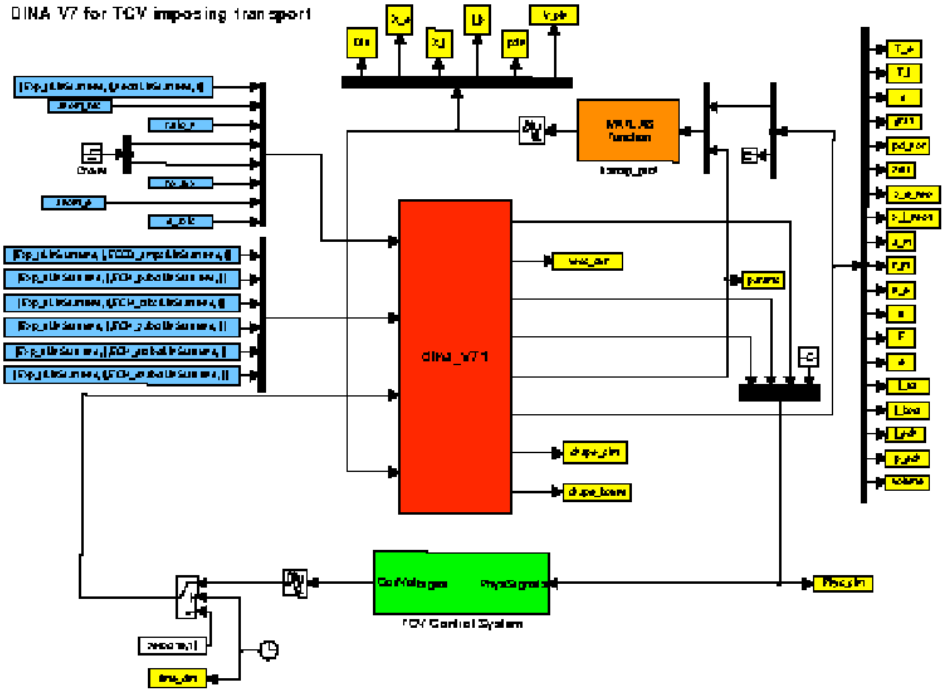

Fig. 2.2.7 *Second phase development of DINA-CH for TCV, with user-specification of the transport coefficients, additional heating and plasma control explicitly defined in the SIMULINK environment*

In the previous phase, we had removed details of the tokamak itself from the DINA code, leaving a generic plasma simulator, solving the free boundary equilibrium, the poloidal flux diffusion within the plasma and heat transport within the plasma. Details of the tokamak construction itself, including diagnostics, were provided externally. Details of the power supplies, their saturation, plasma position and shape control are now explicitly represented in the SIMULINK environment.

In the new second phase, the transport of heat, particles and poloidal flux is implemented internally, but the coefficients can be specified externally, freeing DINA from a set of pre-defined transport models. This has opened DINA up for exploring different transport models in a transparent way. An example of the new implementation is shown in Fig. 2.2.7.

This evolution of DINA-CH has made it possible to re-implement DINA for ITER simulations, which was done this year and an initial simulation of 220 ITER seconds is illustrated in Fig. 2.2.8. This simulation takes roughly one minute per ITER second on a Pentium IV.

In a further development, the MAST tokamak has been modelled. MAST had previously been studied at the CRPP, in collaboration with the UKAEA, to determine the origins of their vertical control difficulties, identifying the probable cause as being an excessive loop delay in the vertical position feedback. Since MAST had already been implemented in the linear RZIP code, it was extremely simple to re-implement in DINA this year. MAST in DINA-CH is now being studied at CRPP to determine the importance of non-linearities in the vertical position control which are a particularity of the spherical tokamak.

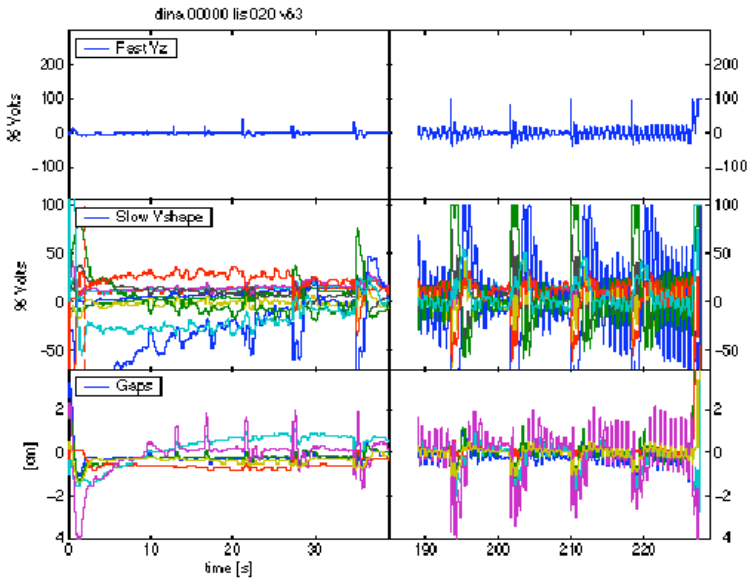

Fig. 2.2.8 *Evolution of the ITER supply voltages and gaps using DINA-CH*

2.3 Basic plasma physics activities

A new TORoidal Plasma EXperiment (TORPEX) has been built at CRPP, mainly dedicated to the study of turbulence and anomalous transport in toroidal plasmas. Low densities and temperatures make it possible to measure and possibly control plasma parameters and wave fields with high resolution locally throughout the plasma. The device provides an ideal training environment for young researchers.

TORPEX is a toroidal device with major and minor radius R=1m and a=0.2m, to which a toroidal magnetic field up to 0.1T is applied using a set of 28 coils. Six poloidal coils can be used to add a small vertical component $B_v \leq 50$mT for the optimisation of the plasma production scheme. Highly reproducible plasmas of Argon and other noble gases, for pressures $p_{gas} \sim 10^{-4}$-10^{-5} mbar, are created by means of waves in the electron cyclotron (EC) range of frequencies. Plasma density and electron temperature are in the range $n_e \sim 10^{16}$-$10^{17} m^{-3}$ and $T_e \sim 5$-10eV, with up to 20kW of microwave power at f=2.45GHz injected during 100ms from the low-field side. Parameters like the neutral gas pressure, the location of the EC resonance and the amount of injected power can be varied to control the density and electron temperature profiles.

Two important milestones were achieved in the first part of 2003: the first plasma was produced in TORPEX, in March, the group was completed, now encompassing two post-doctoral fellows, one with a Euratom Fellowship, and three graduate students (in addition to a number of undergraduate students). During the year we have gone from the first plasma to the optimisation of the plasma production process, and from measurements of the linear properties of the naturally occurring plasma instabilities, aimed at establishing the relationship between the gradients and the fluctuation spectra, to the first characterisation of turbulence.

2.3.1 Plasma production and characterisation

TORPEX plasmas are produced by waves injected in O-mode polarisation using a magnetron source at f=2.45GHz and a truncated wave guide as antenna. The EC

frequency is matched at R_{ec} where B=0.0875T. Primary electrons are accelerated at R_{ec} by resonant interactions, then ionise the neutral gas by collisions. Once a plasma is created, the waves are absorbed at the upper-hybrid resonance location R_{uh} on the low-field side of R_{ec} (Fig. 2.3.1), where the density profile peaks. Electron temperatures of the order of 5eV are measured over the whole plasma column.

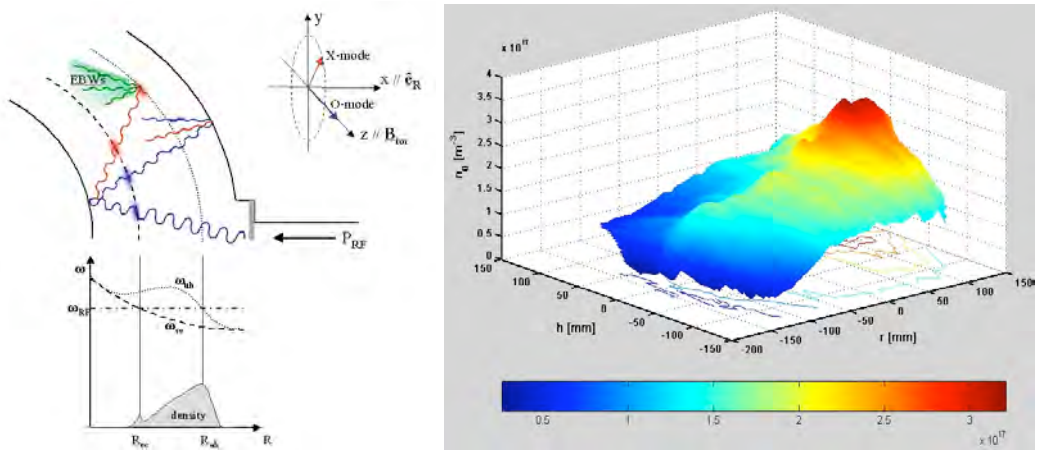

Fig. 2.3.1 ***Left****: schematic of the propagation and absorption mechanisms.* ***Right****: measured density profile for Argon with* $p_{gas}=2\cdot10^{-5}$*mbar,* $B_v=3mT$, $P_{RF}=10kW$*. Coordinates (r,h) are centered on the magnetic axis*

For low power ($P_{RF}\leq10kW$), the lack of a dependence of T_e on the absorbed power, estimated as the difference between injected and reflected power, measured using a bi-directional coupler, suggests that T_e is determined mainly by the ionisation process. The profiles of n_e, T_e and plasma potential are observed to depend on externally controlled parameters like the vertical field B_v, p_{gas}, R_{ec} and the injected power.

2.3.2 Optimisation of magnetic configuration: vertical field

In a simple magnetised torus, i.e with a purely toroidal magnetic field, charge dependent grad–B drifts give rise to vertical electric fields which lead to very fast particle loss due to ExB drifts. The vertical magnetic field is expected to reduce these losses by partially short-circuiting the electric field generated by particle drifts. The zero order particle transport is thus determined by two loss mechanisms: the E_{eq}xB flow and the direct loss where the field lines intersect the vacuum vessel. E_{eq} is the equilibrium vertical electric field that exists for each given field line pitch angle $\tan\theta=B_z/B_\phi$, such that the net direct vertical flux compensates exactly the grad B flux.

The relative importance of these loss channels depends crucially on the pitch angle. By increasing the pitch angle, the end-of-field-line loss comes into play, but the equilibrium electric field decreases, thus the first loss mechanism loses importance. An optimum pitch angle will exist, at which the total loss is minimum and the particle confinement time is maximum.

We calculated the theoretical dependence of the confinement time on the field line pitch angle, as well as the position and value of the maximum. The model was verified experimentally by measuring the typical plasma decay time after the microwave power has been turned off (Fig. 2.3.2). Identifying the plasma decay time with the particle confinement time, we could verify a number of predicted features

(Fig. 2.3.3): the spatial symmetry properties; the existence of a value of vertical field for which the plasma confinement time is maximum; the position and the value of the maximum; the shape of the experimental dependence on position and vertical field. Curiously, both in the model and in the data, higher confinement times correspond to lower overall plasma density.

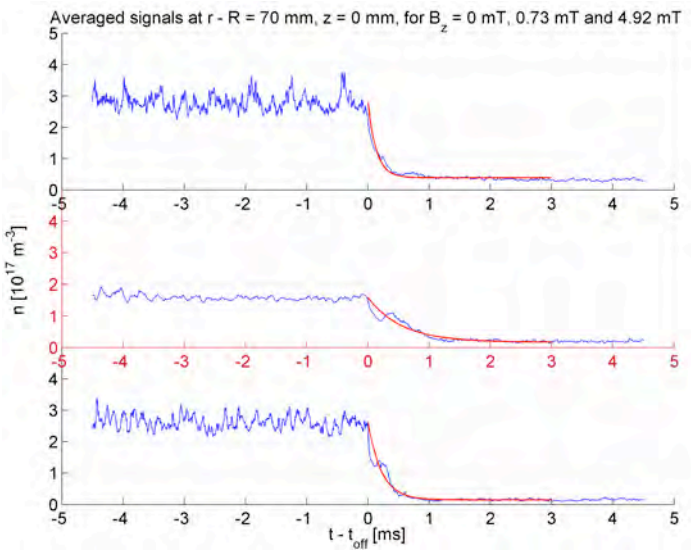

Fig. 2.3.2 *Plasma density decay after the ECR source is turned off, and the exponential fit defining the confinement time τ*

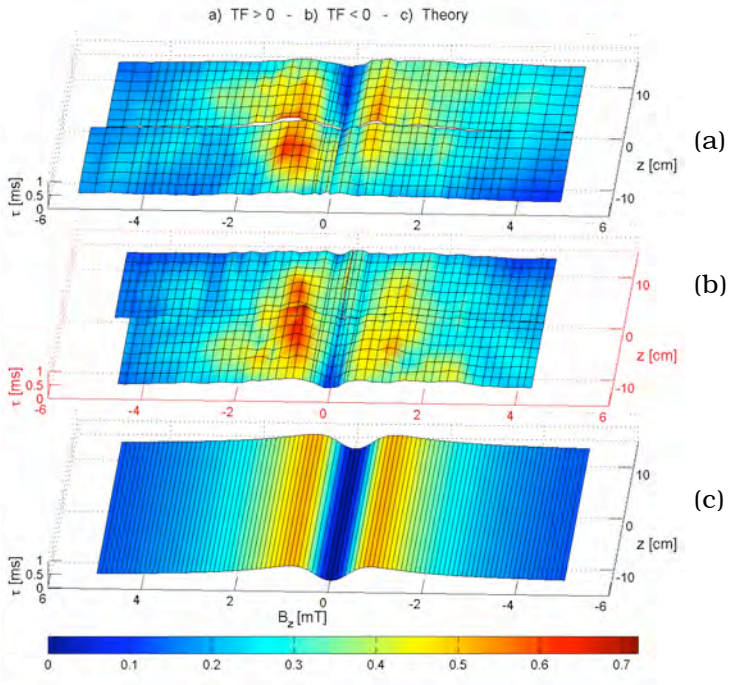

Fig. 2.3.3 *Comparison of theoretical model predictions with experimental data on particle confinement time as a function of vertical magnetic field and vertical position.*

2.3.3 *Linear wave and instability measurements*

The relationship between the plasma gradients and the development of instabilities and turbulent phenomena is a key issue for anomalous transport in toroidal plasmas. In the first measurement campaign both coherent modes and broad spectral features are observed in the different plasma configurations, depending on plasma profiles, and a first attempt at linking the observed fluctuations with the profile parameters was undertaken.

Linear spectral analysis techniques, based on auto- and cross-power spectra corresponding to the second moment of the time series, have been successfully applied in the study of wave phenomena in TORPEX plasmas. For the spectral investigation of the temporal and spatial structure of plasma waves the two-point correlation technique was used, both for the regular and turbulent drift waves. The technique is based on constructing an estimate for the wave-number-frequency spectrum $S(k,\omega)$ from the local phase shift between two single probes. This quantity provides information on the statistical nature of space-time varying fluctuations, including the spectral density in k space, the statistical dispersion relation, the degree of turbulent broadening of the dispersion relation and the spectral indices of turbulent spectra. An example of the application of this method is shown in Fig. 2.3.4. From the evaluation of $S(k,\omega)$ and the Doppler shift due to the ExB drift related to a radial electric field, we conclude that the turbulence observed in TORPEX is consistent with drift waves, characterised by $k_\theta=(0.02\pm0.07)cm^{-1}$ and phase velocity $v_{ph}=4km/s$, propagating in the direction of the electron diamagnetic drift.

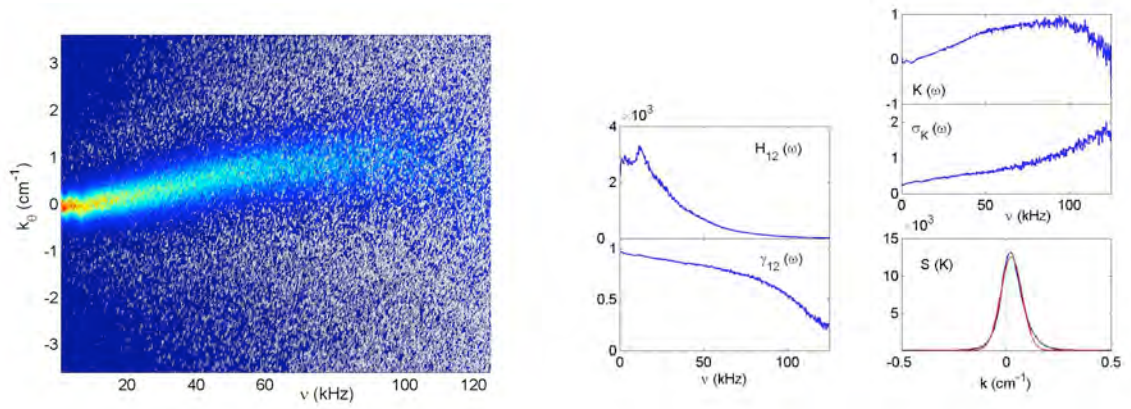

Fig. 2.3.4 *Left: wave-number-frequency spectrum $S(K,\omega)$ evaluated from the signals of two probes separated by 8.7mm, in H plasma, for $p_{gas}=3.5\times10^{-5}$mbar, $B_{TOR}=80$mT, $B_v=1$mT, $n_e\sim2\times10^{17}m^{-3}$, $T_e\sim8$eV. Right: cross-spectrum H_{12}, coherence-spectrum γ_{12}, statistical dispersion $K(\omega)$, broadening of the dispersion relation $\sigma(\omega)$. $S(K)$ is obtained by integrating $S(K,\omega)$ in the range 5-50kHz, where the dispersion relation is linear.*

2.3.4 *Initial nonlinear wave and turbulence analysis*

The statistical properties of turbulence are analysed through the study of the self-affinity parameter or Hurst exponent (H) and the Probability Density Functions (PDFs) of the raw signals. PDFs measured in different plasma conditions show a

strong distortion from a Gaussian shape with well pronounced tails, especially in the case of B_v=0.

The Hurst exponent was computed using two methods: the rescale range analysis and the structure function, Fig. 2.3.5. In this example H>0.5, indicating a long time correlation trend. The stationarity of the fluctuation data, necessary condition for a physical meaning of this kind of analysis, was verified on the TORPEX probe data.

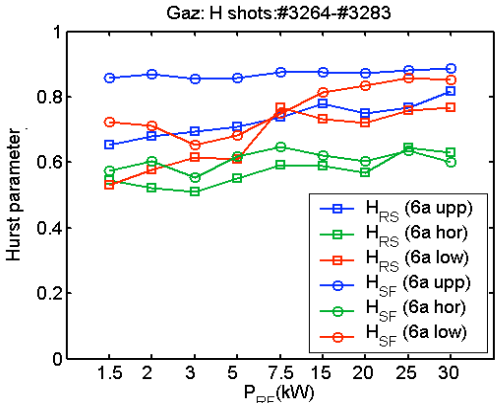

Fig. 2.3.5 *Estimate of the Hurst parameter for one tip from each fast Langmuir probe array, using both the rescale range analysis (H_{RS}) and the structure function (H_{SF}), versus the injected power in H plasma*

The conditional average sampling method was applied to obtain a first example of imaging of turbulent density fluctuations on a poloidal section. Large turbulent structures appear to rotate in opposite directions as the toroidal field is reversed, suggesting that the cells follow the ExB flow (see Fig. 2.3.6).

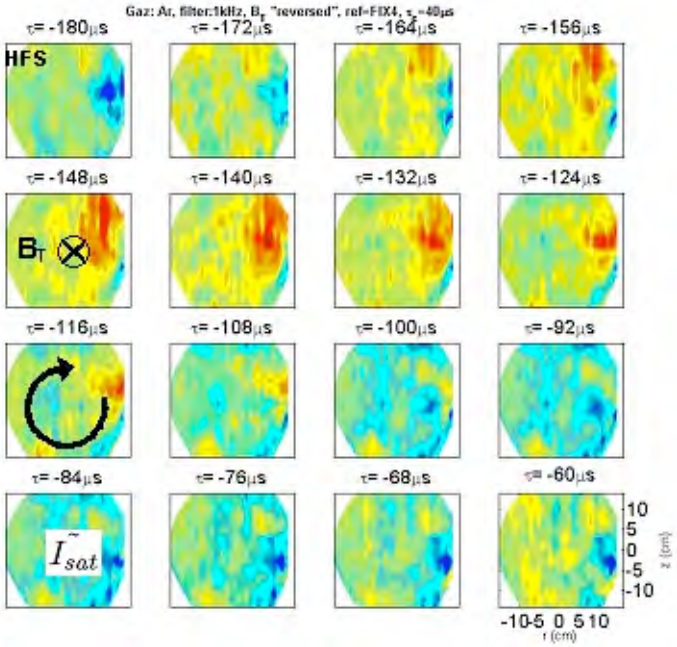

Fig. 2.3.6 *Example of the reconstruction of turbulent structure creation and propagation using the conditional average sampling technique on ion saturation current data from Langmuir probes*

2.4 Materials for fusion

The main objective of the Fusion Technology Materials (FTM) group of CRPP is to investigate the effects of the damage produced by radiation in a variety of materials, in particular candidate materials for structural components of future fusion reactors but also pure metals and model alloys. The group is located at the Paul Scherrer Institute (PSI) in Villigen. It uses the high-energy (590MeV) proton beam of the PSI accelerator, through the Proton Irradiation Experiment (PIREX) and the Swiss Spallation Neutron Source (SINQ) facilities, to simulate experimentally the effects of the 14MeV neutrons that are the product, together with helium nuclei, of the fusion reactions between deuterium and tritium nuclei.

Key parameters for the first wall in fusion power reactors with a fusion power of 3 to 4GW and in quasi-continuous operation include a total neutron flux of 10 to $15x10^{14}n/cm^2.s$, a neutron wall loading of 2 to $3MW/m^2$, an integrated wall load of 10 to $15MWy/m^2$, a surface heat load of 0.1 to $1MW/m^2$ and a power density of 20 to $30W/cm^3$. The accumulated dose will amount to 100 to 150dpa in steels, while the gas produced by transmutation nuclear reactions will amount to 10-15appm He/dpa and 40-50appm H/dpa, also in steels. From the technological point of view, the temperature window of operation of fusion reactors is mainly limited by the mechanical properties of structural materials.

Like 14MeV neutrons, 590MeV protons produce atomic displacement cascades and transmutation nuclear reactions within the irradiated materials. From the point of view of materials science, atomic displacement cascades induce point structure defects, vacancies and interstitial atoms, while transmutation nuclear reactions produce impurities, such as helium or hydrogen gas atoms. The final microstructure of the irradiated material results from reactions between these different defects, leading to defect clusters, dislocation loops, dislocation networks, precipitates, stacking fault tetrahedra (SFT's), voids and/or helium bubbles (Fig. 2.4.1). This microstructure has an important effect on the physical and mechanical properties of the material considered. It can lead to important hardening, loss of ductility and fracture toughness, as well as macroscopic swelling of the material (Fig. 2.4.2). These effects are the main factors limiting the choice of candidate materials. The residual radioactivity of a large amount of exposed material is also a concern and will govern the handling methods, dictate the storage periods and the overall waste management and recycling scenarios. The development strategy that takes into account these limitations has led to the development of the so-called low activation materials.

One of the main advantages of 590MeV protons is to generate a high He/dpa ratio that cannot be achieved with any other currently available irradiation source. While proton irradiations in PIREX produce about 130appm He/dpa and 800appm H/dpa (in steels), irradiations in SINQ with a mixed spectrum of neutrons and protons produce about 50appm He/dpa and 450appm H/dpa (in steels). However, in order to investigate the material properties changes and degradation under different irradiation conditions, the FTM group is also involved in specific neutron irradiations performed in reactors in the USA, the Netherlands and Hungary.

Candidate structural materials for first wall and breeding-blanket applications mainly include reduced activation ferritic/martensitic (RAFM) steels, vanadium alloys and fibre reinforced SiC_f/SiC ceramic composites. Each alternative alloy class exhibits some specific problems arising from radiation damage. For the time being, the most promising class of alloys are the RAFM steels for which the greatest technology maturity has been achieved. Qualified fabrication routes, welding technology and general industrial experience are already available.

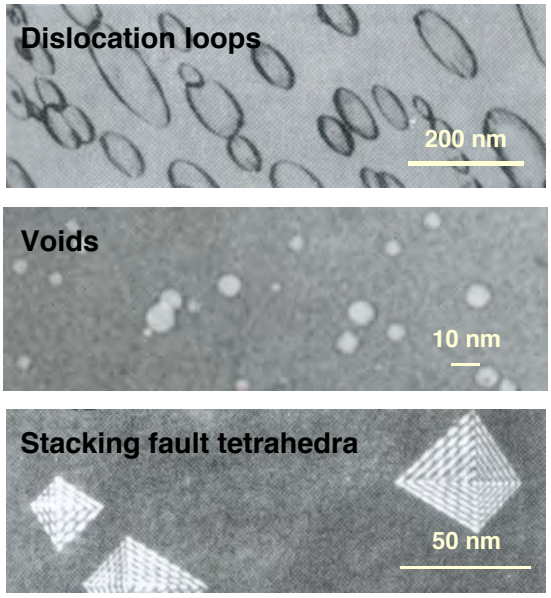

Fig. 2.4.1 *Examples of transmission electron microscopy images of irradiation-induced structure defects*

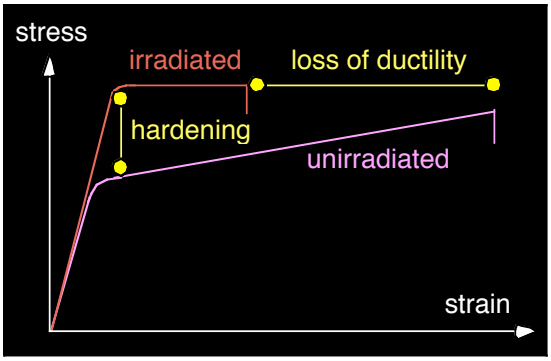

Fig. 2.4.2 *Schematic of irradiation-induced hardening and loss of ductility, as measured in tensile tests*

The design of materials with properties adequate for use in an irradiation environment requires an understanding of the effects of irradiation on their physical and mechanical properties. The FTM group has been active in this field for several years within the framework of the European Fusion Development Agreement (EFDA) and collaborates with many research institutes and industries in Switzerland as well as abroad. The research activities of the FTM group include basic research on radiation damage in pure metals and alloys, characterisation and development of low activation materials for fusion power reactor applications and characterisation of materials destined to ITER. The scientific approach adopted by the FTM group to understand the fundamentals of radiation damage in metals and alloys is based on investigating the structure/mechanics relationships at different length scales (micro-, meso-, and macroscopic). A range of experimental and numerical tools is used to reach these objectives. The main experimental tools include mechanical testing on sub-sized and standard specimens, scanning and transmission electron microscopy (SEM, TEM) and small angle neutron scattering (SANS). The main numerical tools include molecular dynamics (MD), Monte-Carlo (MC) and dislocation dynamics (DD) simulations and finite element (FE) calculations.

2.4.1 Irradiation experiments

The specimens that were irradiated between December 2002 and October 2003 are listed chronologically per material in Table 2.4.1, together with the corresponding irradiation parameters. All the irradiation experiments have been performed in the PIREX facility with 590MeV protons. The beam intensity was around 15μA and the damage rate was approximately 10^{-7}dpa/s.

Specimen name	Material	Specimen type	Specimen number	Irradiation temperature [°C]	Accumulated dose [dpa]
I40T17	Ni (single crystal)	tensile	2	50	0.001
I40T18.1	Ni (single crystal)	tensile	1	50	0.001
I14T18.2	Al (polycrystal)	TEM	1	50	0.001
I40T19	Al (polycrystal)	TEM	2	50	0.001
I29B07	EUROFER 97	bend bar	1	300	0.9
I29B08	EUROFER 97	bend bar	1	300	0.9
I29B09	EUROFER 97	bend bar	1	300	0.9
I32I04	CuCrZr	in situ fatigue	1	100	1.521
I40T26	Ni (single crystal)	TEM	2	350	0.1
I40T27	Ni (single crystal)	TEM	2	350	0.1
I40T28	Zr (polycrystal)	TEM	2	350	0.1
I40T23	Ni (single crystal)	tensile	2	250	0.001
I40T24	Ni (single crystal)	tensile	2	250	0.001
I40T25	Ni (single crystal)	tensile	2	250	0.001
I33T01	Cr (nanocrystal)	TEM	2	50	0.1
I33T02	Cr (nanocrystal)	TEM	2	50	0.1
I33T03	Cr (nanocrystal)	TEM	2	50	0.1
I29B07	EUROFER 97	bend bar	1	300	0.9
I29B08	EUROFER 97	bend bar	1	300	0.9
I29B09	EUROFER 97	bend bar	1	300	0.9
I29B10	EUROFER 97	bend bar	1	300	0.9
I29B11	EUROFER 97	bend bar	1	300	0.9
I29B12	EUROFER 97	bend bar	1	300	0.9
I47T01.1	ODS EUROFER	tensile	1	350	1
I47T01.2	EUROFER Hipped	tensile	1	350	1
I47T02.1	ODS EUROFER	tensile	1	350	1
I47T02.2	EUROFER Hipped	tensile	1	350	1
I47T03.1	ODS EUROFER	tensile	1	350	1
I47T03.2	EUROFER Hipped	tensile	1	350	1

Table 2.4.1 *Specimens irradiated in the PIREX facility in 2003.*

Much of our research work is carried out under mandate by EFDA in so-called Technology Tasks, Underlying Technology Tasks or Next Step Tasks.

2.4.2 Underlying Technology tasks

In-beam fatigue of RAFM steels

This research is aimed at investigating the behaviour of the EUROFER 97 RAFM steel in the condition of in-beam fatigue using an in situ testing facility specially designed for PIREX. The in-beam fatigue experiments performed in 2003 were dedicated to investigating further the role of hydrogen in the condition of in-beam fatigue. The in-beam testing facility failed at the end of 2002 and a new brake had to be installed in the vertical drive system before the testing could proceed again. The testing device was then itself successfully tested. It is now possible to lower the testing equipment into the in-beam position without failure and with no danger of harming the accelerator operation. A first experiment on EUROFER 97 was conducted in August 2003. The test and irradiation temperature was 150°C. The testing system behaved perfectly and the experiment lasted up to the normal fatigue rupture of the specimen. The number of cycles to failure, indicated by a main crack going through the specimen wall, was 1488 cycles. This number of cycles is somewhat lower than the one previously obtained for a specimen of the F82H RAFM

steel tested in similar mechanical conditions but at 300°C. The next in-beam test will be run at a higher temperature (250°C) in order to check the effect of the temperature. Normally the irradiation temperature should not have a very strong effect on the number of cycles to failure, but if such an effect is experimentally demonstrated, it could indicate that the hydrogen produced by the spallation nuclear reactions is playing a role in terms of embrittlement effects. It is known that hydrogen effects in steels are strongly temperature dependent and effective up to 300°C. At least two more in-beam experiments will be performed before the end of 2003. Then, a series of tests (possibly 2 or 3) will be conducted on unirradiated specimens in spring 2004, to compare with the results of in-beam experiments.

Study and development of refractory materials for fusion applications

Neutron irradiation of pure Tungsten in the HFR reactor in Petten (The Netherlands) at 600-650°C and 900-950°C to a dose of about 2.5dpa, has been completed. The cooling down phase is in progress and the irradiated specimens will be transported back to Switzerland in the next few months. Investigation of the microstructure and mechanical properties of neutron-irradiated pure Tungsten will be performed in 2004.

Nanocrystalline (nc) materials are being developed in collaboration with Prof. R. Valiev, Institute of Physics of Advanced Materials, Ufa State/Aviation Technical University, Russia. Preparation of nc Tungsten is still underway. Three samples of nc pure Chromium have been delivered in the shape of 12mm disks that are about 0.3mm thick. They have been produced by applying a pressure of 6.5 and 6GPa and a torsion corresponding to 5 turns, and 6.5GPa and 3 turns, respectively. The grain size has been measured by X-ray diffractometry after electrochemical polishing of the surface. It amounts to 31.5, 14.8 and 15.6nm, respectively. Vickers hardness (Hv) measurements showed that Hv decreases with decreasing grain size, from about 900 to 700, with an error bar of 100 on each measurement. Nanocrystalline samples prepared by severe plastic deformation (SPD) have been compared to nc samples prepared by electrodeposition (ED). In the latter material the grain size was found equal to 28.4nm and Hv was found to be around 1100. Nanocrystalline Chromium has been irradiated in the PIREX facility at room temperature to a dose of 0.1dpa, in the shape of PIREX tensile flat specimens for nc Chromium prepared by ED and in the shape of TEM disks and 3mm long micro-tensile flat specimens for nc Chromium prepared by SPD. A special sample holder, composed of a sandwich of spot welded stainless steel plates, has been developed in order to irradiate TEM disks and micro-tensile flat specimens. The cooling down phase is in progress. Irradiated specimens will be investigated at the beginning of 2003.

Use of spallation neutron source target for irradiating fusion materials

A series of specimens of the EUROFER 97 RAFM steel and the EUROFER 97 RAFM steel reinforced with 0.3wt.% Y_2O_3 particles (ODS EUROFER), has been prepared by spark erosion, destined to be irradiated in 2004/2005 in SINQ at the PSI at temperatures between 300 and 600°C to doses between 5 and 10dpa. They include mini-Charpy specimens (3x4x27mm^3), tensile flat specimens (5mm in gauge length x 1mm in width x 0.4mm in thickness), specimens for TEM observations and small punch testing (3mm in diameter x 0.25mm in thickness), and specimens for small angle neutron scattering measurements (8mm^{2}x1mm). Mini-Charpy's and tensile flat specimens of two kinds of Ti-base alloys, namely Ti-6Al-4V and Ti-5Al-2.5Sn, have also been prepared, which will be also included in the same irradiation. All the specimens have been mechanically polished to get mirror surfaces and benchmarked using a laser device. Mounting of the specimens in irradiation tubes is in progress within the long-term task TW3-TTMS-007 deliverable 8.

Supporting research

Modelling of damage accumulation in Cu, Ni and Au

Our computing power is in the process of being upgraded. In this process the software platform has been migrated to another hardware and operating system (also Unix based), with new compilers (C, C++, Fortran 77 and Fortran 90), optimised for the new hardware. All molecular dynamics (MD) simulation programmes and transmission electron microscopy (TEM) programmes have been successfully posted onto the new platform. New fast data visualisation tools have been incorporated. These are scriptable 3D display software of atomic structures allowing on-the-fly rendering.

A series of simulations was performed for a 5keV cascade in single crystal Au (Fig. 2.4.3). It appears that the cascade generates in the first picosecond (ps) a shock wave that propagates away from the cascade core at the speed of sound (4000m/s from these MD results). It is accompanied by recoil collision sequences that are observed to propagate equally well in all <110> directions (crowdion propagation). The thermal spike occurs at 3ps. The cascade is cooled down at about 15ps. At about 20ps sessile defect clusters (of interstitial type) transform to glissile dislocation loops with a 1/2 <110> Burgers vector. These mobile defects are seen to migrate 1D along <110> directions by thermal activation.

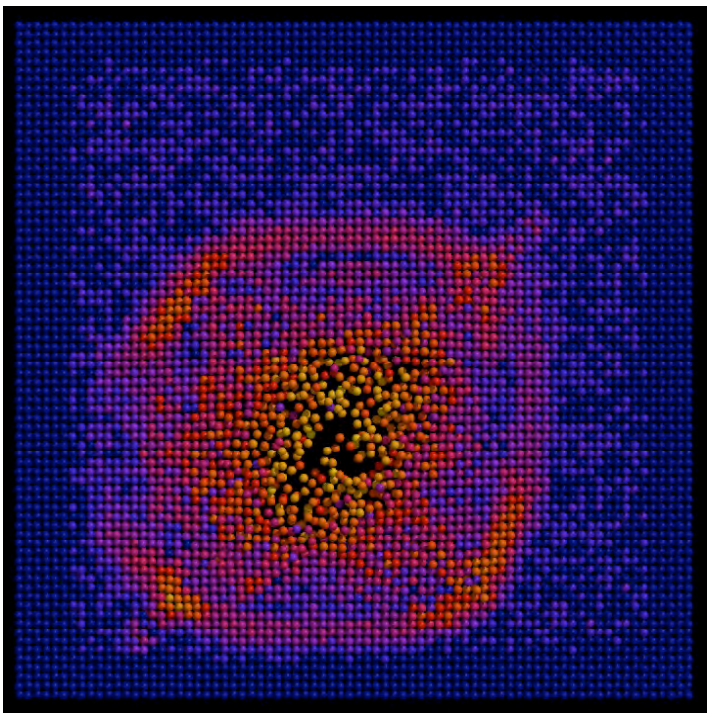

Fig. 2.4.3 *View in cross section of a 5keV cascade at 1.1ps in single crystal Au. The sample contains about 250'000 atoms and its side length is 15.5nm. Colour represents kinetic energy.*

New software has been developed to generate polycrystals, based on a given single crystal. Grain position is randomly generated and grain boundaries are defined similarly to Wigner-Seitz cell boundaries. A given grain is thus made by translating the single crystal and cutting it along its Wigner-Seitz cell boundaries, while respecting full periodic boundary conditions for the resulting sample. Crystallographic orientation of the grains is generated randomly, apart from the

first grain that is put at the centre of the sample and keeps the original orientation of the given single crystal (Fig. 2.4.4).

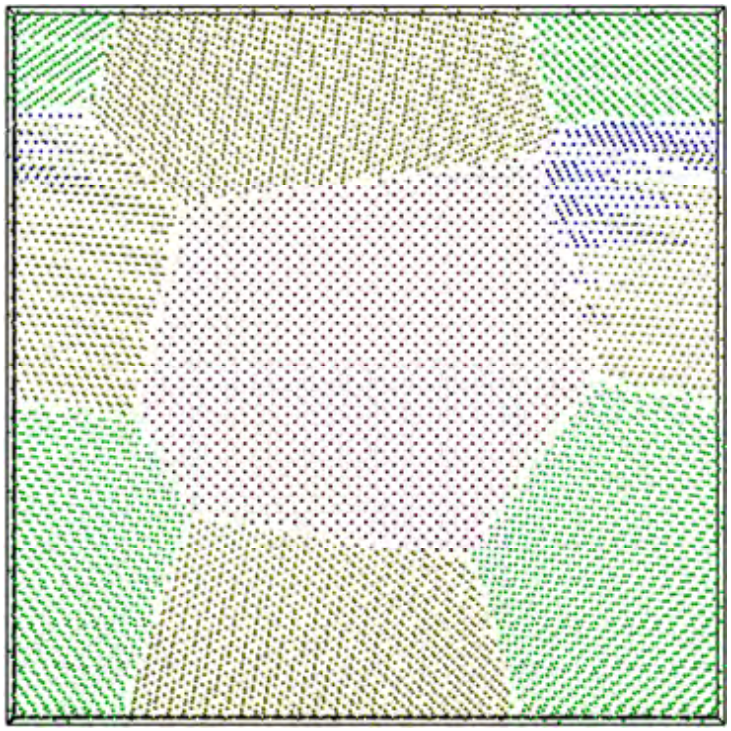

Fig. 2.4.4 *View in cross section of a generated polycrystal of Gold (unrelaxed). Grain size is 10nm and total number of atoms is 500'000.*

Some preliminary tests have also been performed with a cubic sample size of 37×37×37 lattice unit cells, which contains about 200'000 atoms, and Primary-Knock-on Atom (PKA) energies of a few keV in Gold and Nickel. Typical features of the time evolution of displacement cascades could be reproduced, including binary collision stage, thermal spike stage, focusing collision sequences along <110> directions and cooling down (see previous section).

In order to prepare the analysis by TEM of the defect microstructure resulting from the simulated cascades, TEM image simulations of relaxed dislocation loops in Nickel, Aluminium, Gold, Copper were performed, using the Electron Microscopy Software (EMS) code. A simple dislocation loop, made of a number of interstitials placed into a <111> plane, was considered. The loop is built into a MD sample made of about 0.5 million atoms (42x42x42 lattice unit cells). The loop is then relaxed using the Moldy programme and the Al potential. Only this potential is considered for all materials in order to identify contrast differences resulting only from scattering differences between materials, and not from differences in elastic properties. Image simulations are performed for the case of a dark field weak beam diffraction condition of **g**(5**g**), for **g** = {200}, at an acceleration voltage of 200kV. This is the usual diffraction condition used for the identification of dislocation loops and stacking fault tetrahedra in face centred cubic metals. Results indicate that image contrasts increase with increasing size of the loops and reach saturation at a size of about 30 interstitials corresponding to a size of about 2nm. Interestingly, the loop image contrast in the case of Aluminium is similar to the case of Nickel (Fig. 2.4.5), although the scattering power is much lower (Fig. 2.4.6).

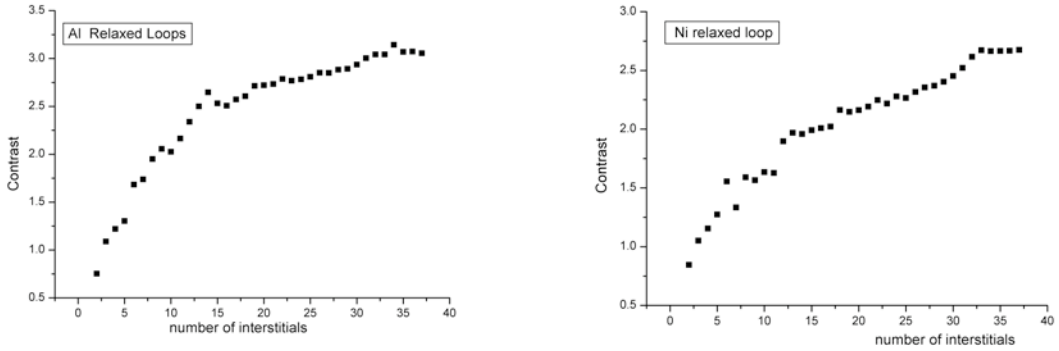

Fig. 2.4.5 *Contrast of the simulated TEM image of an interstitial loop as a function of the number of interstitials contained in the loop, in Aluminium (left) and in Nickel (right). Contrast is defined as the ratio of the maximum and minimum intensities.*

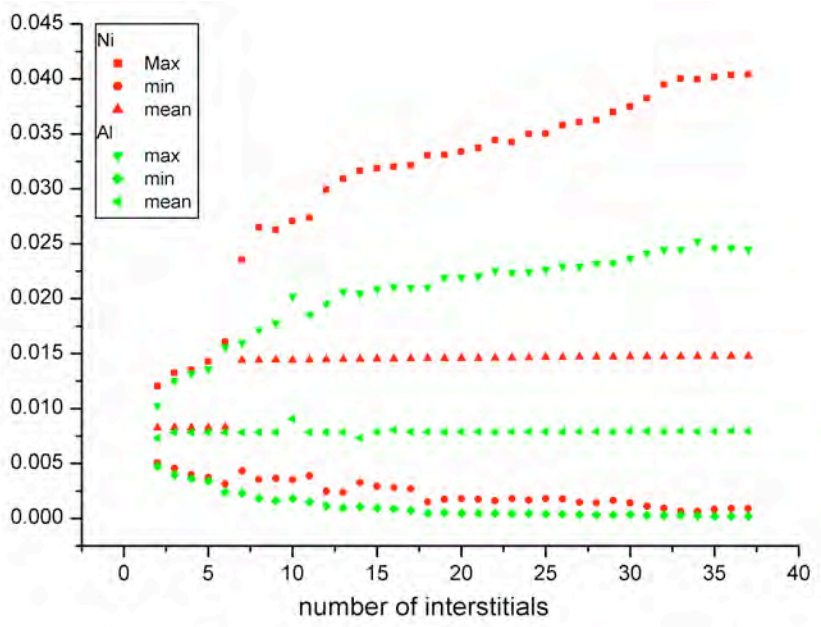

Fig. 2.4.6 *Maximum, minimum and mean intensities of simulated TEM weak beam images of an interstitial loop in Nickel (red) and Aluminium (green) as a function of the number of interstitials contained in the loop. Intensities are normalised to the incident electron beam intensity*

Study of the relation between irradiation-induced microstructure and mechanical properties in Zr alloys

The evolution of the tensile properties after neutron irradiation of Zircaloy cladding tubes have to be assessed from non-conventional tests, like small ball punch tests. The small ball punch test technique has been extensively used in the past to extract tensile and fracture properties. The test consists in clamping a 3mm-diameter disk between two dies and in deforming it with a 1mm diameter steel ball; the load–deflection curve is then measured. From the yield and maximum loads of the curve, calibrations with the yield stress and the ultimate tensile stress obtained from plain tensile tests are usually done. Similarly, calibrations between the ductile-to-brittle transition temperature (DBTT) obtained from punch tests and

standard Charpy impact tests can be done. The DBTT from the punch tests is determined by plotting the temperature dependence of the area below the load displacement curve, which mimics that of the Charpy tests. However, more information regarding the tensile and constitutive behaviours of a material can be obtained by performing finite element simulations of the punch tests and using an inverted procedure to extract the key parameters of the constitutive behaviour. This is of course of primary importance if the constitutive behaviour has to be evaluated from ball punch tests only, when no tensile specimens are available. These parameters are basically the yield stress and the strain-hardening coefficient and are used as input for the finite element simulations. They are iteratively adjusted until the load-displacement curve of the punch test is reproduced. Thus, a finite element model for the punch tests was developed and the preliminary results, obtained for two steels (the EUROFER 97 RAFM steel and the 316L stainless steel) are presented below.

The axisymmetric configuration of the ball punch test experimental device and specimen was modelled with ABAQUS/Standard 6.3. The disk was meshed with 2000 axisymmetric elements, 20 elements in thickness and 100 elements in length. The elements have 4 nodes, with linear integration and are of incompatible mode type. The puncher was modelled as an analytical rigid surface. The interaction between the puncher and the specimen is defined as a contact pair interaction that was chosen to be frictionless. The contact interaction between the disk and the upper and lower dies is defined by clamping the disk with a constant load applied through the dies. Typically, the load applied was 2000N, small enough to avoid plastic deformation. A friction coefficient between the dies and the disk was considered and was taken equal to 0.2. The specimen is deformed by imposing a displacement to the puncher. In Fig. 2.4.7, a schematic representation of the model is shown. The constitutive behaviour used for the simulations was obtained from the experimental tensile curves at room temperature.

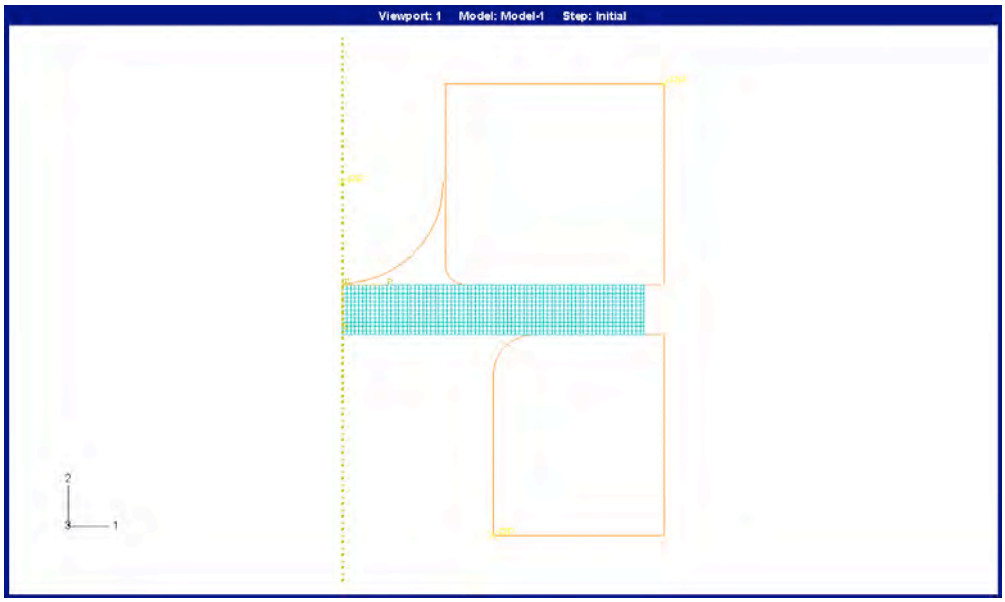

Fig. 2.4.7 *Finite element mesh of the small ball punch device*

Figures 2.4.8 and 2.4.9 show a snapshot of the highly plastically deformed specimen and the simulated curves along with the experimental ones for both steels, respectively. The simulations were run for a displacement of 0.5mm. A reasonably good agreement was found between the simulations and the experiments. Further analysis is currently in progress in particular to assess the sensitivity of the yield stress and strain-hardening coefficient on the simulated

curves. Hence, it will be possible to determine the confidence level in the determination of these last parameters from ball punch tests only.

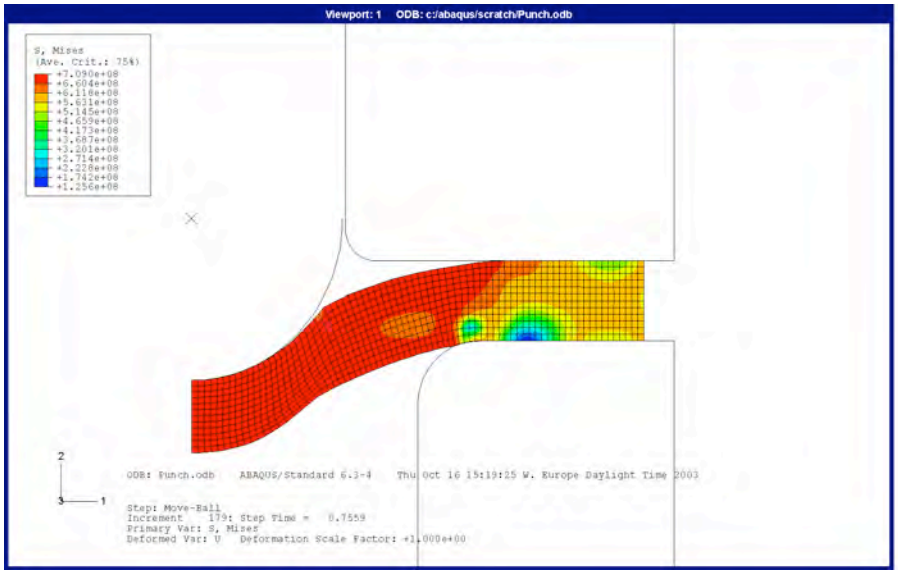

Fig. 2.4.8 *Illustration of the ball punch deformation*

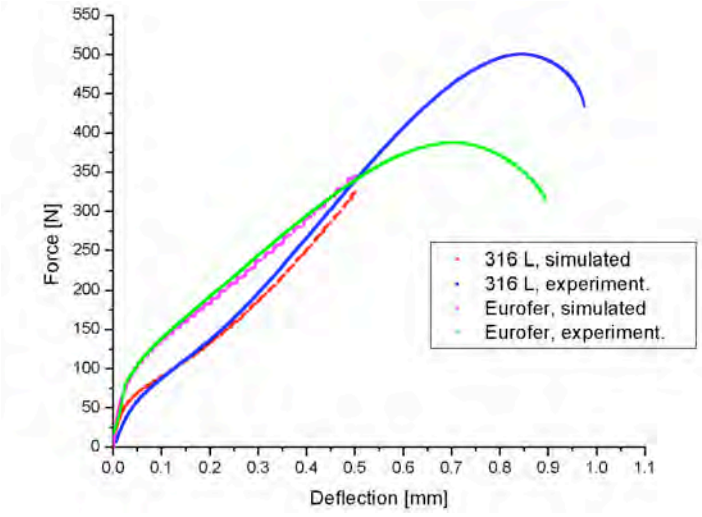

Fig. 2.4.9 *Experimental and simulated ball punch curves*

Irradiation effects on the microstructure, mechanical properties and residual stresses in the heat affected zone of stainless steel welds

The properties of irradiated austenitic stainless steel welds are important for lifetime assessments of reactor internals in Light Water Reactors (LWRs). Typical welds based on the standard austenitic stainless steels 304 and 347 are being studied as part of the project INTERWELD (5th European Framework Program). The mechanical properties, the microstructure and the residual stress distributions in the welds (base metal, heat affected zone HAZ) are being investigated with regard to tensile stress/strain response, TEM characterisation and neutron diffraction.

Figure 2.4.10 shows a comparison of the microstructures near the fusion line (Fig. 2.4.10a), where heavily deformed areas and re-crystallised grains can be seen, and away from it (Fig. 2.4.10b). The structural differences lead one to expect an

increase in yield strength in the HAZ area, as compared to the unaffected base metal, which was experimentally verified (Figures 2.4.11a and 2.4.11b).

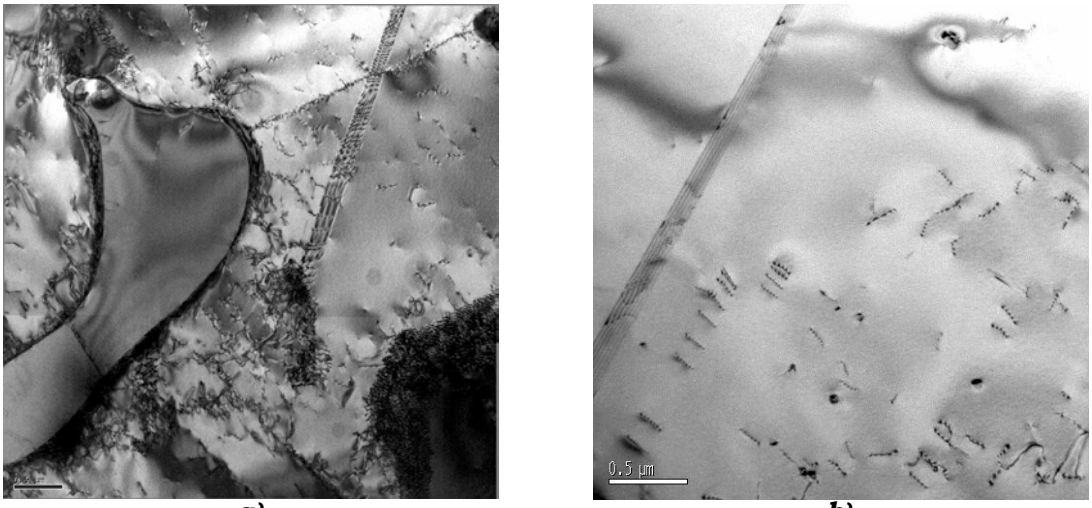

a) ***b)***

Fig. 2.4.10 *a) TEM image of the 347 stainless steel, close to the fusion line; b) TEM image of the 347 stainless steel, far away from the fusion line*

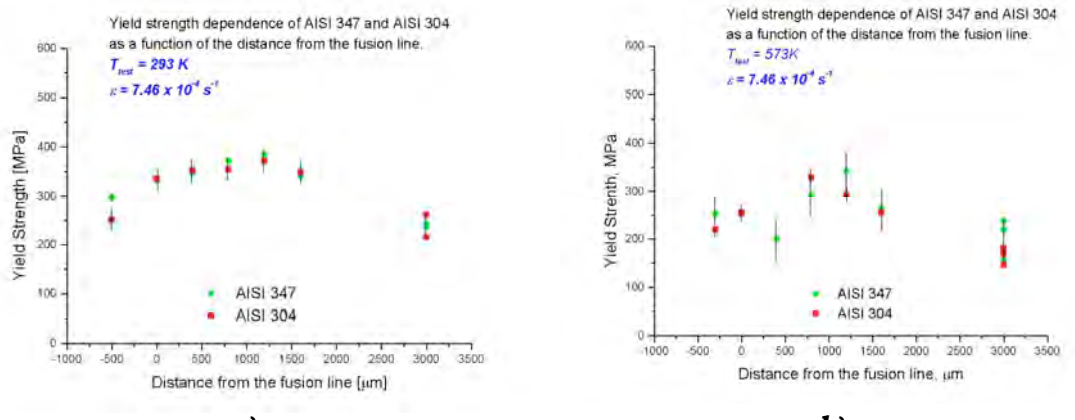

a) ***b)***

Fig. 2.4.11 *a) Tensile yield strength at room temperature as a function of the distance from the fusion line; b) Tensile yield strength at 300°C as a function of the distance from the fusion line*

Preliminary stress measurements using neutron diffraction revealed the presence of high residual stresses in the welds, which might be a direct consequence of the very pronounced differences in the microstructure as a function of the distance from the fusion line.

The deformation behaviour has also been investigated. Twinning was identified as an important deformation mechanism at room temperature (Fig. 2.4.12a). At higher temperature, 300°C, dislocation glide was mainly observed (Fig. 2.4.12b). No strain-rate sensitivity of the stress was seen. During the next stage of this study, materials neutron-irradiated in fission reactors will be investigated.

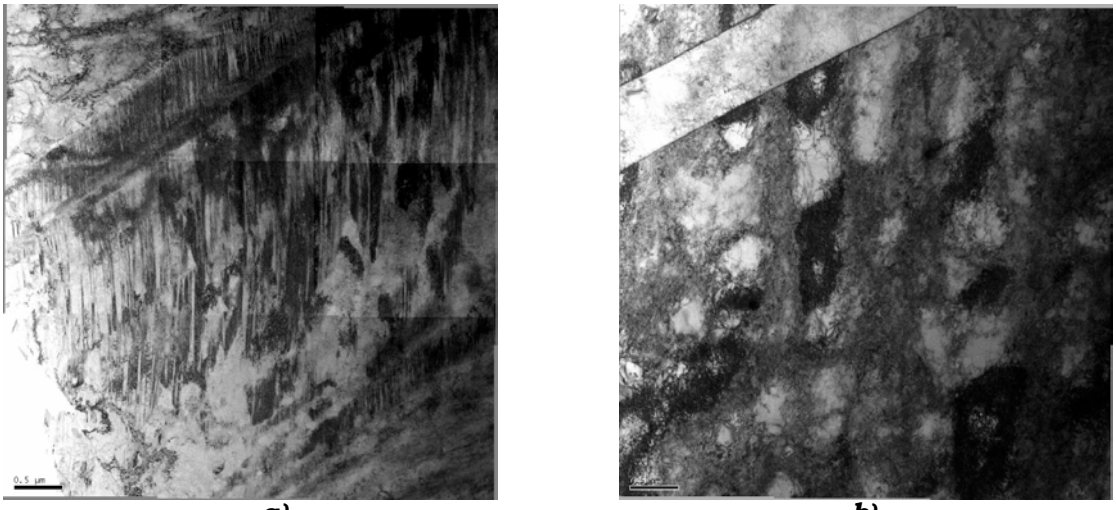

a) *b)*

Fig. 2.4.12 *a) TEM image of the 347 stainless steel, tensile tested at room temperature, close to the fusion line; b)TEM image of the 347 stainless steel, tensile tested at 300°C, close to the fusion line*

Small angle neutron scattering measurements

Small angle neutron scattering (SANS) measurements were carried out on various unirradiated and irradiated body-centred-cubic materials, namely three RAFM steels, the OPTIMAX A, the EUROFER 97 and the F82H based on the 9%Cr/W/V/Ta composition, and pure Iron. For each material, specimens have been irradiated with 590MeV protons in the PIREX facility at the PSI. Different irradiation temperatures and doses were investigated, ranging from 50°C to 350°C and from 0.3 to 2dpa, respectively. The SANS measurements were performed at room temperature with a saturating magnetic field applied to the specimens.

Qualitatively, it was found that a significant additional scattering intensity, with respect to the unirradiated specimens, occurs for all the irradiated ones for Q values larger than $0.7nm^{-1}$. This additional scattering intensity was obtained by subtracting off the scattering of the unirradiated control specimen to that of the irradiated one. In order to characterise the distribution of the irradiation-induced scattering features, we used the equation for the differential coherent small angle cross-section $d\Sigma/d\Omega$, which is proportional to the scattered intensity, for a dilute distribution of a single type of spherical scattering features:

$$\frac{d\Sigma}{d\Omega}(\vec{Q}) = \Delta\rho^2 \int N(R)V_p^2(R)P(\vec{Q},R)dR$$

where N(R)dR is the number of particles per unit volume having a diameter between R and R+dR, $V_p(R)$ is the volume of a particle and P(Q,R) is the form factor of a particle. $\Delta\rho$ is the difference between the scattering length density of the feature and that of the matrix, the so-called contrast. We already showed that the scattering associated with the irradiation-induced defects is consistent with a distribution of nanospheres whose size peaks at about 0.6nm. For the last series of measurement, we applied a saturating magnetic field (horizontal and perpendicular to the beam) to the specimens so that the coherent small angle neutron scattering arises from variations in the scattering length density in nuclear contrast as well as in magnetic contrast:

$$\Delta\rho^2 = \Delta\rho_n{}^2 + \Delta\rho_m{}^2 \sin^2(\phi)$$

where ϕ is the angle between the applied magnetic field direction and the projected observation direction onto the plane perpendicular to the neutron beam. The general equation for the cross-section in the case of magnetic plus nuclear scattering can then be written as:

$$\frac{d\Sigma}{d\Omega}(\vec{Q},\phi) = \frac{d\Sigma_{Nucl}}{d\Omega}(\vec{Q}) + \frac{d\Sigma_{Mag}}{d\Omega}(\vec{Q})\sin^2(\phi)$$

In the Q-range [0.3–1.2]nm^{-1}, it was possible to properly separate the nuclear contribution from the magnetic one. The main advantage of extracting the magnetic scattering is that it represents simultaneously the contributions of the irradiation-induced nanovoids and Helium bubbles, which are both magnetic holes in the microstructure. A typical example is given in Fig. 2.4.13, for the EUROFER 97 RAFM steel irradiated at 250°C to 1dpa, whose the data were analysed by sectors 10° wide. In Fig. 2.4.13, the scattered intensity is averaged on the angular sectors and the angle indicated refers to that of the sector centre. As expected, the scattering increases with the angle ϕ, going from pure nuclear scattering at 0° to nuclear plus full magnetic scattering at 90°. Further, we could deduce the ratio M/N, with $M = \Delta\rho^2_m$ and $N = \Delta\rho^2_n$, by plotting $(\Delta\Sigma_{nucl}/\Delta\Omega+\Delta\Sigma_{mag}/\Delta\Omega)/(\Delta\Sigma_{nucl}/\Delta\Omega)$. The ratio M/N was found equal to about 1.5 (Fig. 2.4.14).

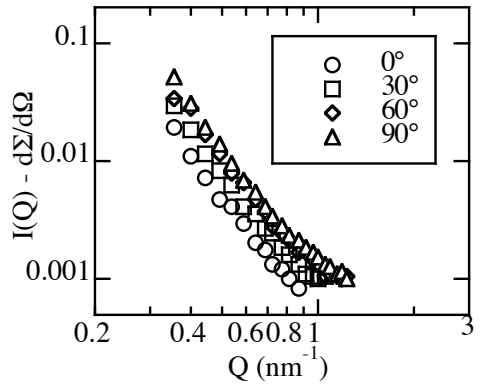

Fig. 2.4.13 *Arbitrary scattered intensity versus Q, averaged on angular sectors 10° wide*

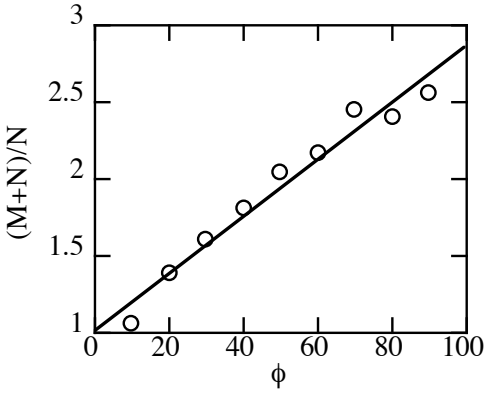

Fig. 2.4.14 *(M+N)/N ratio versus angle ϕ*

Additional measurements are foreseen in order to get the absolute scattering cross sections to determine the actual number density and size distribution of the nano-features and possibly their chemical composition. Ultimately, these data will be integrated into a more comprehensive model of irradiation-induced hardening.

Development of transmission electron microscopy techniques

A new objective aperture has been developed in collaboration with Dr. N. Nita from the University of Sendai, Japan. Following a simulation study, it appeared that a larger directional objective aperture should result in a higher spatial resolution in dark field weak beam imaging. More precisely, the present aperture of 35μm in diameter provides a resolution of about 0.6nm in Copper. We designed a new aperture, rectangular in shape, providing a resolution of about 0.3nm, half the original one. This new aperture, of 40x100μm^2, was milled by focused ion beam (FIB) at Sendai University, inside a 15μm-thick Molybdenum foil provided by the Fusion Technology Materials group (Fig. 2.4.15).

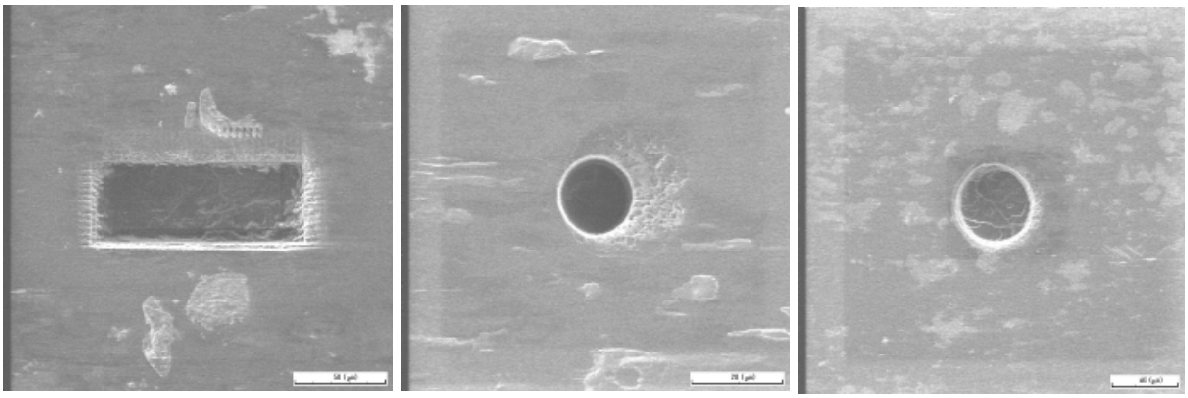

Fig. 2.4.15 *SEM images of the apertures cut by FIB at Sendai University inside a 15μm-thick Mo foil (10, 40 and 40x100μm^2 apertures from left to right)*

Figure 2.4.16 shows the improvement in resolution with this aperture, as obtained in our JEOL2010 transmission electron microscope at the PSI, operated at its nominal acceleration voltage of 200kV. The use of the new aperture allows identification of the truncation of the irradiation-induced stacking fault tetrahedra (SFTs). It appears in Fig. 2.4.16 that the left SFT on the far right image is in fact not truncated on its left wing, contrary to what the first image (left) seems to exhibit with the smallest aperture.

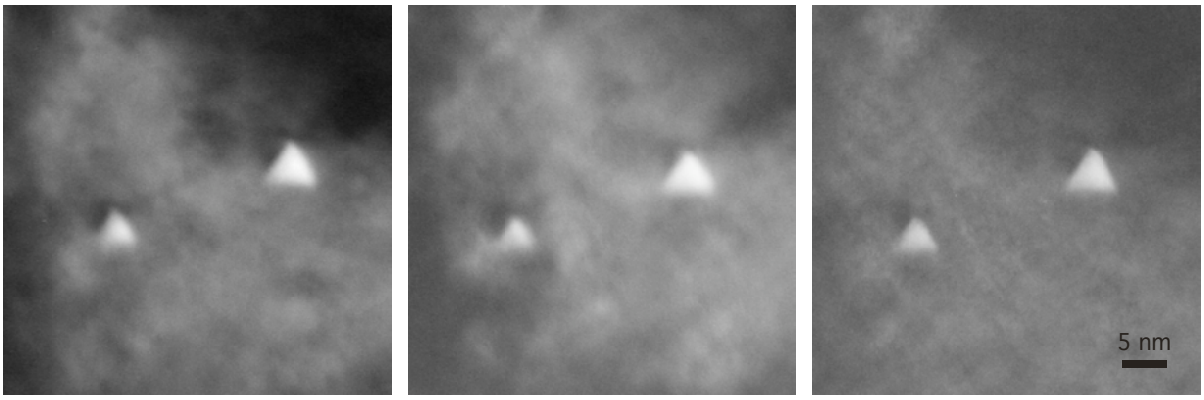

Fig. 2.4.16 *Gold quenched in water from the melting temperature. TEM dark field weak beam image, **g**(6**g**), **g** = {200}, at 200kV, as a function of the objective aperture size. Left: 10μm, middle: 40μm, right: 40x100μm^2 aperture*

2.4.3 EFDA Technology Tasks

Tasks Long Term

TW0-TTMI-003 deliverable 3: Small specimen test technology - Development of experimental fracture testing devices to be used in a hot cell environment and constraint loss assessment on sub-sized compact specimens of EUROFER 97

A completely new traction load train was designed and set up in an electromechanical testing machine Schenck type RMC100. New grips for sub-sized compact tension specimens and tensile specimens were also machined. The system was designed in such a way that it is very easy to set up the specimens so that the necessary handling can be done in a hot cell environment in the future. This new load train has already been used to run a series of tests at room temperature on a variety on tempered martensitic model alloys. Tensile tests were carried out on Fe-Cr-C tempered martensitic model alloys and on the EUROFER 97 RAFM steel. The load train is a self-aligning system and was found to operate very well in terms of the reproducibility of the mechanical test results. Recently, a low temperature chamber was installed. The temperature calibration for a variety of specimen geometries is in progress and the low temperature mechanical testing will be carried out before the end of 2003.

TW1-TTMS-001 deliverable 3: Proton irradiation of EUROFER 97 up to 1dpa of plate, for He effect testing

Proton irradiations at 300°C of mini-bend bars (1mmx1mmx12mm) of the EUROFER 97 RAFM steel were completed during the first semester of 2003. In total, 12 mini-bend bars were irradiated up to about 0.5dpa. Characterisation of the fracture toughness-temperature curve via 3-point bend testing will take place in 2004, after the cooling down period.

TW1-TTMS-002 deliverable 20: Tensile and fracture toughness of EUROFER 97, punch testing

In order to investigate the helium effects on the ductile-to-brittle transition temperature of the EUROFER 97 RAFM steel, determined by small punch tests, a neutron irradiation has been foreseen in the KFKI reactor in Budapest to supplement the proton irradiations previously performed in the PIREX facility. In June, a series of ball punch specimens (3mm diameter disks, 0.3mm thick) and tensile flat specimens (8mm in gauge length, 2.5mm in width, 0.3mm in thickness) of EUROFER 97 was sent to Budapest, Hungary, to be neutron-irradiated in the KFKI reactor at 150°C to 0.5dpa. This irradiation is expected to be completed by the end of 2003 and the specimens sent back to Switzerland in 2004.

TW2-TTMS-006a deliverable 3: Creep testing at RT-750°C on the two improved ODS batches

A number of cylindrical creep specimens, with a diameter of 2mm and a gauge length of 7.6mm, have been cut out by spark erosion from the ODS EUROFER (the EUROFER 97 RAFM steel reinforced with 0.3wt.% Y_2O_3 particles) prepared by the CRPP. Creep testing is in progress, using a locally constructed creep machine operating at constant stress in an argon flow. Creep tests at 600, 650, 700 and 750°C, under creep stresses of 300, 200, 180 and 120MPa, respectively, have been

completed. Preliminary results indicate a significant improvement in creep properties with respect to those presented by the EUROFER 97 alone. A maximum of three creep experiments at three different creep stresses will be performed at each temperature of interest (200, 400, 600, 650, 700, 750°C). A total of 14 experiments still have to be finished. Creep testing of the CRPP material should be completed in November 2003. On the other hand, some amount of the ODS EUROFER prepared by CEA-Grenoble has been received from FZK (Forschungszentrum Karlsruhe) on October 21, 2003. Corresponding creep testing will be performed at the beginning of 2004, following preparation of the specimens by spark erosion.

TW2-TTMS-006a deliverable 6: Tensile testing at RT-750°C on the two improved ODS batches

A number of tensile flat specimens, 2.5mm in width, 0.3mm in thickness and 8mm in gauge length, have been cut out by spark erosion from the ODS EUROFER (the EUROFER 97 RAFM steel reinforced with 0.3wt.% Y_2O_3 particles) prepared by the CRPP. Tensile testing at constant strain rate is in progress, using a Zwick testing machine operating in an argon flow. Preliminary results appear very promising in terms of high strength values and non-negligible tensile elongations. Unfortunately, our high temperature specimen holder in TZM broke at the beginning of June. A new one was designed and built, which was tested successfully last October. Tensile testing of the CRPP material should be completed in November 2003. On the other hand, some amount of the ODS EUROFER prepared by CEA-Grenoble has been received from FZK (Forschungszentrum Karlsruhe) on October 21, 2003. Corresponding tensile testing will be performed at the beginning of 2004, following preparation of the specimens by spark erosion.

TW2-TTMS-004b deliverable 3: Development and testing of coatings to improve the corrosion resistance vs Pb17Li at T>450°C

Following a recent European meeting organised in Brasimone on protection barriers against corrosion by Pb-17Li at 550°C, contacts have been made with a number of companies with the aim of depositing different types of coatings, mostly W-based and Cr-based, on 10-mm diameter cylindrical specimens of the EUROFER 97 RAFM steel. The most interesting coatings include plasma sprayed W, W-Y_2O_3 and W-Re thick coatings and W, Cr, Ti, Ta and diamond-like-carbon thin coatings to be deposited either by physical vapor deposition (PVD) or galvanic methods. Definitive selection of the coatings to be deposited is in progress. Deposition experiments will be performed at the end of 2003, so that corrosion experiments in a turbulent flow of Pb-17Li at 550°C can be started at the beginning of 2004.

TW2-TTMS-005b deliverable 6 : Small-scale fracture mechanics - Modelling of brittle and brittle to ductile transition behaviours using appropriated theories. Formation of rules for transferability to standards and fusion components

The two main activities performed in the frame of this work were i) tensile mechanical testing to investigate the constitutive behaviour and ii) finite element simulations.

i) A series of tensile tests was carried out at room temperature on the EUROFER 97 RAFM steel and different tempered martensitic model alloys to investigate their constitutive behaviour. The model alloys are based on the Fe-9Cr-0.1C and Fe-12Cr-0.1C chemical compositions. They were produced (composition and heat-treatment) in such a way to vary only one microstructural parameter per alloy. In particular, the effects of the prior austenite grain (PAG) size and tempering

conditions were investigated. Alloys with different PAG sizes, namely 30 and 130μm, were produced and heat-treated under two different tempering conditions, yielding either a lath martensite or a sub-grain/lath microstructure. The effect of PAG size on the yield stress and strain hardening was investigated. It was found that the PAG size hardly affects the yield stress while the strain-hardening behaviour is insensitive to it.

The post-yield behaviour was modelled in the frame of dislocation mechanics. In order to model the stress dependence of the plastic strain-hardening, $\theta_p(\sigma_{pl})$, a phenomenological description of strain-hardening was used, based on a one structural parameter model, namely the total dislocation density. The flow stress is decomposed into two components: the yield stress, $\sigma_{0.2}$, and the contribution arising from the plastic strain, $\sigma_{d\text{-}d}$, due to dislocation-dislocation interaction. The component $\sigma_{d\text{-}d}$ is taken proportional to $\rho^{1/2}$, where ρ is the total dislocation density, and is written as:

$$\sigma_{d-d}(\varepsilon_p) = M\alpha Gb\sqrt{\rho} = M\alpha Gb\sqrt{\rho_o + \Delta\rho(\varepsilon_p)}$$

where M is the Taylor factor, α is a dimensionless constant, G is the shear modulus and b the magnitude of the Burgers vector. In this equation $\rho(\varepsilon_p)$ is equal to $\rho(\varepsilon_p) = \rho_o + \Delta\rho(\varepsilon_p)$ with ρ_o being the grown-in dislocation density and $\Delta\rho(\varepsilon_p)$ the net increase in ρ at ε_p. It follows that $\sigma_{d\text{-}d}$ can be written as:

$$\sigma_{d-d}(\varepsilon_p) = \sigma^{o}_{d-d}(\rho_o) + \sigma^{*}_{d-d}(\Delta\rho(\varepsilon_p))$$

with

$$\sigma^{o}_{d-d} = M\alpha Gb\sqrt{\rho_o}\,.$$

Based upon the definition of the plastic strain hardening, $\theta_p = d\sigma_{tot}/d\varepsilon_p$, it follows that θ_p is equal to $d\sigma_{d\text{-}d}/d\varepsilon_p$. Considering the total dislocation density, ρ, as the micromechanical parameter of the model, it appears that the strain hardening is controlled by the evolution of ρ with the plastic strain, i.e., $d\rho/d\varepsilon_p$. Thus, the strain evolution of ρ results from a storage (or multiplication) term due to the locking of dislocations at immobile obstacles and an annihilation term taking into account all the annihilation mechanisms. Assuming a mean displacement distance for the dislocations L, assumed constant for the plastic strain range considered, and assuming that the dynamic recovery is linear in ρ, the dislocation density evolution equation is given by:

$$\frac{d\rho}{d\varepsilon_p} = M\left(\frac{1}{bL} - a\rho\right)$$

where the first term in the brackets relates to the storage mechanisms and the second one to the annihilation processes. By combining the above equations and using the definition of the strain hardening, $\theta_p = d\sigma_{d\text{-}d}/d\varepsilon_p$, the strain hardening can be expressed as:

$$\theta_p(\sigma_{d-d}) = \frac{P_1}{\sigma_{d-d}} - P_2\sigma_{d-d} = \frac{P_1}{\sigma^{o}_{d-d} + \sigma^{*}_{d-d}} - P_2(\sigma^{o}_{d-d} + \sigma^{*}_{d-d})$$

with P_1 and P_2 defined as:

$$P_1 = M^3(\alpha G)^2\frac{b}{2L} \qquad\qquad P_2 = \frac{Ma}{2}$$

An example of this analysis is shown in Fig. 2.4.17, where the strain hardening is plotted against $\sigma_{d\text{-}d}$ and the fit to the data is indicated.

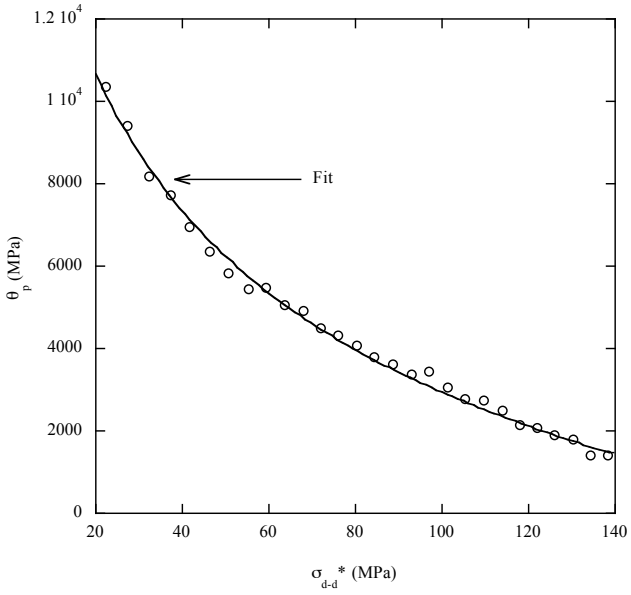

Fig. 2.4.17 *θ_p versus $\sigma_{d\text{-}d}$*, for the Fe-9Cr-0.1C model alloy tensile tested at room temperature.*

For all model alloys, it was found that the mean displacement of the dislocations, L, is independent of the PAG size. The parameter L seems to be controlled by microstructural features whose spacing is smaller than the PAG size and that might be the lath boundaries impeding the dislocation motion in conjunction with the carbide distribution they contain.

ii) In order to assess the transferability of local cleavage criterion, finite element simulations have been initiated, which will be used to determine the local stress/strain fields acting ahead of various stress concentrators. In particular, we are assessing the possibility of using the well-known local critical stress - critical volume criterion for cleavage, when the stress distributions in two specimens are different. Single edge notched bend bars were simulated with in the first case a pre-cracked and in the second case a notch. The specimens were loaded in 3-point bending and a Ramberg-Osgood constitutive law was used for these preliminary simulations. This allows a straightforward comparison with already published work from other authors, but it is planned to run the simulations again with the real constitutive behaviour of the tempered martensitic steel that is under development. The models were built with ABAQUS 6.3. The deformation was applied by imposing the displacement of the punch. The stress fields that develop in the pre-cracked and the notched specimens are presented in Fig. 2.4.18, where the stresses are normalised by the yield stress and plotted against the distance ahead of the stress concentrator. Clearly, the height of the peak stress for the notched specimen is lower than for the pre-cracked specimen and the peak stress is much broader. To be able to check the transferability criterion, mechanical testing at different temperatures using both specimen geometries is under way, while simultaneously running finite element analysis.

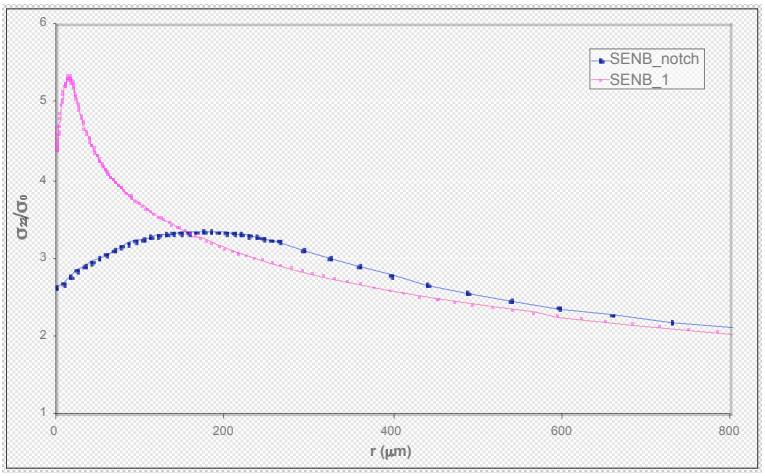

Fig. 2.4.18 *Stress distribution ahead of a pre-cracked specimen (in red) and a notched specimen (in blue).*

TW3-TTMA-002 deliverable 2: W coating onto RAFM alloys

Eight cylindrical specimens, with a diameter of 25mm and a height of 10mm, have been prepared from a plate of EUROFER 97 by spark erosion. A 50μm-thick layer of pure Copper has been deposited using a galvanic method onto the surface of these eight specimens. Pre-coated specimens have been subsequently sent to the Archer company (UK) for deposition of mm-thick Tungsten coatings by chemical vapour deposition (CVD). Note that pre-deposition of a Copper layer onto the EUROFER 97 substrates is needed as the adherence of W-CVD coatings on steel substrates is known to be close to zero. The CVD-W coated specimens should be available at the end of 2003 and characterised by combining bond strength and hardness measurements with scratch testing and microscopic observations.

TW3-TTMS-005 deliverable 1: Low cycle fatigue testing of EUROFER 97

This work is aimed at testing the EUROFER 97 RAFM steel in the condition of low cycle fatigue (LCF). The fatigue will be strain controlled at room temperature, 150°C, 300°C and 550°C. The tests will be run in vacuum using strains of 0.5%, 0.8% and 1.4%. Tests with 500sec hold times will be also run, at the same temperatures and using the same imposed strains. The first step of this project consists in the development of a new fatigue mini-specimen, suitable for irradiation in reactors (small size, small mass) and having a gauge design similar to the existing standard specimens. A visit to FZK (Forschungszentrum Karlsruhe) is being planned for the end of October 2003. European joint discussions will lead to the definition of anew specimen geometry to be used in the next years. The new specimen will be then tested at room temperature in LCF and validated by comparing the obtained results to those previously obtained using standard specimens. The needed load train is already available as well as the testing software. Systematic LCF tests will be started at the beginning of 2004.

TW3-TTMS-005 deliverable 2: Investigation (tensile and Charpy testing) of PHT and PWHT to improve the design limits and to define the acceptable temperature range

No activity has been undertaken yet since the post-weld heat-treated plates are not available for the time being.

TW3-TTMS-006 deliverable 3: Study of the influence of Ti addition on the mechanical properties (Charpy, tensile) with characterisation of the full fabrication process

A literature survey was made in order to determine the adequacy of the selected amounts of additions of Titanium to the ODS EUROFER. The matrix material is the EUROFER 97 RAFM steel. The base reinforcing dispersion is made out of Y_2O_3 particles. It appears that 0.3 and 1.0wt.% Titanium constitute respectively the lower and upper limits of what is used in other laboratories to improve tentatively the Y_2O_3 spatial distribution, reduce the Y_2O_3 particle size and decrease O segregation that is detrimental to fracture properties. Atomised EUROFER 97 has been sieved to particles smaller than 45μm and mixed with 0.3wt.% Y_2O_3 particles, 10 to 30nm in size, and with Titanium powder, by ball milling for 24 hours under Argon atmosphere. Two compositions are being tested, one with 0.3wt.% and the other with 1.0wt.% Titanium. This work is being performed in collaboration with University Carlos III, Madrid, Spain. The resulting ODS powder was sent to the Haute Ecole Valaisanne (Sion, Switzerland) for the final processing. There, the powder will be pre-pressed uniaxially under 35MPa at 1100°C for a few minutes to close as much as possible the porosity, and cooled down. Final compaction will be made in a hot isostatic press (HIP) under 180MPa at 1100°C for 1 hour. Mechanical characterisation of the batches will be performed at the beginning of 2004 via tensile tests and Charpy impact tests.

TW3-TTMS-007 deliverable 7: Molecular dynamics simulations of grain boundaries: evolution of displacement cascades in nanocrystalline Fe samples created with an available Fe potential

Large-scale molecular dynamics simulations of displacement cascade production have been performed in nanocrystalline (nc) face centred cubic (fcc) Nickel with 5nm, 12nm and 20nm average grain diameters. Primary Knock-on Atom (PKA) kinetic energies in a 5-30keV range have been simulated. The high concentration of grain boundaries (GBs) present in our samples, known as sink sources for interstitials and vacancies, enable us to study their role during irradiation.

Introduction of a PKA induces a cascade core region that develops where atoms have been displaced from their lattice positions. During cooling, most atoms return to lattice positions, leaving some damage in the form of interstitials and vacancies that do not recombine. Interstitials left in the grain move via 1D/3D motion to sinks present in the form of GB dislocations, triple junctions and vacancies. The pressure gradient present within the structure influences interstitial movement to the surrounding GBs and therefore the resulting defect structure formed during displacement cascades, shown in Fig. 2.4.19. Initially, the interstitials see the GB region as a 'defect collector plate', a 2D homogeneous region under tension which they move towards. At a certain distance the interstitials are able to distinguish between the local variations in the pressure present in the interphase region, changing their direction 3D to avoid higher compressive regions (red spheres) and move to regions of higher tensile pressure (purple spheres) during their movement to the GB. Consequently, even large interstitial clusters (of up to 6 interstitials) have been seen to move 1D/3D. In contrast, in single crystal simulations pure 1D motion is observed for clusters containing four or more interstitials.

The damage remaining in the grain is affected by the size and proximity of the displacement cascade to the surrounding GBs. Four scenarios have been distinguished: when the cascade is far from the GB (approximating the single crystal); when the cascade is close to the GB; when the cascade periphery touches the GB and when the GB is in the cascade core region. Within these different scenarios, the GB has been found to be flexible, with very local movement

accommodating the influx of interstitials when the GB is outside the cascade core. When GBs are situated within the cascade core no damage or more significant damage has been seen. When a cascade encompasses several grains more significant GB movement occurs which can lead to both grain refinement and grain growth as seen in experiments.

On the other hand, preliminary simulations in body centred cubic (bcc) single crystal and nc Fe have been performed. Initial Ackland potential results show that interstitials are attracted to GB regions; the remaining damage inside the grains is made up of vacancies; the size of these vacancy defect clusters are very small, differing from the vacancy defects seen in the fcc samples.

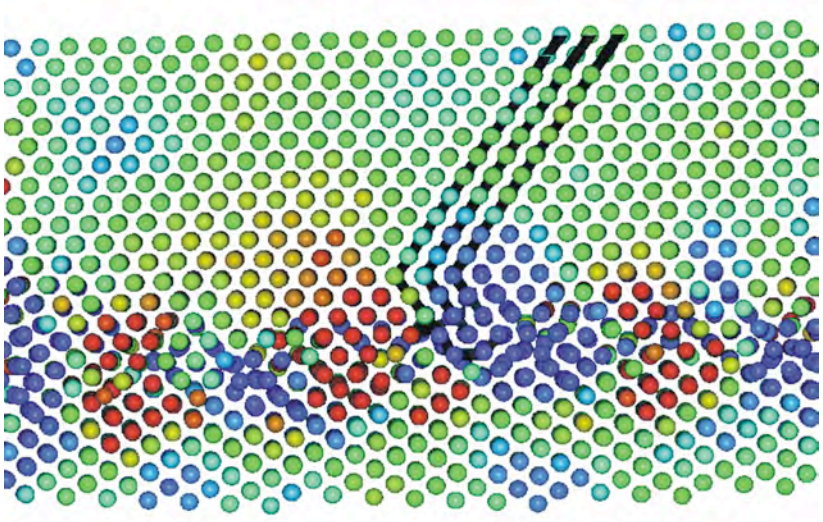

Fig. 2.4.19 *Section of 12nm nc Nickel in the vicinity of a Grain-Boundary. Red indicates regions of high compression and purple represents regions of high tension. The 1D/3D motion of a 6-interstitial cluster (black lines) is superimposed onto the pressure of the sample before introduction of the cascade.*

TW3-TTMS-007 deliverable 8: Irradiation in SINQ

Specimens to be irradiated in 2004/2005 in the Swiss Spallation Neutron Source (SINQ) have been prepared within the Underlying Technology programme. They include tensile flat specimens, mini-Charpy's, TEM specimens and coupons for small angle neutron scattering measurements of the EUROFER 97 RAFM steel, the ODS EUROFER (EUROFER 97 reinforced with 0.3wt.% Y_2O_3 particles) and two Ti-base alloys (Ti-6Al-4V, Ti-5Al-2.5Sn). Specimens are being mounted into specimen holders within this project. The SINQ irradiation will be performed using 9mm internal diameter Zircaloy tubes inserted into the solid target. The specimens are being packed with either Zircaloy or Aluminium. Two or three thermocouples per tube are used to monitor the irradiation temperature. The irradiation spectrum is a mixture of high-energy protons (original energy: 590MeV) and 30 to 50% of spallation neutrons, depending on the position of the tube inside the target. In order to evaluate correctly the dose at each position, activation foils are used. The activation results will be analysed using the high-energy nuclear transport codes LAHET and MCNP-X. The doses and irradiation temperatures vary according to the position of the tube inside the target, as it is irradiated with different regions of the proton beam profile. Both Helium and Hydrogen are produced as result of spallation reactions. Measured values of Helium production in the F82H RAFM steel after a one year campaign in SINQ vary between 1024appm (11.8dpa, T_{irr}=330/360°C) and 214appm (4dpa, T_{irr}=78/91°C), while 360 and 665appm Helium have been measured respectively for the same irradiation conditions. Mounting is being performed so that enough specimens will be

irradiated in a given irradiation condition, which will allow us to perform subsequently systematic, valuable mechanical tests on irradiated specimens. Mounting will be completed at the end of 2003, so that the irradiation can be started in spring 2004, following the annual winter shutdown of the PSI proton accelerator.

Tasks Next Step

TW1-TVV/Titan: Titanium alloy irradiation testing

In order to comply with the working conditions of ITER, it was decided to extend the initial programme and to test titanium alloys (Ti-6Al-4V, Ti-5Al-2.5Sn) at a temperature of 150°C. Tensile flat specimens (8mm in gauge length x2.5mm in width x0.3mm in thickness) and mini-Charpy specimens (3x4x27mm^3) of both materials have therefore been irradiated with 590MeV protons in the PIREX facility at 150°C to 0.2dpa. Results of post-irradiation tensile tests seem to indicate that the Ti-6Al-4V alloy is more affected by the irradiation, in terms of hardening and loss of ductility, as compared to the Ti-5Al-2.5Sn alloy. The crack initiation fracture toughness values appear strongly reduced after irradiation, especially when tested at room temperature. At 150°C the reduction in fracture toughness is more pronounced for the Ti-6Al-4V alloy. Nevertheless, although relatively large changes are obtained in the mechanical test results, before and after irradiation, no difference does show up in the corresponding fractographs. All the fractographs reveal a ductile fracture mode (compare Figs 2.4.20a and 2.4.20b). In addition, a series of six irradiated specimens has been sent to Battelle, Richland (USA), in order to measure the Hydrogen amount generated by the high-energy proton irradiation. The information is necessary for understanding if the irradiation-induced Hydrogen actually plays a role in the observed embrittlement effects.

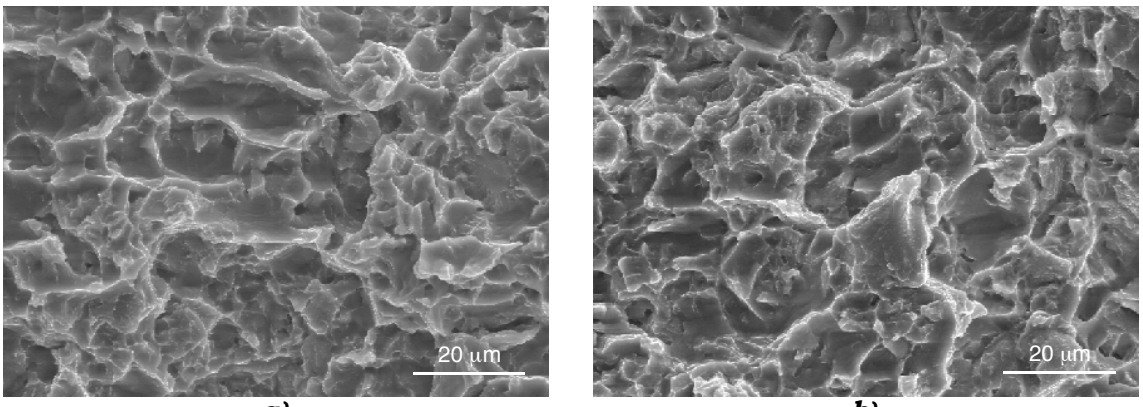

a) ***b)***

Fig. 2.4.20 *a) Fractograph of unirradiated Ti-6Al-4V; b) Fractograph of irradiated Ti-6Al-4V*

TW1-TVV/Beam: In-beam mechanical testing of CuCrZr

The object of this work was to investigate the mechanical behaviour of the CuCrZr alloy in the condition of in-beam fatigue. A series of experiments have been conducted using an in situ fatigue device to study the behaviour of the CuCrZr alloy under cyclic deformation and concurrent irradiation with 590MeV protons, at 100°C. Three experiments have been carried out, a test on an unirradiated specimen, the in-beam fatigue test and a post-irradiation fatigue test. The dose reached at the end of the in-beam test was 0.23dpa. The post-irradiation tested

specimen was irradiated to 0.11dpa. A series of deformation tests with and without concurrent irradiation were also performed, to measure the flow stress in-beam-on condition. The in-beam specimen reached the longest fatigue life. The post-irradiation tested specimen had the shortest fatigue life. The total plastic strain measured for the in-beam specimen was larger than the plastic strain measured for the statically irradiated specimen and the unirradiated specimen. It is envisaged that the observed strain effects result from precipitate coarsening. The flow stress measured in-beam-on condition increases with decreasing cyclic frequency. The increase in flow stress is a direct consequence of the interaction of the mobile dislocations with the irradiation-induced defects. The nature of the interaction with the dislocations is viscous drag. Assuming high strain levels for the CuCrZr components and depending on the dynamic conditions at the first wall of ITER, the effect of the in situ deformation could be beneficial for the fatigue resistance. The consequence for ITER is that the life of a CuCrZr component could be improved compared to that of a post-irradiation component.

TW3-TVM-TICRFA: Effect of low dose neutron irradiation on Ti alloy mechanical properties

This research work is a continuation of the project TW1-TVV/Titan, but with neutrons as irradiating particles. A series of specimens of titanium alloys (Ti-6Al-4V, Ti-5Al-2.5Sn) have been irradiated with neutrons at 150°C to 0.3dpa in the KFKI reactor in Budapest, Hungary. For each material, one tensile flat specimen (8mm in gauge length x2.5mm in width x0.3mm in thickness) and four mini-Charpy specimens ($3x4x27mm^3$) have been irradiated. One mini-Charpy specimen per material was loaded with 150wppm Helium and another one was annealed in order to remove most of the Helium content. Two more Charpy's were irradiated in the as received condition. In this way an interesting irradiation matrix was produced, which should deliver a good database for comparison with the results obtained within the project TW1-TVV/Titan (see above). The specimens have been delivered in the summer of 2003. They have been decontaminated, sorted and are ready for mechanical testing. The specimens will be tested in a three-point bend fixture, for fracture toughness. The tensile tests have been started. The testing should be finished at the end of 2003.

2.5 Superconductivity

The R&D activity of 2003 was again focused on cable-in-conduit superconductors for fusion magnets, with preparation and testing of short samples for SULTAN. The facility has been fully loaded during 2003 and the waiting list of available samples to be tested (disregarding the samples still on manufacturing) extends at least to the mid of 2004 (sections 2.5.8 and 2.5.5). About five months of SULTAN operation was devoted to the testing of the ELRES samples (section 2.5.1), about two months each for the improved full size Nb_3Sn ITER TF conductor (section 2.5.3), the two W7-X samples (section 2.5.2), and one of the two subsize Nb_3Sn samples of the CRPP-MIT collaboration (section 2.5.5).

Beside the SULTAN related projects, advanced Nb_3Sn strand characterisation, $I_c(B, T, \varepsilon)$ for future ITER conductor has been carried out. Analysis of TF Insert results is carried out in the scope of superconductivity studies (section 2.5.6).

In a collaboration with FZK, the preparation of a prototype 70kA High Temperature Superconductor Current Lead is in progress with some delay. The test is now re-scheduled in the Toska facility (Karlsruhe) for 2004.

2.5.1 Experiment with imposed current imbalance

In the task ELRES, CRPP proposed to investigate systematically the correlation between resistance imbalance at the electrical connection and the V-I characteristic. The rationale for the work program is based on:

- Use of conductors with a large number of strands (at least one fourth of the ITER full size) to give relevance to the test results
- Precise control of the level of resistance imbalance at the joint, by insulating a known fraction of the strands in the termination
- Comparison of identical conductors with different inter-strand resistance, to draw practical conclusions and applicable feed-back to the design

The NbTi CICC, prepared and tested by CRPP in 2001-2002 with parametric variations, offered an unique opportunity to achieve the goals of the ELRES task in a very short time and at a minimum cost.

The three conductors named #2, #3 and #4 of the NbTi parametric studies at CRPP are made out of the same basis superconducting strand, are cabled to the same total number of strands and same cable pitches and have identical outer size. The only difference is the strand coating and/or the sub-cable wraps, which affect the inter-strand resistance, i.e. the ability to redistribute the current.

The conductor layout is summarised in Table 2.5.1 and Fig. 2.5.1 illustrates the conductor cross-sections.

NbTi Conductor No	#2	#3	#4
Strand Coating	SnAg	Ni	Ni
Subcable Wrap	No	No	Yes
Cable Pattern	(1 + 6) x 3 x 4 x 4 *288 NbTi strands and 48 Cu cores*		
Cable Pitches	42 / 70 / 122 / 182 mm		
Cable Space Diameter	16.5 mm		
Conduit Diameter	18.5 mm		
Cu : non-Cu in strand	≈1.05		
Strand Diameter	0.70 mm		
Number of Filaments	690		
Twist Pitch	7 mm		
RRR	≈140		

Table 2.5.1 *Main parameters of the tested conductors*

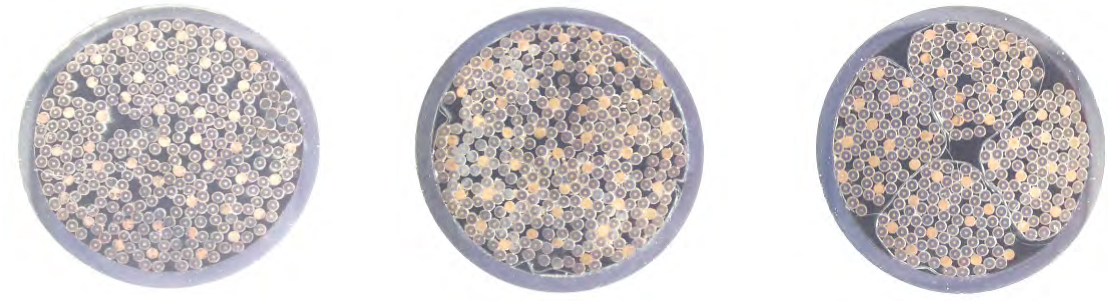

#2 #3 #4

Fig. 2.5.1 *Polished sections of the tested conductors*

The three conductors are assembled as hairpin samples, with the lower joint replaced by a U-bend. The resistance distribution can be controlled at one of the sample top terminations (the connection to the current source.

The modification of the electrical connection must allow opening the steel-copper box several times to change the fraction of strands contacted to the copper body of the steel-copper box. The cable is split into the four sub-cables, each of them soldered into a copper U-profile. The U-profiles with the soldered sub-cables can be either connected (Fig. 2.5.2) or insulated (Fig. 2.5.3) of the contact copper plate of the termination shoe.

Each sample has been tested at three current imbalance conditions: 100% with all four sub-cables connected to the copper shoe; 75% with three of four sub-cables connected and one insulated; 50% with only two of the four sub-cables in contact with the copper shoe and the other two insulated.

Fig. 2.5.2 *Sub-cables encased in the steel-copper box, with 100% connection*

Only DC tests have been performed for the ELRES samples. From the results obtained in CONDOPT experiments the general behaviour of the samples is known. A smooth current sharing is observed in the V-I characteristic only at low current density, I_{op}<25kA. The test program was focused on the low current range, i.e. in the range of high temperatures where the critical current and *n*-index can be distinguished.

Fig. 2.5.3 *Termination of the sample after the first test run. An insulation tube is slid over one of the sub-cable to obtain 75% connection*

As an example, Fig. 2.5.4 shows the comparison of critical current and quench current results for the three conductors at 5T background field and a temperature

of 6.4K. It is seen that conductor #2 with SnAg coating is less sensitive to the current imbalance and there is no difference in quench and critical current at 100% and 75% connection. The conductor #4 with Ni coating and sub-cable wrap is extremely sensitive to the current imbalance, quench and critical current drop by 30% at 75% connection and does not change at 50% connection. There is marginal difference between conductors #3 and #4 at 50% connection.

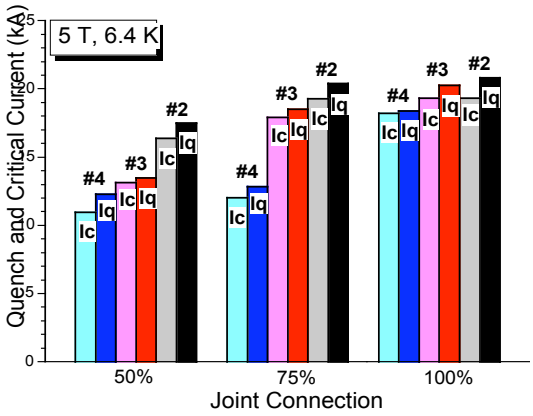

Fig. 2.5.4 *Conductors #2, #3 and #4. Quench and critical current at different level of the current unbalance in 5T background field and temperature of 6.4K.*

An evolution of the *n*-index with a reduction of the connected sub-cables is shown in Fig. 2.5.5. When all the four sub-cables are connected to the copper shoe (100%) the *n*-index fits very well to the strand database. A significant drop of the critical current density (about 40%) is observed in conductor #4 with Ni coating and sub-cable wrap. The conductor #4 shows an "acceleration" of the V-I curve from the very beginning starting from 75% connection, while conductor #3 shows an "acceleration" only at 50% connection. The conductor #2 does not show any "acceleration", all points of the *n*-index fit the strand database.

It has been found that the conductor with Ni coating and sub-cable wrap is extremely sensitive to the current imbalance in the joint, and current can be not redistributed even at 75% connected strands.

The conductor with SnAg coating is not sensitive to the current imbalance in the joint, there is no change in quench and critical current at 75% connected strands, and there is a marginal drop of the quench and critical current at 50% connected strands. Taking into account that the distance of the sample from the termination where the current imbalance is imposed to the measurement section is only about two meters, it is possible to imagine that in a real coil with much longer distances between joint and high-field region, the current becomes uniformly distributed.

The conductor with Ni coating and without sub-cable wrap is able to redistribute the current imbalance up to 75% connected strands.

The practical conclusion from this experiment is the allowed tolerances on non-homogeneous current distribution in the joints of a real coil for conductors with different inter-strand resistance. A further analysis allows a prediction of how far the current imbalance can be tolerated for the actual conductor.

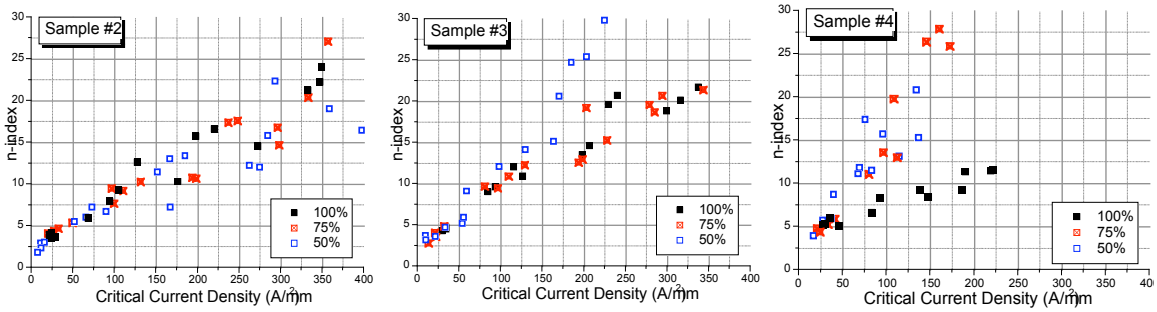

Fig. 2.5.5 *n-index evolution at different levels of the current imbalance*

2.5.2 Test of two samples of W7-X conductor[*]

Two samples of the W7-X conductor have been prepared by IPP, according to the interface specification of CRPP and delivered in June 2003. One sample (named W7-Xa) has been tested only for the electrical connection between the two conductors, the joint. The second sample (named W7-Xb) has been tested for both joint and conductor. This work does not aim at a final judgement of the samples, but only at quantifying their performance.

The conductor for the W7-X coils is a cable-in-conduit made from 243 NbTi strands (3^5, five stages cable). The strand has 0.57mm diameter, no surface coating, Cu:non-Cu=2.6, twist pitch 24mm, 144 filaments about 25μm thick. The pitches of the five cable stages are 25, 60, 90, 126, 147mm. The jacket is a co-extruded aluminium alloy. The conductor has a square cross section, 15.9x15.9mm. The average diameter of the cable space is 11.4 mm. The void fraction is 37.6%.

The main object of the collaboration between IPP and CRPP is to verify the performance of the electrical connections to be built between the series connected coils of the W7-X fusion device. The samples tested in SULTAN contain one electrical connection manufactured by IPP according to the design planned for the coil-to-coil connections, see Fig. 2.5.6.

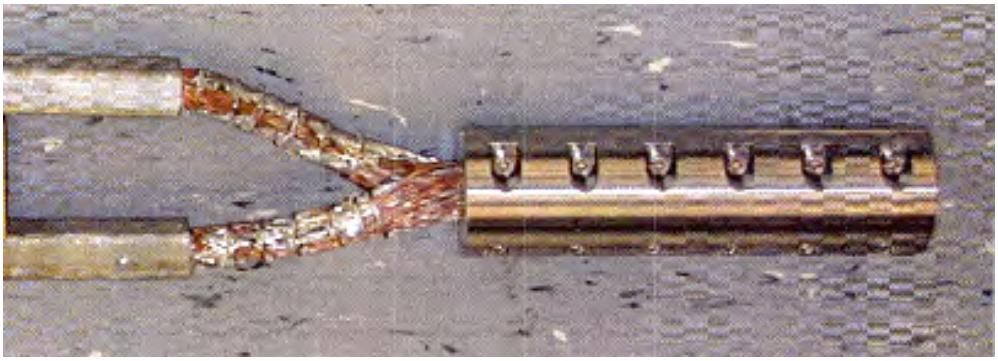

Fig. 2.5.6 *A prototype joint, without joint box, compacted into the steel halves*

The two samples prepared by IPP and tested in SULTAN have the same conductor, joint layout, supporting structure and instrumentation scheme. The differences between the two samples are the length (2.9 vs. 3.5m) and the solder alloy (PbSn vs. SnAg).

[*] (Collaboration with IPP Greifswald, Germany)

Results of joint ac loss

The ac loss has been measured by gas flow calorimetry. The sinusoidally varying field is orthogonal to the dc field of SULTAN (always set at 2T). One set of measurement is taken at constant amplitude (±0.05T) and frequency range from 2 to 20Hz, at 0 and 18kA operating current, see Fig. 2.5.7, left. Another set of measurements is at constant frequency (20Hz) and varying field amplitude, see Fig. 2.5.7 right. The loss is either normalised to the energy per cycle per strand volume in the joint (25.68cm3) or just shown as overall power loss in the joint.

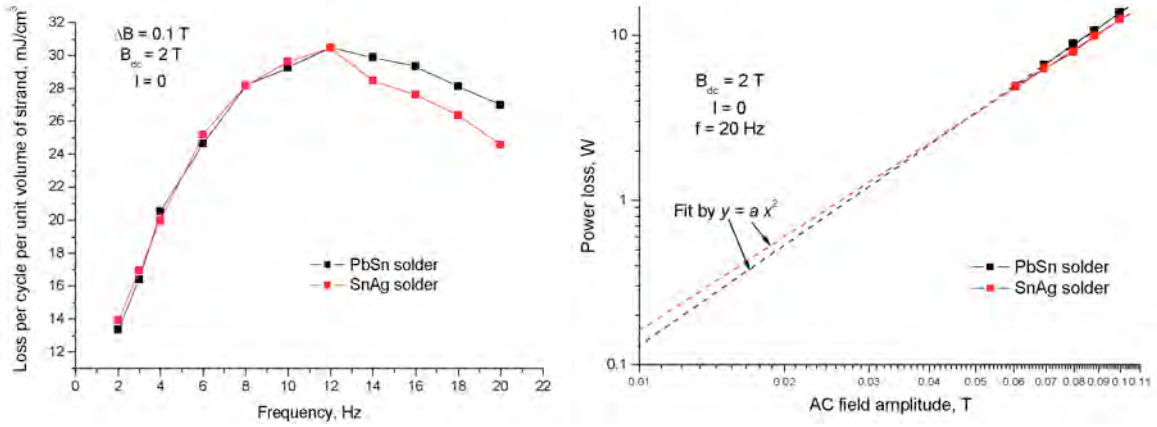

Fig. 2.5.7 *Loss curve vs. frequency for both joint samples (left) and power loss of the joint assembly vs. field amplitude in log-log plot (right)*

The loss is virtually identical for both samples: at higher frequency, the joint with SnAg solder shows a slightly lower loss. The energy density, arbitrarily normalised to the strand volume in the joint, is higher than the magnetic field energy density. This means that, in this range of frequency, other components, e.g. the joint box and the aluminium in the eye-glass piece, contribute substantially to the loss.

From the maximum of the loss curve at about 12Hz, the time constant of the joint assembly, τ is about 13ms. Such a small time constant is likely to be due to the steel joint box. The actual coupling current time constant of the soldered joint is largely screened in the range of frequency of the test. From purely geometric considerations, the time constant of the soldered strand bundle is expected to be in the range of 1s, i.e. the peak of the (partial) loss curve should be well below 1Hz. Indeed, the NbTi strand, with a pure Cu matrix and a twist pitch of 24mm, should have a time constant of few tens of msec, see conductor results.

The power loss results vs. field amplitude, $\Delta B \equiv 2B_0$, at 20Hz frequency is shown in Fig. 2.5.7, in a log-log scale. The measured points are well matched by a square fit. The extrapolation suggests that, at 10mT ac field amplitude, the ac power loss in the joint is of the order of 0.1–0.2W.

Results of joint resistance

The joint resistance is measured over a field range up to 2T and a current range up to 25kA. The joint resistance is very low. The results of joint resistance are gathered in Fig. 2.5.8, where the resistance is plotted vs. the background magnetic field. The resistance is evaluated at 25kA to improve the signal/noise ratio. The impact of the magnetoresistance of the copper matrix in the strand is visible. As expected, the joint soldered with SnAg alloy has a lower resistance compared to the PbSn solder.

However, from an engineering point of view, the impact of magnetic field and solder resistivity is marginal. The power, RI^2, is limited to about 30mW, well below the resolution of the calorimetric method. In operation, it is likely that the ac loss power load exceeds the ohmic load at the joints.

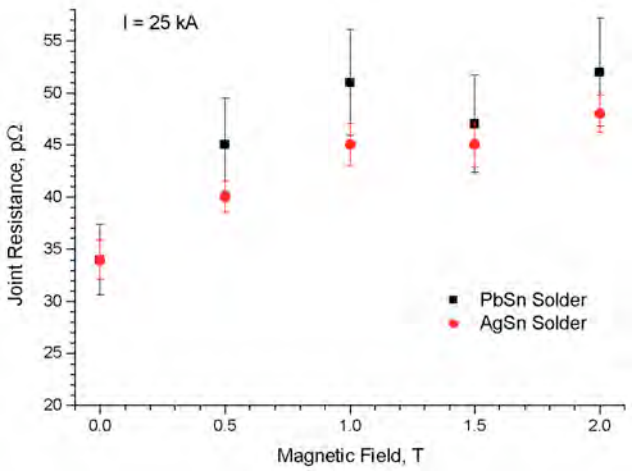

Fig. 2.5.8 *Joint resistance, as $10^{-12}\Omega$, vs. background magnetic field at 25kA operating current*

Results of conductor ac loss

The ac loss characterisation of the W7-X conductor was carried out applying a sinusoidal field of amplitude ±0.1T (twice as much compared to the joint) transverse to the conductor axis. The frequency of the applied field ranges from 0.2-6Hz. The effective length of the applied ac field is 390mm. The energy loss, measured by gas flow calorimetry, is normalised to the strand volume enclosed in the ac field, 24.03cm^3.

The results are gathered in Fig. 2.5.9. The hysteresis loss Q_h, i.e. the extrapolation to zero frequency of the loss curve, can be reliably estimated from the filament diameter (25μm) by the formula

$$Q_h = \oint_{a-b-a} M_\perp(B)dB \approx \frac{4\Delta B}{3\pi} D\bar{J}_{c\parallel}$$

where ΔB is the peak-to-peak amplitude of the ac field (0.2T), D is the filament diameter (25μm) and $\bar{J}_{c\parallel}$ is the average current density over the field cycle (retained 4.75.10^{9}A/m^2). The hysteresis loss normalised to the overall strand volume (Cu:non-Cu=2.6) is 3.87mJ/cm^3.

The loss curve is linear (within the error bar) at low frequency. From the initial slope of the loss curve the coupling loss constant $n\tau$, is estimated from the loss formula for sinusoidal applied field,

$$n\tau = \frac{Q}{f}\frac{4\mu_0}{2\pi^2\Delta B^2} = 45\ ms$$

The result is in the range expected for a multi-filamentary strand with copper matrix and 24mm pitch, i.e. there is no significant contribution to the loss by the inter-strand coupling, despite the absence of resistive barrier (coating) on the strand surface. This indicates that the copper oxide has built on the strand surface, e.g. during the manufacturing process.

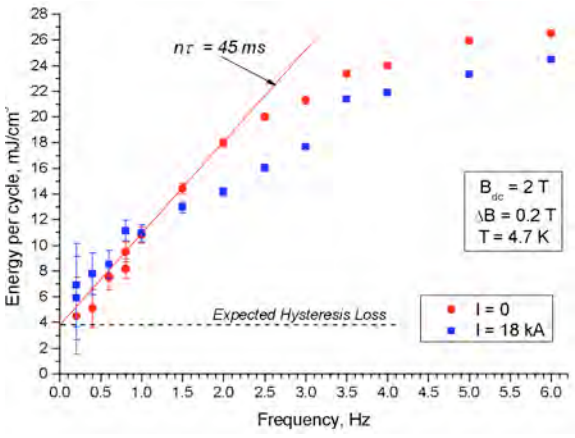

Fig. 2.5.9 *The ac loss versus frequency of the W7-X conductor at 0 and 18kA operating current*

Results of conductor dc performance

The critical current and the current sharing temperature are defined using a 0.1μV/cm electric field criterion. To determine the current sharing temperature the current and the magnetic field were kept constant, while the helium inlet temperature was increased. The quench and the critical currents measured for applied magnetic fields of 5 and 6T are shown in Fig. 2.5.10. The data points (stars) obtained from the T_{cs} measurements at I=18kA are in good agreement with the results of the I_c measurements.

As observed in other NbTi conductors, the sample quenches at high current density (low temperature) before the voltage of the critical current criterion has been reached. The quench properties seem to be dominated by the local electric field enhancement on the high field side of the cable. The quench occurs when the local heating exceeds the cooling provided by the supercritical helium. In some cases this occurs at average electric fields well below 0.1μV/cm, the critical current criterion, and is the reason for the observed "sudden quenches". The critical current is determined by the average electric field along the strand. Due to the twist pitch the strands cycle in and out of the high field region. The measured average electric field is therefore considerably lower than the value at the magnetic peak field, even for insulated strands.

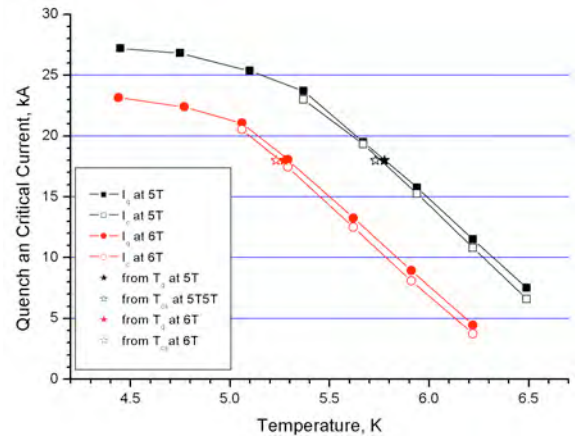

Fig. 2.5.10 *Quench and critical currents, I_q and I_c, of the W7-Xb sample at background fields of 5 and 6T*

The current-voltage relation of the W7-Xb sample has been investigated. Close to the superconducting transition, the electric field is well described by the power law expression $E=E_c(I/I_c)^n$, which defines the *n*-index. The *n*-indexes of cable (measured in SULTAN) and the strand (from the QA documents) are compared in Fig. 2.5.11. Both the cable and the strand *n*-indexes increase with increasing non-copper critical current density. A similar behaviour was found in other NbTi conductors. The results suggest that the relatively high cable *n* values are close to the strand data. This behaviour may be understood as an even current distribution among the strands. In the case of a strong current imbalance, the *n*-index of the cable is expected to be substantially lower than in the strand.

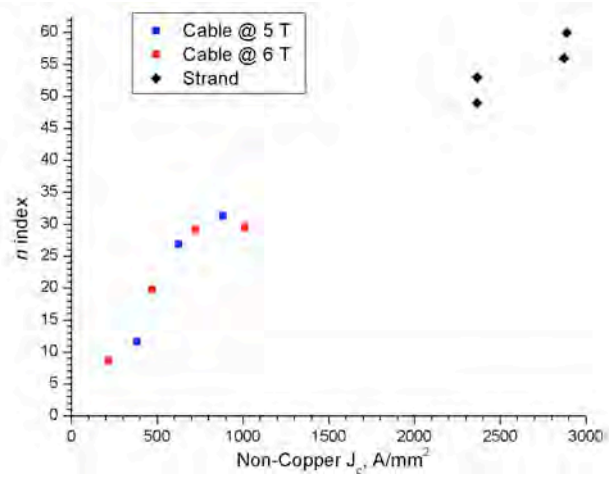

Fig. 2.5.11 *Cable and strand n-indexes as a function of the non-copper critical current density*

The results of the current sharing measurements at I=18kA in a background field of 5, 5.5, 6 and 6.5T are shown in Fig. 2.5.12. Due to the transport current of 18kA the magnetic peak field is 0.71T higher than the background field. The current sharing temperature depends linearly on the magnetic field. The results of the T_{cs} measurements are in reasonably good agreement with the I_c data. To estimate the temperature margin in the W7-X coils, the line labelled "peak field" should be used. For example, assuming an operating current of 18kA, an operating temperature of 4.3K and a peak field of 6T in the non-planar coil, the temperature margin can be estimated from Fig. 2.5.12 to be $\Delta T \approx 5.6–4.3=1.3K$

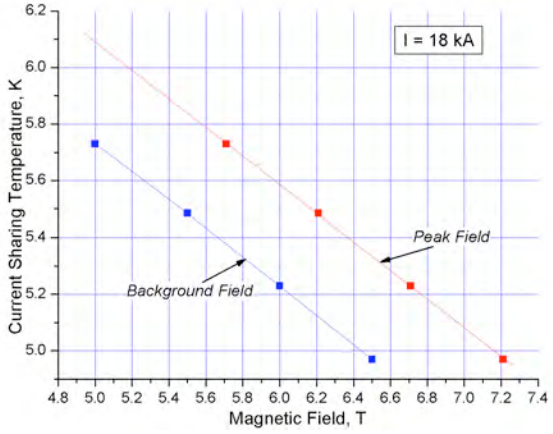

Fig. 2.5.12 *Current sharing temperature at I=18kA plotted vs. the background and the peak field*

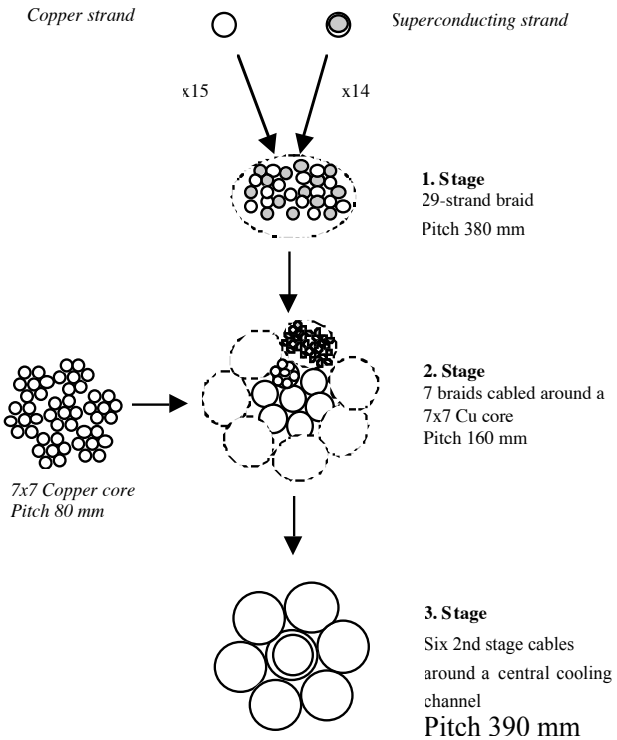

Strand Characteristics	Specified	Measured
Cu:non-Cu Ratio	0.8 ± 0.05	0.86
Non-Cu J_c, 12T, 4.2K, 0.1μV/cm (A/mm^2)	800	795-803
Non-Cu hysteresis Loss, ±3T (mJ/cm^3)	≤ 400	293-303
RRR, 273K/20K	> 100	60 (Cr-plated) 380 (bare)
Cr-Plating (μm)	1 ~ 1.5	1.3 ± 0.1

Table 2.5.2 *Strand characteristics and cable layout*

2.5.3 Development and test of a new Nb_3Sn full size conductor

Results obtained on the ITER Model Coils and a number of conductors tested in the SULTAN facility revealed that Nb_3Sn strand properties are reduced in the cable either after first energising and/or after applying a number of current cycles. Based on these observations, the ITER-IT initiated an action devoted to conductor redesign

for the ITER coils. Although the present task is not explicitly part of the redesign effort, it is aimed at clarifying conductor design issues which have the potential to influence the magnitude of performance degradation during operation of ITER coils. The developmental conductor subject to this study, denoted as sample A, follows the specifications of the ITER TF conductor but wants to make use of the lessons learned during the last 8 years of conductor R&D within ITER. Among other issues, the new conductor should take advantage of the 'post model coil' advanced strand with improved properties reflecting the state of the art of Nb_3Sn manufacture thus contributing to strand cost control for ITER.

In order to assess the effect of bending and/or the effect of enhanced local pressure at cable crossings on the deterioration of strand properties in the cable, a companion conductor denoted as sample B, has been prepared. This conductor has the same cable pattern as conductor A but its annular space is filled with solder. Solder-filled conductors have the potential to eliminate the internal disturbances caused by the strand movements and to reduce the bending and the transverse stress effects.

The cable configuration is a multistage arrangement of Nb_3Sn and pure copper strands. The first cable stage is a braid containing 14 superconducting and 15 pure copper wires. The second cable stage consists of 7 braids twisted around a core of 49 copper strands. The third and last cable stage consists of six second stage cables twisted around the central cooling channel. No wrapping is applied to the last but one cable stage.

The Outokumpu strand employed in the present developmental conductor is the first pilot quantity which has been procured and tested after starting the redesign action within ITER. Half of the produced length has been Cr-plated and half was left bare according to the requirements of the soldering operation conductor B underwent after reaction heat treatment. The main characteristics of the manufactured Nb_3Sn strand are summarised in Table 2.5.2. The Swiss company Marti-Supratec performed the braiding while the subsequent cabling and jacketing into Ti pipes was completed by the Russian company VNIIKP in January 2003. Two conductor lengths based on the two types of braids, each 5.6m long, were produced.

Strand test results

A series of wires was heat treated in argon flow and some of the relevant properties for magnet applications were examined. The tests included I_c versus B and T, the uniaxial strain dependence of I_c and Residual Resistivity Ratio. The heat treatment schedule recommended by the manufacturer was based on the one used for the ITER CSMC (800hrs). A shorter heat treatment schedule (400hrs) has also been considered. Tests have been carried out with both schedules.

Critical current measurements in magnetic fields ranging from 9 to 12T and at temperatures between 4.2 and 8K were performed on 1m long helically wound samples. The preparation of critical current specimens was made according to the procedure developed during the ITER strand benchmark i.e. a TiAlV grooved mandrel with copper rings attached for current contact. The effect of uniaxial tensile strain on the critical current was measured in the same 12T laboratory solenoid previously used for critical current measurements. The tensile strain apparatus is designed to measure the critical current of short straight specimens exposed to a transverse magnetic field while being strained.

An example of measured critical current density as a function of temperature at 9, 10, 11 and 12T and at zero applied strain is shown in Fig. 2.5.13. The short heat treatment provides superior performance at high magnetic fields and temperatures.

At 9T for example, the short heat treatment supplies superior J_c values above 7K, while at 12T the critical current densities obtained with the short heat treatment are already higher at 6K. However, both short and long heat treatment achieve at 12T and 4.2K the target value of 800A/mm^2.

The intrinsic strain of the wire was determined experimentally by measuring the critical current as a function of strain. The critical current at 12T and 4.2K as a function of applied uniaxial strain is shown in Fig. 2.5.14. The solid line is a fit to the measured points to determine the maximum of the $I_c(\varepsilon)$ curve. The resulting intrinsic strain is ε_0=-0.21%.

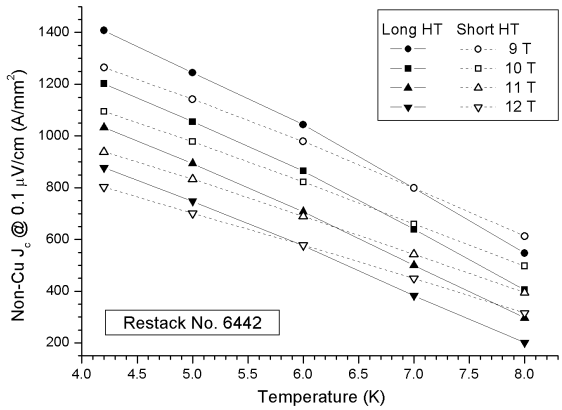

Fig. 2.5.13 *Critical current density as a function of temperature for fields ranging between 9 and 12T. Two sets of data points are shown corresponding to the original (long) and the short heat treatment schedules.*

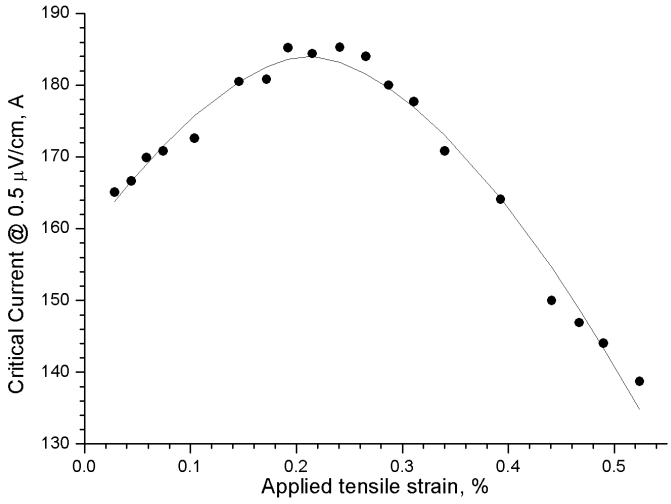

Fig. 2.5.14 *Critical current versus applied tensile strain at 12T and 4.2K*

The index n of resistive transition in Fig. 2.5.15, determined from the V-I characteristic, is roughly constant over the investigated range of field and temperature in contrast with strands tested in the past which show a pronounced dependence on critical current density. The same range of results is obtained for long and short heat treatment.

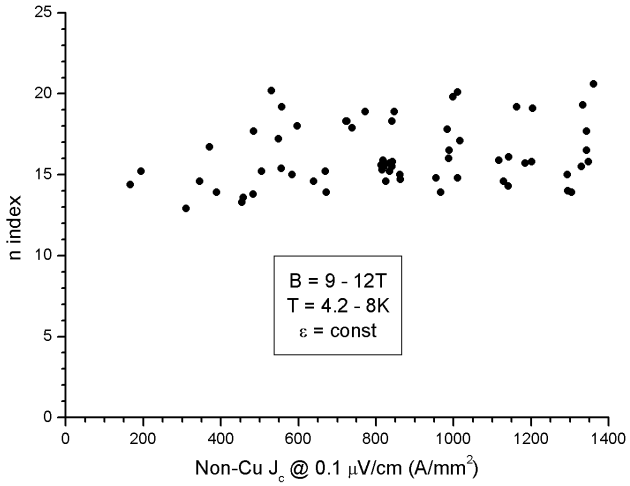

Fig. 2.5.15 *n-index of resistive transition determined from the voltage-current characteristic of strand samples within the investigated range of temperatures and fields*

Full size test results

Measurements on conductors A and B are under way in the SULTAN test facility to characterise the conductors regarding ac losses, dc properties and cycling behaviour. Preliminary dc measurements show clear indication that the performance of conductor A is degraded as compared to the strand data applied at a criterion of 0.1μV/cm even with the strain effect of jacket and the peak-field effect taken into account. On the other side, applying a 1μV/cm, the Summers fit lies close to the quench curve which is an indication that the cause of the degradation is not intrinsic to the strand but rather a property of the cable. This is illustrated in Fig. 2.5.16, where the measured critical and quench currents for conductor A at 11T magnetic background field.

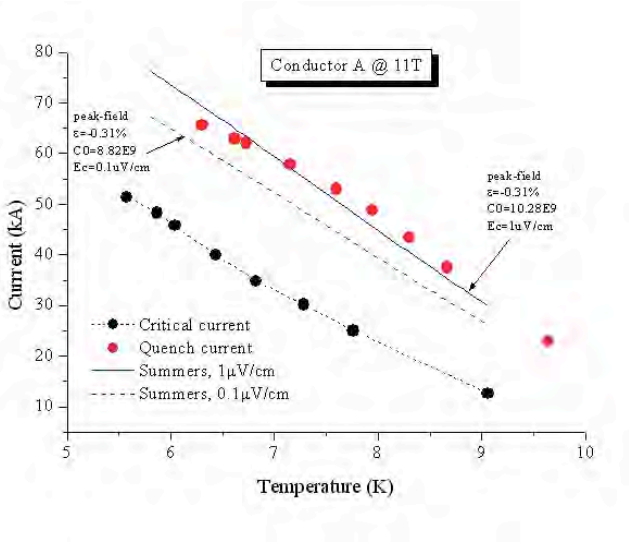

Fig. 2.5.16 *Measured dc data of conductor A at 11T compared with predictions based on Summers scaling relation at 0.1 and 1μV/cm*

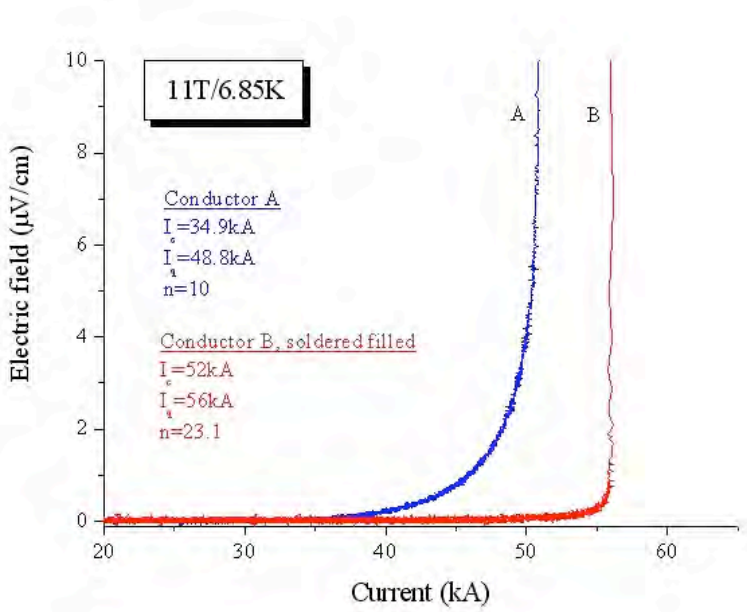

Fig. 2.5.17 *Typical voltage-current curves for conductor A and B at 11T and 6.85K*

A direct comparison between conductors A and B revealed an unexpected high performance of conductor B, which shows practically no degradation. This is illustrated in Fig. 2.5.17 where the voltage-current curves for the two conductors at 11T applied field and a temperature of 6.85K are shown. The key issue here is the degradation in the power-law index of conductor A from around 20 for strands to 10, while in conductor B no degradation is seen, n_B=23.1. A lower *n*-index, as for conductor A, means the conductor will run earlier into current sharing and will reach the 0.1μV/cm at a lower current. Therefore we conclude that the apparent degradation of conductor A is a collective effect of assembling a large number of strands in a conduit which manifests itself as a decrease in the power-law index. It seems that braiding the strands does not improve this situation, compared with twisted cables. On the other side, filling the cable with solder, as for conductor B, seems to be a good solution to eliminate this unwanted effect. This also suggests that the collective degradation of *n*-index is a mechanical effect.

2.5.4 High temperature superconducting current leads

In a collaboration with the Forschungszentrum Karlsruhe (FZK) a 70kA current lead is being developed to demonstrate the feasibility of high temperature superconductors (HTS) for the toroidal field (TF) coil system of the ITER. In an earlier design of the ITER magnet system it was found that the cooling power required by conventional current leads is about 1/3 of the total dissipated power of the whole system. Using an HTS current lead in the temperature range from 4.5 to 65K the resistive losses are eliminated and only the losses due to heat conduction remain. Taking into consideration the power required to cool the heat exchanger operating between 65K and room temperature, a reduction in the power consumption by a factor of 3 to 4 compared to a conventional current lead is obtained.

The HTS current lead consists of an HTS part and a conventional copper part operated in the temperature ranges 4.5 to 65K and 65K to room temperature, respectively. The HTS part is cooled by heat conduction from the 4.5K level and the

copper part is actively cooled with helium gas with a 50K inlet temperature. The optimum temperatures of both the helium and the conductor at the cold end of the heat exchanger depend on the assumed refrigerator efficiency, the engineering critical current density of the AgAu/Bi-2223 tapes at the envisaged temperature and the cross-section of the stainless steel support. Studies performed at CRPP indicate that the optimum temperature at the warm end of the HTS part is around 65K for a helium inlet temperature of 50K. An artist's view of the current lead is shown in Fig. 2.5.18. On the left hand side, the clamp contact to the NbTi bus bar is visible. On the right hand side, the connection to the water-cooled flexible cable is located. In the centre the HTS current lead module including the copper end caps and the heat exchanger are shown. The main parameters of the 70kA HTS current lead are listed in Table 2.5.3.

Parameter	Value
HTS part	
HTS tape/stainless steel cross-section	9.04/49.55cm^2
Engineering critical current density (77K, self-field)	12 kA/cm^2
Lower/upper end temperatures	4.5/65K
Length of HTS stacks	692mm
Contact resistance at lower/upper end	0.65/5nΩ
Length of HTS-Cu transition at lower/upper end	54.4/44.5mm
Length of HTS current lead module	715mm
Heat load at 4.5K (I = 0)	5.4W
Heat exchanger part	
Material of heat exchanger and *RRR*	SE copper, 50-100
Length of heat exchanger	700mm
Lower/upper end temperatures	65/290K
Helium inlet temperature and mass flow rate	50K/4.69g/s at 68kA

Table 2.5.3 *Current lead parameters*

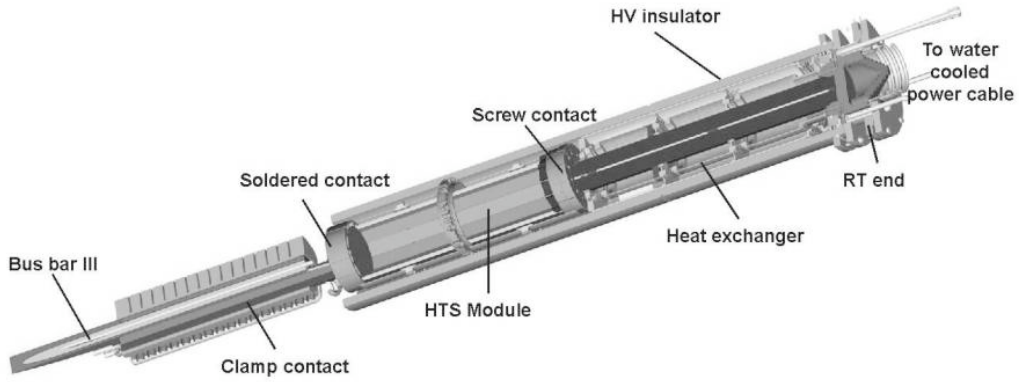

Fig. 2.5.18 *Artist's view of the 70kA current lead*

The resistive part of the current lead made of copper forms a heat exchanger. The design is similar to that of other conventional high capacity current leads fabricated at FZK. A central circular copper rod of 90mm diameter conducts the current from room temperature to the intermediate stage at 65K. Perforated plates are brazed onto the outer surface of the copper rod acting as a heat transfer unit. The residual resistivity ratio (*RRR*) of the electrolytic copper (SE copper) used to fabricate the central rod as well as the perforated plates is between 50 and 100. The length of the

heat exchanger is optimised for 70kA steady state operation. The HTS current lead module consists of the HTS part and two copper end caps, which provide the current transfer to the other parts of the current lead (see Fig. 2.5.19). To simplify the fabrication a modular design has been chosen for the HTS part. The basic component is the CryoBlock™ current lead wire of American Superconductor (AMSC) with cross-sectional dimensions of $4.1\times0.2mm^2$ and a critical current >100A at 77K and zero applied field. The wires are sintered into stacks during the wire fabrication process. Each stack is formed of 13 tapes leading to dimensions of $2.6\times4.1mm^2$. The length of the stacks is 700mm.

Seven of the stacks are soft soldered into stainless steel carriers with copper tips (so-called panels). The panels have been soft-soldered into the end caps to form a 12-fold prism. This is an approximation of the most advantageous circular design, which minimises the magnetic field perpendicular to the ab-planes of the textured Bi-2223 filaments parallel to the broad face of the tapes. The chosen monolithic assembly will withstand all forces experienced by the lead during installation and operation. The total design current at 77K and self-field is 68kA. Pre-tests of the stacks and the panels at 77K and zero applied field provided average critical currents of (893±64)A and (5691±143)A, respectively. The estimated total current of 68296A reaches the design value.

The module has been instrumented with temperature sensors and voltage taps. Two sets of 5 Cernox temperature sensors are available to determine the temperature profile along the HTS current lead module. Additional 12Pt sensors close to the upper end cap are used to estimate the maximum temperature of each of the panels in the event of a quench. The current distribution in the panels will be deduced from the signals of 12 small-sized Hall probes attached on top of the G10 protection tube. The test of the current lead in the TOSKA facility of FZK is foreseen for the first half of 2004.

2.5.5 Preparation of Nb_3Sn subsize samples

The objective of this task is to make a study using two identical Nb_3Sn cables, but with two different jacket materials, stainless steel and titanium in order to complement the existing conductor data, in particular investigate if the transverse load degradation (including cycling) is affected by the thermal expansion of the jacket material.

Two subsize Nb_3Sn conductors have been prepared by MIT using strand material (IGC) left over from the Model Coil manufacture. The cabling and jacketing has been contracted by MIT to VNIIKP (Moscow). The two conductor sections, jacketed respectively with Ti and stainless steel, have been received at CRPP in December 2002.

The preparation of SULTAN samples from the raw conductor sections includes: straightening and shaping of the conductor lengths into two hairpin sections (i.e. with a U-bend at the bottom). Dismantle the jacket from the four ends of the two sections. Remove chemically the Cr plating from the strand surface. Swage the four cable ends into a copper pipe, to a void fraction of about 27%. Prepare ceramic spacers to slide over the Cu pipe. Cover the cable ends with respectively SS and Ti pipes and weld them to the conductor jacket on one side and to reduction piece and extension pipes on the other side. Fix the two samples on a rigid support for the heat treatment. Add I_c sample holders (witness barrels) manufactured at CRPP. After completion of the above work, in February 2003, the two samples were shipped to MIT for heat treatment.

The heat treated samples have been received at CRPP in July 2003. The preparation of samples after heat treatment for testing includes design and manufacturing of joints and clamps parts, soldering and welding of the termination, instrumentation, sensors, assembly, wiring. By the end of October 2003, the two samples are ready for test in SULTAN. The start of the tests with the stainless steel jacketed conductor, is planned by mid November 2003. The test program includes dc performance and ac loss as a function of the cyclic load.

The sample strand specimens are also being tested at CRPP to provide the necessary database for the performance assessment of the subsize samples.

2.5.6 Superconductivity studies

The ITER Toroidal Field Conductor Insert (TFCI) coil was developed and built to simulate the conductor performance under ITER TF conditions. The TFCI was charged without training to 46kA in the background field of the Central Solenoid Model Coil (CSMC) in Naka, Japan (~13T). One of the objectives of the TFCI tests was to measure the current sharing temperature (T_{cs}) behaviour of the conductor and to compare it with predictions based on strand measurements. The TF Insert is a one-layer solenoid featuring Nb_3Sn dual channel cable-in-conduit conductor (CICC) with Titanium wall conduit. The TFCI is cooled by forced-flow of supercritical helium. The CICC is embedded in a stainless steel mandrel, cooled by separate circuits at 4.5K. During the T_{cs} runs the He inlet temperature is slowly ramped by means of a resistive heater located upstream the lower joint. The TFCI met the design objectives but showed results which require further investigation.

The goal of our analysis is to derive the strand performance in the cable by simulating the temperature profile along the conductor length. A preliminary analysis assessed the consistency of the experimental data and has defined the strategy used in the simulation model. We consider the last-but-one cable stage, modelling the CICC as 6 twisted super strands, characterised by the Summers scaling parameters and by the non-linear voltage current equation $E=E_0(I/I_0)^n$. The cable *n*-index is estimated from the resistive voltage signals. The total magnetic field is obtained by adding the CSMC external field to the self field of the TFCI last-but-one cable. The coupled thermal, hydraulic and electrical analysis is performed with the code THEA, validated in several experiments in the SULTAN test facility. Having derived upper and lower *n*-index, the only fitting parameter in the simulation is a global cable variable which includes the contributions of bending strain, thermal strain and electromagnetic load.

A subset of T_{cs} experiments has been analysed. An acceptable agreement of simulated and measured results is achieved if the fitting parameter is ~ -0.60% and independent of electromagnetic load (the strain at zero loading in conductors with Ti jacket is < -0.30%). The *n*-index and the T_{cs} of the cable are considerably lower than the respective values measured from the strand. These results can be explained either by strand interactions in the cable, e.g. non-uniform current distribution, or by change of strand intrinsic properties, e.g. factors in fabrication, cool down or electromagnetic loading responsible for the reduction of the critical current of individual strands, and their *n*-index. Due to this unidentified degradation of the CICC, it is not possible to describe the strands in the cable by the Summers equation for the original strands. A more accurate model of the joints was included to assess the relevance of non-uniform current distribution.

2.5.7 Testing of MgB_2 high temperature superconductor

The research division of Edison Spa developed the Reactive Liquid Infiltration (LRI) technique providing the possibility of preparing MgB_2 bulk material and wires with high critical current densities. The field and temperature dependencies of the critical current of MgB_2 bulk material prepared by Edison Spa have been investigated at CRPP using a temperature variable cryostat. In addition, the voltage-current characteristic of the material has been studied. The electric field close to the transition to the normal state can be well described by the power law $E=E_c(I/I_c)^n$, where E_c=1μV/cm is the electric field criterion used to define the critical current I_c. The results have been compared with the n-index measured for a mono- and a 7–core wire. The n-index was determined in the electric field range of 0.5 to 5μV/cm. The critical currents of the MgB_2 bulk material can be well represented by the scaling law

$$I_c(B,T) = \frac{C_0}{B}\left(1-\left(\frac{T}{T_c}\right)^{\beta}\right)^{\gamma}\left(\frac{B}{B_{sc}(T)}\right)^{p}\left(1-\frac{B}{B_{sc}(T)}\right)^{q} \quad \text{where} \quad B_{sc}(T)=\left(1-\left(\frac{T}{T_c}\right)^{\alpha}\right)$$

Assuming T_c=39K a reasonably good fit results for p=0.1 and q=5. The other scaling parameters are: $B_{sc}(0)$=(12.8±0.5)T, α=0.91±0.07, C_0=(13490±220)AT, β=3.00±0.20 and γ=3.97±0.48. Because of the existence of an irreversibility field in MgB_2 the scaling field B_{sc} may be lower than the upper critical field. The n factors found for the bulk, the mono- and the 7-core wire have been fitted with the following relation

$$n(B,T)= n_0 \exp\left(-\varepsilon B/\left(1-T/T_c\right)^{\delta}\right)$$

where n_0, ε and δ are scaling parameters. The scaling parameters found from a fit based on T_c=39K are:

MgB_2 Samples	n_0	ε (1/T)	δ
Bulk (#62)	103	0.30	1.33
Monocore wire (#58)	130	0.38	1.00
7-core wire (#40A)	37	0.145	1.33

Table 2.5.3 *Scaling parameters*

The existence of an irreversibility line well below the upper critical field indicates that above the irreversibility field the vortices are movable, and hence the critical current is zero. As in high temperature superconductors thermally activated depinning may be of importance in MgB_2 at sufficiently high temperatures and fields. The factor $1/\varepsilon\times(1-T/T_c)^{\delta}$ may be considered as the irreversibility field. Very recently it has been reported that the irreversibility field of MgB_2 bulk material is in agreement with the above expression proportional to $(1-T/T_c)^{1.5}$. The δ value of 1.33 obtained for the MgB_2 bulk material is close to the exponent of 1.5 found for the irreversibility field.

The values of n_0 found for the MgB_2 bulk and wire samples vary considerably. It can be expected that at low temperatures and fields the broadening of the $E(I)$ curves is dominated by the sample homogeneity. A variation of the critical current density along the conductor due to variations in the microstructure results in reduced n factors. The observed deviations from the n scaling law at low fields and temperatures may reflect this effect. In multicore wires the variation of the cross-section of the thin filaments leads to a variation in I_c, which is an additional

mechanism to reduce the n factors. The low n_0 value for the 7-core wire may be caused by this effect.

2.5.8 Preparation of a low cost NbTi full size conductor

A simplified joint concept for the ITER Poloidal Field (PF) coils is being developed. The main feature of this concept is a fully welded steel joint box enclosing the contact surfaces. The box is weldable using Tungsten Inert Gas (TIG) technique and capable of being opened and re-welded. The joint has the following parameter targets:

- Void fraction of the compacted joint section ≥30%
- Joint quench current >90% of conductor quench current
- Resistance at 5T field and 40kA current <1.5 nΩ
- Overall eddy current / AC loss time constant nτ<100 ms

In order to reach joint target parameters the following technique for the joint fabrication has been developed:

- Coating removal (chemical)
- Pre-soldering of the cable
- Wrapping by a solder foil
- Compaction of the cable in joint section and welding of the joint box will be done in one go. The cable assembled with the insulated copper saddle pieces will be enclosed into the stainless steel join box. The pressure will be applied onto the cover of the steel box, and welding of the cover will be done under pressure.
- Heating of the joint box to melt the solder foil

The NbTi conductor sections have been delivered to CRPP in June 2003 after a long delay, completed by certificate and “Quality Book”. The manufacturing drawings of the joint and the sample itself have been completed. The sample contains two joints. One, a hairpin configuration for the lower joint to connect two pieces of the conductor sections, and the second one is a lap configuration in the centre of one of the conductor section. Because of complex sample configuration and the limited space in the SULTAN test well (full-size PF conductor and two joints in one sample) the trials on bending of the conductor have been performed successfully.

The sample will be tested in both the “raised” and “lowered” position in SULTAN, under steady and pulsed conditions, in order to characterise both the lap joint in the middle of the sample and the hairpin joint at the bottom.

In a second campaign, the length of the lower joint may be reduced by about 50% by cutting and reassembling, and the joint retested.

2.6 Gyrotron development

118GHz Gyrotron development

The TH1506A 118GHz/0.5MW/2s gyrotron produced by Thalès Electron Devices which had suffered from a window failure in 2002 was repaired by Thalès and reinstalled in the TCV premises in July. The tube has then been successfully conditioned, tested and incorporated in the TCV ECH system. It is now being operated routinely on TCV.

In parallel, the contract placed between CEA-Cadarache, Thalès and CRPP to improve the performance of the long pulse version of the tube (TH1506B) is running and the modified prototype will be ready for factory tests by the end of the year. The CRPP will attend and contribute to the tests, particularly by doing frequency measurements, detecting the presence of parasitic oscillations and by measuring the mode purity at the output window of the tube.

140GHz Gyrotron development

The 140GHz 1MW/CW Gyrotron to be used on W7-X is a continuing project, the prototype tube which had achieved 0.85MW in 180s pulses in 2002 has been opened and inspected by Thalès Electron devices and refurbished. It will be further investigated in FZK. In parallel, negotiations for the series production are underway. CRPP was invited to participate during the procurement phase.

ITER 170GHz gyrotron gun (TW3-TTHE-CCGDS1) (Section 4.2.2)

The design of the ITER 170GHz gyrotron gun along with the geometry of the super-conducting magnet coils has been performed according to the specifications and the final report has been sent to EFDA. Sensitivity studies with respect to the position of the bucking coil along the axial coordinate of the gyrotron show that the sensitivity properties of the 170GHz gun are similar to those of the 140GHz gun. The simulations have been extended in order to include the electron beam propagation through the mode converter and the collector of the gyrotron. Double check of the simulations, which were performed with the code DAPHNE, has been initiated in collaboration with the Forschungzentrum–Karlsruhe in Germany (using the code ESRAY) and the National Technological University of Athens in Greece (using the code ARIADNE).

Gyrotron mode converter

The two codes written last year have been further developed. The first one calculates the power in each TE mode as a function of the converter axial coordinate z and the second one simulates the microwave bunch formation; both codes treat the case of a constant converter radius R). Some parts have been rewritten in a more concise and clear way and detailed comments have been added. The derivation of the coupling coefficients formulas for the TE-TE modes interaction in the case of linearly varying converter radius ($R = \kappa z$, where κ is a constant) has been performed. The formulas were verified at the transition to the case with a constant converter radius (formulas for this case were previously derived). An extension of the first code mentioned above has been started. The extended part is intended to perform the same calculations as the first version of the code but for the case of a linearly varying converter radius.

*2.7 Industrial process plasmas**

Most of the research projects in the industrial plasma group of the CRPP are carried out in close collaboration with Swiss industries and are mainly funded by the CTI or Topnano. The main topics during 2003 were capacitively coupled RF reactors for

* The work described under this section was performed outside the frame of the Association Euratom – Confédération Suisse.

the deposition on large areas for flat display and solar cell applications. The latter project is of particular interest since it allowed a Swiss equipment manufacturing industry to enter into the market for equipment for thin film solar cell production. In addition, a newly-designed capacitively coupled RF reactor has been tested in order to obtain highly uniform film thickness at very high plasma excitation frequencies for substrate areas bigger than $1m^2$. Besides these deposition plasmas, new research and development topics such as atmospheric plasma and electrical discharge machining (EDM) emerged. Discharge plasma physics is the main topic in these two interesting projects linked to successful applications. Modelling of process plasmas, in particular of large area RF plasmas, has been started with a first CTI project of a purely theoretical nature. A basic National Science Foundation project in collaboration with the Laboratoire de Thermique Appliqué et de Turbomachines (LTT) and the Laboratoire d'Ingénierie Numérique (LIN) of the Energy Institute (ISE), all part of the EPFL Faculty of Engineering (STI) on the influence of a weakly ionized boundary layer on transonic and supersonic air flows show that there is still demand for new applied topics as well as for pure fundamental research.

2.7.1 The physics of plasma enhanced CVD for large area coating

The aim of this CTI project is to develop a large area, high throughput coating system for mass production of silicon thin film solar cells, based on plasma enhanced chemical vapour deposition (PECVD) in a single chamber reactor. The work was carried out in a collaboration between CRPP Lausanne, IMT Neuchatel, and Unaxis Display Truebbach. The CRPP investigated the reactor design, the deposition of the intrinsic layer, and contributed to investigations of the boron contamination between the p- and i-layers. The IMT concentrated on layer properties and interface optimisation, boron contamination, and cell fabrication and evaluation. Unaxis developed an industrial reactor system.

The reactor parameter investigated in this project was the influence on the plasma uniformity of an asymmetric electrode construction. This asymmetry is intrinsic to the plasma-box design where the planar RF electrode is surrounded by a grounded sidewall. It was shown analytically that the RF plasma potential, and therefore the plasma, is more intense near the walls, extending into the plasma by a damping length given by the Telegraph equation. This gives rise to circulating DC currents which were measured using surface probes, thereby confirming the model. The influence of the side walls can therefore be predicted and it was shown that a symmetric electrode design would eliminate this source of plasma and film non-uniformity.

Film porosity appears to be linked to excessive degradation of the final solar cell and a density of at least 90%, measured by spectral ellipsometry, was taken as a guideline for obtaining high quality cells. It is therefore crucial to identify any possible errors in the ellipsometric method. For example, film surface roughness, due to deposition on a rough SnO_2-coated substrate, artificially reduces the ellipsometric density estimate. This was proven by systematically polishing a rough film surface (a method obtained from the CIME-EPFL) and noting that the density estimate converged to a higher value. Smoothing the surface was monitored by atomic force spectroscopy (in collaboration with the LPCM-EPFL). The conclusion is that the film density must always be measured using a smooth substrate such as a silicon wafer. Another source of error can be the imperfect angular alignment of the ellipsometer - the density estimate depends sensitively on this angle as shown in a collaboration with the EICN at Neuchatel. Reliable relative density estimates can be made by always using the same, fixed angle ellipsometer.

In addition, a basic version of a novel in-situ interferometric film growth rate diagnostic developed at the CRPP was especially adapted for a large area machine. This diagnostic will be used in further large area deposition projects at the CRPP and it is planned to also implement it in commercial KAI reactors on customers demand.

A critical issue for the single chamber system used in this project is the question of boron contamination of the i-layer following deposition of the boron-doped p-layer in the same reactor chamber. It was previously found that a simple flushing of the reactor with gases such as argon, hydrogen, and oxygen is not effective in reducing the contamination. It has also been checked that the origin of the contaminating boron is not from outgassing of physisorbed TMB, nor from the boron in the p-layer of the film itself. Many different scenarios were evaluated for their effectiveness in inhibiting boron contamination without damaging the final solar cell. An original in situ 'oxidation' process using water vapour without plasma application was developed at IMT. Speculating from previous experience at the CRPP, a new process was tested. SIMS measurements showed that the boron contamination was reduced. Subsequent tests on complete solar cells in IMT proved conclusively that this novel technique is a successful solution to the problem of single chamber operation, a crucial milestone in this CTI project. Moreover, the new treatment avoids the problems of oxygen contamination and degassing associated with water vapour. A patent concerning the flushing method is pending.

Transfer to industry

The present and preceding CTI project together with the excellent results of the micromorph solar cell developed at the University of Neuchatel are leading to important industrial implications. The board of Unaxis decided in view of the positive results concerning the application of Unaxis KAI reactors for the production of thin film silicon solar cells to create a new Unaxis business unit: Unaxis Solar. The clear goal of Unaxis is to become the leading supplier of advanced production equipment and processes for silicon-based thin film solar cell manufacturing. The present project opened the door to the final decision of Unaxis. Due to this decision the Swiss photovoltaic community and Swiss PV market now have a domestic manufacturer of equipment for the production of thin film solar cells, an important position for future developments of the solar cell market.

2.7.2 Plasma spraying

Characterisation of supersonic low pressure plasma jets by electrostatic probes

Unlike atmospheric pressure plasma jets, which have been extensively studied experimentally and theoretically, the growth of interest in low pressure DC plasma jets has only occurred recently. Low pressure plasma jets present unconventional properties such as their low collisionality, their large dimensions and their supersonic flow. Therefore specific diagnostics have to be adapted for these conditions. Studies of plasma jets using optical emission spectroscopy (OES) are mostly based on the assumption of local thermodynamic equilibrium (LTE) which is no longer satisfied at lower pressure. Enthalpy probe measurements in compressible supersonic plasma jets have been reported but were limited to a pressure above 200mbar. These limitations show the need to develop a diagnostic to characterize DC plasma jets covering a pressure range from 2 to 80mbar which is independent of the LTE assumption.

Electrostatic probes are widely applied in low density plasmas such as glow discharges to measure the electron temperature and density. Unlike other diagnostics like the optical emission spectroscopy (Boltzmann plot) or the enthalpy probe, this technique does not require the assumption of the local thermodynamic equilibrium.

The investigated plasma jet is generated with a Sulzer Metco F4-VB gun with a conical nozzle of 6/12mm inner/exit diameters. It is mounted on a 2-axis (radial and axial) displacement system inside a 2 m^3 vacuum vessel (Fig. 2.7.1).

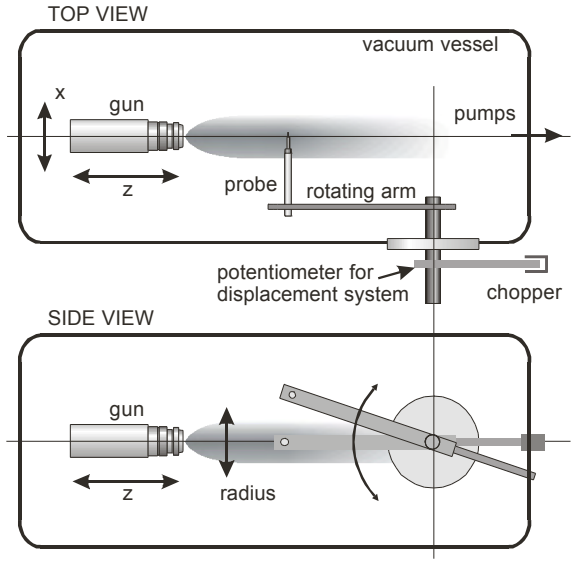

Fig. 2.7.1 *Schematic view of the experimental arrangement*

The double Langmuir probe is made of two parallel tungsten wires of 0.15mm diameter sticking out 1.5mm from a thin ceramic sheath used as shield. The two wires are 1mm apart and the probe is quickly swept radially through the plasma jet by a rotating arm with calibrated position to obtain radial profiles. The current circulating between the electrically floating probes once immersed in the plasma jet is measured as a function of the voltage difference. The Mach probe construction is similar to double probe, except that the two probes are mounted with their axes perpendicular to each other. Therefore one probe is parallel to the plasma jet flow, the other being perpendicular. Each probe is polarised at the same potential in the ion saturation current region of the Langmuir characteristic. The ratio of the currents collected by the two probes allows the Mach number of the plasma flow to be determined.

Probe measurements have been made in under-expanded jets in the pressure range from 6 to 40mbar in the chamber chamber. Figures 2.7.2, 2.7.3 and 2.7.4 show light emission and radial profiles of Mach number, electron density and temperature at axial positions corresponding to the middle of successive expansion and compression zones which are indicated by vertical markers in Fig. 2.7.2. These positions correspond to the local extrema of the axial light emission profile.

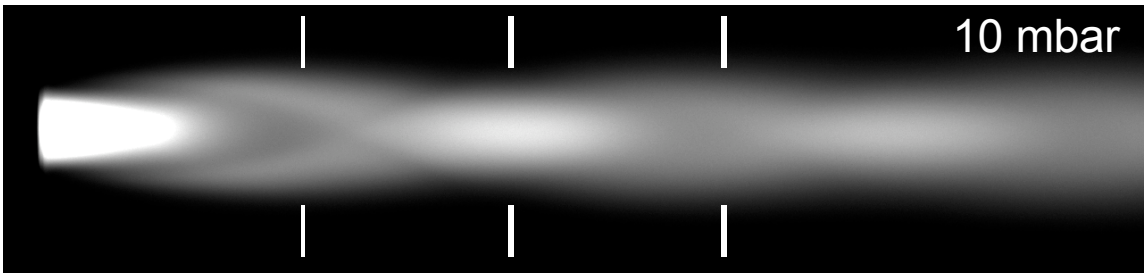

Fig. 2.7.2 *Images of the plasma jet at 10mbar chamber pressures.*

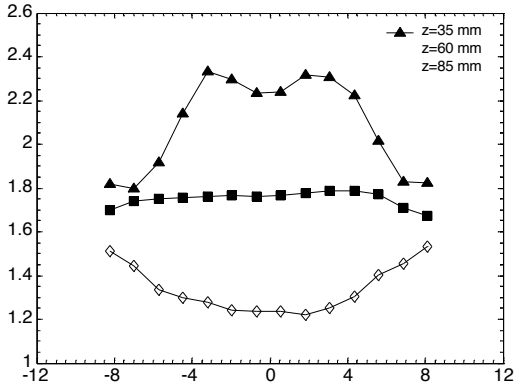

Fig. 2.7.3 *Radial profiles of the Mach number at different axial locations*

The Mach number radial profile (Fig. 2.7.3) in the first expansion zone at z=35mm is broad and slightly hollow on axis. The two bumps correspond to the inner part (r=3.5 mm) of the visible barrel shocks at the edge of the plasma jet where the flow reaches Mach 2.4. The flow velocity is then reduced radially to Mach 1.8 which is still supersonic because the shocks at the plasma fringe are oblique. In the compression zone (z=60mm), the Mach number radial profile has a minimum on the jet axis, its value strongly drops from the first expansion zone close to the subsonic transition at Mach 1.2 but the flow still remains supersonic, which means that there is no Mach reflection here. In this area, where the local static pressure is higher than the surrounding pressure, the jet starts to expand again, but due to the viscosity and turbulence of the surrounding cold gas, the plasma jet does not reach the speed of the first expansion zone and the profile is rather flat at Mach 1.7 in the second expansion zone (z=85mm) where there are no barrel shocks.

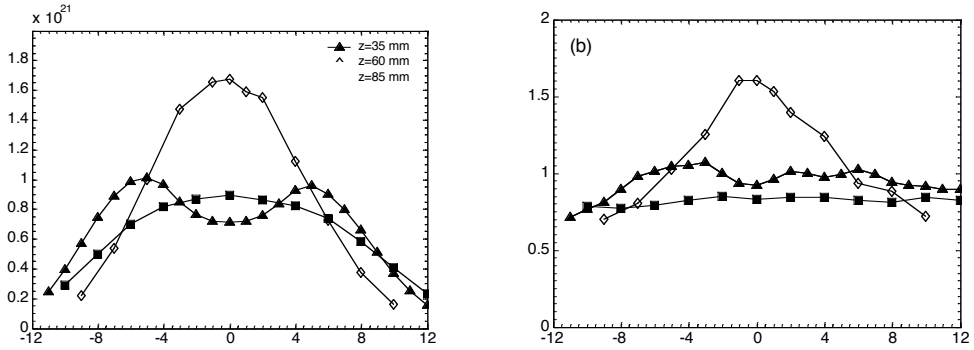

Fig. 2.7.4 *Radial profiles of the electron density (a) and electron temperature (b) at 10mbar, 400A current and 40SLPM Ar flow*

The radial profiles of the electron density shown in Fig. 2.7.4 reproduce the structure of the jet topology characterised by the plasma jet light emission. The electron density is broad and hollow in the first expansion zone, as is the radial intensity profile. At the maximum expansion region the electron density is at its lowest value of $7 \cdot 10^{20} m^{-3}$ on axis. On the other hand the electron temperature radial profiles present a rather flat profile for both expansion zones at values between 0.8 and 1eV. However, it peaks in the compression zone where the axial value (1.6eV) is two times higher than on the plasma edge. There is substantial heating of the electrons in the compression zone.

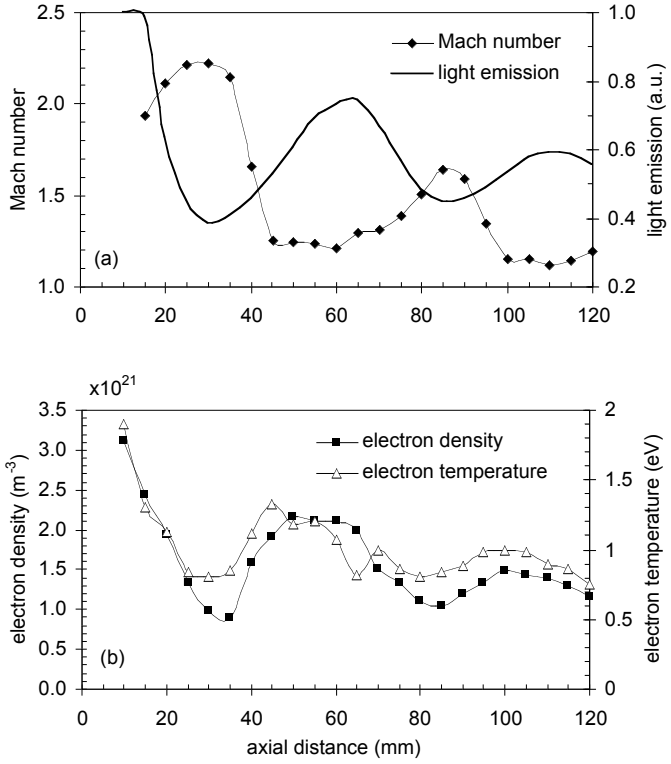

Fig. 2.7.5 *Axial profiles of the light emission and Mach number (a), and of the electron density and temperature (b) at 10mbar, torch parameters: 400A, 40SLPM Ar*

Figure 2.7.5 shows axial profiles of the Mach number, electron density and temperature and a direct comparison with the axial light emission of the plasma jet for the same conditions. The Mach number clearly reaches its maximum when the jet is at its maximum expansion which corresponds to the region where the light emission is the weakest. Because of this expansion the electron density and the electron temperature also reach their minimum at z=30mm.

The oblique shock waves which allow the flow to change direction after the expansion reflect fromeach other further downstream on the jet axis at an axial distance of about z=44mm. This region corresponds to a transition zone between the expansion and the compression zone (Fig. 2.7.2). The Mach number drops strongly at this location and stays minimum as far as z=60mm which corresponds to the maximum of light emission of the compression zone. The electron density and the electron temperature rise to their local maxima because the flow is strongly slowed down and compressed.

The jet exhibits two completely different behaviours of the electron density and temperature considering either the radial expansion or the axial flow in the

compression zone. The radial increase of the electron density at the fringe in the first expansion zone is due to the fact that the plasma jet is compressed at the edge by the cold surrounding gas, with only a slight increase of the electron temperature from 0.9 to 1.1eV and a slight reduction of the Mach number. On the other hand, in the axial compression zone, the electron density increases axially but this time with a major heating of the electrons from 0.8eV to 1.6eV, which is shown up by the axial profile in Fig. 2.7.7. This is because the plasma jet is strongly compressed and slowed down at the same time with a decrease of the Mach number from 2.4 to 1.2. Therefore a substantial fraction of the kinetic energy is converted into thermal energy.

Beyond that point, the flow velocity already starts to increase till it reaches its maximum in the second expansion zone but remains still lower than in the first expansion zone. Axially, the electron density and temperature follow the structure of the plasma jet emission. However the Mach number strongly drops already upstream of the bright visible compression zone, even though the maximum of the Mach number occurs where the light emission is the weakest.

A novel approach to interpret enthalpy probe measurements in low pressure supersonic plasma jets

To improve the control and quality of the processes further and to develop new applications, a more quantitative approach is required in which the fundamental physics of the process should be investigated. In particular, the phenomena controlling the expanding plasma jet should be studied both experimentally and by numerical simulation. This requires knowledge of key parameters such as the temperature, pressure, chemical composition, velocity or local heat flux.

To measure these parameters, the enthalpy probe measurement technique has been extensively applied in Atmospheric Plasma Spraying (APS) jets assuming Local Thermodynamic Equilibrium (LTE) and incompressible flow. However, the latter is not valid in low pressure plasma jets and the formation of a normal shock wave (NSW) in front of the probe must be taken into account. Although specific technological constraints (low gas density) have been recently overcome, there are still severe conceptual complications in the use of enthalpy probes for low pressure plasma jets.

The first steps of a new approach have been presented to interpret enthalpy probe measurements performed in supersonic plasma jets which are not in aerodynamic equilibrium. This technique is based on the resolution of the fundamental governing flow equations throughout the normal shock wave (NSW) induced by the probe and towards stagnation. It uses the second law of Thermodynamics to include non-isentropic effects and relies on the measurement of the post shock static pressure using a specially developed probe. The advantages of this new approach over previous ones are the less restrictive assumptions and the possibility to include non-LTE effects. In addition, the unknown static pressure of the free jet (usually wrongly approximated by the chamber pressure) is not required as an input, but is obtained as a result of the method.

This new technique has been tested and compared with previous approaches for the case of an under-expanded argon plasma jet produced by a DC plasma torch operated at 10 mbar. The results obtained, in terms of static pressure, temperature and velocity profiles, are consistent with the jet flow phenomenology. Moreover, agreement is found with previous methods at the fringe of the jet where non-aerodynamic equilibrium effects are negligible.

2.7.3 Design of a new large area high density RF plasma source (HDS)

Capacitively coupled parallel plate RF reactors are commonly used for plasma enhanced chemical vapour deposition (PECVD) and dry etching of thin films such as amorphous silicon or silicon oxide. Large area (>1m^2) reactors are used for the production of photovoltaic solar cells and thin film transistors for flat screens. These industrial applications typically require a uniformity in film thickness to better than 10%.

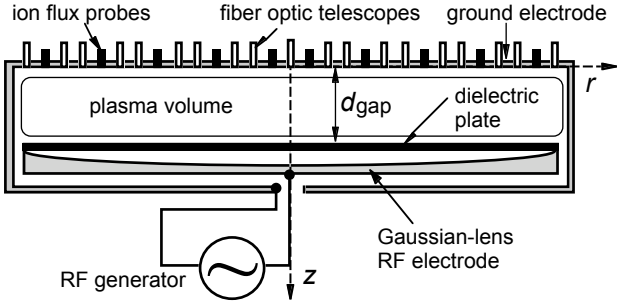

Fig. 2.7.6 *1m diameter cylindrical RF test reactor*

The non-uniformity considered is due to finite wavelength effects associated with high frequencies in large area reactors, such that the reactor size is comparable to, or larger than, a tenth of the free space wavelength at the excitation frequency. Non-uniform RF plasma potential will generally result in non-uniform power dissipation and consequently non-uniform deposition or etch rates. Many other phenomena can give rise to non-uniform deposition or etching in RF parallel plate reactors, including imperfect contact of the substrate with the electrode inappropriate gas flow distribution, clouds of dust particles, and various edge effects due to fringing fields, electrode asymmetry etc.

A schematic of the 1m diameter cylindrical reactor is shown in Fig. 2.7.6; a cylindrical reactor was used to facilitate comparison with the 2D cylindrical vacuum theory. Moreover, cylindrical symmetry means that a single line of probes across a radius should suffice to characterise the plasma uniformity, in contrast to a rectangular reactor where a 2D array is necessary. In these experiments, measurements were made across a whole diameter to check the cylindrical symmetry. The lens design of the RF electrode is intended to compensate the standing wave effect by creating a uniform vertical electric field over the plasma volume. To be uniform, the plasma requires not only a constant electric field, but also a constant geometrical thickness. The plasma was therefore confined between parallel boundaries by a disc of glass placed on the profiled electrode (see Fig. 2.7.6). A special RF electrode was designed whose surface was machined according to a Gaussian profile. The electrode was constructed for uniform electric field at a design frequency of 100MHz. Conventional parallel plate electrodes were also used for comparison, replacing the glass with a metal disc.

A dielectric convex "lens" can be used to fill the gap below the glass to prevent any possible ignition of a parasitic plasma. Taking this into account, the design frequency with PTFE changes to 69MHz. All reported experiments were performed using argon and frequencies of 13.56, 67.8 and 100MHz. The vacuum RF electric field radial profile was measured by drawing a calibrated diode probe across the reactor diameter at mid-gap height through a small window in the sidewall. The plasma uniformity was monitored by means of two probe arrays positioned along the same diameter. Nineteen fibre optic telescope probes with photodiode sensors

measured the optical emission intensity averaged over the vertical profile to give a rough indication of the plasma power radial profile. Ten surface mounted biased (-50V) electrostatic probes measured the ion Bohm current through the RF sheath to give an estimate of the ion flux onto the plane ground electrode.

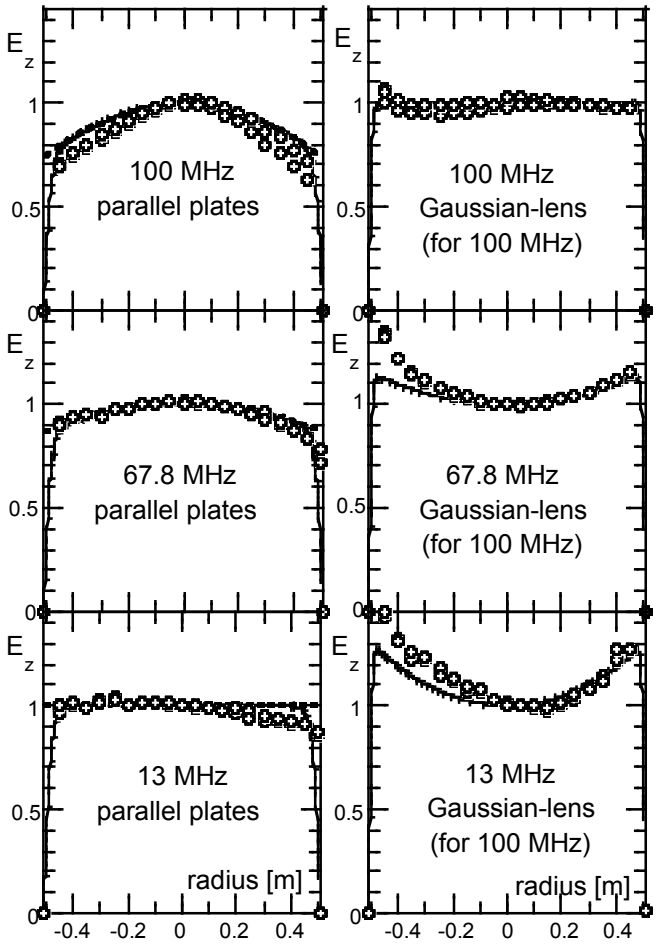

Fig. 2.7.7 *Measured and modeled radial profiles of the vertical electric field in vacuum*

The solution for Gaussian profile electrodes predicts a uniform radial profile for the vertical electric field at the design frequency of the lens. Convex (under-compensated) or concave (over-compensated) curves are observed for frequencies above or below the design frequency respectively. The measured profiles in Fig. 2.7.7 agree well with the theoretical curves, as expected for the vacuum case. The theory and the design and construction of the reactor with a gaussian-lens electrode are therefore validated for the case of vacuum (no plasma).

In Fig. 2.7.8 it is shown that it is possible to select pressures and RF powers for good uniformity of the ion flux at 67.8MHz using the Gaussian-lens electrode. However, the profiles obtained with the parallel plate electrode at this frequency remain dominated by standing wave non-uniformity for all plasma parameters. This demonstrates the effectiveness of the Gaussian-lens electrode for compensating the standing wave effects for VHF plasmas in large area reactors.

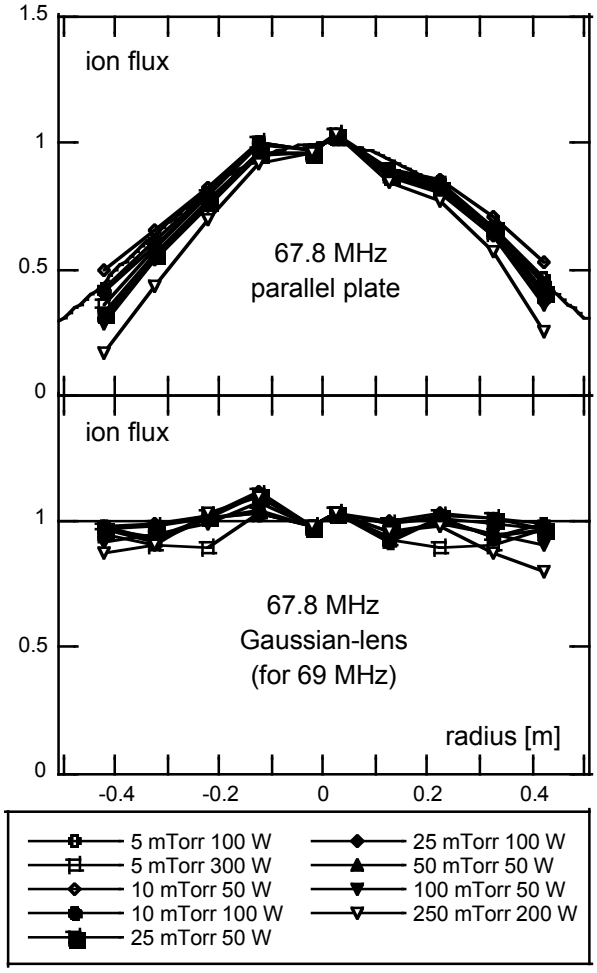

Fig. 2.7.8 *Measured radial profiles of the ion flux at 67.8MHz for the Gaussian-lens electrode filled with PTFE (design frequency 69.0MHz)*

2.7.4 Plasma diagnostics for electrical discharge machining (EDM)

Electrical Discharge Machining (EDM) is a well-known machining technique for more than fifty years. Nowadays it is widely used in a large number of industrial areas, mainly to produce moulds, dies and finished parts with complex shapes.

This technology uses the eroding effect of electric spark discharges on the electrodes. Thus, the machining consists of successively removing small volumes of electrode material, which are molten or vaporised during the discharge. The electrical discharges are created between the conductive workpiece and a shaped electrode (die-sinking machine) or a metallic wire (wire cutting machine). Thus EDM can be used to machine any material that conducts electricity, whatever its hardness may be. The sparks are created in a flowing dielectric fluid, generally water or oil, for several reasons. It guarantees a high plasma pressure and therefore a high removing force on the molten metal when the plasma collapses, it solidifies the molten metal into small particles, and it also enhances the flushing of these particles.

Figure 2.7.9 shows a schematic of the experimental set-up, a small and versatile die-sinking EDM machine. The dielectric, the electrode and the workpiece can

easily be changed. We used pure water, mineral oil and liquid nitrogen as dielectric; copper, tungsten and graphite electrodes; and W300 steel workpieces.

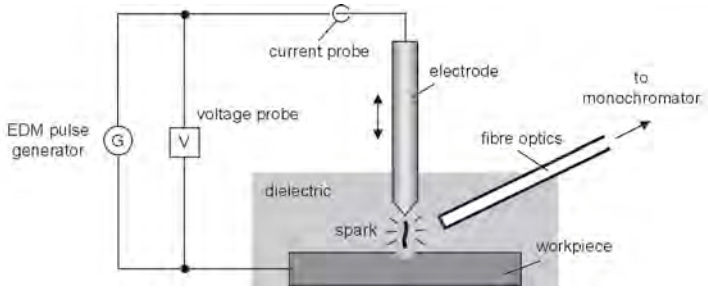

Fig. 2.7.9 *Schematic drawing of the experimental setup*

Figure 2.7.10 is a close-up image of the electrodes during machining. This image was obtained with an endoscope composed of 10'000 fibres coupled to a CCD camera. The plasma is clearly visible, along with gas bubbles created by the discharge.

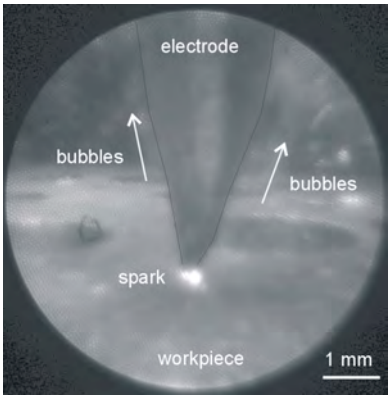

Fig. 2.7.10 *Image of an EDM discharge in water obtained with an endoscope*

For Optical Emission Spectroscopy, the emitted light is collected by a quartz fibre. The fibre is immersed in the dielectric, located a few millimeters from the spark to optimise the collected light intensity and to reduce absorption from the dielectric. A typical spectrum from EDM discharge changes for different experimental conditions such as electrode material/workpiece material, dielectric, discharge current and discharge on-time (see Fig. 2.7.11). The dominant line within the spectra is the Balmer H_α line emitted by atomic hydrogen, which comes from the cracking of the dielectric molecules. Although the H_α line is dominant, the remaining Balmer series lines such as H_β or H_γ are not observed. Furthermore, the H_α line is broadened. The plasma is contaminated by impurities: several lines of atomic copper from the electrode are present, along with many lines originating from atomic iron, chromium and carbon of the removed material of the steel workpiece. The fact that all observed lines are atomic lines (and a few neutral molecular lines) and that no ionic lines are visible is a first indication that the electron temperature is low.

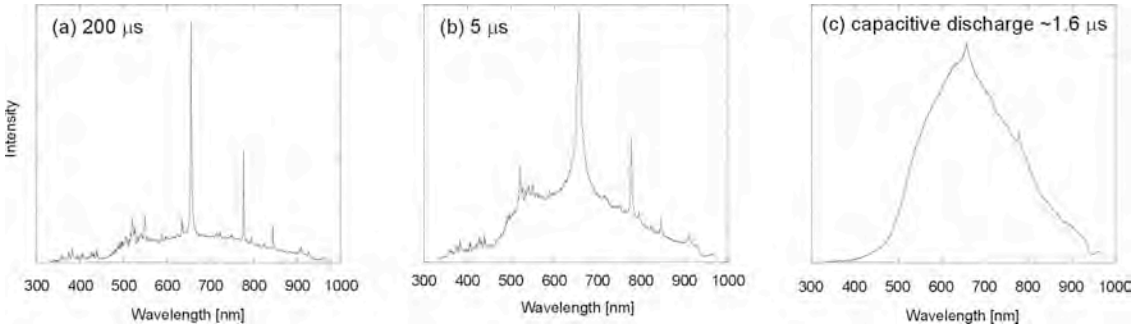

Fig. 2.7.11 *Effect of the on-time on the emission spectrum (Cu/steel, water, (a) 12A, 200µs; (b) 12A, 5µs; (c) ~1.6µs)*

The broadening of the H_α line increases drastically with decreasing on-time as shown in Fig. 2.7.11 (a) and (b). Such an important broadening can only be due to dynamic Stark broadening, which by far dominates the pressure broadening or Doppler broadening. Stark broadening of the H_α line depends strongly on the electron density and can be used to evaluate it. The H_α line is also shifted to higher wavelengths with increasing electron density. Figure 2.7.12 shows time-resolved emission spectra of a spectral region where numerous metal lines are visible. The iron, chromium and copper lines are completely merged during approximately the first microsecond, which again indicates a particularly high electron density.

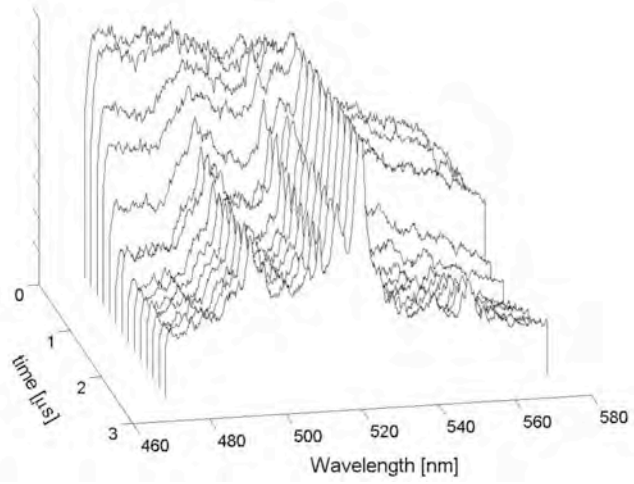

Fig. 2.7.12 *Merging of the Fe, Cu and Cr atomic lines (Cu/steel, water, 12A, time resolution 200ns)*

The electron temperature found from the Boltzman plot method assuming thermal equilibrium is about 0.7eV (~8100K) and remains rather constant within the error margin during the discharge.

To calculate the evolution of the electron density, we use FWHM and shift measurements from time-resolved spectra of the H_α line, shown in Fig. 2.7.13. In spite of some differences, the FWHM and the shift measurements give comparable density values and evolution. As expected, the electron density is extremely high during the first microsecond (above $10^{18}cm^{-3}$) and then decreases rapidly with time. In the very beginning of the discharge, the plasma has to overcome the extreme pressure imposed by the dielectric.

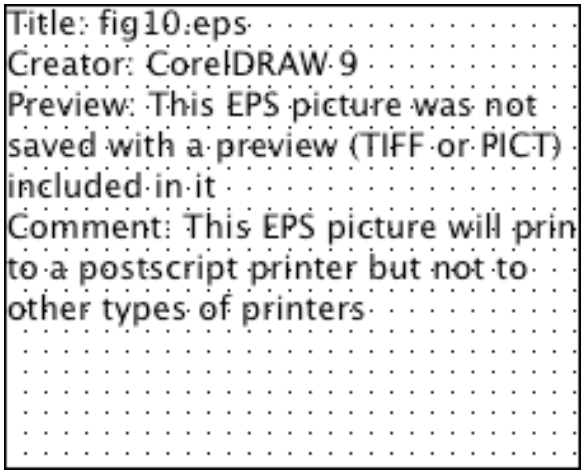

Fig. 2.7.13 *FWHM and shift measurements from time-resolved spectra of the H_α line are used to derive the electron density*

The plasma parameter Γ given by the ratio of Coulomb interaction divided by thermal interaction is in our case around 0.45. Thus, EDM discharges produce cold and dense plasmas, which are weakly non-ideal. In addition, the spectroscopic results indicate directly that the plasma is non-ideal. First of all, the extreme density lowers the ionization energy threshold and thus "erases" the upper energy levels of atoms. This results in absence of the H_β and H_γ lines for example, along with an increase in continuum radiation. These effects can only occur in non-ideal plasma and can clearly be observed on our spectra as said previously. In addition to broadening and shift, the H_α line gives other useful information. Figure 2.7.14 shows a typical example of a spectrum around the H_α line. If a Lorentzian fit is applied, it is observed that the shape of the line is slightly asymmetric and deviates from the fit. This asymmetry is due to interactions between ions and the emitter (hydrogen atom in our case), and is another sign of plasma non-ideality.

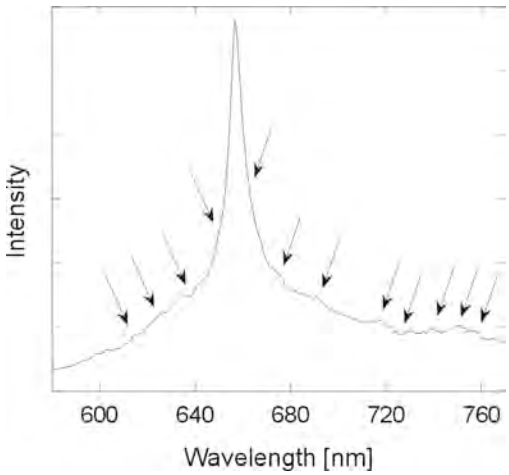

Fig. 2.7.14 *Complex structures around the H_α line (Cu/steel, water, 12A, 2μs)*

We also see complex structures around the line arising from the strong static electric field in the plasma (~ MV/cm) causing splitting of energy levels in the hydrogen atoms (Stark effect). Transitions between these new levels create several lines around H_α. Furthermore, if Langmuir or ion acoustic turbulence is present in the plasma, an oscillating electric field is superimposed on the static field. In the case of Langmuir turbulence, the turbulence creates satellite lines located at 656.2nm$\pm n\bullet\lambda_p$, where n=1, 2, … and λ_p is the wavelength associated with the

Langmuir wave frequency (~10nm under our conditions). Finally, if resonant interactions between the Stark separation and the oscillations of the dynamic field occur, depressions or "dips'' appear on the spectrum. The combination of these effects, typical in non-ideal plasma, results in multiple modifications in the H_α profile as seen on Fig. 2.7.14. The complexity of the emission spectrum reflects the complexity of the plasma itself: it is a cold and dense plasma, highly collisional, with strong electric field, turbulence and resonance phenomena.

2.7.5 Atmospheric plasmas for thin film coating

Avoiding vacuum technology for depositing coatings on polymer films is certainly one possible route for cost reduction. Vacuum technology has several economic drawbacks. The process for coating deposition is not continuous, the machine has to be stopped and opened for the loading and unloading of film reels, and pumping down time is tightly linked to the pumping speed and cleanliness of the pumping system. The maintenance of equipment for production is costly and time consuming. Plasmas at atmospheric pressure are thought to be an alternative way for the production of coatings for various applications.

However, there are different problems related to the process by RF plasmas operated at atmospheric pressure. First of all, the applied RF voltage must be in the kV range, giving rise to considerable problems in the design and construction of the RF generator, circuit and of the RF electrodes. RF plasma discharges at this pressure often show a discharge consisting of many different discharge filaments similar to the one observed in the so-called silent discharges. However, under certain conditions a uniform plasma can be obtained, as required for uniform film deposition. The control of the discharge type is one of the difficulties in atmospheric RF plasma applications. The control parameters for the discharge transition are the plasma excitation frequency and the electrode gap distance.

During the year three principal topics have been investigated: the HV circuit and its optimisation and modeling and design of the electrodes.

Careful design of the HV circuit to create the atmospheric plasma is of prime importance for the success of the project. The plasma excitation circuit with a frequency response from 1kHz to 20kHz was built. Various experiments have been performed to determine the electrical components of the circuit in order to make a model of the circuit. PSpices (simulation program for electronics) was used to simulate the circuit and good agreement with measurements of the circuit response have been found. Besides the simple electrical circuit, matching circuits have been investigated in order to optimise the RF power in the atmospheric plasma. The experiment has been equipped with the necessary large frequency response voltage and current measurement equipment and the corresponding signal treatment.

The dielectric barrier material is as well of prime importance for well-behaved discharges. Several different materials (glasses, Teflon, ceramics), material qualities (purity) dimensions (thickness, surface) and preparation (welding, printing) have been investigated and evaluated. At present, by far the best solution is obtained with a thin (≈1mm) alumina dielectric with screen printed electrodes (in collaboration with the Laboratoire d'électrochimie physique et analytique) finally glued to the electrode supports by means of a conductive epoxy glue. The screen printing technique used allows a lot of freedom in the design and patterning of the electrodes. In addition, it turned out that this type of electrode was rigid enough to withstand long duration plasma operation.

The gas distribution between the electrodes also turned out to be important for obtaining well behaved glow discharges at atmospheric pressure. The design of the

gas distribution system has been optimized for the operation at atmospheric pressure. The assembly of the reactor at the CRPP is shown in Fig. 2.7.15.

Fig. 2.7.15 *View of the atmospheric plasma reactor at the CRPP*

In addition, the installation of the electrodes into a vacuum chamber has been completed. This system can be used to investigate RF discharge in various gases at pressures from 1bar down to about 1mbar.

2.7.6 Nano powder synthesis by thermal plasmas

The goal of the project is to monitor and to develop *in-situ* process monitoring for nano-particle processing in thermal RF induction plasmas. To produce the nano-powders with the desired properties and high reproducibility it is necessary to understand the interior of the plasma where reactions between powders and different plasma components take place. These reactions and phenomena include phase transformations, particle melting, evaporation and recondensation etc. Fundamental study of these chemical, physical and thermal reactions and phenomena in the plasma will be carried out by applying various *in-situ* particle monitoring methods. These *in-situ* monitoring measurements will be correlated to ex-situ characterization of the synthesised nano-powders which will allow us to understand and control the process of nano-powder synthesis.

In the frame of TOPNANO 21, a project has been started on the nano-powder synthesis in thermal plasmas in collaboration with the EMPA in Thun. The project intends to contribute to the understanding of the nanometer-sized powder formation and production in RF thermal plasmas through a multidisciplinary approach involving material scientists (EMPA-Thun) and plasma physicists (EPFL-CRPP). *In-situ* diagnostic methods are of prime importance to guarantee high purity, good dispersion, ultra fine particle size.

As a first step, an enthalpy probe system was adapted to the synthesis chamber to characterize the inductively coupled plasma (ICP). The experimental set-up used consists of three parts. At first the ICP-torch which is operated by max. 30kW RF

(13.56MHz) power, secondly a water cooled cylindrical reactor which is connected to a filter unit and lastly the enthalpy probe system.

The enthalpy probe system has a radial position displacement system and cooling water supply and is connected to a computer for data acquisition. The measurements were carried out in three different axial positions by help of the viewports which are especially designed in several levels for in-situ powder diagnostics. Various plasma parameters were investigated. (gas composition, gas flow rate in different gas inlet line and pressure). In order to better understand gas flow effects on plasma temperature and velocity, the local plasma composition will be investigated by a gas sampling system (mass spectrometry). Taking into account the introduction of powders into the plasma centre line through injector it is necessary to have a high RF power to be able to evaporate or melt powders which have a very high melting point such as tungsten carbide.

In addition, laser extinction measurements have been designed, tested and installed on the device and first in-situ powder measurements have been made. These preliminary results helped to optimise the powder feeder and torch operation.

2.7.7 Plasma induced surface modifications for biomedical applications

Various studies on surface modifications for biomedical application have been performed in a CTI project in collaboration with Prof. H. J. Mathieu from the Laboratoire de Métallurgie Chimique (LMCH) of the STI.

Plasma surface treatments are potentially very useful for the covalent incorporation into polymer surfaces of extraneous reactive groups suitable for participation in further, conventional chemical reactions at the surface. The plasma modification can be carried out in the presence of specific gases, such as O_2, Ar, He, NH_3, N_2, and H_2. This results in the generation of active species, which can activate and modify the material depending on the nature of the gaseous medium.

Polystyrene (PS) is a popular substrate for disposable ware in medical diagnostic, primarily due to its optical transparency, durability, low cost, and good mouldability. Non-modified polystyrene may cause non-specific adsorption. Therefore it is customary to modify it with hydrophilic polymers.

The aim of this work is to prepare chemically reactive yet specific PS surfaces for subsequent high-density bio-immobilisation. These modified surfaces are potentially efficient substrates of medical diagnostic tools for use in a proprietary ADS fluorescence reader.

One of the great problems in polymer processing is the upgrade from the laboratory reactor to an industrial reactor treating a large number of items cost effectively. In most cases the laboratory reactor conditions are poorly or even completely unknown. The aim of the present study is to diagnose the laboratory reactor and its processing in order to translate the process onto a large reactor for industrial application. To activate the specific surface properties of the polymer, ion bombardment is the crucial process. In order to characterise the activation process the bombarding ion species and their ion energy impinging on the film must be known. In addition the ion fluence, respectively the ion dose, is an important parameter in the activation process.

Plasma treatment of PS chips was carried out in a capacitively coupled RF reactor operating at 13.56MHz. For plasma diagnostics only commercial equipment has been used in order to demonstrate that basic plasma diagnostics are now

commercially available and are sufficient for an advanced understanding of the surface modification by plasmas and the industrialisation of the processes. A Scientific System ion flux probe (IFT) has been applied to measure the ion flux on the grounded electrode. A Balzers PPM 422 system has been used to measure the ion composition and the energy of the impinging ions. Both measuring systems have been incorporated into the grounded electrode. This experimental arrangement permits a measurement of the characteristics of the ion bombardment at the same place as the treated substrate. Therefore correlation between plasma parameters and surface analysis can be obtained.

A comparison of N_2-H_2 and NH_3-H_2 plasmas with varying admixture of H_2 using commercial diagnostic equipment is carried out. The data are correlated with PS surface activation controlled by XPS. The main results are that the maximum ion energy is around 10-15 eV. This energy is given by the asymmetric construction of the processing reactor. Interestingly to create a functionality on the film 10^4-10^5 ions/molecule per cm^2 are necessary. It was also found that under the same experimental conditions a NH_3-H_2 plasma is almost two times more efficient than a N_2-H_2 plasma to create active nitrogen-containing (C-N) sites.

2.7.8 Modeling for industrial plasmas

In collaboration with Unaxis a new project on the modelling of industrial plasmas has been elaborated and accepted by the CTI. Until now, the development of the next large area PECVD reactor generation has essentially been done empirically, based on the experience acquired with the preceding reactor generation. Due to the rapid increase of the substrate size, which now reaches more than 1m, in the flat display industry, the development of the PECVD reactors used for the fabrication of the TFTs becomes more and more costly and difficult, especially if technological innovations have to be tested and introduced to reach the required specifications. In order to reduce the development cost, a project of numerical simulation of large area PECVD reactors has been started in collaboration with UNAXIS. The main goals of this project are first to identify the origin of the film thickness and property non-uniformity, and then to dispose of a tool which should permit an evaluation of different reactor designs and choose the most promising one. The different aspects that have to be treated in the development of the model are first the simulation of the gas flow distribution across the porous showerhead RF electrode, and then the development of the neutral chemistry model which has to be coupled to the plasma physical model (fluid description). In order to fulfil this project in a relatively short time scale of only two years, it has been decided to use a commercial software package (CFD-RC ACE+) and to adapt it to our specific reactor geometry and process conditions.

2.7.9 Influence of a weakly ionised boundary layer on transonic and supersonic air flow

During 2003, the National Science Foundation accepted a project which involves a close collaboration between the Laboratoire de Thermique Applique et de Turbomachines (LTT) and the Laboratoire d'Ingénierie Numérique (LIN) of the Energy Institute (ISE) from the Faculty of Engineering (STI) and the CRPP.

The goal of the project is to study the effect of ionised gases in the proximity of leading edge surfaces on the shape, strength and absorption of the shock envelopes present within oncoming air flow in transonic and supersonic regimes. The project proposes an experimental investigation of the modification and dispersion of shocks

that arise in transonic and supersonic flow by use a weak ionisation of the gas generated by a surface discharge.

The experiments will consist of an installation of a typical aircraft wing section in one of the Laval nozzles at LTT. The Laval nozzle available at the LTT produces an outlet Mach Number that can be regulated between 0.2 and 1.6. An atmospheric uniform glow discharge will be used as plasma source to obtain the required plasma layer covering the necessary wing surfaces. This surface plasma source consists of a parallel arrangement of electrode strips on a suitable dielectric between which the plasma is created. Different electrode geometries and arrangements are possible which need to be optimised for the application on the wing section surface. The choice of the dielectric is of prime importance for the discharge. Different dielectrics materials are possible however these should also be functional with demands concerning mechanical properties and temperature resistance. Furthermore in a first attempt, common dielectrics shall be used for the initial investigations on a model in the wind channel. Later on, different materials compatible with the constraints of the aircraft shall be used and tested. The plasmas obtained will be investigated with different diagnostic methods, in particular the crucial power efficiency shall be studied.

The modification of the flow structure and shock wave structure with the ionised air will be investigated and compared with the model and the former experiments without the plasma layer. The investigations will also include studies on the effect of the surrounding flow on the stability of the glow discharge.

2.7.10 Other collaborations and industrial mandates

During the year, the industrial plasma group obtained two complete microwave plasma systems with 2 and 6kW power from the Institute of Materials. The equipment has been transferred to the CRPP and rebuilding of the experiments is underway. This new equipment is an excellent contribution to the group which aims to have in the future an experiment based on this commonly used plasma source.

Numerous industries consulted us during the last year and this resulted in many small experiments and tests which have been performed on the existing plasma reactors at the CRPP.

At this point it should be added that the collaboration with industry is excellent and a high degree of confidence between the collaborating industry and the plasma processing group exists. This working atmosphere is extremely stimulating for the different members such as PhD students and senior physicists.

3 Technical achievements of the CRPP in 2003

3.1 TCV operation

During 2003, the way of operating TCV was modified with the aim of saving on the consumption of liquid helium for the ECH gyrotron magnets. The rhythm of four operational days per week, three weeks every four weeks has been replaced by compact blocks of continuous operation.

The operation was interrupted by a few minor incidents, some of them attributed to the new Thomson scattering system, whose increased laser power puts additional load on the optics near the tokamak. Another was due to overheating of a flange by unabsorbed microwaves.

3.2 TCV diagnostics

After 10 years of operation, with all essential diagnostics and many TCV-specific systems routinely operational or nearing completion, the issue of future diagnostic developments for TCV is intimately linked with the medium-to-long term future of the TCV programme, which will continue to have both a scientific and an educational mission. The possibility of major investments is expected to be restricted due to an increased involvement of CRPP in ITER. As a result, progress on TCV is likely to be driven to a lesser extent by performance enhancements. The TCV scientific programme is expected to put more emphasis on aspects of fundamental fusion physics and generic technology issues within the areas of the competence of CRPP.

3.2.1 Magnetic measurements

X3 absorption measurements in H-mode

For high β in H-mode plasmas using X3 heating, a measurement of the absorbed X3 power is required. The normal diamagnetic flux measurement is strongly affected by ELMs (edge localised modes observed during H-mode). A new process has been developed to identify and compensate for the ELM effect by modelling the DML response to the ELMs as top-hat functions as shown in Fig. 3.2.1. The method consists of identifying the transfer functions H_m such that $\hat{y}_k = \sum_m H_m(z) x_{m,k}$ where each x_m represents a single ELM and $\hat{y}$ is the modelled response signal. The identification is performed minimising $J = \sum_k [y_k - \hat{y}_k]^2$ using a non-linear method leading to a model of type:

$$\hat{y}_k = \sum_m \frac{\alpha_m}{1 - a z^{-1}} x_{m,k} + \sum_s A_s \varphi_{s,k}$$

where a (the pole), $\{\alpha_m\}$ (the amplitudes) and $\{A_s\}$ are the free parameters, z is the Z transform variable and $\{\varphi_s\}$ are B-spline base functions (to follow the slow variations). Figure 3.2.1 shows the DML signal and the modelled compensation for

the ELM response. The power modulation contribution will be added in the model in order to be able to extract the absorbed power.

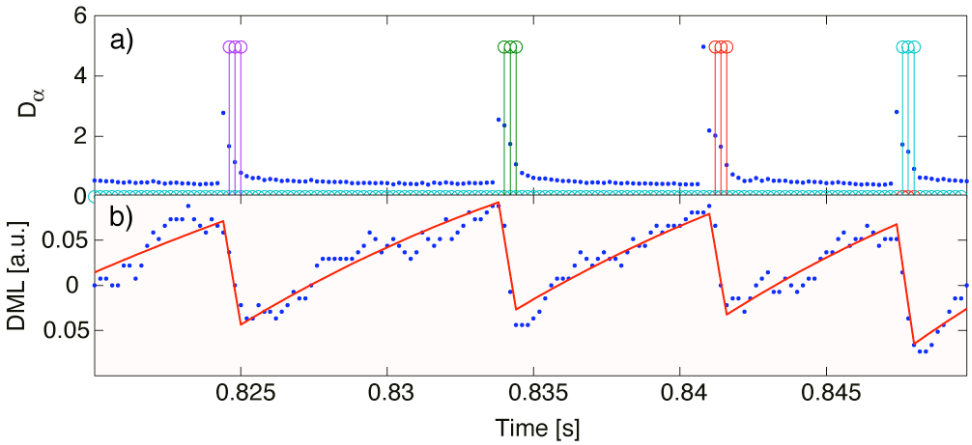

Fig. 3.2.1 *a) D_α measurement (blue dashed line) showing the ELMs and model x_m (multicolour stems); b) DML measurement y (blue dashed line) strongly affected by ELMs shows the model $\hat{y}$(red line) compensation performing well*

3.2.2 Thomson scattering

Measurements of T_e and n_e with improved spatial resolution for a limited number of chords have become possible on TCV with the installation of additional spectrometers on loan from Consorzio RFX, Padova, Italy. Nine spectrometers with 4 spectral channels each and a complete data acquisition system have been integrated into the existing Thomson scattering diagnostic on TCV.

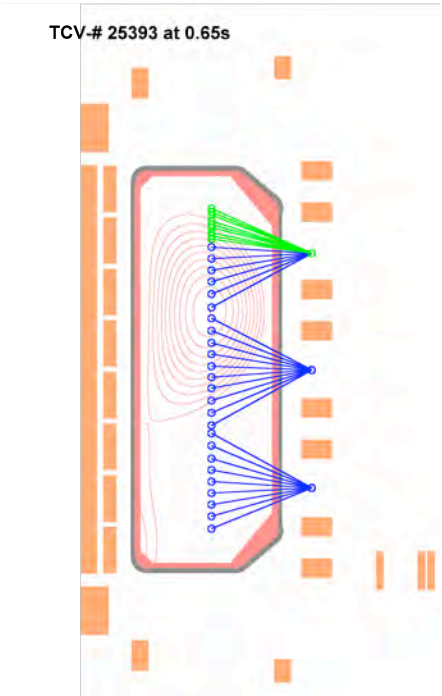

Fig. 3.2.2 *View of TCV poloidal cross section showing the arrangement of spatial channels of the Thomson scattering diagnostic (blue: main system, green : edge system).*
The flux surfaces for pulse #25393 at t=0.65s are given as reference.

For the 2003 experimental campaign the 9 high-resolution channels (dz=10mm instead of 30mm) have been aligned to cover a range of z = +506mm to +624mm,

near the top of the TCV vessel. This arrangement was chosen to optimise the edge profile measurements for H-mode studies. Figure 3.2.2 shows the coverage of a poloidal cross section of TCV by the Thomson scattering volumes after addition of the edge channels together with the flux surfaces of a plasma in a typical H-mode configuration (#25393).

The extended system has provided valuable information for the study of the L-H transition and the evolution of edge pedestals in the T_e and n_e profiles. Examples of profiles recorded during pulse #25393 are shown in Figs 3.2.3a,b.

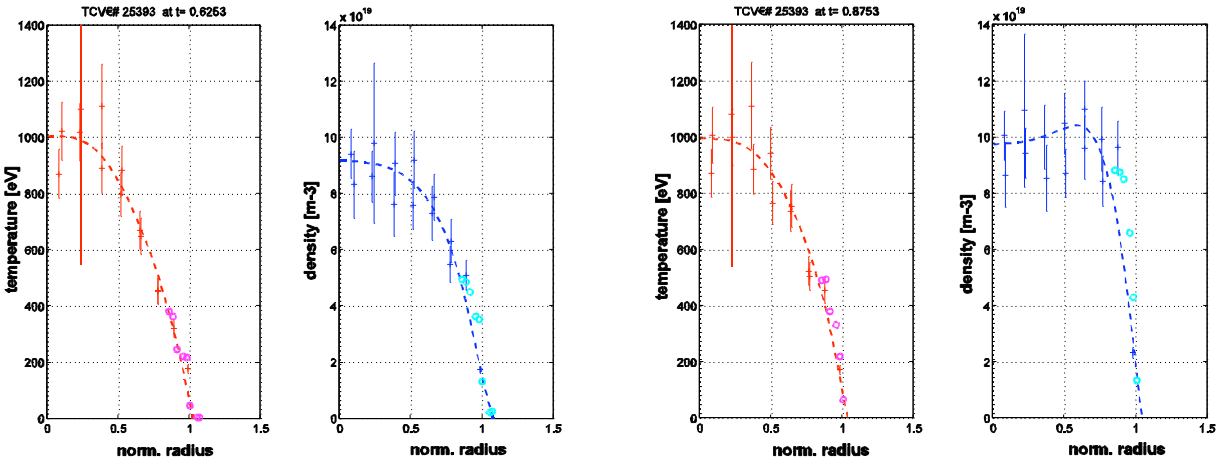

Fig. 3.2.3 *Spatial profiles of electron temperature (left) and density (right) for TCV #25393 at 2 time steps: left) during an ELMy H-mode phase, right) during a phase without ELMs. The points obtained from the edge TS-system are shown as circles*

3.2.3 Plasma core diagnostics

Diagnostic Neutral Beam Operation

The DNBI was operated throughout the 2003 campaign following the upgrade of the beam current to ~3A. The beam and control software were reliable with relatively few discharges lost to maintenance requirements such as cryopump regeneration. In order to improve the beam luminosity to encompass higher plasma density TCV operation, an exploratory contract was established with the Budker Institute of Nuclear Physics, Novosibirsk, Russia to investigate possible routes to increasing the injected neutral density in the CXRS observation region. Preliminary conclusions indicate that the current system can be enhanced by re-conditioning the RF source box, to reduce cumulated metal coating and to improve the beam optics by a more accurately machined acceleration grid assembly. To obtain better performance, the source could be replaced by an “arc” device which features higher temperatures leading to increased beam purity and a higher luminance that can lead to a reduced beam divergence.

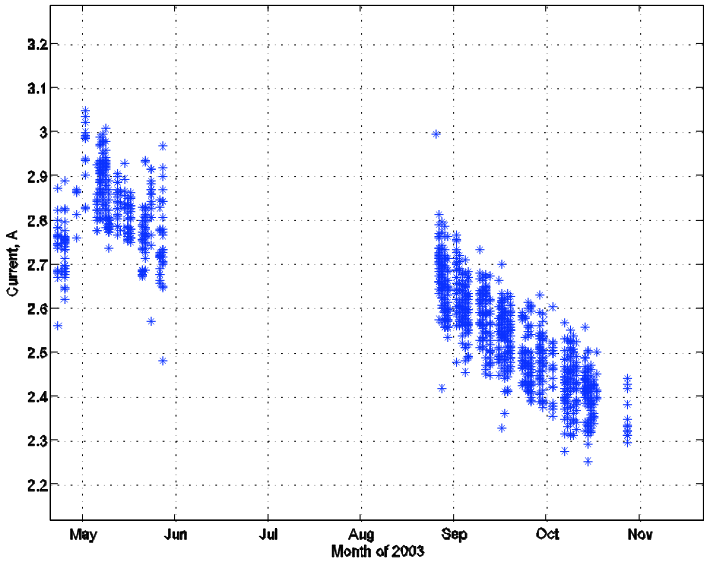

Fig 3.2.4 *Beam current from the DNBI during 2003. There is a clear degradation in the RF source output that may possibly be recovered by re-conditioning, e.g. with an oxygen rich discharge which would oxidise any accumulated metal deposits.*

Charge Exchange Recombination Spectroscopy

In order to measure the plasma electric field with CXRS, it is necessary to measure the ion velocity vector, which can be done by measuring the toroidal and poloidal velocities via their respective Doppler shifts. The toroidal rotation profile is already measured by the primary Ion Temperature camera, and a vertical plasma view is required to measure the poloidal velocity component. Awkward port access on TCV required careful design compromises. The final design required modification of the carbon tiles on the TCV floor and provides a poloidal plasma profile when the plasma configuration is close the centre of the machine, Fig. 3.2.5.

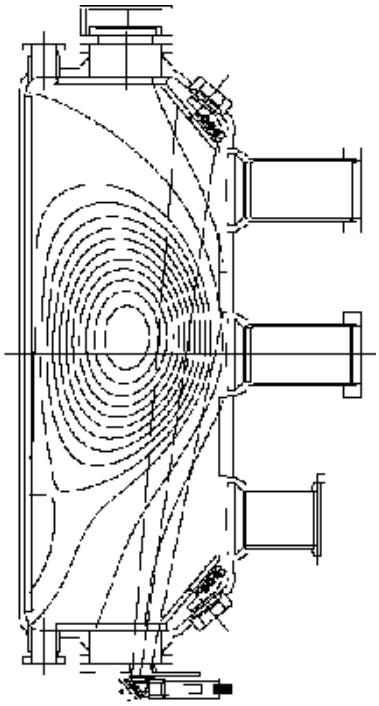

Fig. 3.2.5 *Vertical view of TCV plasma through a port situated under the machine vessel. The incident optics are fabricated in a solid tube for stability and external alignment*

Soft X-ray Pulse Height Analysis

A 4-DSP VME crate module has been installed in TCV to perform real-time analysis of the data stream from a Peltier-cooled solid-state diode observing soft X-ray radiation from TCV. The diode is installed to observe the plasma along a vertical chord and analysis of the measured radiation, in the form of a pulse stream, can be used to determine the plasma temperature, the presence of impurities in the plasma and deviations from a Maxwellian velocity distribution.

The DSP hardware and software are provided by a collaboration with the IST/CFN Institute, Portugal. Preliminary tests of the DSP code demonstrated data acquisition from the diode during a TCV discharge and an initial pulse-height spectrum on which the data analysis is based. When completed, it is hoped data can be acquired and analysed in real-time for real-time optimisation of TCV discharges.

MultiWire Proportional X-ray detector

A new soft X-ray detector which consists of two superposed wire chambers, each similar to the detector prototype (MPX) currently installed on TCV is nearing installation, Fig. 3.2.6. It will measure temperature profiles to be obtained by the differential absorber method, with both high spatial and temporal resolution. This will be used for heat pulse transport studies at high density, in X2 overdense conditions, by modulated EC power deposition (edge X2, X3, EBW).

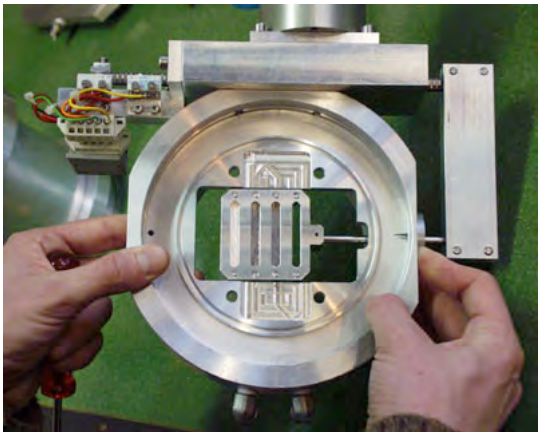

Fig. 3.2.6 *Picture of the new filter holder in front of the MPX chamber in a modification which places it closer to the TCV vacuum port. The primary filter may now be changed remotely.*

Compact Neutral Particle Analyser

A compact neutral particle analyser has been ordered from the A.F. Ioffe Physical-Technical Institute, St-Petersburg, Russia, Fig. 3.2.7. This device uses electric and magnetic fields to disperse both the neutral particle energy and the mass onto two separate arrays of channeltron detectors. This will be mounted on a horizontal port intersecting the diagnostic neutral beam injector primarily for high energy ion physics with the separation of the Hydrogen and Deuterium spectra.

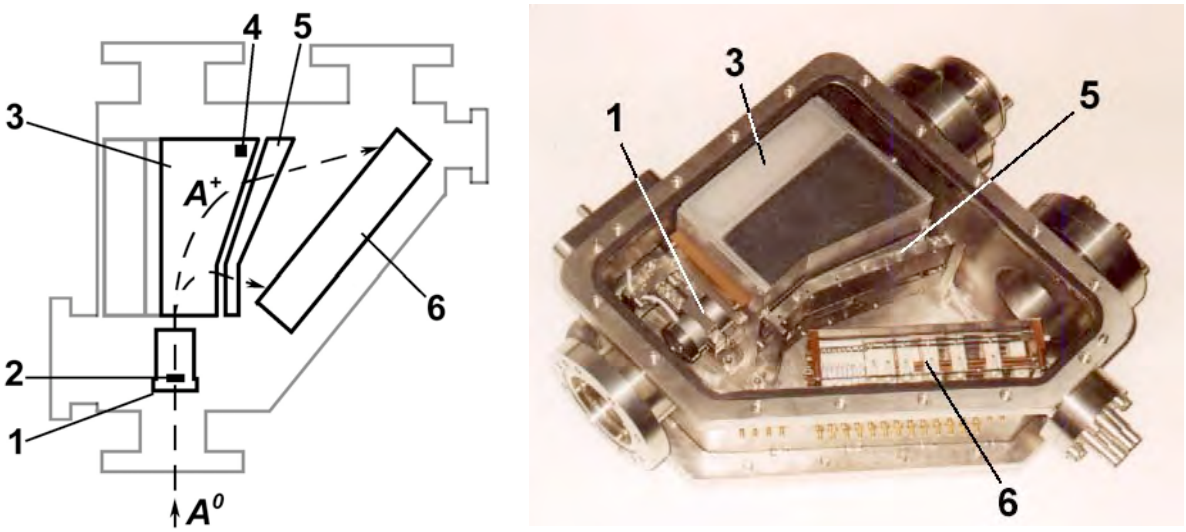

Fig. 3.2.7 *Schematic and photograph of the device. Incoming neutral particles follow the path from 1) the carbon foil stripper to 6) the channeltron detector array*

Fast Bolometry

This twin, seven camera diagnostic is in the final manufacturing stage and is scheduled for installation by the end of 2003, Fig. 3.2.8. An ex situ calibration of the camera optics is planned before installation in which the angular étendue of each channel will be measured using a test light source and compared with the camera design. Measurements of the channel overlap will provide the empirical basis for tomographic reconstruction. For example, these measurements will determine the angular resolution of each channel, and will enable evaluation the susceptibility of reconstructed images to spatial aliasing. The data acquisition system for the bolometer arrays will include the capability of performing simplified tomographic reconstructions in real time during the plasma discharge, which may then be used in the TCV plasma control system.

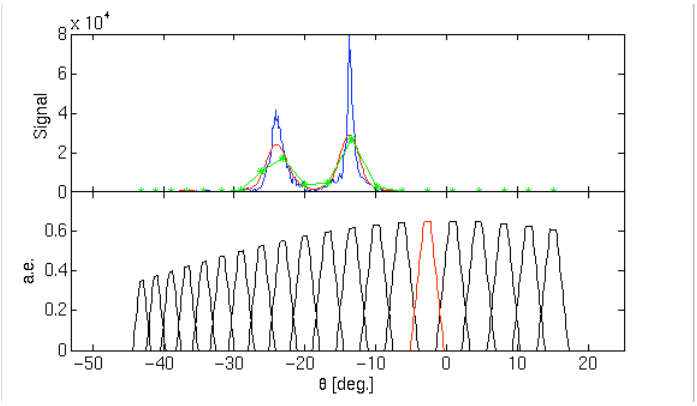

Fig. 3.2.8 *A phantom emission profile showing the effects of finite resolution and spatial aliasing. Top: The received emission profile (blue curve), the profile convolved with the instrument response (angular étendue, a.e., red curve), and the discrete measurements (green line with stars). Differences between the red curve and green sample points are the result of spatial aliasing. Bottom: The calculated angular étendue for one of the seven bolometer arrays. The channel coloured red is used for the instrument response convolution in the top figure.*

Electron Cyclotron Emission (Low Field Side ECE)

A 65-100GHz, 24 channel, 750MHz bandpass radiometer was installed on TCV in 2003. Oversized waveguides were installed on an upper (z=21.2cm) antenna and central (z=0cm) chords, though the antenna cannot be installed until the a major TCV opening, scheduled for the end of 2003, Fig. 3.2.9. ECE LFS measurements using z=0 quasi-optical line have been available on TCV since April 2003 using radiation transmitted through a quartz window.

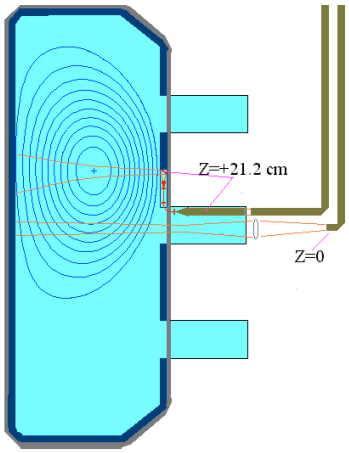

Fig. 3.2.9 *Position of the central observation chords. Position at z=0cm will be augmented by view at z=21.2cm after installation of an internal waveguide and antenna*

Z_{eff} from Bremsstrahlung plasma emission

The Z_{eff} measurement is provided by an optical telescope installed on the top of TCV using a vertical view and collecting the visible continuum Bremsstrahlung radiation around 536nm, Fig. 3.2.10.

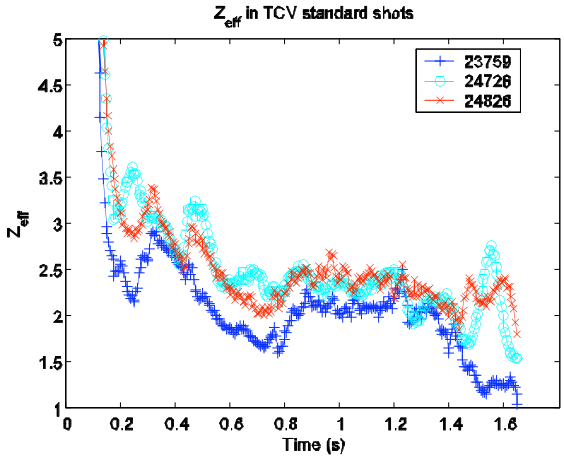

Fig. 3.2.10 *The deduced temporal evolution of Z_{eff} for 3 standard TCV discharges. Despite a large variation in the plasma density during the main portion of the discharge, (0.2->1.4s), the Z_{eff} values are very similar.*

A classical set-up consisting of a collection optics with lenses, interference filter with a bandwidth <6 nm onto a compact photomultiplier light detector. The system, calibrated in absolute intensity, gives a direct measure of Z_{eff} since the brightness of the continuum radiation in this spectral region is proportional to n_e^2, $T_e^{1/2}$ and Z_{eff}. This implies that a good knowledge of the electron density and temperature is necessary. The system is reliable for densities higher than $3x10^{19}m^{-3}$. Below this, molecular lines of C_2 and H_2 appear to become more important than the continuum radiation and the measurement of Z_{eff} is clearly wrong.

Hard X-ray Spectrometer

A hard X-ray Camera is again installed on TCV on loan from Tore Supra. It is used to measure the spatial and spectral distributions of Bremsstrahlung emission from suprathermal electrons during ECH and ECCD experiments.

Millimeter wave Sniffer

In collaboration with CNR-Milano, three "sniffers" have been constructed and mounted on TCV, Fig. 3.2.11. The main property of these detectors is a highly isotropic response which allows measurement the level of stray radiation independently of the RF incidence angle. In the present configuration, some of the detectors are situated behind the graphite tiles without a direct view to the plasma. Modified tiles allowing a direct view to the plasma will be installed in by the end of 2003. An absolute calibration of the system will be made once the tiles are modified.

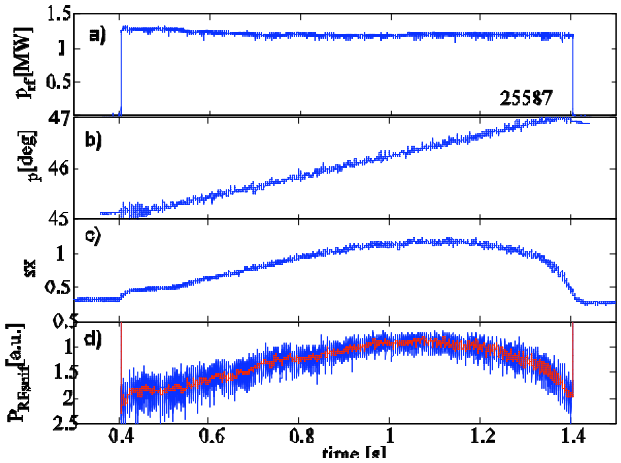

Fig. 3.2.11 *Preliminary measurement is shown in which 1.5MW of RF power was injected with a top-launch a) and the launcher mirror was swept in the poloidal plane (b)); c) Temporal evolution of the soft x-ray signal indicates the angular position of maximum absorption in the plasma (t=1.1s, theta-poloidal = 46.5°) and, in excellent agreement, the stray radiation d) shows a minimum (negative voltage on the detector) at maximum absorption.*

3.2.4 Plasma edge diagnostics

Fast reciprocating Langmuir probe

The new probe head described in the previous report has been extensively deployed throughout 2003 for measurement of radial profiles in turbulent electric fields and particle fluxes. Due in part to the recent interest within the community in the possible link between fluctuation driven cross-field particle flux and parallel flow, a second probe head has been designed and installed on TCV. Shown in Fig. 3.2.12, the new head redistributes the five possible single Langmuir probe elements such that two are placed on either side of a central separating bar permitting the measurement of flow in the scrape-off layer. The three central pins in combination with the "Mach" probes now also render possible the measurement of fluctuations in the radial gradients of turbulent quantities.

Fig. 3.2.12 *A Mach probe head installed in late 2003 on the TCV fast reciprocating probe drive. As before, the head is constructed of Boron Nitride with 5 graphite probe tips. The two pins on either side of the central bar yield the SOL Mach flow via the ratio of collected ion saturation currents. In common with previous designs, the probe head is shaped to match the poloidal curvature of the standard lower single null magnetic equilibrium in which the majority of measurements are made.*

IR Thermography

The two of IR thermography systems commissioned in late 2002 have now begun to provide routine measurements of the surface temperatures in the TCV vessel and hence power flux distribution. The diagnostic yields spatial resolution of ~2mm across wide FOVs encompassing the vessel floor and the lower half of the central column separated by ~90° toroidally. Each system views arrays of tile embedded Langmuir probes and thermocouples and each has been absolutely calibrated in the laboratory using a wide field black body source in the presence of the full system of relay optics. An example of the surface temperature distribution near the end of an ohmic H-mode, SNL discharge is presented in Fig. 3.2.13.

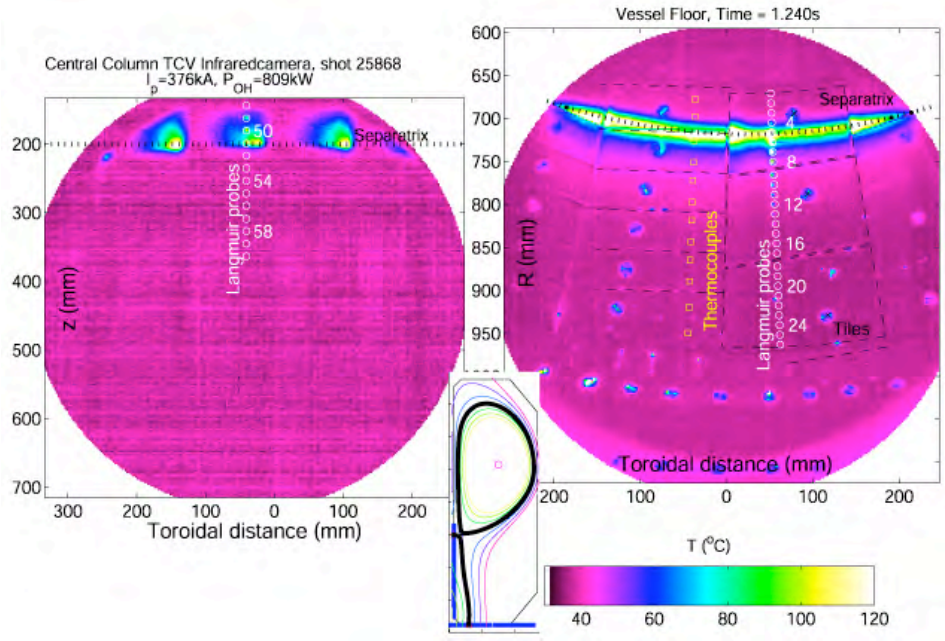

Fig. 3.2.13 *Surface temperature distribution at the graphite divertor targets near the end of an ohmic H-mode discharge with magnetic equilibrium shown in the inset at lower centre (the thick blue lines denote the approximate field of view). The positions of Langmuir probes and tile embedded thermocouples are also indicated.*

CCD-digital

Four 12bit digital CCD cameras were installed to view the TCV divertor through a single coherent fibre bundle with a 1-12ms frame time. By splitting the same image onto the 4 cameras equipped with interference filters, radiation from different impurity features are observed, Fig. 3.2.14. The software was upgraded to allow un-assisted acquisition for a sequence of TCV discharges and survey the maximum intensity evolution on each camera to optimise the exposure parameters.

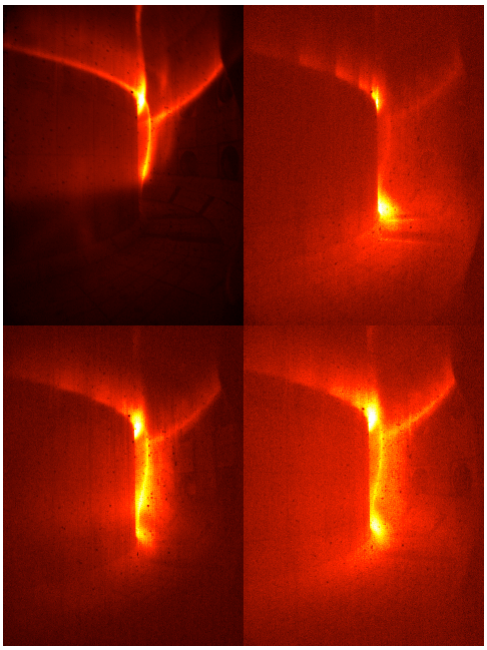

Fig. 3.2.14 *One image from each camera for TCV discharge #23927 at 0.54s*
The top left camera is acquiring radiation from CIII ions whilst the other cameras are observing radiation from different excited states of Deuterium neutrals.
The difference in the intensity distributions indicates differences in the plasma density and temperature.
Note: the figures are coloured artificially to enhance the image contrasts.

3.2.5 Long term diagnostics requirements for TCV

Major components of the scientific mission will arise naturally from existing technical and scientific competences and will include ECH/ECCD, plasma control, MHD theory, transport theory and modelling. These constitute the tools for experimental investigations of electron transport (thermal and suprathermal) and MHD stability aimed at validating (or refuting!) theoretical predictions. Investigations of these topics will require the measurement of internal magnetic fields, electrical fields and local measurements of plasma turbulence in addition to those provided by existing diagnostics. The lack of local field measurements is already felt today.

The presently disused Far Infrared Polarimeter is not suitable for internal magnetic field measurements in the low density, low current plasmas required for ECH and ECCD regimes where the current density profile is modified. A comparison of the merits of two other systems has been undertaken, namely the Motional Stark Effect (MSE) diagnostic (with help from UKAEA staff) and the Heavy Ion Beam Probe (HIBP, in collaboration with RRC Moscow). In its simplest, and least expensive, implementation, MSE can provide measurements of sufficient accuracy albeit with modest time resolution for a limited range of conditions, using the existing Diagnostic Neutral Beam. The practical implications and limitations of a HIBP are still under investigation. Although implementation of a HIBP would be likely to take longer than an MSE system, it has the potential of providing measurements of both the local plasma potential and the poloidal flux distribution, as well as local measurements of density, potential and magnetic field fluctuations, which would be

of great value for comparisons with anomalous transport theory. The conclusions of this study are expected to be available early in 2004.

3.3 Plasma control system

To date, TCV has most exclusively been operated using analogue signal processing in its control system. This is based on analogue matrix multiplication with preprogrammed coefficients plus a matrix PID controller with 24 inputs and 24 outputs. This system has the 200kHz bandwidth necessary to stabilise the vertical position but it can neither implement non-linear control algorithms nor be used to take real time decisions on the control strategy. The control of advanced tokamak regimes as well as that of the ECH launcher geometry clearly require a digital system that offers a more flexible and extended functionality. In order to keep a continuity with the present system and not to degrade its performance, we choose to replace the PID matrix by an array of 32 Digital Signal Processors (DSP) with 32 inputs, 32 outputs and a data interchange bus. This upgrade of the plasma control system consists of the following steps.

- Replacement of the 128 channel wave generators with a sampling rate of 1kHz with a wave generator at 125kHz, necessary in experiments such as ECH power modulation or ELM control. This new system has been delivered and will be operational for the next experimental campaign.
- Replacement of the 24 by 24 matrix PID by an array of 32 DSP. This system is being built by the CFN, Portugal under a CRPP-CFN collaboration agreement and will be delivered early in 2004.
- Development of a user friendly programming environment for the control algorithms. Such an environment is crucial to give access to the calculation power of the processors without using low level languages and also to make the integration in the control processes of TCV and the evolution of these algorithms easier. This development is done in collaboration with the CEA, Cadarache.

3.4 Heating system

3.4.1 X2 heating system

Gyrotrons

The oldest of the X2 gyrotrons (designated gyrotron 3 - accepted 8/9/96) developed a vacuum leak during an operation session (but not during a pulse) on 25/4/03. Gyrotron number 5 was exhibiting evidence of poor vacuum since the beginning of 2002 and attempts to recondition the tube during the winter 2002/3 shutdown proved ineffective. The gyrotron was replaced by a spare tube before the beginning of operations, requiring a realignment of the matching optics unit (MOU) and a recalibration of the power. Both tubes have been sent back to the manufacturer for repair. The total available X2 power for the majority of the 2003 campaign was thus limited to the 2.35MW delivered by 5 gyrotrons.

Matching Optics Units (MOUs)

The polariser rotation mechanism of the MOU of gyrotron 6 failed to turn reliably at the start of operations and required manual intervention for each shot. During calibration tests with the plasma at the start of operations, it was discovered that the malfunctioning MOU produced incorrect polarisation and thus poor power absorption in the plasma. This was due to an occasional slip in the drive chain of the polariser mirrors. The mirror position measurement system cannot detect this slippage. All polarisers were subsequently inspected and while some other polarisers had also suffered minor changes in polarisation, only MOU6 caused significantly reduced 1st pass absorption. A modification has been carried out on all MOUs to prevent this in the future.

Launchers

The fast moving mirrors of launchers 3 and 4 both stuck at one end of their operating range. This severely limited the utility of launcher 4 during plasma experiments (launcher 3 had no power delivered to it due to the vacuum leak in gyrotron 3 mentioned above). Both launchers were removed during a short opening in July and launcher 4 was replaced by a spare and was thus restored to its full operating range. Both launchers stuck due to fracturing of ceramic insulators. A new simplified design of the launcher has been made which eliminates the insulators, minimises the number of parts in the launcher, requires a minimum of fabrication or modification of existing parts and which should remove the possibility of sticking. The new design is more modular, requiring less assembly and is more rigid, reducing the sensitivity to geometric particularities of the different vacuum ports in which the launchers are mounted. The new launchers will be ready for installation during the 2003/4 winter shutdown.

3.4.2 X3 heating system

Gyrotrons and transmission lines

All gyrotrons of the 3rd harmonic heating system are now installed in the final configuration and have functioned reliably. Gyrotron 7 was returned in July after repair of the window broken in April 2002. The gyrotron was successfully reconditioned in August. During the summer, the transmission line configuration was changed so that the gyrotron injected power from the top of the tokamak (as do gyrotrons 8 and 9). Previously the power from gyrotron 7 was injected from the side via launcher 3. The switch allowing operation of either an X2 or X3 gyrotron in transmission line 3 was moved to its final location in the TCV zone and the remainder of line 7 was installed. Plasma heating by 1.5MW of X3 power was achieved during the fall campaign. Transmission line 3 will be completed once the repaired gyrotron 3 has been accepted.

RHVPS

All regulated high voltage power supplies used to power the gyrotrons have been modified to allow 10s pulses. This modification was made in preparation for testing a 110GHz gyrotron under study for JET-EP. Although the JET-EP project was cancelled, this modification proved very useful for rapid conditioning of the repaired X3 gyrotron which, although used for 2s pulses at TCV, is designed for 210s pulse use on Tore Supra.

3.5 The TORPEX basic plasma physics device

The construction of the educational TORoidal Plasma Experiment, TORPEX, was completed in 2003. First plasmas were obtained in March 2003, after which regular experimental campaigns have followed. TORPEX is characterised by a major and minor radius R=1m and a=0.2m, Fig. 3.5.1. A set of 28 coils provides a toroidal magnetic field up to 0.1T. Six poloidal coils are used in the present configuration to add a small vertical component $B_v \leq 50$mT for the optimisation of the plasma confinement.

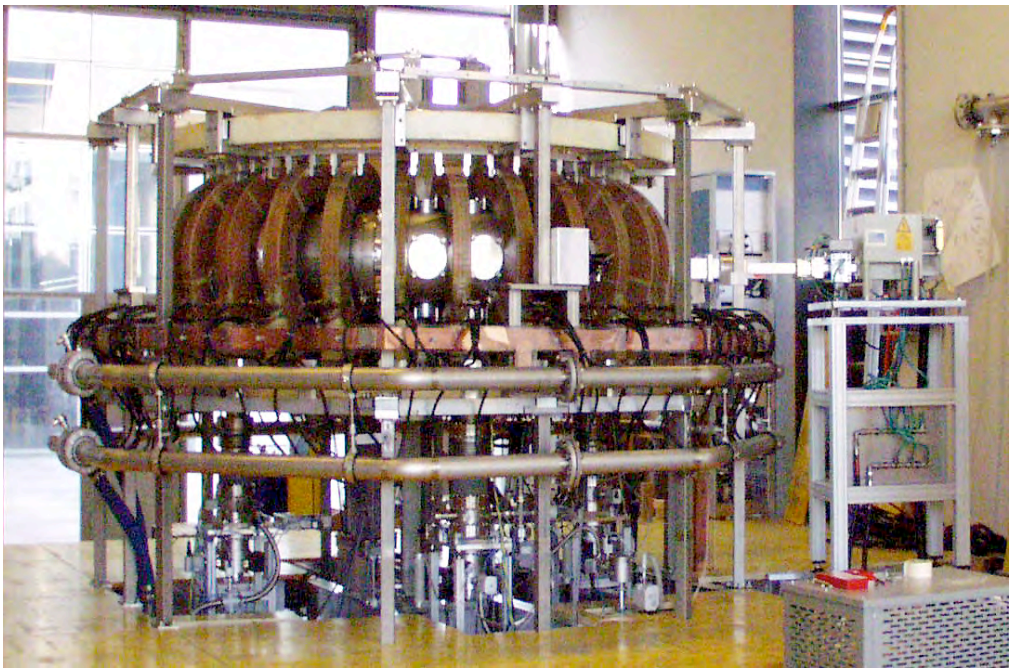

Fig. 3.5.1 *The TORPEX device*

The systems that remotely control the power supplies, the vacuum pump and diagnostics, the electronic gains and mechanical drivers for probes, are conceived following the same solutions adopted on the TCV tokamak, allowing exchanges of software and hardware modules.

Diagnostic developments on TORPEX

Sets of remotely controlled, movable electrical probes and analysers were developed to reconstruct the profiles of the main plasma parameters over the poloidal section, Fig. 3.5.2. The fluctuation spectra are measured using 33 pairs of capacitively coupled fixed Langmuir probes (1.3mm between tips, 8mm between pairs) installed at the same toroidal location and measuring the fluctuating component of the ion saturation current I^+_{sat}. They provide frequency spectra in the range 100Hz-125kHz, and a determination of perpendicular wave numbers $k_\perp$ up to 24cm^{-1}.

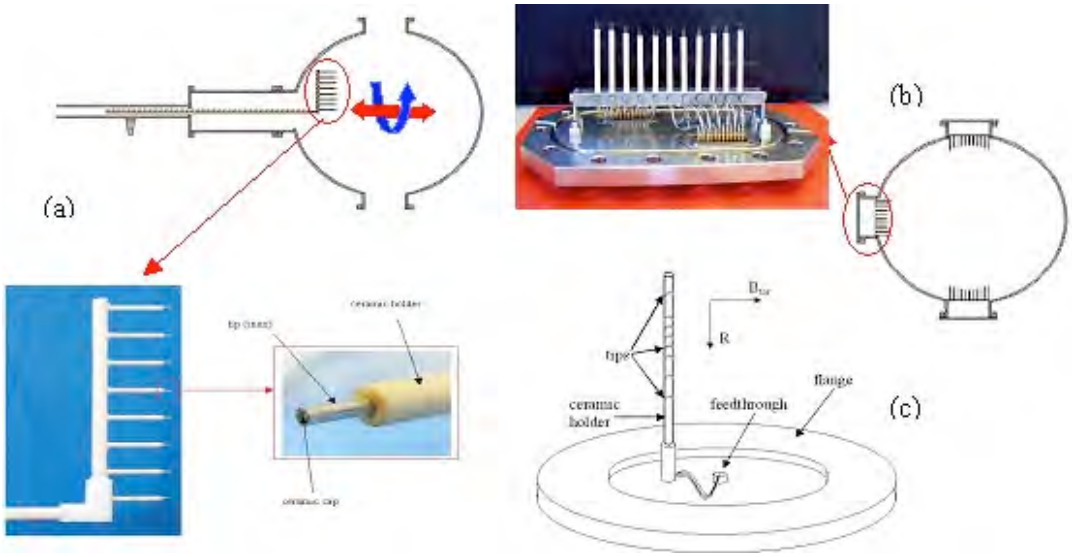

Fig. 3.5.2 *Examples of TORPEX Langmuir probe diagnostics: (a) movable low frequency set; (b) 3 arrays of high frequency (coaxial) double probes; (c) multiple ring probe for gradient measurements*

Two pieces of optical equipment have been installed on TORPEX: a camera operating in the visible range, and an Ocean Optics S2000 spectrometer, used to estimate the number of photons emitted by the plasma, in particular with a view to confirming the feasibility of optical diagnostics such as laser induced fluorescence and fast imaging of the plasma turbulence. Examples of the data produced are shown in Fig. 3.5.3.

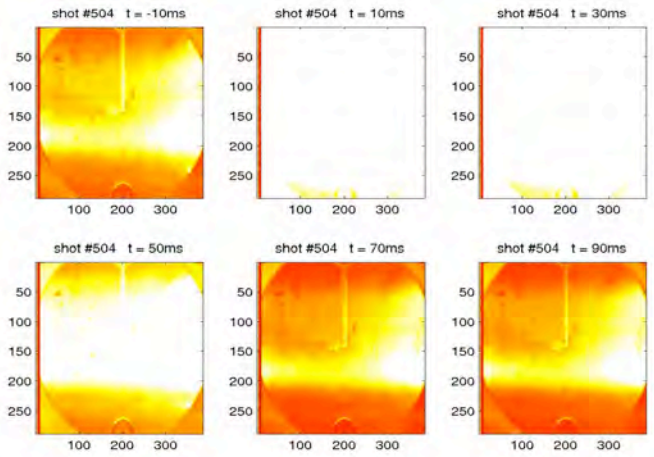

Fig. 3.5.3 *An image of the shot sequence on TORPEX obtained using the visible camera*

The data acquisition is based on two CAMAC based systems with 64 channels sampled at 1kHz and 16 channels at 10MHz, and a C-PCI based system with 96 channels sampled at 250kHz. The data is organised using MDS-plus.

3.6 Superconductivity

3.6.1 The SULTAN facility

After the January shut down of PSI services, the operation of the SULTAN facility was resumed at the beginning of February 2003. The shut down was also used to repair a leak in the main vacuum, which limited the operation of the facility in the last months of 2002. Part of the super-isolation had to be replaced as it was heavily polluted by oil from the vacuum pump.

The facility was operated continuously from February 2003 to the end of the year, testing short length conductor and joint samples as described in section 2.5.

3.6.2 The JORDI Facility for Resistance Distribution Test on Joints

The commissioning of the facility, planned in 2003, could not be done because of late delivery (summer 2003) of the conductor sections from which a sample must be manufactured. The higher priority of other tasks and the non-planned test of the W7-X samples (section 2.5.2) forced a redirection of the required manpower. Final commissioning and sample tests are now planned in 2004.

3.6.3 Procurement and commissioning of a heat treatment furnace for Nb_3Sn

The procurement and installation of a vacuum furnace to heat treat the Nb_3Sn short samples to be tested in SULTAN was agreed in July 2002 among EFDA and CRPP as a deliverable of contract Art 5.1a TW1-TMC-JSPREP. The need of a vacuum furnace for the SULTAN samples was recognised due to the practical difficulties of carrying out the heat treatment on industrial plants.

A call for tender for the furnace was sent out in September 2002. The minimum homogeneous heated length was specified as 3800mm (i.e. a SULTAN short sample). The tubular furnace has a diameter ≥200mm, to heat treat two SULTAN full size short samples in one go, if necessary. The company Thermcraft (North Carolina) was eventually selected based on price consideration.

Thermcraft had already delivered ten years ago a similar furnace to LLNL, later re-installed at MIT. Contrary to the LLNL furnace, the CRPP furnace has access at both ends of the retort vacuum tube and uses water cooling for the flanges, which are vacuum sealed with Viton O-rings. The maximum nominal temperature is 750C, the power requirement is 90kW. Five heated zones are individually controlled by thermocouples attached to the outer surface of the retort to obtain a homogeneous temperature profile. The controller unit allows setting a heat treatment schedule with several segments of ramp (at a controlled rate) and soak.

A step down, 90kVA transformer was procured in February 2003 to supply the furnace, operating at 240V 3 phase – 216A, from the 400V power net. The vacuum system has been designed to achieve and maintain 10^{-7}mbar in the tube furnace. To minimise the gradients through the 5m long tube, a layout has been selected with two turbomolecular pumps, one at each end of the tube. The vacuum connection at the ends of the tube furnace is obtained by standard T connectors (NW250), see

Fig. 3.6.3 The furnace can be loaded and unloaded without disassembling the vacuum system. The gate valves and the turbomolecular pumps are placed just below the T connectors. Vent ports (not shown in the sketch) allow flushing the tube furnace with N_2 gas after breaking the vacuum in the last section of the cool down process, at temperature <80C.

The water cooling of the ends of the furnace tube is designed to maintain the flange connections with Viton O-rings at room temperature and improve the removal of the overall heat loss in operation. The two cooling sleeves are connected to the PSI water cooling circuit and the inlet valve is set to provide a water flow of about 5litre/minute. A failure of the water cooling could have serious consequences during the heat treatment (end flanges temperature increasing above 200C, Viton O-ring melting, vacuum breaking, etc.). To prevent the risk of loss of cooling, an additional cooling circuit with tap water is connected in parallel to the main circuit through an overpressure valve: in case of loss of pressure in the close loop circuit, water flows automatically from the tap water circuit.

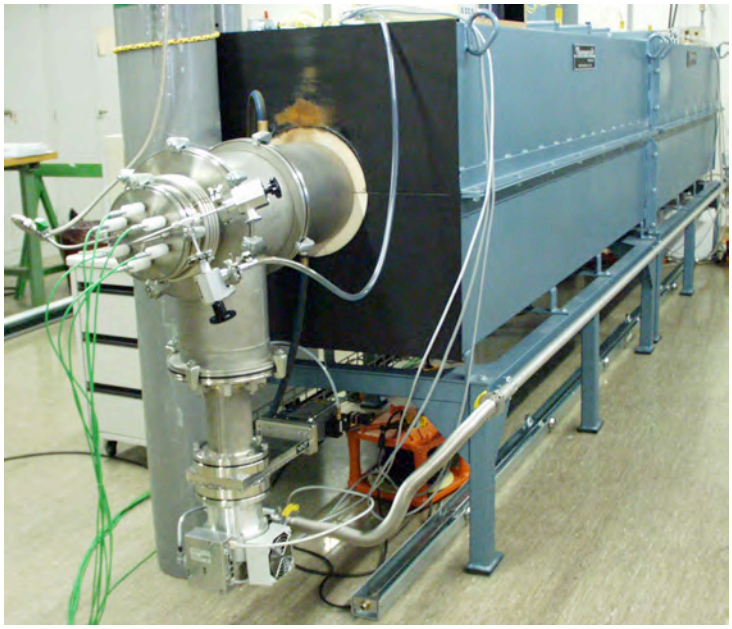

Fig. 3.6.1 *One end of the vacuum tube, with cooling water, vacuum T connector (gate valve and turbomolecular pump underneath) and end flange with thermocouples and gas feed-through.*

The Thermcraft furnace is equipped with a Honeywell controller regulating the power of the five heating zones in a feedback loop with thermocouples sensing the temperature on the outside surface of the steel tube. To be able to save the recorded temperature data and to monitor the temperature behaviour from the thermocouples attached to the heat treated object, the controller had to be upgraded. A dedicated PC is connected to the controller for monitoring all the temperatures. SpecView® software was procured to save on-line the data.

An Argon bottle supplies purge gas to the conductor sections to be heat treated. Gas feedthroughs swagelock fittings are placed at the front flange, together with six thermocouple feedthroughs. The flow of the purge gas can be tuned by a set of reduction valves. After flowing through the conductor sections, the purge gas bubbles out and is dispersed in the environment.

The Thermcraft furnace was received at CRPP by the end of January 2003 and was first assembled in beginning of February. The commissioning was delayed by a

severe leak at the welds of the two end flanges to the tube furnace (a smaller leak was also detected and repaired in the water cooling sleeves). After negotiations with Thermcraft, it was decided to do the repair in Switzerland. The two flanges were cut. The tube length was reduced by only 20mm. New flanges were adapted to the tube, to avoid machining the 5m long tube. A structural, discontinuous weld has been made from the outside and a thinner, vacuum tight continuous weld was made from the inside. After leak test, the repaired tube was placed back in the furnace and commissioning was carried in March 2003, applying a short heat treatment up to 700°C.

The vacuum inside the tube is satisfactory, in the range of 10^{-7}mbar. The temperature inside the vacuum tube is homogeneous and consistent with the temperature at the outer surface of the tube. The temperature ramp up could be easily set from very low rate up to about 100°C/h. The ramp down is limited by the good insulation of the heating elements and by the vacuum inside the tube.

A full cycle heat treatment of a short section of Nb_3Sn conductor was carried out in May 2003, without any interruption. The heat treatment of the "new full size Nb_3Sn conductor" (section 2.5.3) was carried out in June 2003. To place the conductor sections inside the tube furnace, a cart has been built, Fig. 3.6.2. The two sealed conductor sections are first placed on thin steel supports, spaced by about half meter. The cart is a steel U profile with retractable reels. After sliding the cart under the assembly of conductor and spacers, the reels of the cart are lowered so that the weight of the assembly rests on the cart. The cart is inserted into the furnace and the assembly is positioned as required. Then the reels are partly lifted and the spacers of the assembly are brought to rest on the furnace tube. Eventually the "empty" cart is retracted from the tube and the furnace is closed. The reverse procedure is applied to extract the sample assembly from the furnace.

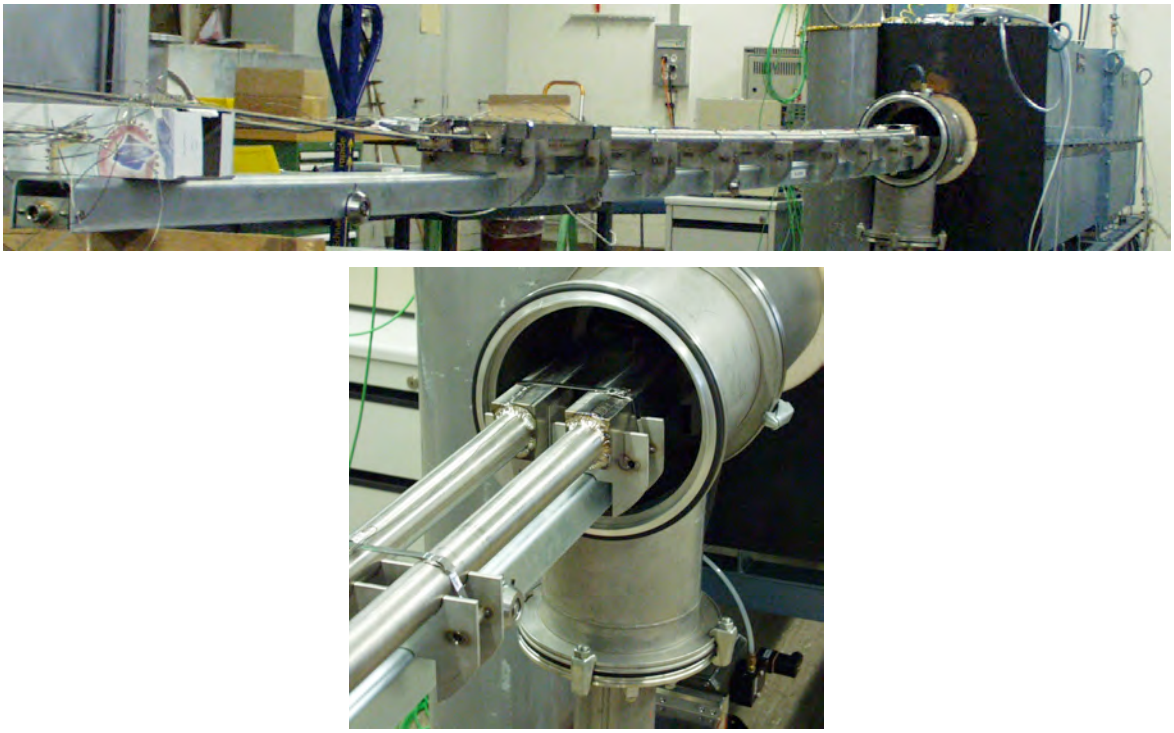

Fig. 3.6.2 *The two sections of "new full size Nb_3Sn conductor" assembled on the steel spacers resting on the cart during insertion into the furnace (June 2003)*

4 International and national collaborations

4.1 Exploitation of the JET facilities

A number of CRPP staff members spend time as part of the EFDA-JET team which includes all Associations. Their major contributions are detailed in this section. This work was partly funded from preferential EURATOM support.

Collaboration with the JET-EFDA Task Force M (MHD)

CRPP collaboration with Task Force MHD for JET-EFDA experiments has focussed on leading experiments and finalising analyses of experimental data and of simulations of 2002 experiments.

The main experiments performed in 2003 in which CRPP was directly involved in coordinating the sessions for TF-M were related to Neoclassical Tearing Modes (NTMs), sawteeth and Toroidal Alfvén Eigenmode (TAE) physics. Otherwise CRPP collaborators continued to offer expert analyses of MHD phenomena in all types of discharges.

The NTM experiments concentrated on sawtooth physics and control, in particular trying to control sawteeth stabilised by fast particles using local Ion Cyclotron Current Drive (ICCD). The first demonstration of the destabilisation of sawteeth, which are stabilised by fast particles as will be the case in burning plasmas, has been performed as shown in Fig. 4.1.1. Therefore the modification of shear near q=1 can also destabilise sawteeth with a strong fast particle contribution, similar to sawteeth modified by Electron Cyclotron Current Drive (ECCD) in TCV.

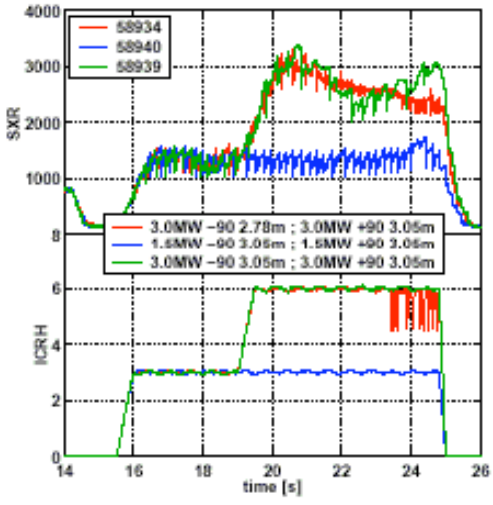

Fig. 4.1.1 *Long sawtooth periods are obtained with ICRH heating in the centre, 3MW. Then 3MW is added off-axis near the inversion radius, pulse #58934. In this case the sawteeth are strongly destabilised.*

Other sawteeth experiments were dedicated to the effects of rotation on the sawteeth and comparing sawteeth in forward and reverse magnetic field configurations, Fig. 4.1.2.

The effect of plasma rotation on the internal kink instability and thus on the sawtooth period was investigated in two experiments jointly led by CRPP staff in the forward and reverse magnetic field configurations. The momentum injection was varied from pulse to pulse by changing the Neutral Beam Injection (NBI) power. These studies confirmed previous observations that sawteeth are shorter with counter- than with co-NBI, but mapped out the dependence of the period in considerably more detail, revealing that the period reaches a minimum at 4MW in counter-NBI, corresponding to an angular rotation frequency of ~-20krad/s, as Fig. 4.1.2. The existence of a minimum at a negative value of the rotation frequency was predicted by theory, although the experimental value appears to be approximately one order of magnitude larger.

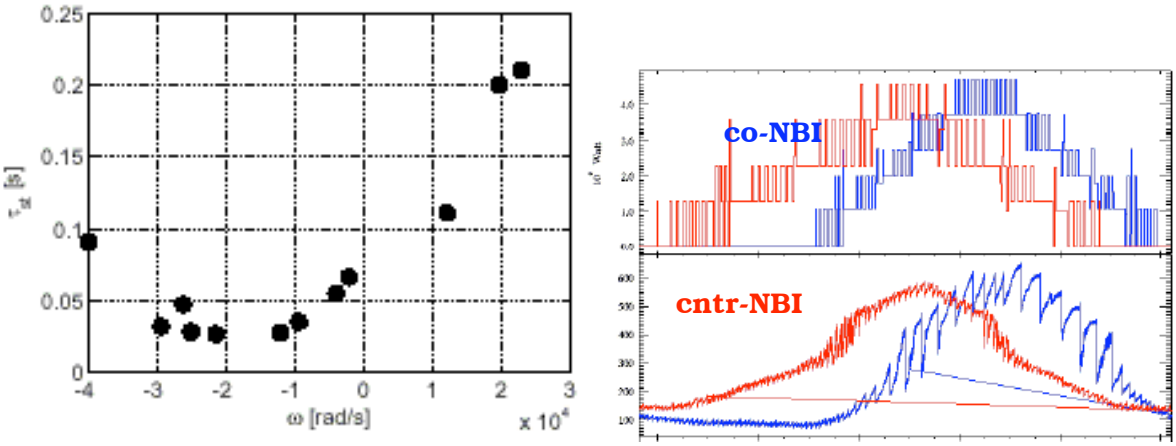

Fig. 4.1.2 *a) Sawtooth period as a function of toroidal rotation frequency (positive for co-NBI). b) Comparison between co-NBI (blue) and counter NBI cases, the change in sawteeth is evident in the bottom (SXR) traces.*

Experiments related to the effects of long sawtooth periods on NTMs were led by CRPP. Real-time control experiments were performed parasitically and β control has been tested. Due to the lack of reliability of JET, some sessions had very few useful pulses.

One experiment led by the CRPP was devoted to investigating in more detail the dependence of the onset β for m/n=3/2 NTMs on the sawtooth period, by means of Ion Cyclotron Resonance Heating (ICRH) power ramps at near-constant β. The study was compromised by poor ICRH coupling, but resulted nonetheless in a significant addition to the NTM triggering database, comprising a broad range of sawtooth periods and β values which did not result in a 3/2 NTM, thus highlighting the need for a better understanding of the triggering mechanism.

An additional study of the dependence of 3/2 NTM stability on plasma rotation was hampered by poor vessel conditions, although the limited dataset obtained confirmed the expected stabilising effect of rotation, resulting in an increased onset β.

The analyses of NTM onset characteristics of previous campaigns were completed. Further analyses are underway, including recent experiments performed on DIII-D in collaboration with JET. These include the comparison of marginal β scaling for the 3/2 and the 2/1 with results obtained in ASDEX-UG, DIII-D and JET. A particularly interesting example of a ramp-down experiment aimed at determining the marginal β limit of the 3/2 mode is shown in Fig. 4.1.3. In this discharge a 3/2 and a 2/1 mode are destabilised. During the power ramp-down the 3/2 mode is

stabilised before the 2/1 mode, about 1s earlier, and therefore the marginal β limit of the 2/1 mode is lower than for the 3/2 mode.

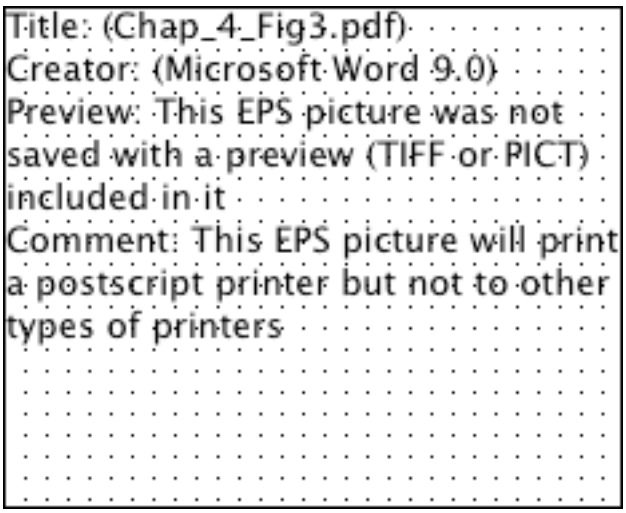

Fig. 4.1.3 *RF and NBI power stabilise a long sawtooth period during ramp-up phase which triggers both 3/2 and 2/1 modes.*

Using the present saddle coil antennas to excite low-toroidal mode number AEs modes, dedicated experiments were performed to investigate weakly damped modes that can exist in advanced tokamak scenarios. In reversed shear discharges, in the presence of a strong internal transport barrier, the strong pressure gradient raises the ion diamagnetic drift frequency to values that are comparable to the Alfvén frequency. In this regime, weakly damped modes have been driven and detected by the saddle coil system. Confirming this result, fast ion driven instabilities have been observed in the absence of an external antenna drive for values of additional heating power that would be well below excitation threshold in conventional scenarios and for modes in the TAE or Ellipticity induced Alfvén Eigenmode (EAE) gap. These findings illustrate a possible issue for the alpha particle confinement in ITER advanced scenarios.

In conventional scenarios, investigations have continued to assess the main damping mechanisms that determine the mode stability via measurements of the dependence of the damping rate of stable low-n TAEs and EAEs on a number of plasma parameters. These parameters included the ion Larmor radius, the plasma β, the plasma rotation and the direction of the ion grad-B drift. The data shows a weak dependence of the frequency and damping rate of stable TAEs with low toroidal wave number on the ion Larmor radius, in contradiction with the prediction of theory based on the fluid model. The dependence of the measured damping on the bulk β, the core safety factor and the value of central magnetic shear also suggest that gyro-kinetic models are needed to reproduce the damping measurements, hence to provide reliable predictions of the mode stability limit in burning plasmas.

The previous experimental finding of the importance of the edge magnetic shear in providing a strong damping to radially extended AEs has been confirmed by direct observation of the stability limits of AEs driven by resonant NBI generated ions in low magnetic field discharges.

The spectrum of AEs driven unstable by ICRH-generated fast ions is correlated with new measurements of the fast ion distribution using the Neutral Particle Analyser diagnostic. Various ICRH heating and fuelling schemes are considered, in view of possible control schemes for the fast ion populations. A comparison of experiments using monochromatic and polychromatic ICRH heating was performed. In the polychromatic case EAEs are driven unstable and TAEs are driven to much smaller amplitudes than for monochromatic heating. As the excitation of TAEs and EAEs

are indicative of the existence of a fast particle pressure gradient close to the core or towards the edge, respectively, these observations indicate a broader radial profile of fast particles for polychromatic ICRH, with a weaker drive for TAEs in the core, and a larger drive for EAEs closer to the edge. Neutral Particle Analyser measurements of the ion temperature confirm that the polychromatic heating is less effective than monochromatic heating in creating a high-energy tail in the plasma core.

As part of the JET Enhancements, CRPP has the responsibility for the new antenna system to excite MHD modes in the Alfvén wave frequency range (20–500kHz) with intermediate toroidal mode numbers (n≤15). This will provide direct measurements of the stability properties of the modes that are considered the most prone to instability in large burning plasmas such as ITER. The design of the two groups of 4 antennas to be installed in-vessel and the relevant interfaces is now almost complete, Fig. 4.1.4. Engineering analysis of the forces and stresses on the antennas during disruptions has been conducted in collaboration with MIT.

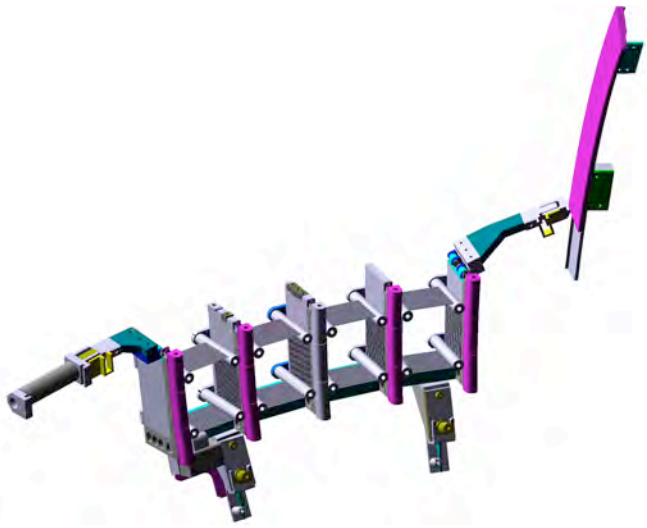

Fig. 4.1.4 *Final design of one of the two antenna structures to excite intermediate n AEs, developed as part of the JET Diagnostic Enhancements*

Collaboration with the JET-EFDA Task Force E (Exhaust)

During 2003, CRPP continued its strong support of Task Force Exhaust (TF–E) activities, both in terms of data analysis and participation in 2003 experimental campaigns, in many cases as scientific coordinator. A CRPP staff member was appointed Deputy TF-E Leader in late 2002, responsible for the experimental period 2003/04 (including the selection of experimental proposals and construction of the programme). Duties in the TF-E leadership have included an important role in the planning, execution and reporting of experiments conducted during campaign C8 and overall responsibility for coordination and execution of the extensive TF-E experimental activity, in which JET was operated with reversed (ie positive) toroidal magnetic field and plasma current. Research has also continued using the CRPP constructed, bi-directional Retarding Field Analyser (RFA) probe installed on one of the two JET fast reciprocating probe drive systems.

Magnetic field reversal is important for edge and divertor physics studies since the directions of drift flows present in the scrape-off layer (SOL) of all tokamaks depend on only on the field direction. These drift flows in turn may have a strong influence on divertor asymmetries and material migration in the edge, the latter of great

importance for issues of tritium retention and divertor re-deposition and erosion. Although next step reactors are unlikely to operate in reversed field, experiments of this nature on a large tokamak like JET can be of enormous assistance in understanding the physics of drifts. As shown in Fig. 4.1.5, the CRPP RFA probe has provided new, higher quality data for the flow speed in matched forward and reversed field discharges. The data confirm earlier JET measurements, but now much with higher radial spatial resolution. Strong Mach flows (Mach 1 is plasma flow at the sound speed in the SOL), reaching M~0.6 are present in the forward field SOL, with the flow stagnating through most of the edge (and sometimes slightly reversing) in reversed field. Such flow speeds are anomalous and cannot be explained in magnitude by current theories describing classical drifts. Interestingly, for both field directions, a common flow velocity is clearly reached at or near the separatrix. These are strong indications that excess ballooning transport at the outside mid-plane may be responsible for a component of the anomalous flow.

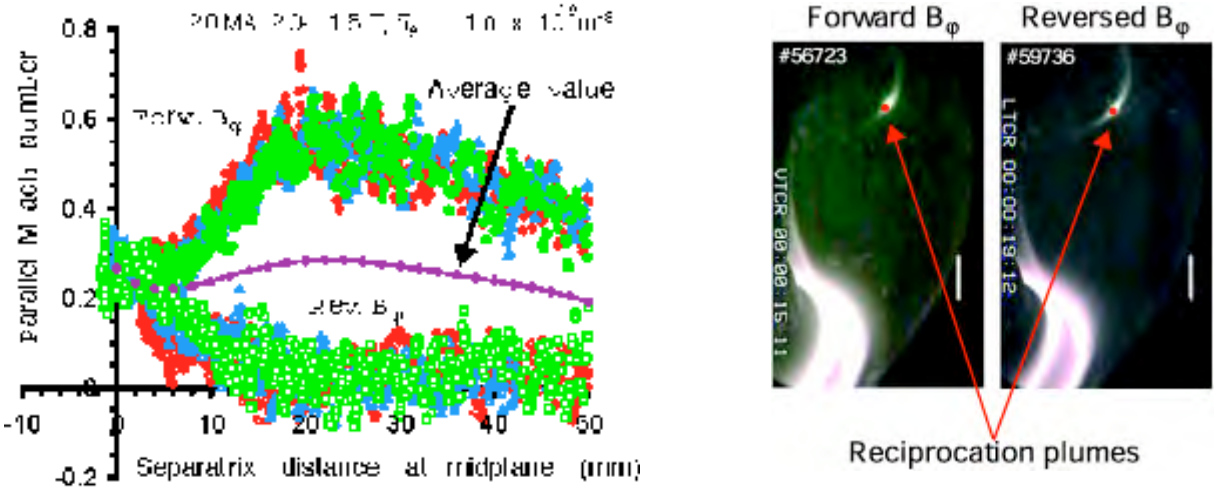

Fig. 4.1.5 *New measurements of parallel flow speeds have been made possible by the new CRPP RFA probe head in both forward and reversed toroidal field – here the strong flow from outer to inner divertor in forward field is observed to stagnate through most of the SOL in reversed field. The flow differences in these otherwise perfectly matched L-mode discharges can even be qualitatively discerned in the video frames capturing the "reciprocation plume" as the probe moves into the SOL and generates visible light emission due both to fuel recycling and carbon evolution. Note also the differences in divertor recycling emission as the field direction is changed.*

Further strong evidence that the flow is indeed a real effect comes again from the CRPP RFA which, in addition to providing a direct measurement of the flow itself (by collecting ions on the slit plates facing the outer and inner divertors), also yields the local parallel ion temperature, T_i, on the ion-side (facing the outer divertor in forward field) and electron-side (facing the inner divertor) drift directions of the probe. The unique new result of Fig. 4.1.6, shows how the ion-side/electron-side T_i ratio exceeds unity for forward field whilst in reversed field, the ratio switches in favour of the electron-side. Such behaviour was recently theoretically predicted as a consequence of the depletion, by the probe itself, of density on the downstream side of the flow. This modifies the local parallel electric fields and hence the ion velocity distribution, producing a higher T_i value on the upstream (ion) facing side. Since the probe provides both Mach No. and T_i simultaneously, the results can be compared with theory. Agreement is qualitative in forward field but it is not presently understood why the T_i ratio switches strongly in favour of a strongly

reversed flow in reversed field even though the probe measured flow would appear to be only slightly negative.

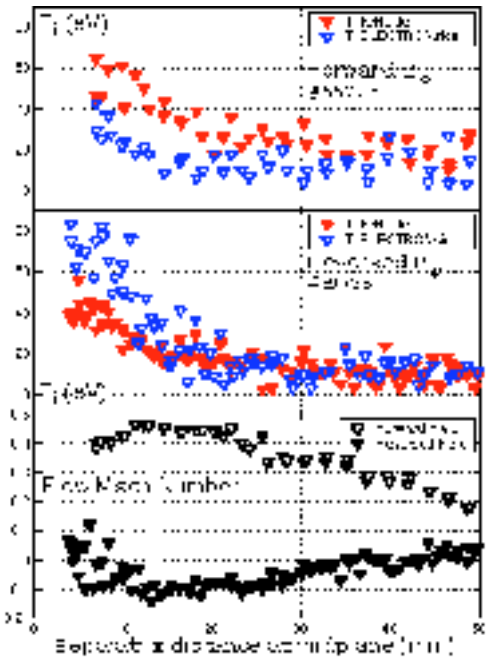

Fig. 4.1.6 *First known demonstration of the effect of SOL plasma flow on the ratio of ion temperatures measured in the upstream and downstream directions. This data are from matched low density, ohmic JET discharges in which the delicate edge probe functions most reliably.*

Modelling work on detachment in L-mode JET helium plasmas using the SOLPS5.0 coupled fluid-Monte Carlo edge code package has progressed and has been extended to matched deuterium fuelled cases. For the most part, good agreement has been found between theory and experiment, though the approach to detachment in deuterium is particularly difficult to simulate with the code and has not been seriously attempted in past efforts at modelling JET discharges. A long research article documenting the principal results of this activity is in preparation at the time of writing.

In addition to the above activities, CRPP staff have coordinated and are actively involved in the data analysis of a number of other TF-E experiments. In particular, an interesting new study of Type I ELM driven divertor target currents for matched forward and reversed plasmas is underway to compare and contrast with similar analysis performed and recently published for TCV ELMs. Experimental sessions with pure helium discharges and L-mode deuterium divertor detachment have also been executed in reversed field for comparison with matched forward field cases.

Collaboration with other JET-EFDA Task Forces

Evidence for the existence of the curvature pinch in source-free L-modes in JET

Experiments dedicated to the study of fuelling and impurity particle pinches in source-free L-modes were led by CRPP staff. The existence of an anomalous inward particle pinch and its origins are still a subject of controversy. Turbulence theories suggest that both $\nabla q/q$ (curvature pinch in fluid theory or 'Turbulent EquiPartition' in kinetic theory) and $\nabla T_e/T_e$ ('Anomalous Thermodiffusion') may play a role in addition to the Ware pinch. The goal of the experiment was to obtain measurements, allowing us to distinguish which of the shear and the temperature gradient effects is the most important. This implied experimental conditions with a variety of quasi-stationary q profiles and electron temperature profiles in discharges

without central fuelling by neutral beams. Safety factor profiles were measured using the JET interferometer-polarimeter diagnostic to constrain the equilibrium reconstruction. The edge particle source was modelled using the K1ND code provided by PSFC, MIT. It shows that the particle source is insignificant in the bulk of the plasma and cannot, by a vast margin, explain the peaking of the density profiles. The Ware pinch was minimised by operating at high electron temperature in the presence of lower hybrid current drive, leading to a wide range of q profiles between reversed central shear and positive shear, all with $q_0>1$. Due to the difficulty of efficiently coupling Lower Hybrid power at the same time as Ion Cyclotron Resonance Heating, it was unfortunately not possible to create discharges with as wide range of $\nabla T_e/T_e$ as expected.

Nonetheless a useful dataset was created by including discharges from other, similar JET experiments. The final dataset includes off-axis Lower Hybrid Current Driven plasmas with full ($V_{loop}=0$) or partial current replacement, as well as Ohmic discharges and a few ICRH plasmas. It shows that the density profile width parameter $<n_e>/n_{e0}$ clearly follows the current profile width parameter q_0/q_{95} for normal shear discharges with $q_{95}<8$ and $1.5<q_0<3$, while no direct effect of V_{loop}, $\nabla T_e/T_e$, nor P_{aux} is discernible. This complements previous observations in normal shear sawtoothing TCV plasmas, where $q_0\approx1$ and $2<q_{95}<10$ (section 2.1). Together, combined observations in the two devices allow $<n_e>/n_{e0}$ to be expressed as a function of $<j>/j_0 \propto q_0/q_{95}$ in normal shear plasmas.

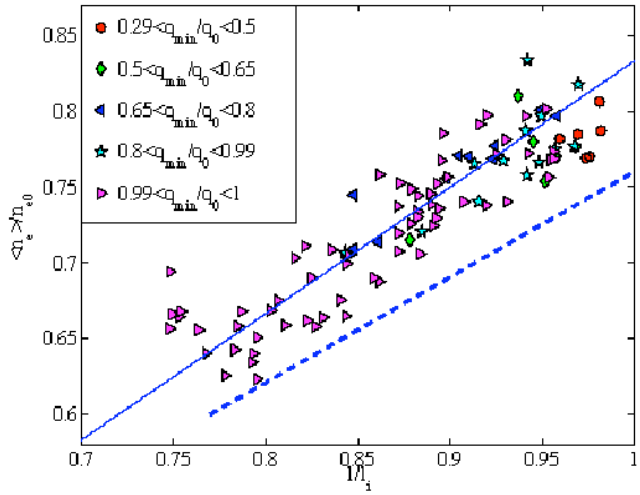

Fig. 4.1.7 *Density peaking factor $<n_e>/n_{e0}$ as a function of internal inductance in LHCD and Ohmic source-free JET L-mode plasmas. The symbols refer to classes of reversal parameter q_{min}/q_0. The broken line is a prediction based on the curvature pinch.*

Interestingly, reversing the shear, does not lead to hollow density profiles, as might be expected from some TEP predictions. This suggests that the turbulence responsible for the anomalous pinch may be absent in the reversed shear region or the effect of shear term in these discharges does not overcome the effect of aspect ratio, which always produces peaking, as predicted by theory. An empirical fit including both normal and reversed shear discharges suggests that the plasma normalised internal inductance l_i may be a general scaling parameter with $<n_e>/n_{e0}\approx0.83l_i$, irrespective of the other discharge parameters including loop voltage, Fig. 4.1.7 and shows that the Ware pinch is of little importance in these plasmas. The observed l_i dependence is in agreement with the prediction of a simple theoretical curvature pinch model, shown as a broken line in the figure.

CRPP staff provided extensive support for the development of NTM free S1 scenarios. CRPP has also contributed to the analyses of L-H transition and ELMy plasmas, in particular the transition in RF heating only discharges.

The study of the effects of externally applied radial electric field on the micro-stability of specific JET plasmas has been started. The linear code LORB5 is used to analyse the self-consistent linear growth rate of ITG with ExB shear. In particular the effect of reverse shear and Te/Ti will be studied in detail. The interface with the code GLF23 has also been installed for further comparisons.

4.2 ITER Tasks and R&D

The CRPP continues to place a high priority on work directly related to ITER, some of which is described here. This work was largely supported by EURATOM preferential support.

4.2.1 International Tokamak Physics Activities (ITPA)

H-mode transitions

A major activity of the ITPA group 'Confinement Database and Modelling' consists of gathering and analysing data provided by many tokamaks to predict the confinement in L-mode and in H-mode and to predict the threshold power for accessing the H-mode. The 'Threshold Database' contains data dealing with the L-mode to H-mode transition. It is now managed from the CRPP. New data were added and a new version was released. The influences of the aspect ratio and Z_{eff} on the threshold power were studied and included in the power law scaling for predictions.

MHD, disruptions and plasma control

The CRPP is also represented in this topical group, both for its experience of MHD and of plasma control.

ITER Physics Basis: All ITPA Topical groups are presently preparing a complement to the ITER Physics Basis for publication in 2004.

4.2.2 ITER ECRF 170GHz gyrotron development

Gyrotron (subtask 1.1)

Within the TW3-THHE-CCGDS1 task agreement, subtask 1.1, support was given to the industrial partner Thalès Electron Devices mainly by means of electron gun simulations, among other contributions.

The Technical Specifications and General Requirements for the Coaxial Gyrotron Development Prototype 1, 170GHz/2.0MW/1s were prepared. On the basis of these specifications the Call for Tender EFDA/03-960 was issued in June with a closing date for the Tender submission in August. The CRPP was represented in the Technical Evaluation Group (TEG) whose conclusion was that the only offer received was technically receivable and in compliance with the specifications.

The contract negotiation phase, in which CRPP is also involved, has begun and should lead to the placement of a contract by end of 2003 or early in 2004.

Magnet (subtask 2)

In parallel with the design of the gyrotron a finalisation of the design of the superconducting magnet has been performed. The 220mm warm bore of the designed magnet is compatible with the gyrotron technical design performed by Thalès. An electron beam alignment system has been included, similar to that used in the 165GHz coaxial gyrotron magnet operated at FZK. The feasibility of construction, from the superconductivity and cryogenic point of view, has been assessed by CRPP/PSI. The Technical Specifications and General Requirements for the magnet have been written in May. The CFT has been sent in June and replies have been received in September from 2 companies. The responses to the CFT are being evaluated by the TEG, in which the CRPP is represented.

Test facility (subtask 5 and future work)

The gyrotron will be tested at the test facility to be installed at the CRPP. Power supplies are needed for CW testing. The CFT for the main high voltage power supply (MHVPS), the body power supply (BPS) and the series high voltage solid state switch (HVSSS) have been written in collaboration with the other project partners. The MHVPS is under the responsibility of the CRPP. The Technical Specifications and General Requirements for the MHVPS have been included in a CFT issued in September. The CRPP will be represented in the TEG.

The gyrotron hall in the PPH building has been cleared and will soon be ready for new equipment. Contacts have been made with the competent services to have a crane installed for moving the gyrotron and magnet and for piercing the floor to pass cooling pipes. The transmission line CFT is in preparation and should be ready for issue by the end of the year. The cryogenic requirements of the ITER gyrotron form a significant enough part of the overall LHe use at the CRPP to justify a global study of helium use and recovery. Quotes have been received for refurbishing or upgrading the liquifier and recovery system. A detailed list of data acquisition signals has been compiled and preliminary contacts have been made with firms to help define possible solutions for both fast (μsec) and slow (hour) acquisition. The plant control system is under study.

4.2.3 Upper launcher design

In collaboration with EFDA-CSU Garching, ITER-IT, and the Associations ENEA-CNR-Milano, FOM, FZK, IPP-Garching, IPF-Stuttgart, the CRPP participates in the design of the ECW upper launcher of ITER. In this frame, the CRPP also organised meetings for the ECW Coordinating Committee aiming to discuss the requirements of the system for neo-classical tearing mode control in ITER.

4.2.4 Development of a feedback control technique for combating power supply saturation

The control of the vertical position instability is well modelled by linear equations. However, when the power supply saturates, the system becomes fundamentally non-linear and a tuned controller may no longer be optimal. We have investigated

this in collaboration with the Laboratoire d'Automatique of the EPFL with the aim of developing an optimal controller in the presence of voltage saturation.

The linear system possesses a single unstable mode, or pole, corresponding to the unstable growth rate. It is this quantity, the unstable mode, which must be optimally controlled during saturation, since all other modes are stable and can be left uncontrolled while the power supplies are saturated. We investigated a method of estimating this unstable mode for TCV found it accurate enough.

When saturation occurs, the feedback controller must only stabilise the unstable mode, in which case the region of attraction of the controller becomes the controllable region in the presence of the saturation. All other controllers are sub-optimal, which had not been realised previously.

The method proposed consists of smoothly changing from a full controller with small power supply requests to a state control only controlling the unstable mode, using a continuous function $(1- x_1^2)$ applied to all states except the unstable state, where x_1 is the value of the state, normalised to its maximum controllable value given the saturation level.

Using this method, we have demonstrated an increase in the controllability of ITER during large perturbations to the control system. Work is now progressing on completing the details for practical implementation of the method.

4.2.5 Superconductivity

A large number of specific R&D tasks were dedicated to studies of different superconductivity issues, some described in detail in section 2.5, partly funded by EURATOM preferential support. These are summarised as:

- TW3-TMC-SULTAN, Operation of the SULTAN facility and conductor test
- TW3-TMSC-HTSCL, Test of high temperature superconducting current leads, in collaboration with FzK, Karlsruhe
- TW3-TMSC-ELRES, Preparation and test of three NbTi samples with impressed current unbalance
- TW3-TMSC-SULSAM, Preparation and test of two Nb_3Sn subsize samples in collaboration with MIT
- TW2-TMSC-LCJOIN, Adaption for testing of two full size NbTi sample and test of a low cost NbTi joint sample
- TW1-TMC-JSPREP Del.1, Fabrication of a low transfer resistance Nb_3Sn full size sample
- TW1-TMC-JSPREP Del.5, Procurement of a heat treatment furnace for Nb_3Sn full samples to be tested in SULTAN
- TM-G02.01, M29, Development and manufacture of a low cost NbTi full size joint sample
- TM-005.G1, M12, Analyses of TF insert results. Preparation of an organised, accessible database for the test results of SULTAN short sample

4.2.6 Materials

A large number of specific R&D tasks were dedicated to studies of different fusion material issues, described in detail in section 2.4. These studies are partly funded by EURATOM preferential support, summarised as:

- TW0-TTMI-003 deliverable 3: Small specimen test technology - Development of experimental fracture testing devices to be used in a hot cell environment and constraint loss assessment on sub-sized compact specimens of EUROFER 97

- TW1-TTMS-001 deliverable 3: Proton irradiation of EUROFER 97 up to 1dpa of plate, for He effect testing

- TW1-TTMS-002 deliverable 20: Tensile and fracture toughness of EUROFER 97, punch testing

- TW2-TTMS-006a deliverable 3: Creep testing at RT-750°C on the two improved ODS batches

- TW2-TTMS-006a deliverable 6: Tensile testing at RT-750°C on the two improved ODS batches

- TW2-TTMS-004b deliverable 3: Development and testing of coatings to improve the corrosion resistance vs Pb17Li at T>450°C

- TW2-TTMS-005b deliverable 6 : Small-scale fracture mechanics - Modelling of brittle and brittle to ductile transition behaviours using appropriated theories. Formation of rules for transferability to standards and fusion components

- TW3-TTMA-002 deliverable 2: W coating onto RAFM alloys

- TW3-TTMS-005 deliverable 2: Investigation (tensile and Charpy testing) of PHT and PWHT to improve the design limits and to define the acceptable temperature range

- TW3-TTMS-006 deliverable 3: Study of the influence of Ti addition on the mechanical properties (Charpy, tensile) with characterisation of the full fabrication process

- TW3-TTMS-007 deliverable 7: Molecular dynamics simulations of grain boundaries: evolution of displacement cascades in nanocrystalline Fe samples created with an available Fe potential

- TW3-TTMS-007 deliverable 8: Irradiation in SINQ

- TW1-TVV/Titan: Titanium alloy irradiation testing

- TW1-TVV/Beam: In-beam mechanical testing of CuCrZr

- TW3-TVM-TICRFA: Effect of low dose neutron irradiation on Ti alloy mechanical properties

4.3 Plasma-surface interactions, in collaboration with the University of Basel

Inclined mirror plates (100 mm x 60 mm x 2.5 mm) will be positioned in the scrape-off-layer of TEXTOR at the FZ-Jülich (Germany) to allow the exposure at different radial distances from the last closed flux surface in order to study influence of a growing carbon deposit as well as the reflectivity evolution after erosion or after carbon implantation into the surface. Several polished mirrors of polycrystalline molybdenum, of tungsten and stainless steal have been prepared and pre-

characterised by spectrophotometry and spectroscopic ellipsometry to determine the spectral dependence of the reflectivity for different angles of incidence. Due to our newly designed mechanical component allowing us to precisely position the large mirror sample relatively to the light beam of the optical instruments, we could realise systematic cartographies of the optical constants. Two Mo mirrors have already been exposed to the plasma in TEXTOR and will be investigated by our optical methods and by photoelectron spectroscopy in order to get information about the thickness, the composition and the electronic structure of the deposits and the surface morphology. These measurements will be completed by SIMS. The next step will be the exposure to the TEXTOR plasma for a longer periods of time.
First experiments on the magnetron sputtering deposition of Mo thin films on silicon substrates and carbon layers have been made. We were specially interested in the oxygen contamination and the surprisingly high reactivity with the transition metal layer. We investigated the interface formation of MoO_3//Si, MoO_x//Si and MoO_3/C//Si using low deposition powers implying a low growth rate. As the formation of molybdenum carbide plays a crucial rule during the exposure to the plasma, we realised a large number thin films of dual magnetron co-deposition. The optical constants depend strongly on the composition of the film which, in general, consists of a mixture of Mo, C, MoC and MoO_2. The characterisations will be completed by AFM, SEM and X-ray diffraction and repeated on other first-wall materials like tungsten and vanadium.

4.4 Socio-Economic Studies

Risk and Novelty in Energy scenarios, TW1-TRE-FPOA

(Work performed by the CEPE (EPFL, ETHZ, PSI) for the Association, on behalf of EURATOM, under preferential support from EURATOM)

The project investigates the risk perception (familiarity, event/occurrence, damages/loss, effects/consequences, extent, reduce/decrease, resolve/mitigate) and novelty (attractiveness/goodness, newness, introduction/disclosure, acceptance/ agreement) attitudes of communicators (groups of experts or organisations) as found in their respective publications in the energy scenario literature and finally to compare the outcome with data collected from different groups of advanced students in Switzerland, Belgium, France and Austria as well as from a focus group established in the frame of socio-economic studies for the proposed Cadarache site for ITER (Project POFFICAD) .

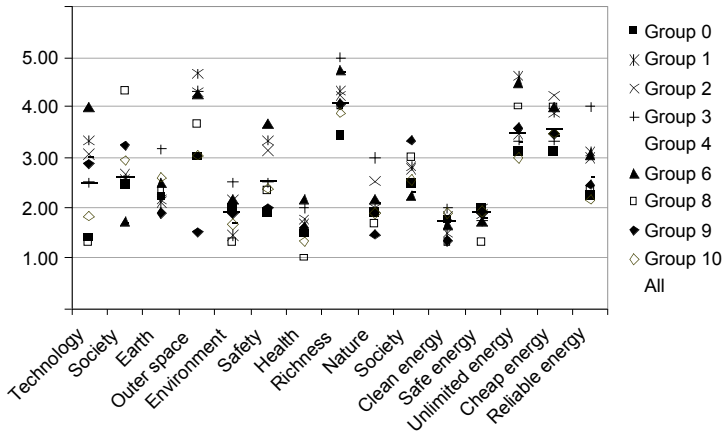

Fig. 4.4.1 *Ranking of different items from the various groups. The vertical axis is the rank, 1 being the highest.*

For this last purpose, specific questionnaires were developed and tested with the help of two groups of electrical engineering students, one group of social science students, one group of process engineering students, and one group of astronomy students. The average ranking of the different items is shown in Fig. 4.4.1. A significant increase in the spread in the average ranking per group was observed, except for the ranking of the items *earth*, *society*, *clean energy* and *cheap energy*. Strongest agreement throughout the groups was observed for the items *clean energy* and *safe energy*, stating high importance (rank 1-2) with 68.6% and 46.2% standard deviations of the averages respectively. The high standard deviations were due to low sample numbers of some of the groups.

Fusion as part of the energy system, TW2-TRE-FESA/A1

(Work performed by the LASEN (EPFL) for the Association on behalf of EURATOM)

The objective of the research was to explore the global potential of fusion power plants and to quantify their advantages and drawbacks. The problem is to build consistent multi-regional global electric markets scenarios for the horizon 2100, including fusion as an energy supply option. The research makes use of the PLANELEC/PRO software, developed by LASEN/EPFL. It determines the generating expansion plan, which adequately meets electricity demand at minimum cost while respecting constraints given by the user, such as CO_2 emissions. When comparing alternate expansion patterns, the objective function to be minimised is the present value of total costs, including investment cost, operation cost, maintenance and fuel cost. PLANELEC/PRO uses probabilistic simulation to estimate generating system production costs and dynamic programming to determine the optimal expansion pathway. The allocation of natural resources to satisfy the constraint of the demand is based on recent systemic approaches to allow technologies which may not be economically optimal to be taken into account in the energy supply scenarios, and particularly the electricity supply.

Fusion technologies are defined as candidates and compete with other technologies under environmental and resources constraints. The problem with this approach is that several unknown parameters have to be quantified, such as plant availability statistics or maintenance characteristics and cost. The methodology developed permits the establishment of long-term global and multi-regional electric generation scenarios to evaluate the potential of the fusion option in comparison with other complementary or competing new technologies.

4.5 Collaborations with other EURATOM Associations

The Association is actively collaborating with other Associations. A full list of the collaborative activities has been reviewed and endorsed by the EFDA Scientific and Technical Advisory Committee. The following list gives specific themes where such collaboration occurred. Those marked (*) are the subject of specific preferential support by EURATOM.

C. Angioni, M. Maraschek, A. Mück, G. Pereverzev, F. Ryter, H. Zohm, IPP Garching, Germany, *"Sawtooth tailoring experiments for NTM control" (*)*

F. Ryter, IPP Garching, Germany, *"Measurement of electron transport in electron temperature gradient variation experiments at high ECH power density in TCV as a function of plasma shape; comparison with ASDEX-Upgrade" (*)*

J. Bakos, KFKI Budapest, Hungary, *"Laser ablated impurity transport using Nickel"*

G. Cunningham, G. McArdle, Association UKAEA Fusion, UK, **J. Qin**, Imperial College, London, UK, *"Comparing the plasma equilibrium control of tight and conventional aspect ratio tokamaks" (*)*

A. DellaCorte, P. Gislon, Association EURATOM-ENEA, Italy, **D. Ciazynski and L. Zani**, Association EURATOM-CEA, France, *"Test in SULTAN of the PS-FSJS sample" (*)*

V. Grandgirard, CEA, France, *"Eulerian gyrokinetic code development" (*)*

R. Heller, Association EURATOM-FzK, Germany, *"EFDA task on design of high temperature superconducting current leads" (*)*

Y. Ilyin and A. Nijhuis, University of Twente, Holland, *"The assessment of current distribution results from test in SULTAN"*

T. Madeira, **P. Amorim**, CFN/IST, Lisbon, Portugal, *"X-ray spectroscopy of the TCV plasma" (*)*

M. Maraschek and S. Guenter, IPP Garching, Germany, *"NTM marginal β limit on ASDEX-Upgrade Tokamak" (*)*

D. Mazon, M. Jouve, Association EURATOM-CEA, France, *"Temporary installation of imaging hard-X-ray camera*"

P. Nielsen, R. Pasqualotto, G. Manduchi, Consorzio RFX, Padova, Italy, *"Thomson scattering from the edge plasma of TCV"*

J. Nuehrenberg, S. Sorge, A. Koenies, V. Kornilov, IPP Greifswald, Germany, **A. Peeters**, IPP Garching, Germany, *"Linear and nonlinear gyrokinetic simulations" (*)*

V. Piffl, IPP Prague, Czech Republic, *"Ultra Soft X-ray spectroscopy using a multi-layer mirror to observe He- and H-like emission from Boron, Carbon, Nitrogen and Oxygen" (*)*

***L. Popova**, Institute of Mathematics and Informatics, Bulgarian Academy of Sciences, Sofia, BG), **S. Kuhn and D. Tskhakaya** (Association Euratom-OAW, Innsbruck, Austria, **A. Loarte** (EFDA-CSU Garching),* "PIC simulations of ELM-produced particle and energy pulses and their effect on the SOL"

A.P. Rodrigues, CNF/IST, Lisbon, Portugal, *"Multiple DSP based controller for TCV digital control system" (*)*

F. Volpe, B. Lloyd, Association UKAEA Fusion, Culham, UK, "*Installing the ray tracing code ART and the Fokker-Planck code Bandit-3D at the CRPP and participation in the planning of EBW experiments in TCV*"

G. Zvejnieks, Institute of Solid State Physics, University of Latvia, Latvia, **O. Dumbrajs, V. Hynönen,** Helsinki University of Technology, Finland, **W. Suttrop, H. Zohm**, Max-Planck-Institut fuer Plasmaphysik, EURATOM-Association, Germany, *"Dynamical properties of Edge Localised Modes (ELMs) occurring in the ASDEX-Upgrade and TCV experiments" (*)*

4.6 Other international collaborations

J. Egedal, W.Fox, M.Porkolab, PFSC, MIT, USA, *"Magnetic reconnection on the Versatile Toroidal Facility"*

G. Giunchi, Edison, Milan, Italy, *"Test of MgB2 high temperature superconductors"*

V.E. Lukash, RRC Kurchatov, Institute of Nuclear Fusion, Moscow, Russia, **R.R. Khayrutdinov**, **V. Dokouka**, TRINITI, Troitsk, Russia, **D. Raju**, IPR, Bhat, India, *"Simulation of TCV experiments using the non-linear DINA code"*

J. Minervini, PFSC, MIT, USA and **N. Martovetski**, LLNL, USA, *"Preparation and test of two subsize Nb3Sn cable-in-conduit superconductos"*

N. Mitchell, ITER International Team Naka and D. Bessette, ITER International Team Garching, Germany, *"Analysis and interpretation of the the ITER TFCI Tcs experiments"*

V.D. Shafranov, Kurchatov Institute, Moscow, Russia, **S. Medvedev**, Keldysh Institute of Applied Mathematics, Moscow, Russia, **V. Nemov**, Kharkov Institute of Physics and Technology, Ukraine, **J. Nuehrenberg**, Greifswald, Germany (*), *"Novel Approaches to Improve Confinement in 3D Systems"* (INTAS grant)

J. Snipes, R. Parker, M. Porkolab, J. Freidberg, PFSC, MIT, USA, *"Fast particle physics and Alfven waves on the Alcator C-Mod tokamak"*

A. Sushkov, Kurchatov Institute, Moscow, Russia, *"Implementation of a double layer multiwire proportional soft X-ray (MPX) detector for high spatial and temporal resolution temperature profiles in TCV"*

Wendelstein Group, IPP Greifswald, Germany, *"Test of 2 W7X conductor joint samples"*

S.Yu. Medvedev, A.A. Martynov, A.A. Ivanov, Keldysh Institute of Applied Mathematics, Moscow, Russia, **M.Yu. Isaev, V.D. Shafranov, A.A. Subbotin**, RRC Kurchatov Institute, Moscow, Russia, *"Equilibrium and Stability of 2D and 3D plasma configurations"*

E. Zapretilina, Efremov Research Institute Of Electrophysical Apparatus (NIIEFA), Russian, *"Electromagnetic behaviour of the large NbTi cable-in-conduit conductors for the ITER Poloidal Field coils"*

4.7 Other collaborations within Switzerland

Ph. Mullhaupt, D. Bonvin, B. Srinivasen, Laboratoire d'Automatique, EPFL, *"Development of saturating controller algorithms for ITER"*

Many industrial collaborations within Switzerland are underway with the plasma processing group, see Section 2.7.

5 The Educational Role of the CRPP

The CRPP plays a role in the education of undergraduate and postgraduate students, particularly in the Faculté des Sciences de Base (Faculty of Basic Sciences) of the EPFL. Advanced education and training in fusion physics and technlogy and plasma physics topics is carried out as part of the research activities of the Association. Section 5.1 presents the 7 courses given to physics undergraduates and to engineering undergraduates. In their fourth and final year, physics undergraduates spend time with a research group at the EPFL, typically 12 hours per week for the whole year. During this period, they perform experimental or theoretical studies alongside research staff, discovering the differences between formal laboratory experiments and the "real" world of research. After their final examination at the end of the 4th year, physics students are required to complete a "diploma" work with a research group, lasting a full semester. This diploma work is written up and defended in front of external experts. The CRPP plays a role in all of these phases of an undergraduate's education, detailed in Sections 5.2 and 5.3.

As an academic institution, the CRPP supervises many Ph.D. theses, also in the frame of the Physics Section of the EPFL. 3 PhDs were awarded in 2003. At the end of 2003 we have 29 Ph.D. students supervised by CRPP members of staff, mostly in Lausanne but also 5 at the PSI site in Villigen. Their work is summarised in Section 5.4.

5.1 Undergraduate courses given by CRPP staff

N. Baluc, *Chargée de cours – "Material Physics"*
Basic course on material physics, presented as an option to 4th year Physics students. The course covers the theory of diffusion, dislocation and plasticity as well as the characterisation of materials. Experimental techniques used in materials studies, as well as analysis methods are presented for super-alloys, quasi-crystals, ceramics, composites and polymers.

A. Fasoli, Assistant Professor – *"Plasma physics II"*
One semester option course presented to 4th year Physics students, introducing the theory of hot plasmas via the foundations of kinetic and magnetohydrodynamic theories and using them to describe simple collective phenomena. Coulomb collisions and elementary transport theory are also treated. The students also learn to use various theoretical techniques like perturbation theory, complex analysis, integral transforms and solution to differential equations.

J.B. Lister, *Chargé de cours – "Plasma Physics III"*
An introduction to controlled fusion, presented as a one semester option to 4th year Physics students. The course covers the basics of controlled fusion energy research. Inertial confinement is summarily treated and the course concentrates on magnetic confinement from the earliest linear experiments through to tokamaks and stellarators, leading to the open questions related to future large scale fusion experiments.

M.Q. Tran, Professor – *"General Physics I"*
Winter semester 2002-2003 (2 hours of lecture and 2 hours of exercises) for the "Communications Systems" section. The course covers kinematics and basic Newtonian mechanics of material points.

M.Q. Tran, Professor – *"Plasma Physics I"*
An introduction to basic plasma physics, presented as a one semester optional course to 3rd year Physics students. The course treats the fundamental physics of magnetised and non-magnetised plasmas.

L. Villard, *Maître d'Enseignement et Recherche (MER) – "General Physics II"*
Summer semester (4 hours/week lecture and 2 hours/week exercises). Introductory course in physics for students in the "Communication Systems" section. The course covers Newtonian systems dynamics, special relativity and thermodynamics.

L. Villard, *Maître d'Enseignement et Recherche (MER) – "General Physics III-IV"*
Winter semester course given to students in their 2nd year Mechanical and Electrical Engineering.

5.2 Undergraduate work performed at the CRPP

EPFL 4th year students (2003 Summer semester)

Lukas DERENDINGER: *"Infra-red absorption spectroscopy measurements in a radio-frequency glow discharge used for the deposition of teflon-like layers for bio-medical applications"*
Fluoro-polymer (Teflon-like) layers can be deposited at ambient temperature on various surfaces by radio-frequency glow discharge using fluoro-carbon gas precursors diluted with hydrogen. These coatings have interesting properties like hydrophobicity which make them candidates for bio-medical applications. Even if such layers of sufficient quality have been obtained by empirical developments, the underlying plasma chemistry mechanisms remain to be determined.
Infra-red absorption spectroscopy in the gas phase has been used to measure the concentration of several molecules and radicals formed in the plasma. The concentration of these species have been correlated with the properties of the deposited fluoro-polymer layers, measured by X-ray Photoelectron Spectroscopy (XPS) and contact angle (collaboration with STI-IMX-LMCH of EPFL, Prof. H. J. Mathieu).

Sébastien JOLLIET: *"Particle trajectories in a curvilinear magnetic field: perturbation method"*
The aim of this work was to assess the applicability of the perturbation approach, in which the electric and magnetic drifts are considered as small corrections to the uniform parallel motion. Both ions and electrons in toroidal axisymmetric configurations were considered, assuming concentric or Shafranov-shifted circular magnetic surfaces. An equilibrium radial electric field was also considered. The deviations from exact trajectories were analysed. Both Shafranov shift and radial electric fields break the symmetry in velocity space. The variation of parallel velocity is in fact the dominant correction for electron motion and a supplementary perturbation term was included to take this into account.

Nicolas MELLET: *"Resolution of equations for the Alfvén resonant magnetic surfaces"*
In this work the equation giving the Alfvén resonant surfaces (Alfvén continuum) was solved with a Fourier method in various model axisymmetric configurations. The effects of finite aspect ratio, Shafranov shift and elongation were investigated. The study has focused in the low frequency part of the spectrum for which the various geometrical couplings induces gaps. The size of the gaps was calculated as a function of the corresponding geometrical factors.

Samantha PAVON: *"A study of the ionisation source of a high current DC arc reactor"*
The objective of the project was to study the ionisation source of a high current DC arc reactor used for low energy plasma deposition of epitaxial silicon. The filament current asymmetry and resistance were measured, from which the temperature and current distribution were deduced and compared with a numerical model which accounted for ohmic heating, black body radiation, thermionic emission and hot spot formation due to ion bombardment.
An interpretation of why the plasma preferentially attaches to one end of the filament was proposed. The interpretation includes an initial transitory phase where thermionic emission is dominant. This induces a peaked temperature distribution near the ends. Then there is formation of a "hot spot" near one of these peaks due to the dominance of ion bombardment. The stable configuration is reached when the hot spot is fixed. The geometry of the ionisation chamber had no influence, but the behaviour of the filament depends strongly on its form and whether it is made of tungsten or tantalum.

Karin SCHOMBOURG: *"Analyseur électrostatique à grilles pour TORPEX"*
The knowledge of particle distribution functions is an important issue for the characterisation of plasmas. A Retarding Field Analyser (RFA) has been developed and installed in the toroidal device TORPEX. The first tests in Argon and Hydrogen plasmas confirm the values of electron temperature, independently measured by means of electrostatic Langmuir probes. They also indicate that the design of the RFA could be simplified, and parameters like the distance between grids optimised to achieve a better response in terms of signal-to-noise ratio (SNR). The low SNR ratio is actually limiting the capabilities of the RFA for the measurement of ion parameters.

EPFL 4th year students (2003-2004 Winter semester)

Olivier PISATURO: *"Design and construction of a Mach probe for the TORPEX experiment"*
A multiple face, movable electrostatic probe is designed to measure the flow created by a combination of electric and magnetic fields in the plasmas produced by Electron Cyclotron Resonance in TORPEX. Such a measurement is important in relation to the study of drift wave turbulence and related anomalous transport. As the drift waves are Doppler shifted by the plasma flow, knowledge of the value of the flow is necessary to reconstruct the wave characteristics in the plasma frame. In addition, the gradient in the plasma flow plays a fundamental role in the process of 'anomalous' transport, as it can reduce the radial extension of turbulence structure and the related transport of particles and energy.

Martin PYTHON: *"Design and construction of an optical probe for the TORPEX experiment"*
A movable optical probe is being designed and built, collecting visible light emitted by the pasma in a localised volume,. The probe consists of an interference filter, a mirror, a lens, and an optical fiber. It will be mounted on a movable arm, so that a localised measurement will be possible even in passive spectroscopy. Information on the state population, electron temperature from line intensity ratio, upper limits for the ion temperature will be obtained. The probe will be tested in view of the in situ application of laser induced fluorescence for a reconstruction of turbulence structures resolved spatially and by energy.

Jonathan ROSSEL: *"Determination of the breakdown conditions on TCV"*
This work aims at determining the precise conditions required for plasma breakdown in the TCV tokamak, to increase the reliability of this badly understood phase of the discharge. Use can be made of all existing diagnostics.

External students

Alexandre BLAIS, from the Department of Mechanical Engineering, University of Ottawa, Ottawa Canada: "*A novel approach to interpret enthalpy probe measurements in low pressure supersonic plasma jets*"
The development of a new numerical method to interpret enthalpy probe measurements in supersonic plasma jets needs the input of experimental data. This collaboration allowed the student to perform measurements of the (unknown) static pressure downstream of the shock induced by a special post-shock probe. The results of this research was presented and published in the 16th International Symposium on Plasma Chemistry, Taormina, Italy.

Alberto ALFIER, from the Universita degli Studi di Padova, Italy: *"Edge Thomson Scattering"*
In continuation of a collaboration with Consorzio RFX, Padova (started in 2001), Alberto Alfier spent 1 month at CRPP to work on the Thomson scattering diagnostic measuring electron density and temperature in the edge region of TCV. His work concentrated on processing of the data and preparation of software for presentation of the results in the form of density and temperature profiles on normalised flux coordinates. The data sets form the main Thomson scattering system and the extension for high resolution measurements near the plasma edge can now be combined to obtain profiles with better coverage even beyond the last closed flux surface.

Eric CELLIER, from the Ecole Nationale Supérieure de Physique de Marseille: *"Study of MHD activity in elongated TCV discharges in presence of ECW"*
Discharges at high elongation stabilised by far off-axis X2 current profile broadening and at high central density are dominated by continuous MHD activity on q=1, replacing the usual sawtooth activity. This activity is studied using a poloidal array of 64 soft X-ray chords (MPX) and toroidal arrays of 16 magnetic probes and 4 soft X-ray diodes, with Fourier and SVD techniques. Magnetic and soft X-ray measurements show a mode structure with high harmonic content m/n=1/1, 2/2, 3/3 resonant on the q=1 surface. When X3 central heating is applied, the mode amplitude typically decreases on a local resistive time scale while the current profile is measured to peak. In the case sawteeth are present, the amplitude of the m=3 signal deduced from the MPX can be substantially modulated sawtooth activity.

János MÁRKI, from KFKI, Budapest: *"Investigation of impurity transport"*
This undergraduate student spent a total of 4 weeks at the CRPP, in the framework of an ongoing collaboration with Prof. Bakos of KFKI, Budapest. He received training for the operation of the laser ablation system operated in collaboration with KFKI Budapest and with the data analysis of impurity transport experiments. Following his second visit, he continued data analysis remotely from Budapest of a set of experiments he had participated in.

5.3 EPFL Diplomas awarded in 2003

Nicolas FREMAUX: *"Emissivity reconstruction of TCV plasma divertor emission using multiple digital CCD cameras"*
In a diverted plasma configuration on TCV, the contact of the plasma leg with the machine walls has been observed to diminish at sufficiently high density, a phenomena termed "detachment". As particles follow the last closed flux surface and are directed to the machine walls, they lose momentum and the current to the walls diminishes. Volume recombination in the high density divertor is one possible

mechanism for this momentum loss and may be observed by comparing the relative intensities of the Balmer alpha, beta and gamma (etc.) radiation of deuterium neutrals. A fibre optic telescope image of the divertor was split onto 4 digital CCD cameras, each equipped with an interference filter to isolate a particular spectral feature. In this work, the optical arrangement and calibration were obtained and algorithms developed to interpret the acquired images in terms of light emissivity. Changes in the intensity ratios of the Balmer series lines during plasma detachment were observed indicating that recombination is occurring.

Joël GROGNUZ: *"Investigation of electron Bernstein waves"*
With a view to extending the operational space of additionally heated plasmas on TCV efforts are being made to develop Electron Bernstein Wave Heating of overdense plasmas. At electron density $>4.2\times10^{19}m^{-3}$ electromagnetic waves at the first cyclotron harmonic in the extraordinary mode do not propagate. By mode converting these electromagnetic waves to electrostatic waves that can propagate irrespective of density it should be possible to heat overdense plasma.
For direct mode conversion, fast X-mode to Bernstein wave (XB) there must be a very large density gradient ($>10^{22}m^{-4}$) in a region of the plasma where the extraordinary mode at the first cyclotron harmonic is evanescent. For Ordinary to slow X-mode to Bernstein wave (OXB) conversion to occur the plasma frequency and the upper hybrid frequency must concide in a region of the plasma where there exists a substantial density gradient ($>10^{21}m^{-4}$) on TCV.
Studies performed by the student revealed that direct XB conversion scheme will be extremely difficult on TCV but that the OXB scheme may be possible on TCV in high density H-mode. Attempts have been made to produce plasmas that will allow mode conversion to occur. It has been found possible to produce discharges suitable for mode conversion studies in ELM-free H-mode. The conditions to allow OXB conversion have been attained only briefly (< 100msec).

Christian SCHLATTER: *"Radiation losses study in the regimes with improved confinement on T-10 using AXUV-detectors"*
An array of fast bolometers (16 channel pinhole camera) based on Absolute eXtreme UltraViolet (AXUV) silicon photodiodes covering the plasma cross-section of the T-10 tokamak was calibrated and successfully used for the measurement of the total radiated power as well as for the reconstruction of the radial plasma emissivity distribution by an algebraic Abel inversion method. The suitability of the semiconductor-based detector for the environment of T-10 was carefully checked by analysing its behaviour exhibited in a variety of plasma discharges but also by characterisation of the detectors response after 18 months of operation on the tokamak. Different regimes of better confinement (T-10 H-mode, density limit, biasing) investigated in recent experimental campaigns were studied and the important contribution of AXUV as valuable diagnostic facility for the further understanding of localised radiation processes was demonstrated. The outstanding fast temporal resolution (less than 20μs) allows studying of short timescale processes – for example the injection of fast pellets – which cannot be performed by other diagnostics.
This diploma was carried out at the Russian Research Centre “Kurchatov Institute” in Moscow.

Daniel TAMBURRINO: *“Characterisation of a supersonic low pressure DC plasma jet by optical emission spectroscopy”*
The Low Pressure Plasma Spraying (LPPS) processes, which use plasma torches at reduced pressure, have emerged as reliable technologies, with broad industrial successes for the deposition of numerous coatings. A diagnostic has been developed using optical emission spectroscopy in order to study the deviation of the local thermodynamic equilibrium (LTE) of low pressure plasma jets as a function of the pressure. Measurements of excitation temperatures by means of Boltzmann plots and electron density by Stark broadening have been performed in an argon and

argon-hydrogen plasma jet at pressures varying from 2 to 400 mbar and 2 to 20 mbar respectively. It is shown that the Ar/H_2 plasma jet is not in local thermodynamic equilibrium for pressures between 2 to 20 mbar because the excitation temperatures of argon and hydrogen are not the same. The study of the LTE deviation in function of the pressure is not straightforward for pure argon plasma jets because the measured points of the Boltzmann plot are close to form a line even when the plasma is not in thermodynamic equilibrium. However, it is shown that the plasma jet is closer to the thermodynamic equilibrium in the compression zones than in the expansion zones. The study also showed the difference in the plasma jet structure between an Ar and Ar/H_2 plasma jet, the Ar/H_2 plasma jet presenting a higher density and temperature on the plasma jet fringes.

Pierre WEBER: *"Investigation of the plasma dynamical response for transport studies in toroidal plasmas"*
Transport phenomena are naturally investigated on tokamak devices, like TCV. A specific tool to investigate the transport properties is the modulation of the plasma heating or production source, in this case the electron cyclotron heating (ECH). Experiments in which the ECRH power is modulated have already been performed on TCV with the aim of investigating the generation and thermalisation of energetic electrons and the heat transport phenomena.
The diploma work is focused on the analysis of experimental data from TCV, and their interpretation on the basis of 'system identification' analysis to extract the information about transport properties, both of the plasma bulk and of the suprathermal component.
The possibility of exploiting similar techniques on the toroidal device TORPEX (operating at CRPP/EPFL) has been explored, together with the possible experimental scenarios.

Diploma studies presently underway (Winter semester 2003)

Lukas DERENDINGER: *"Experimental Investigation of the Telegraph Effect in a Large Area Plasma Reactor and Comparison with a 2-D Numerical Simulation"*
Parallel plate RF reactors are commonly used for plasma-enhanced chemical vapour deposition and dry etching of thin films such as amorphous silicon or silicon oxide. Large area ($>1m^2$) reactors are used for the manufacture of photovoltaic solar cells and thin film transistors for flat screens. In these reactors, the RF plasma potential can vary over a long range across the reactor due to the finite plasma conductivity, resulting in plasma non-uniformity. A perturbation of RF current due to the grounded sidewall is propagated along the resistive plasma between capacitive sheaths in order to maintain RF current continuity between the electrodes; the damping length is determined by the Telegraph equation. This diploma work is an experimental study of the 2-D non-ambipolar DC current flow pattern in a large area rectangular reactor, KAI-S, using the installed array of 82 surface probes. The measurements are to be compared with a 2-D numerical solution of the Telegraph equation.

Chong DING: *"Study of Dielectric Barrier Discharges as a Function of Pressure using Optical Emission Spectroscopy and Electrical Measurements"*
Plasma processing using uniform discharges near atmospheric pressure requires electrodes covered with a dielectric barrier to limit the risk of arcing. There are several regimes of operation, of which the uniform luminescent discharge provides the most appropriate conditions for a wide range of high quality, low cost plasma applications. A low frequency (kHz) high voltage (kV) source is operated in a pressure range of 10 to 1000mbar. This study aims to characterise the electrical properties and use optical emission spectroscopy to identify the excited species and gas composition.

Sebastien JOLLIET: *"Gyrokinetics in straight-field-line magnetic coordinates"*
The aim of this work is to formulate and solve the problem of electrostatic gyrokinetics in a straight-field line magnetic coordinate system for both particle motion and field solver. The intent is to reduce the number of operations by avoiding coordinate transformations at every time step. The method will also make further optimisations easier. The relevant modifications will be implemented first in linear, then in nonlinear gyrokinetic global codes.

Nicolas MELLET: *"Alfvén continuous spectra in 2D and 3D configurations"*
In this work the differential equations determining the Alfven continuum magnetic resonance surfaces will be written and solved in axisymmetric and general 3D configurations. Tokamak configurations, then stellarator configurations will be examined. Results will be compared with the mode conversion surfaces computed with a full wave code.

Samantha PAVON: *"Electrical, Optical and Mass Spectrometric Characterisation of a Low Energy DC Arc Plasma"*
Low energy plasmas have only recently been considered as an alternative to Chemical Vapour Deposition for epitaxial deposition of layers for semiconductors. This diploma work is carried out in the High Current DC Arc BAI 450D reactor at the CRPP in collaboration with UNAXIS. The reactor has been adapted for low pressure operation, suitable for epitaxial deposition, and the plasma profiles will be measured using Langmuir probes, CCD camera and optical spectroscopy. The low energy aspect will be verified using an energy-resolved mass spectrometer. The radial profiles of the plasma column will be modelled using a 1D numerical simulation.

Karin SCHOMBOURG: *"Transport studies in TORPEX plasmas"*
The aim is to investigate the cross-field transport of particles and energy across B in TORPEX, and add important information to the characterisation of TORPEX plasmas, already under way from the point of view of turbulent phenomena and instabilities. Plasma parameters are measured with arrays of electrostatic Langmuir probes. They will be used to infer the transport properties by applying well-established techniques based, for example, on the correlation of signals from different tips. A Retarding Field Analyser (RFA), can be employed to identify the contributions to transport of different energy classes of particles, for example to distinguish between bulk and suprathermal components. A technique specifically developed for this kind of studies is the modulation of the microwave (MW) power that produces and sustains the plasma. The transport coefficients can be evaluated by inducing a small perturbation to the plasma density and/or temperature, and analysing their spatial and temporal responses on the basis of existing transport models. During the first part of the diploma the candidate will study and implement the hardware modifications of the MW source required for the exploitation of MW modulation technique in TORPEX. The optimum parameters, like modulation frequency and amplitude, will be identified. The second part will be focused on the measurement of the transport properties, and possibly on their relation to the measured properties of turbulence.

5.4 Postgraduate studies

Postgraduate courses given in 2003

Nadine BALUC, Robin SCHAUBLIN, Philippe SPAETIG, Max VICTORIA: *"Effects of Radiation on Materials"*

This 14-hour class is given by four lecturers from the CRPP and one lecturer of the PSI (Dr. D. Gavillet). It is aimed at providing extensive information on the effects of radiation (neutrons, protons, ions) on the structure and mechanical properties of structural materials for nuclear power plants. It is divided into five chapters: 1) introduction to radiation damage and nuclear installations, 2) radiation damage and analysis tools, 3) fracture mechanics and radiation damage, 4) radiation effects in materials for fission reactors, 5) materials for fusion reactors.

Laurent VILLARD: *"Numerical Methods for Partial Differential Equations"*
This course is part of the EPFL Doctoral School in collaboration with the Swedish NetUniversity. It unites 50 PhD students from the EPFL, the Paul Scherrer Institute, the Haute Ecole du Valais, KTH Stockholm and CTH Gotheborg.

Roland BEHN, **Prof. Peter BOCHSLER** (University of Bern), **Christoph HOLLENSTEIN**, **Henri WEISEN**: *"Plasma Diagnostics"* (course PY-12 of the EPFL doctoral school)
This course consisted of 56 hours, of which roughly half were lectures and half were class exercices. It covered the topics of diagnostics for industrial plasma applications (12 hours), fusion plasmas (32 hours) and diagnostics of space plasmas (8 hours). It was taught jointly by three members of the CRPP and for the part on space plasmas, by Prof. P. Bochsler as an invited lecturer from the Institute for Solar Physics at the university of Bern. I was regularly attended by 11 students, three of which were not PhD students at CRPP. Four of the students followed the course to meet the requirements of the newly established doctoral school of the EPFL; two of these were CRPP PhD students.

Doctorate degrees awarded during 2003

Juliette BALLUTAUD: *"Study of high deposition rate amorphous silicon in Plasma Enhanced Chemical Vapor Deposition (PECVD) reactor for silicon thin-film solar cells"*
EPFL PhD thesis 2900(03)
Plasma enhanced chemical vapour deposition (PECVD) of thin films such as amorphous silicon has widespread applications especially in the field of photovoltaic solar cells and thin-film transistors for flat screen production. Industrial applications require high depositions rates over large areas with a good uniformity in layer thickness. In this thesis, some aspects of PECVD in large surface, industrial type, capacitive radio frequency reactor are investigated. The aim of this work is to study the plasma process conditions to increase the deposition rate of uniform, good quality, a-Si:H layer for solar cell application in a single chamber reactor.
The studies realized during this thesis have necessitated the development and the comprehension of diagnostics such as deposition rate measurement by in-situ interferometry, plasma power measurement and layer density measurement by ellipsometry. During the thesis, we have also elaborated a matching-box circuit for using process frequencies of 27.12MHz and 40.68MHz.
Deposition of a-Si:H in small electrode gap reactor has been studied. At present industrial reactors have a standard electrode gap of 2.4cm. We modified a reactor to reach a small gap of 1.7cm. It appears that we have obtained faster deposition rate in the small gap reactor but non-uniformity problems increase due to edge focusing and powder effects. One solution, based on a teflon jigsaw to keep the plasma away from the edge confined spaces, is proposed to suppress focusing effect but the operation parameter space is still reduced by the powder effect.
Systematic measurements of a-Si:H layer density was also done by ellipsometry. It is shown that the layer density decreases when the deposition rate increases, independently of pressure, gas flow and frequency (27.12MHz/40.68MHz) of the plasma. At high deposition rate, ~6Å/s, only an increase of the process temperature from 200°C to 230°C can significantly improve the layer density. We have noted

also a slight improvement of layer density for layers deposited in the small gap reactor. Nevertheless industrial constraints impose a process temperature of 200°C and a standard gap reactor. By optimising the process parameters, keeping the temperature process at 200°C, good quality, uniform, a-Si:H layer were deposited at 3Å/s on 37cm x 47cm glass substrates at 40.68MHz.
A particular source of non-uniformity in large area reactor has been examined. In large area reactors, a perturbation in RF plasma potential, due to the electrode edge asymmetry, propagates towards the plasma center with a characteristic damping length λ. The variation of RF plasma potential at the edge implies a variation of the deposition rate across the reactor area and then a non-uniformity of the deposited layer. A theoretical study was done to understand of this phenomenon and experimental results confirmed the model.
Finally, for solar cell applications, a study of the boron cross-contamination during solar cell deposition in a single chamber process has been done. During the deposition of the intrinsic layer, for a p-i-n cell, i-layer is contaminated by the residual boron radicals present in the reactor after the deposition of the boron-doped layer. This contamination decreases cell performance. Several reactor treatments have been tested to solve this contamination problem. The effectiveness of these treatments was evaluated by secondary ion mass microscopy (SIMS) measurements. It appears that an ammonia flush or a water vapour flush of a few minutes, between the deposition of the p-layer and i-layer, reduces the boron contamination at the p-i interface. The performance of cells made with these treatments, in a single chamber process, are comparable to performance of cells done in a multi-chamber process.

Paolo BOSSHARD: *"Charge exchange spectroscopy measurements of ion temperature and impurity ion density"* EPFL PhD thesis no. 2723(03)
The ion temperature profile of the TCV plasmas have been measured for the first time using a Charge eXchange Recombination Spectroscopy (CXRS) diagnostic working with a Diagnostic Neutral Beam Injector (DNBI). The diagnostic has been optimised to obtain ion temperature measurements with relative errors lower than 15% at electron densities ranging from $1.10^{19}m^{-3}$ to $7.10^{19}m^{-3}$, implying major upgrades both of the DNBI (the injected neutral current has been increased by a factor ~2 since the original installation) and of the spectroscopic diagnostic (the transmission efficiency has been enhanced by a factor of ~20). These measurements were used to estimate the plasma ion energy fraction in ohmically (15%-40%) and ECR heated discharges (<10%) and to study the behaviour of the ion energy confinement time as a function of the plasma shape. A strong degradation of the confinement was observed as the plasma shape triangularity increases from negative to positive values in good agreement with the previous confinement observations for the electrons. It was found that ion temperature behaviour was, in most cases, well modelled by collisional energy transfer from the hotter electrons. The CXRS measurements show that the ion temperature profiles are strongly correlated with the presence of sawteeth instabilities and the plasma current profile width.

Thierry DELACHAUX: *"Study of carbiding and nitriding plasmas in a high current arc reactor, with application to zirconium coating"* EPFL PhD thesis no. 2782(03)
The aim of this thesis was to develop and study a process which allows the chemical transformation of the surface of tetragonal zirconia (t-ZrO_2) into zirconium nitride (ZrN). The idea is to combine the optical properties of ZrN, which has a yellow-gold colour, with the mechanical properties of hardness and resistance to crack propagation of t-ZrO_2. Moreover, this kind of chemical treatment allows to eliminate usual problems related to adhesion at the deposit-substrate interface. To perform this nitriding process, that is, the substitution of oxygen by nitrogen, we have successfully used a high current arc discharge in gas mixtures of argon-hydrogen-nitrogen or argon-ammonia.
The results of the study of our non-equilibrium plasmas show that discharges in mixtures of argon-hydrogen-nitrogen and argon-ammonia are very similar from the

point of view of optical characterisation. Both are efficient sources for the production of atomic hydrogen and NH molecules which react favorably with tetragonal zirconia to facilitate nitriding. For a better understanding of the complex chemistry in the plasma phase, a preliminary numerical modelling of the discharge was started involving diffusion of a multi-species mixture and non-equilibrium chemical reactions. The results show that the density profile of the reactive species is strongly influenced by the plasma profile temperature.
Our analyses of the interaction of the plasma and of the zirconia surface have shown that the thermodynamic nitriding process is efficient for plasmas in the gas mixtures of argon-hydrogen-nitrogen or argon-ammonia when two conditions are satisfied:

- The temperature of the ceramics must be higher than about 600°C so that the surface reactions are fast enough to form a layer with a yellow-gold colour after about two hours of nitriding treatment. On the other side, the temperature has to be kept below 1000°C to avoid grain growth in the zirconia, which blisters the surface.
- A reducing atmosphere is necessary to desorb oxygen from the zirconia and to allow the incorporation of nitrogen by the redox reaction:

$$(NH)(g) + 3\ O_O^x \rightarrow (H_2O)(g) + 2\ N_O' + V_O^{\cdot\cdot}$$

The substitution of the oxygen by nitrogen is accompanied by the creation of a vacant site ($V_O^{\cdot\cdot}$). The presence of atomic hydrogen in the plasma enables this condition to be fulfilled.
Our X-ray diffraction studies of the development of the crystalline structure of the nitrided zirconia have indicated that the nitrogen incorporated in the ceramic acts as a stabiliser of the high temperature phases enabling the metastable retention of the tetragonal and cubic phases of zirconia. These studies have shown that the formation mechanism of the zirconium nitride layer occurs in successive steps as follows:

$$\text{tetragonal-}ZrO_2 \text{ -> cubic-}ZrO_2 \text{ -> } ZrN$$

When the nitrogen concentration increases in the original tetragonal zirconia, the ceramic first starts to transform into the cubic phase, then when the threshold of nitrogen solubility is reached, there is precipitation of grains of zirconium nitride (ZrN).

External Students

Walter ZAMBONI from the Departement of Electrical Engineering, Università degli Studi di Napoli "Federico II", Italy: "*Modelling of superconducting cables*"
This student visited the CRPP Superconductivity Group from September to November. His activity is cantered on the electromagnetic models (1D/3D) for superconducting cables. The 1D models are based on a Multi-conductor Transmission Line code (THEA®). The 3D models use a field approach. These two models have been used to investigate the self-field effects on the resistive transition parameters of multiplets and cables, such as the critical current and *n*-index. He has used experimental data of tests in SULTAN for developing the models. After the visit in Villigen, he kept working on these topics back in Naples.

Ph.D. Theses supervised by CRPP staff at the end of 2003

Laura ABRARDI: *"Study of density fluctuations in JET"*
The aim of this work is a better understanding of turbulent phenomena through the study of density fluctuation characteristics in fusion plasmas, particularly in the edge region during ELMs. Microwave reflectometry in particular provides access to short-scale turbulence with good temporal and spatial resolution. We started the analysis of the data provided by the two reflectometers installed on JET. The first

one is a multichannel O-mode reflectometer, working in the range 18-70GHz, whose phase measurements are used to determine the positions of the corresponding reflection layers; the second one is a correlation reflectometer, working in the range 76-106GHz, used in direct measurements of the radial correlation length of the plasma fluctuations. Future work will also include a feasibility study for fluctuation diagnostics in TCV.

Paolo ANGELINO: "*Gyrokinetic model for electron and ion dynamics in axisymmetric plasma configurations*"
EM-GLOGYSTO is a 2D global linear electromagnetic spectral code. The model includes both passing and trapped particles. Trapped particles are taken into account with the bounce averaged drift kinetic model. Recent developments in the code include the description of both passing ion and electron dynamics by the linearised electromagnetic gyrokinetic equations. Comparison with earlier results (obtained with a drift kinetic quasi-adiabatic approximation for electrons) shows the necessity of a more accurate electron dynamics description for electromagnetic modes. A more efficient parallelisation has been introduced in the code, which has lead to a reduction in the execution time by an order of magnitude and saving of memory resources. The latest development in the code is the inclusion of the ExB flow, for both circulating particles and trapped ions. The new version of the code has been benchmarked with an electrostatic code for ITG modes and it allows us to further analyse linear mechanisms for stabilisation. The radial electric field has two effects: it removes the toroidal ITG mode from its main drive region with unfavourable magnetic curvature and it tilts the eigenmode structure. Finally, for the first time, the behaviour of electromagnetic microinstabilities (Alfvénic-ITG) has been investigated in presence of an equilibrium radial electric field.

Gilles ARNOUX: *"Plasma heating at the 3rd harmonic of the electron cyclotron frequency"*
The preliminary study on the absorption properties of the 3rd harmonic electron cyclotron heating in a top-launch configuration (X3 ECH) has shown that a real time feedback control of the launcher poloidal angle is needed and that the fast electrons play a significant role in the absorption efficiency.
An analog signal processing system based on a synchronous demodulator has been implemented on TCV in order to generate an error signal. This error signal is obtained from the soft X-ray measurement that gives the dynamic response of the plasma to a small perturbation obtained by modulating the wave injection angle at a frequency around 40Hz. In preliminary experiments, it was shown that the signal can be obtained and used via a PID controller. After some fine adjustment, the control loop and its effectiveness will be tested.
The X3 top-launch system has been used as a fast electron diagnostic. Experiments have been performed by scanning the electron energy population on which the RF beam is coupled, by varying the radial position of the launching mirror. In plasmas where fast electrons are generated by CO-ECCD via the injection of X2 power, this method allows a measurement the energy distribution of the electron population (bulk and fast electrons).
The absorption measurement of the RF power is obtained by analysing the diamagnetic flux variation induced by the modulation of the injected power. In case of H-mode plasmas, the perturbation caused by the ELMs on the diamagnetic signal make this measurement unusable. A digital signal processing has been developed using system identification method in order to separate the two dynamics (ELMs and modulation) and allows to obtain the absorption measurement of X3 wave even in H-mode scenarios.

Raul BONADE: *"A Study of the constitutive behaviour and fracture behaviour of ferritic and martensitic alloys"*
The constitutive behaviour of various tempered martensitic model alloys was determined at room temperature from tensile test results. The model alloys are based on the Fe-9Cr-0.1C and Fe-12Cr-0.1C chemical composition and were heat-

treated to get various prior austenite grain sizes with different degrees of tempering. Lath martensite and sub-grain martensite were so obtained. The effect of prior austenite grain size on the yield stress and strain-hardening was investigated. It was found that the prior austenite grain size hardly affects the yield stress while the strain-hardening behaviour is insensitive to it. The post-yield behaviour was modelled in the frame of the dislocation mechanics. A strain-hardening law, based upon the basis of a net increase of the total dislocation density, was used to reconstruct the overall tensile curve. The characteristic parameters (length, dislocation density) of the strain-hardening laws were found quite consistent with the microstructures in consideration. The tensile tests were supplemented with metallographic and transmission electron microscopy observations performed before and after tensile testing. Further tensile tests at lower temperatures are in progress.
Finite element simulations of cracked and tensile notched specimens were initiated. The defined finite element models will be used to model the fracture testing to come for a variety of fracture specimens and tests, including static fracture toughness, static tests and dynamic tests on notched specimens.

Alberto BOTTINO: *"Modelling of magnetically confined plasmas"*
The global electrostatic code LORB5, developed during this thesis work, has been adapted to simulate experimental discharges of TCV. In particular, it has been used to study the linear stability of electrostatic microinstabilities in TCV electron internal transport barrier (ITB) discharges. Results show that, for the TCV tokamak, the dominant microinstability is a trapped electron mode (TEM) localised outside the barrier region. The negative magnetic shear appears to have a strong stabilising effect and plays a crucial role in the formation of electron ITBs even in the absence of a sheared radial electric field. These results have been benchmarked against the transport model GLF23, for which an interface with the TCV database has been created. The code LORB5 has also been used to simulated ion internal transport barrier plasmas in JET equilibria. The interface between JET experimental data and the code LORB5 has been provided by an adapted version of the MHD equilibrium code CHEASE. Preliminary results show that both the sheared radial electric field and the reversed magnetic shear contribute to the reduction of the transport in the region of the barrier.

Yann CAMENEN: *"Confinement studies in shaped and extremely shaped plasmas heated by electron cyclotron waves"*
During this year, we tried to get more insight in the energy confinement dependence on plasma shape in tokamak L-mode discharges. To detect a possible variation of the cross-field electron heat transport with plasma triangularity, δ, we achieved transport experiments based on temperature gradients variation at $\delta\sim0.2$ and $\delta\sim0.4$ in plasmas predominantly heated by electron cyclotron waves. These experiments were carried out in TCV in collaboration with F. Ryter from ASDEX-Upgrade. The electron temperature gradient ∇T_e and the normalised electron temperature gradient $R\nabla T_e/T_e$ were varied at constant edge heat flux by changing the radial distribution of the EC power deposition at constant total EC power. The high EC power density available in TCV has allowed us to extend the range of $R\nabla T_e/T_e$ obtained in other tokamaks by a factor 4, showing that the electron thermal diffusivity χ_e exhibits a threshold behaviour at low gradients and increases with $R\nabla T_e/T_e$ for $R\nabla T_e/T_e<15$ as in other tokamaks, but was found to stop increasing at the highest temperature gradients ($15<R\nabla T_e/T_e<25$). The reduction of transport at high $R\nabla T_e/T_e$ values is more pronounced at $\delta\sim0.2$ than $\delta\sim0.4$, but it is not clear at present whether the difference observed at the two triangularities is intrinsic to the plasma shape or depends on another plasma parameter, like the ion temperature for instance. These transport experiments also enlighten last year experiments on current profile tailoring where the current profile was broadened acting on the temperature profile by radially localised far off-axis EC power deposition to stabilise high elongation plasmas at low current. Moreover, the new soft X-ray detector

which consists of two superposed wire chambers, each one similar to the first detector prototype (MPX) is to be installed and will allow us retrieving fast temperature profiles by the absorber method, with both high spatial and temporal resolution, opening the door to heat pulse transport studies, even in overdense situations, by modulated EC power deposition.

Emiliano CAMPITELLI: *"Study of the relation between irradiation-induced microstructure and mechanical properties in Zr alloys"*
The evolution of the tensile properties after neutron irradiation of Zircaloy cladding tubes have to be assessed from non-conventional tests, like small ball punch tests that consists of deforming a 3 mm diameter disk clamped between two dies with a 1 mm diameter steel ball. In order to extract the usual tensile properties (yield stress and work-hardening coefficient) from such tests, finite element simulations with ABAQUS have been undertaken, as well as punch and tensile tests, on a variety of materials, including tempered martensitic steels, austenitic steels and aluminium alloys, to model the experimental load deflection curves obtained from the punch tests. A finite element model has been defined and tested with these materials. It was possible to reconstruct the load-deflection curves by using the constitutive behaviour obtained from standard tensile tests. A parametric study is in progress to evaluate the influence of the constitutive behaviour parameters on the shape of the load-deflection curve with the ultimate goal to extract those parameters from the punch test curves only for the Zircaloy material, from which no standard tensile tests can be carried out.

Antoine DESCOEUDRES: *"Application of plasma emission spectroscopy to the electrical discharge during EDM"* (Top Nano 21 project n° 5768.2)
Electrical Discharge Machining (EDM) has been a well known machining technique for more than fifty years. Nowadays it is widely used in a large number of industrial areas, mainly to produce moulds, dies and finished parts with complex shapes. This technology allows the production of mirror surface finishing with nanometre roughness and high machining accuracy. However, to improve on the performance of EDM, it is necessary to understand the electrical discharge in detail. The plasma created during the machining process is systematically investigated with optical emission spectroscopy. Typical spectra show strong H_a and continuum radiation, with many lines emitted by impurities coming from electrode and workpiece materials. The molecules of the dielectric (water or oil) are cracked by the discharge. Atomic hydrogen resulting from this cracking is the source of the H_a emission. Changing electrode polarity affects the electrode wear and workpiece erosion rates, which can be qualitatively seen on spectra. Time-resolved spectroscopy has been used to measure the electron density evolution from Stark broadening of the H_a line. The electron density reaches $2 \cdot 10^{18} cm^{-3}$ at the beginning of the discharge. This extreme density causes merging of atomic lines, strong Stark broadening and shift of the H_a line. The density decreases afterwards rapidly with time. The electron temperature remains roughly constant around 0.7eV. The low temperature and the high density measured prove that the EDM plasma is weakly non-ideal (plasma coupling parameter $\Gamma \cong 0.45$). Absence of the H_b line, asymmetric shape of the H_a line and complex structures around H_a are other spectroscopic evidences of the plasma non-ideality.

Jean-Yves FAVEZ: *"Application of modern control methods to a tokamak plasma"*
All present-day tokamaks routinely use PID controllers, designed on simple assumptions and tuned by experience. Thus, as a result, the control performance can be rather limited. Recently, considerable attention has focused on optimal controllers with enhanced robustness like LQG and H_∞. Although these linear controllers have shown valid results, they usually fail to maintain control in the presence of large disturbances (ELMs). This weakness is due to the saturation of the actuators and can cause considerable damages to the plant. The future work aims at the investigation of non-linear methods, which could avoid this problem by

maintaining the tokamak into a stable and save operational domain even if large disturbances occur. A further goal in tokamak control research is to find a way to reduce the power consumption and the ac-losses while maintaining a fast response time. This work is targeted at the TCV, JET and ITER tokamaks.
The first part of the work has concentrated on understanding the modelling of the tokamak and on studying the controllability regions of linear systems with only one saturated input. We have considered planar systems with one stable and one unstable pole under saturated linear state feedback and analysed its region of attraction. We have shown that there is a topological bifurcation in the region of attraction, i.e. the region of attraction changes between being an unbounded hyperbolic type region and a region bounded by a limit cycle. The main contribution of our work is to provide an analytical condition under which bifurcation occurs. This condition is based on the characteristics and position of the stable and unstable manifolds. Furthermore, the exact shape of the region of attraction has been provided.
The second part of the work has focused on the enhancement of the tokamak control in the presence of power supply voltage saturation. The aim was to improve the existing controller in the sense of increasing the region of attraction while retaining the local performance and avoid chattering in the control signal. For second order systems with one unstable and one stable pole under saturated input, it has been demonstrated formally that these requirements can be achieved using an additional nonlinear term in the existing linear control law. The extension to this nonlinear control law for higher order systems, like the tokamak, has been applied by analogy and with conviction. The validation of this new controller has been done via simulations. Work has been carried out on a separate issue, namely the simulation of the full feedback control on TCV in the presence of ECH, using the DINA free boundary simulation code, developed in collaboration with the Kurchatov and TRINITI institutes.
This project is carried out in collaboration with the Laboratoire d'Automatique (LA) at the EPFL.

Sergi FERRANDO: *"Bootstrap Current and Stability in the Asymptotic Regime in Quasi-Symmetric Configurations"*
Bootstrap Current (BC) is calculated in the collision-less regime for two reactor-size quasi-symmetric configurations: a 3-period Quasi-Axisymmetric (QAS) and a 4-period Quasi Helically Symmetric (QHS) device. The research is focused in assessing the effect of the BC on the rotational transform and on stability when beta is increased and determine the relevance of the non-symmetric modes on the BC. It has been seen that for QAS configurations the BC enhances the rotational transform. Converged BC-consistent equilibria have been obtained up to beta=6.1%. When increasing beta the BC is also increased, enhancing the rotational transform. For beta around 6% the rotational transform crosses the n/m=2/3 rational surface, destabilising the configuration. The non-symmetric modes have proved to be relevant. When non-symmetric modes are neglected the system is unstable for beta=5.3%, but when 25% or more of each non-symmetric mode is considered, the BC decreases enough to put the rotational transform below the n/m=2/3 rational surface, stabilising the configuration. For the QHS case the BC goes in the direction which decreases the rotational transform. Convergence has been achieved up to beta=3%, and it has been shown that the BC is strongly sensitive to the increase of beta. The non-helically symmetric modes, however, have shown little impact on the BC and the rotational transform for the cases studied. The study of the stability of the QHS configuration is in process.

Malko GINDRAT: *"Experimental study of the behaviour of a DC plasma spraying torch operated at low pressure"*
Low Pressure Plasma Spraying (LPPS) processes, which use DC plasma jets expanding at low pressure, are used for fast deposition of thin, thermally sprayed coatings on large surfaces. During the third year of this thesis the aim was to improve and complete the measurements using electrostatic probes. Measurement

of key plasma jet properties, such as the Mach number, electron density and temperature were performed using double electrostatic probes and Mach probes. In particular, under-expanded jets were studied more into details by performing complete mappings of the Mach number, electron density and temperature at 10 and 2mbar. These results show that the measured physical properties are consistent with the jet phenomenology like the presence of expansion and compression zones, the effect of the pressure and the location of the shocks. These results contribute to improve the understanding of the supersonic plasma jet behaviour at low pressure and can allow quantifying the deviation from the LTE. The extensive mapping of the measured physical properties of the jet will also serve as input for modelling.

Jan HORACEK: *"Measurement of edge electron temperature and turbulence in the tokamak plasma boundary"*
A significant quantity of new edge turbulence measurements in TCV were made this year using the modified fast reciprocating probe head installed in late 2002. Experiments in Spring provided the first, high quality data for fluctuations in poloidal electric field and particle flux in matched forward and reversed toroidal magnetic field discharges, as a function of plasma density and during ELMing H-mode. This new data has confirmed the "bursty" nature of edge transport and a great deal of detailed statistical analysis has been performed demonstrating the "skewed", non-Gaussian nature of the probability distribution functions (PDF) describing the turbulent ion flux. This asymmetry in favour of positive (ie outgoing) transport events at large amplitude increases with increasing distance from the separatrix, confirming the "long range" nature of non-diffusive edge transport and its potential importance in determining plasma-wall interactions in the main chamber.
Unfortunately, the available electronics support has not been sufficient to provide for hardware necessary to execute the planned electron temperature fluctuation measurements (though this should become possible in 2004). Efforts to use a DSP based approach were abandoned after initial attempts, largely through lack of the required expertise and concerns for the timescales involved in providing a working system. Instead, efforts have concentrated on the development of a new probe head, designed specifically to measure parallel flow, turbulence in this flow and the fluctuations in radial gradients of poloidal electric field and ion flux. At the time of writing the first ever measurements of parallel flow Mach Number in the TCV scrape-off layer have been obtained, in addition to a wealth of new fluctuation data including measurements in close proximity to the ohmic density limit. Further H-mode data and measurements in helium plasmas are planned before the end of the current experimental campaign.
Unconnected to the turbulence work, some effort has also been devoted to the processing of data from the two new TCV infra-red thermography systems. This has included the development of a software suite for the production of appropriate calibration matrices and the easy visualisation of video images of surface temperature evolution.

Igor KLIMANOV: *"Study of the electron distribution function during Electron Cyclotron Current Drive (ECCD)"*
The study requires the development of new diagnostic and analysis tools. A new 24-channel Low Field Side (LFS) radiometer has been built. The second antenna at Z=21cm will be installed during the opening at the end of the 2003. ECE LFS measurements of electron temperature using Z=0 optical line are available since April 2003. It allows LFS and High Field Side (HFS) measurements simultaneously. A numerical module to simulate the ECE emission spectra for any distribution function has been developed. The code is combined with the best available plasma ray-tracing code TORAY-GA. The code was also used as ECE module for Fokker-Plank code CQL3D. The code was applied to X3 (3rd electron cyclotron harmonic, X-mode) heating regime of low density X2 preheated plasma (ECCD) when X3 power was launched laterally from the LFS. The reconstruction of the electron distribution

function that can explain 100% absorption (measured by DML) of the X3 gyrotron power has been proposed. Surprisingly good agreement between all available diagnostics (Thomson scattering, ECE HFS, HXR camera) is found.

Andrei MARTYNOV: *"MHD activity of tokamak plasmas"*
The analysis of ideal stability of TCV shots with eITBs was performed using the numerical code KINX. The influence of pressure profile peaking, of the shape of reversed shear current profile and of the value of q_{min} was investigated.
It was shown that:

- The reversed shear configurations with eITB can be ideally unstable at low normalised beta because of high localised pressure gradient.
- The profiles are unstable at lower pressure gradient when q_{min} is close to rational surfaces, (1.5, 2, 2.5, 3,...)
- Avoidance of disruptions triggered by ideal modes might be possible by changing the q_{min} values to the stability windows between rational surfaces by fine tuning the EC heating and current drive configuration.

Based on previously obtained results on the influence of plasma triangularity on the ideal internal kink mode stability, the experimental study of dependence of the sawtooth oscillations on plasma triangularity was carried out on TCV tokamak. It was shown that in ohmic conditions the dependence of the sawtooth period on plasma triangularity has minimum close to zero triangularity and the sawtooth period increases with both positive and negative triangularity. This corresponds to the numerically predicted effect of stabilisation of ideal internal kink mode by positive and negative triangularity.

Stefan MUELLER: *"Basic investigation of turbulence and transport in toroidal plasmas"*
Before the beginning of operation of TORPEX in March 2003, the focus of this work was on contributing to the design and construction of the device (electromagnetic fields; computer system, data-acquisition and control system).
After the beginning of operation, work concentrated on the optimisation of the discharge parameters, especially the optimisation of the confinement scheme using vertical magnetic fields. A model for the particle confinement time, based on particle drift motion and comparison of different loss channels, was developed and experimentally verified.
Using the dispersion relation solver developed in 2002 the measured fluctuation spectra were compared with a drift-wave model.
Another element of this work is to contribute to the diagnostic development in TORPEX, including a large Langmuir probe array for measuring the propagation of turbulent structures as well as optical diagnostics, like spectroscopy, rapid plasma imaging and laser induced fluorescence.

Petri NIKKOLA: *"Simulations of electron cyclotron wave propagation in TCV"*
The Fokker-Planck modelling with radial particle transport of TCV ECCD/ECRH plasmas has continued. The code has been applied to plasmas with varying confinement properties, i.e., for conventional plasmas and in discharges with an increasing electron internal transport barrier. The transport model of the code can distinguish between these different plasmas both qualitatively and quantitatively. Simulations with varying launching geometries are being carried out for X3 waves. The code agrees well with TORAY-GA and experiments in the X3 absorption calculation. However, the observed 100% absorption of X3 waves in the presence of X2 waves, the X2-X3 synergy, has proven to be difficult to model even though some increase in X3 absorption due to X2 waves has been obtained. In these calculations a large numerical mesh is needed.

Mario PODESTA: *"Experimental studies of transport properties in toroidal plasmas"*
The new toroidal device TORPEX is now operating, and plasmas in noble gases (Argon, Hydrogen) are routinely obtained by injecting microwaves in the electron cyclotron (EC) range of frequencies.

The first experimental campaign focused on the characterisation of plasmas obtained in TORPEX. First, the ECRH system (including the microwave generator and the transmission line) has been integrated with the other systems required to operate the machine (timing unit, acquisition system). The identification of the working regimes has then required the optimisation of parameters like gas pressure, injected power, position of the EC resonance inside the vacuum chamber. Electrostatic probes (different arrays of Langmuir probes and a Retarding Field Analyser) have been installed for the measurement of plasma parameters across the poloidal section.

Francesca Maria POLI: *"Study of fluctuations and turbulence in toroidal plasma"*
A multi-tip Langmuir probes array was installed last February on TORPEX and is now fully operational. The diagnostic allows the measurement of fluctuations with frequency up to 125kHz and the resolution of wavelengths as small as 0.065mm. A new electronic module for the measurements of fluctuations with a frequency resolution of 10MHz is under study and will be built within the next few months. Mathematical techniques have been explored that can be applied in the study of fluctuations, including methods of spectral analysis to study the linear and nonlinear interaction of fluctuations, and statistical methods to infer an estimate of the broadening of turbulence spectrum from local measurements. Novel methods suitable for a representation of the dynamics of plasma turbulence, such as wavelet analysis, are under study.
The multi-tip array, which provides the measure of fluctuations at a fixed radial position (*i.e.* 4cm from the edge), has been tested for the design of a new generation multi-tip array that will provide a complete poloidal mapping of the turbulent structures, including their size and dynamics.

Pavel POPOVITCH: *"Electromagnetic wave propagation in 3D plasma configurations"*
The code LEMan has been developed to investigate global wave propagation and absorption properties in 3D plasma confinement configurations. It solves the Maxwell equations using the full cold plasma model. Special care is taken at the magnetic axis to ensure the unicity of the solution and to minimise an unphysical energy sink on the axis. Cubic finite elements for the radial discretisation have been implemented which improves the convergence. The energy balance is used for the self-consistence and convergence check of the solution. The studies in 2D geometry show very good convergence with the radial grid size and harmonic number, especially for the global energy conservation. The algorithm for the main equation matrix construction has been improved, largely reducing the number of calculations. Several simplified geometries with selected symmetries (toroidal, mirror, elliptical, helical) have been analysed, all showing the expected behaviour of the modes and gap structures. Two fully 3D geometries have been studied, the CHS and LHD stellarators. In both cases, the spectrum is very complex because of both poloidal and toroidal mode coupling. Still, a comparison with the corresponding cylindrical branches helps to distinguish the main modes and mode conversion surfaces.

Andrea SCARABOSIO: *"Studies on MHD activity as a function of plasma shape in standard TCV scenarios and MHD phenomena in advanced scenarios"*
In highly elongated discharges with far off-axis heating and at high core density, sawtooth activity is replaced by a continuous rotating mode. Magnetic and soft X-ray measurements show a mode structure with several (m/n=1/1, 2/2, 3/3) modes resonant on the q=1 surface. In the presence of off-axis heating and high density, the electron temperature and consequently the current density profile strongly flatten creating a region of decreased current density and low magnetic shear around q=1. Due to this flat current profile, a magnetic island can grow and saturate with its higher harmonics. This is supported by the observation that when

central X3 power heating is added, the j_ϕ profile peaks again and the mode vanishes.
The collaboration with EFDA-JET has continued with experiments on the effects of plasma rotation on the β threshold for Neo Classical Tearing triggering, the so-called β_{onset}. Plasma rotation is expected to increase β_{onset} through the shielding of resonant magnetic surfaces and/or polarisation current effects. Analysis of the data is currently in progress.
At TCV, experiments on plasma rotation and its interaction with MHD modes have just started and will continue during the next year. Strong changes in the plasma rotation are observed with local ECH power deposition.

Christian SCHLATTER: *"Studies of the fast particle distribution in TCV and JET"*
The thesis is devoted to fast particles. Experimental data from the Neutral Particle Analysers (NPA) of TCV and JET will be used to estimate the fast ion distribution function for regimes involving both fast ions and electrons. With the arrival of the new compact NPA on TCV, the study of highly energetic neutrals will be possible for the first time. The following topics should constitute the thesis:

- Simulation of the ion neutralisation probability with the aim of modelling the ion distribution function on TCV;
- Characterisation of the slowing down of the fast ions by injection of neutrals using the Diagnostic Neutral Beam Injector (DNBI);
- Study of the link between the fast ion tail of the ion distribution function and ECCD efficiency (TCV) or plasma rotation (JET) in discharges with ECH (TCV) or ICRH (JET);
- Study of the radial transport of fast ions on both tokamaks and their relation to instability control.

Hannes SCHMIDT: *"Characterisation of a high density, large-area VHF Plasma Source"*
The objective of this project is a feasibility study of a novel, large-area plasma-based thin film production technique. In a first phase a cylindrical reactor has been designed and constructed to show the "proof of principle" of a novel electrode design. The reactor parameters are 100cm electrode diameter at an excitation frequency of 67.8MHz. It has been shown that uniform electric fields can be obtained (a necessary condition for plasma homogeneity) and it was proved that the special electrode design can compensate the standing wave effect at VHF.
In a second phase, the development of a high density rectangular industrial plasma reactor for PECVD application has been started. The fabrication of a rectangular-shaped electrode and the development of process compatible in-situ optical uniformity measurement system should be finished by the end of 2003. This project is carried out in collaboration with UNAXIS Displays.

Lukas STINGELIN: *"Beam Cavity Interactions in High Power Cyclotrons"*
(This work is performed at the Paul-Scherrer-Institute in Villigen)
Excitation of the 10th beam harmonic mode is observed in the main cavities during normal operation of the PSI 590MeV ring cyclotron. Refined measurements of this Higher Order Mode (HOM) signal showed a linear dependence as a function of the proton beam current as predicted by the Eigenmode expansion method. One of these cavities was removed from the cyclotron for a precise measurement of the HOMs in the corresponding frequency range of 553 to 562MHz. It showed strong mode coupling to the beam-slot, the vacuum pump port and the coaxial input line increasing the losses and bandwidths and modifying the resonance frequency.
A simplified cyclotron model was developed to simulate the beam deformation due to the excitation of HOMs. It assumes that particle oscillations can be decoupled into movements in vertical and horizontal direction. The space charge effects on vertical movements can be calculated analytically and the horizontal movements are simulated by a 2D Particle In Cell Needle (PICN) model.

Raluca STOENESCU: *"Irradiation effects on the microstructure, mechanical properties and residual stresses in the heat affected zone (HAZ) of stainless steel welds"*
The objective of the study is to correlate the residual stress state induced by welding in the HAZ with the microstructure and the mechanical properties following neutron irradiation in an experimental fission reactor, and to compare these results with those obtained for a similar material irradiated in a real fission reactor. During the last year, the materials irradiated at low doses (10^{-4}–10^{-5}dpa) in a real fission reactor were investigated by the way of small specimen technology tensile testing and transmission electron microscopy. A strong increase in the yield strength of the irradiated material was evidenced, although, due to the low doses investigated, no irradiation-induced defects were detected in transmission electron microscopy. Investigation of the materials irradiated in the experimental reactor will be performed next year.

Alban SUBLET: *"Study of RF atmospheric and near atmospheric pressure glow discharges"*
Atmospheric Pressure Glow Discharges have many applications as an alternative to classical PECVD. Our study concerns silicon dioxide film deposition, in a capacitive discharge, using organo-silicon compounds. A new vacuum reactor has been built to work in a controlled atmosphere. Special electrodes were designed using the techniques of screen-printing on alumina substrates. The electrical source has been optimised by the adjunction of an adjustable resonant circuit, high voltage feedthrough and Teflon sleeving to avoid arc transitions inside the reactor. Specific diagnostics (current shunt, test capacitor and electrical probes) have been used to measure the electrical characteristics of the plasma. These measurements were completed by photocurrent measurement. Plasmas in Helium and Nitrogen have been studied in the range of 10-1000mBar Pascal and for different excitation frequencies. Particular discharge modes have been highlighted such as filamentary, multi-peak, glow, and transition regimes. To better explain these different regimes optical spectroscopy will complete the electrical diagnostics. This will also permit a vertical spectral resolution of the discharge. A second reactor has been designed for future dirty process with organo-silicon compounds like HMDSO.

Marco WISCHMEIER: *"Divertor detachment in the TCV and JET tokamaks"*
Further refinement of the SOLPS5.0 code package simulations of detachment in JET pure helium, L-mode plasmas has continued in 2003, extending now this earlier work to simulation of matched cases in deuterium. In helium, improvements in the quality of the match to experimental data have been obtained but have not modified the essential conclusions published at the 2002 Plasma-Surface Interactions conference: divertor detachment is driven by enhanced loss (due to the long mean-free paths) of He neutrals to the X-point region where He neutrals and He^+ ions radiate strongly, starving the divertor plasma of the energy required for re-ionisation of recycled fuel. In deuterium, using a large fluid/Monte-Carlo package to simulate detachment represents a major challenge due to the increased complexity of the phenomena at work during the detachment process. A further two JET visits this year (two weeks each) under secondment have helped in solving some of the many problems encountered with these D cases – simulation of D detachment on JET has not previously been attempted using SOLPS5.0. A long research article documenting the principal results of the comparison between D and He from the modelling point of view is in preparation at the time of writing and will represent closure of these thesis activities at JET.
With regard simulations of deuterium detachment on TCV, progress has been made in eliminating further candidate processes as explanations for the anomalous detachment seen at the outer target in standard SNL diverted discharges. In particular, more refined treatments of the D_2 molecules, long suspected (via molecular assisted recombination (MAR) processes) as being the most likely candidate, have now been ruled out. Similarly, a more realistic treatment in the Eirene neutrals code of the full three dimensional geometry of the TCV vacuum

vessel has not significantly improved agreement with experiment. A detailed summary of these results was presented in September 2003 at the 9th Plasma Edge Theory (PET) Workshop in San Diego, CA, USA. Efforts through the remainder of this thesis will now concentrate on the inclusion of hydrocarbon species in the simulations in an attempt to demonstrate if one of the few remaining candidate processes – hydrocarbon driven MAR – can account for the experimental observations.

Zhongwen YAO: *"Mechanical properties and microstructure of irradiated metals"*
For future investigation of the damage microstructure resulting from high dose irradiation, specimens of pure Ni single crystal were irradiated to 1dpa at room temperature (RT). The damage microstructures of specimens previously irradiated to 0.001, 0.01 and 0.1dpa at 523K, to 0.1dpa at 623K and to 0.3dpa at RT, were observed by using the weak beam technique in transmission electron microscopy. The results showed that: (a) For a given dose, the defect density decreases with increasing temperature; (b) The irradiation-induced defects (stacking fault tetrahedra, SFTs, and dislocation loops) grow with increasing temperature; (c) Very small voids can be seen in the specimens irradiated at 523K, but with a low density. At 623K, density of the voids is higher and they exhibit larger sizes, of about 10nm for some of them; (d) The SFTs are present even at 623K (0.36Tm) and their size increases from 1.5nm at RT to ~6nm at 623K; (e) The defect density already saturates at about 0.1dpa.

Gang YU: *"Small angle neutron scattering investigation of radiation damage in metals and alloys"*
A number of defects produced by high energy proton- or neutron-irradiation in metallic materials are too small to be resolved using transmission electron microscopy (TEM), i.e. they have a size below 1 nm in diameter. However, it is thought that these small defects actually contribute to radiation hardening and embrittlement of metallic materials. It is then proposed to investigate these small irradiation-induced defects by using the Small Angle Neutron Scattering (SANS) and Small Angle X-ray Scattering (SAXS) techniques. Final characterisation of the defects (type, size and density; evolution with accumulated dose and irradiation temperature) will be made by combining results of SANS and SAXS measurements with TEM observations and molecular dynamics simulations. The impact of the characterised irradiation-induced defects on the hardening and fracture behaviour of investigated materials will be assessed.

Alexei ZABOLOTSKY: *"Particle transport in TCV"*
Study of electron density peaking on TCV performed in 2002 showed that because of the strong correlation of the electron temperature and parameter $\langle j \rangle / j_0 q_0$ ($\langle\ \rangle$ means the volume average) in TCV discharges it is very difficult to separate the influence of Turbulent Thermo-diffusion and Turbulent Equipartition on density profile peaking. Several experiments aimed to resolve this uncertainty were performed this year in collaboration with JET. Density peaking in source-free L-mode JET plasmas with LHCD and ICRH was observed, as for the TCV plasmas, to increase with increasing peaking of the current profile. For the discharges investigated the relationship was summarised as $\langle n_e \rangle / n_{e0} \sim 0.83 l_i$, where l_i is the normalised internal inductance. This observation, which was made in a series of discharges with a variety of MHD-quiescent LHCD discharges including fully current driven plasmas and no core particle source, supports theories explaining particle convection by Turbulent Equipartition.
Parallel experiments aimed at determining the steady state transport parameters of carbon using the vacuum-ultraviolet multichannel spectrometer were carry out on TCV in collaboration with IPP Prague. The extreme shaping capability of the TCV tokamak allowed us to perform changes of plasma shape to obtain a compete scan of the CVI or CV emission along the radii in a single discharge with good spatial resolution. The diffusion coefficient was determined from these profiles by means of

the STRAHL code. Such experiments give a unique opportunity to derive the transport parameters of carbon as intrinsic TCV impurity. Studies of the dependence of the carbon diffusion coefficient on plasma parameters are under way.

6 Public relations activities in 2003

6.1 *Official visits*

The General Consul of France in Geneva, François Laumonier visited in June 2003 in the company of delegates from the French Embassy, Fig. 6.1.1.

Scientific attachés from the Swiss Embassies visited in October 2003.

The CRPP also welcomed a US Science Policy Delegation.

Fig. 6.1.1 *P.J. Paris of the CRPP presenting the TCV tokamak to the French delegation led by M. le Consul Général de France in Genève, M. François Laumonier.*

6.2 *General outreach activities*

An outreach activity presenting the progress in fusion and plasma science and their related activities was set-up for different levels of education: undergraduates, high school students, elementary school students, teachers at all levels, the general public and government officials. New brochures, posters and flyers were edited on fusion and plasma physics. We have been active via public colloquia, "round tables" and talks on energy issues especially on fusion energy.

We have been maintaining contact with the medias, through press releases and interviews, as well by participating in radio and TV broadcasts, mostly as a result of the nomination of Prof. M. Q. Tran as EFDA leader.

Organised visits to the CRPP

We welcomed about 1000 visitors to the CRPP in Lausanne, mostly in groups of about 20 to 40 people. About 60 % of the visitors came from schools, high schools

or universities. Some 15 to 20 % of the total number came from abroad. Among the many visits in 2003 were:

- Students from HES - Yverdon
- Students from the HES Valais
- Equipe patronale de la Côte
- Students from TU Delft
- Students from the Czech Technical University in Prague
- Staff from Bobst SA Technical R&D division
- Members of the Atout (Radical & Liberal parties) Association
- ASTHEC: PhD Students from CEA Cadarache
- Ecal- Ecole Arts Graphiques de Lausanne
- Members of the Fédération Romande des Entrepreneurs
- Institut National Polytechnique de Grenoble- Congrès INPG at EPFL
- Students from the Gymnase de la Cité (Lausanne)
- High school students from the eastern part of Swizerland and from Tessin

During the summer of 2003 we welcomed the so-called "Passeports-Vacances" for 30 young people 13-15 years old who were able to visit different laboratories at the EPFL.

EPFL Open Days and meetings

Around 2500 people visited the CRPP installations during three Open Days in May 2003.

In 2003, a conference was organised at the EPFL entitled "Energy: a challenge for Mankind". Professor H. Bruhns, from the EU Commission presented the integrated European fusion programme.

Talks and conferences

Many staff members of the CRPP presented the research activities of the centre in Switzerland and abroad, listed in Appendix B.4.

"**CRPP Clip**"

A short 2 minute film on CRPP, requested by EFDA to present the work of the Associations at the European Expo, was produced in 2002 and delivered to EFDA in 2003. A second, longer version for open days and school visits should be finalised in 2003 - 2004.

Starmakers

"The Starmakers" movie has been translated in Korean and presented in 3D at the European Fusion Expo in Seoul. Another version in Hungarian was made for the Fusion Expo in Budapest, for the Autumn 2003. The movie is now available in English, French, German, Italian, Portuguese, Spanish, Basque, Hungarian and Korean.

Web activities on http://crppwww.epfl.ch

The main CRPP website is regularly kept up to date, including links to other sites, mainly fusion oriented The home page as well as all pages directly accessible from the home page under the heading "more about CRPP" have been converted to the new layout adopted for the whole of the EPFL. The pdf-formatted pages (CRPP in brief) providing direct information on the CRPP have been updated. The full archives of the CRPP are now available on the web site, including listings of all scientific work from 1960 to the present day. Access to almost all LRPs has been provided and the same system is also progressively being used for journal publications and conference contributions. Future plans include experimenting with and introducing multimedia features.

All web pages are now regularly backed up and a new host server has been acquired. This will bring the 5 year old system up to date and in particular it will enable authentication to access the protected area (internal web pages) for our colleagues at PSI and for all members of CRPP on mission outside the EPFL or at home.

APPENDICES

APPENDIX A Articles Published in Refereed Scientific Reviews During 2003

(see CRPP archives at http://crppwww.epfl.ch/archives)

Anghel A., *"A simple model for the prediction of quench point in cable-in-conduit conductors"*, Cryogenics 43, 223-232 (2003)

Angioni C., Goodman T.P., Henderson M.A., Sauter O., *"Effects of localised electron heating and current drive on the sawtooth period"*, Nucl. Fusion 43, 455-468 (2003)

Bruzzone P., Stepanov B., Vogel M., Gloor T., Wesche R., *"Parametric studies of subsize NbTi cable-in-conduit superconductors for ITER FEAT"*, IEEE Transactions on Applied Superconductivity 13, 1456-1459 (2003)

Bruzzone P., Wesche R., Stepanov B., *"The voltage/current characteristic (n value) of the cable-in-conduit conductors for fusion"*, IEEE transactions and applied superconductivity 13(2), 1452 (2003)

Buttery R.J., et al., Sauter O., Testa D., *"Onset of neoclassical tearing modes on JET"*, Nucl. Fusion 43, 69-83 (2003)

Campbell D.J., et al., Sauter O., *"Report on the 10th European Fusion Physics Workshop (Vaals, The Netherlands, 9-11 December 2002)"*, Plasma Phys. & Contr. Fusion 45, 1051 (2003)

Coda S., Alberti S., Blanchard P., Goodman T.P., Henderson M.A., Nikkola P., Peysson Y., Sauter O., *"Electron cyclotron current drive and suprathermal electron dynamics in the TCV tokamak"*, Nucl. Fusion 43, 1361 (2003)

Cooper W.A., Isaev M. Yu., Okamura S., Yamazaki K., *"MHD stability of 3D plasma confinement systems with finite plasma current"*, Journ. Plasma and Fusion Research SERIES, 5, 57 - 62 (2002) (ISBN4-9900586-7-4)

Cooper W.A., with International Collaboration, *"Impact of heat deposition profile on global confinement of NBI heated plasmas in the LHD"*, Nuclear Fusion 43, 749 - 755 (2003)

Crisanti F., Albanese R., Ambrosino G., et al., Lister J.B., *"Upgrade of the present JET shape and vertical stability controller"*, Fusion Eng. And Design 66-68, 803-808 (2003)

DeAlmeida P., Victoria M., *"Channeling effects in heavy-ion irradiated NiAl (100) single-crystals: a TEM assessment in cross-section geometry using weak-beam imagning"*, Sol. State Com. 125, 195-199 (2003)

Degeling A.W., Martin Y.R., Lister J.B., Villard L., Dokouka V.N., Lukash V.E., Khayrutdinov R.R., *"Magnetic triggering of ELMs in TCV"*, Plasma Phys. & Contr. Fusion 45, 1637-1655 (2003)

Delachaux T., Hollenstein Ch., Levy F., Verdon C., *"Nitriding of tetragonal zirconia in a high current dc plasma source"*, Thin Solid Films 425, 113-116 (2003)

Descoeudres A., Sansonnens L., Hollenstein Ch., *"Attachment-induced ionization instability in electronegative capacitive RF discharges"*, Plasma Sources Science and Technology 12, 152-157 (2003)

Egedal J., Fasoli A., Nazemi J., *"Dynamical plasma response during driven magnetic reconnection"*, Phys. Rev. Lett. 90, 135003 (2003)

Falchetto G.L., Vaclavik J., Villard L., *"Global-Gyrokinetic Study of Finite beta Effects on Linear Microinstabilities, "*, Phys. of Plasmas 10, 1424-1436 (2003)

Fenstermacher M.E., Erents S.K., Lawson K.D., et al., Pitts R.A., and contributors to the EFDA-JET workprogramme, *"Comparison of Carbon and main ion radiation profiels in matched Helium and Deuterium plasmas in JET"*, Journal of Nuclear Materials 313-316 (2003)

Furno I., Weisen H., and TCV Team, *"Observation of inward and outward particle convection in the core of ECH and ECCD plasmas in the TCV tokamak"*, Physics of Plasmas 10, 2422 (2003)

Garbet X., et al., Weisen H., *"Turbulent Particle transport in magnetized plasmas"*, Phys. Rev. Lett. 91, 35001 (2003)

Giunchi G., Ceresara S., Ripamonti G., et al., Wesche R., Bruzzone P., *"High performance new MgB2 superconducting hollow wires"*, Supercond. Sch. Technol. 16, 285-291 (2003)

Graves J.P., Sauter O., Gorelenkov M.N., *"The internal kink mode in an anistropic flowing plasma with application to modelling NBI sawtoothing discharges"*, Phys. of Plasmas 10, 1034-1047 (2003)

Guenter S., Gantenbein G., Gude A., et al., Sauter O., *"Neoclassical tearing modes on ASDEX Upgrade: Improved scaling laws, high confinement at high β_N and new stabilization experiments"*, Nucl. Fusion 43, 161-167 (2003)

Henderson M.A., Alberti S., Angioni C., Arnoux G., Behn R., Blanchard P., Bosshard P., Camenen Y., Coda S., Condrea I, Goodman T.P., Hofmann F., Hogge J.-Ph., Karpushov A., Manini A., Martynov An., Moret J.-M., Nikkola P.,Nelson-Melby E., Pochelon A., Porte L., Sauter O., Ahmed S.M., Andrebe Y., Appert K., Chavan R., Degeling A., Duval B.P., Etienne P., Fasel D., Fasoli A.,, Favez J.-Y., Furno I., Horacek J., Isoz P., Joye B., Klimanov I., Lavanchy P., Lister J.B., Llobet X., Magnin J.-C., Marletaz B., Marmillod P., Martin Y., Mayor J.-M., Mlynar J., Paris P.J., Perez A., Peysson Y., Pitts R.A., Raju D., Reimerdes H., Scarabosio A., Scavino E., Seo s.H., Siravo U., Sushkov A., Tonetti G., Tran M.Q., Weisen H., Wischmeier M., Zabolotsky A., Zhuang G., *"Recent results from the EC heated plasmas in the TCV"*, Phys. Plasmas 10(5), 1796-1802 (2003)

Hidalgo C., Gonalves B., Pedrosa M.A., et al., Pitts R.A., *"Experimental evidence of fluctuations and flows near marginal stability and dynamical interplay between gradients and transport in the JET plasma boundary region"*, Journal of Nuclear Materials, 313-316 (2003)

Hillis D.L., Laorer T., Bucalossi J., et al., Pitts R.A., and EFDA-JET workprogramme contributors, *"Deuterium to Helium plasma-wall change-over experiments in the JET MkII-Gas Box Divertor"*, Journal of Nuclear Materials, 313-316 (2003) (15th International conference on Plasma-Surface Interactions in Controlled Fusion Devices, 27-31 May 2002, Gifu, Japan)

Hogge J.-P., Alberti S., Porte L., Arnoux G., *"Preliminary results of top launch 3rd harmonic X-mode electron cyclotron heating in the TCV tokamak"*, Nucl. Fusion 43, 1353 (2003)

Horacek J., Pitts R.A., Stangeby P.C., Batishchev O., Loarte A., *"On the effect of parallel field temperature gradients on the overestimation of Te measured by TCV divertor target Langmuir probes"*, Journal of Nuclear Materials 313-316, 931-935 (2003)

Ilyin Yu, Nijhuis A., TenKate H.H.J., Bruzzone P., *"Self field measurements fy Hall sensors on the SeCRETS short sample CICCs subjected to cyclic load"*, IEEE Trans. Appl. Supercon. 13(2), 1752-1755 (2003)

Isaev M.Yu., Grebenshchikov S.E., Shcheptetov S.V., Nuehrenberg J., Cooper W.A., *"Compact torsatron with improved a-particle confinement"*, Plasma Physics Reports 29, 727 - 739, 2003

Isaev M.Yu, Nuehrenberg J., Mikhailov M.I., et al., Cooper W.A., *"A new class of quasi-omnigenous configurations"*, Nucl. Fusion, 43, 1066-1071 (2003)

Ivanov A.A., Abdrashitov G.F., Anikeev A.V., Bagryansky P.A., Deichuli P.P., Karpushov A.N., Korepanov S.A., Lizunov A.A., Maximov V.V., Murakhtin S.V., Smirnov A. Yu., Zouev A.A., Noack K., Otto G., *"GTD device - recent recults and future plans for GDT upgrade"*, Transactions of Fusion Science and Technology 43, No 1T, Fuste8, 51 - 57 (2003) ISSN: 0748-1896

Kuntze M. et al. (FZK), Alberti S., Tran M.Q. (CRPP), Giguet E. et al. (Thales Electron Devices), *"Advanced high-power gyrotrons"*, Special Issue on Plenary and Invited Papers from ICOPS 2002, IEEE Trans. Plasma Science, 31(1), 25 - 31 (2003), (ISSN 0093-3813)

Lukash V.E., Raju D., Dokouka, Favez J.-Y., Khayrutdinov R.R., Lister J.B., *"DINA simulations of TCV electron cyclotron heating discharges"*, Fusion Engineering and Design 66-68, 767-770 (2003)

Manini A., Moret J.-M., Ryter F., & ASDEX-Upgrade Team, *"Signal processing techniques based on singular value"*, Nucl. Fusion 43, 490-511 (2003)

Mao S., Luongo C., Marinucci C., *"Quench simulation in superconducting cables using optimzed DRP scheme"*, IEEE Trans. Appl. Supercon. 13(2), 1692-1695 (2003)

Maraschek M., Sauter O., Guenter S., Zohm H., ASDEX-Upgrade Team, *"Scaling of the marginal β_p of neoclassical tearing modes during power ramp-down experiments in ASDEX Upgrade"*, Plasma Phys. and Contr. Fusion 45, 1369-1384 (2003)

Marinucci C., Bottura L., Bruzzone P., *"Analysis of the Measurement of the Current Sharing Temperature in the ITER TF Model Coil"*, Fusion Eng. Des. 66-68, 1001-1005 (2003)

Marmy P., Luppo M., *"Effect of hydrogen on the fracture toughness of the Titanium alloys TI6AL4V and TI5AL2.5SN before and after neutron irradiation"*, Plasma Devices and Operations 11(2), 71-79 (2003)

Martin Y.R., Henderson M.A., Alberti S. and TCV Team, *"Accessibility and properties of ELMy H-mode and ITB plasmas in TCV"*, Plasma Phys. and Contr. Fusion 45, A351-A365 (2003)

Martynov A.A., Medvedev S.Yu., Villard L., *"Tokamak equilibria with negative core current density"*, Physical Review Letters 91(8), Article 085004 (2003)

Mlynar J., Coda S., Degeling A., Duval B.P., Hofmann F., Goodman T., Lister J.B., Llobet X., Weisen H., *"Investigation of the consistency of magnetic and soft X-ray plasma position measurements on TCV by means of a rapid tomographic inversion algorithm"*, Plasma Phys. & Contr. Fusion 45, 169 - 180 (2003)

Moret J.-M., Buehlmann F., Tonetti G., *"Fast single loop diamagnetic measurements on the TCV tokamak",* Rev. Sci. Instrum. 74(11), 4634 (2003)

Narushima Y., Sakakibara S., Watanabe K., Nishimura K., Yamada H., Nakajima N., Yamazaki K., Cooper W.A., and LHD Exp. Group, *"Low-n ideal MHD analysis in limiter plasma on LHD",* Journ. Plasma and Fusion Research SERIES, 5, 514 - 518 (2002) (ISBN4-9900586-7-4)

Nelson-Melby E., Porkolab M., Bonoli P.T., et al., *"Experimental observations of mode-converted ion cyclotron waves in a tokamak plasma by phase contrast imaging"*, Phys. Rev. Lett. 90(15) (2003)

Nikkola P., Sauter O., Behn R., Coda S., Condrea I., Goodman T.P., Henderson M.A., Harvew R.W., and TCV Team, *"Modeling of the electron cyclotron current drive experiments in the TCV tokamak",* Nucl. Fusion 43, 1343 (2003)

Noterdaeme J.-M., et al., Sauter O., *"Heating, current drive and energetic particles studies on Jet in preparation of ITER operation",* Nucl. Fusion 43, 202-209 (2003)

Pitts R.A., Alberti S., Blanchard P., Horacek J., Reimerdes H., Stangeby P.C., *"ELM driven divertor target currents on TCV",* Nucl. Fusion 43, 1145 (2003)

Pitts R.A., Andrew P., Coad P. et al., Wischmeier M., and contributors to the EFDA-JET work programme, *"Comparing scrape-off layer and divertor physics in JET pure He and D discharges",* Journal of Nuclear Materials 313-316, 777-786 (2003)

Pitts R.A., Chavan R., Davies S.J., Erents S.K., Kaveney G., Matthews G.F., Neill G., Vince J.E., Duran I., and JET-EFDA workprogram contributors, *"A retarding field energy analyser for the JET plasma boundary",* Rev. Sci. Instrum. 74, 4644 (2003)

Raju D., Sauter O., Lister J.B., *"Study of nonlinear mode coupling during neoclassical tearing modes using bispectrum analysis",* Plasma Phys. Control Fusion 45, 369-378 (2003)

Sansonnens L., Bondkowski J., Mousel S., Schmitt J.P.M., Casagne V., *"Development of a numerical simulation tool to study uniformity of large area PECVD film processing",* Thin Solid Films 427 (2003) 21-26

Sansonnens L., Schmitt J., *"Shaped electrode and lens for a uniform radio-frequency capacitive plasma",* Appl. Phys. Lett. 82(2), 182 - 184 (2003)

Scavino E., Bakos J.S., Dux R., Weisen H., and TCV Team, *"Effects of plasma shape on laser blow-off injected impurity transport in TCV",* Plasma Phys. & Contr. Fusion 45, 1961 (2003)

Testa D., Fasoli A., Solano E. and JET-EFDA contributors *"Diagnosis and study of Alfvén eigenmodes stability in JET",* Rev. Sci. Instrum. 74, 1694-1700 (2003)

Testa D., Fu G.Y., Jaun A., Fasoli A., Sauter O., *"Experimental test of damping models for n=1 Toroidal Alfvén Eigenmodes in JET",* Nucl. Fusion 43, 479-482 (2003)

Testa D., Fasoli A., Jaun A. and JET-EFDA contributors, *"Measurement of the damping rate of n=1 toroidal Alfvén eigenmodes as a function of the neutral beam heating power and plasma beta on JET"*, Nucl. Fusion 43(2003), 724-728

Texier M., Bonneville J., Proult A., Rabier J., Baluc N., Guyot P., *"On the yield point of AlCuFe quasicrystals",* Scripta Materiala, 49, 41 (2003)

Turnbull A.D., Lao L.L., Osborne T.H., Sauter O., et al., *"Edge localized modes in DIIII-D high performance discharges"*, Plasma Phys. & Contr. Fusion. 45, 1845-1872 (2003)

Verhoeven A.G.A., Bongers W.A., Elzendoorn B.S.Q., et al., Alberti S., Goodman T., Henderson M., *"The design of an ECRH system for JET-EP"*, Nucl. Fusion 43, 1477-1486 (2003)

Weng P.D., Bruzzone P., Chen Z.M., Stepanov B., et al., *"Test results and preliminary analysis of HT-7U short samples"*, Cryogenics 43, 165-171 (2003)

Wischmeier M., Coster D.P., Bonnin X., et al., Pitts R.A., and contributors to the EFDA-JET work programme, *"An overview of JET edge modelling activities"*, Journal of Nuclear Materials 313-316, 980-985 (2003)

Zabolotsky A., Weisen H., and TCV Team, *"Observation and empirical modelling of the anomalous particle pinch in TCV"*, Plasma Phys. & Contr. Fusion 45(5) 735-746 (2003)

APPENDIX B Conferences and Seminars

(see CRPP archives at http://crppwww.epfl.ch/archives)

B.1 Conference proceedings published in 2003

Behn R., Sauter O., Zhuang G., Camenen Y., Coda S., Condrea I., Goodman T., Henderson M., Nikkola P., Pochelon A., Scarabosio A., *"Formation of eITBs in EC-heated TCV plasmas with and without inductively driven current component"*, Proc. 30th EPS Conference on Controlled Fusion and Plasma Physics, St Petersbourg, Russia, July 2003, ECA Vol. 27A, P-3.208

Coda S., Alberti S., Blanchard P., Klimanov I., Moret J.-M., Weber P., *"Dynamical studies of suprathermal electron relaxation by modulated ECCD"*, Proc. 30th EPS Conference on Controlled Fusion and Plasma Physics, St Petersbourg, Russia, July 2003, ECA Vol. 27A, P-3.134

Degeling A.W., Martin Y.R., Lister J.B., Villard L., Dokouka V.N., Khayrutdinov R.R., Lukash V.E., *"Magnetic triggering of ELMs in TCV"*, Proc. 30th EPS Conference on Controlled Fusion and Plasma Physics, St Petersbourg, Russia, July 2003, ECA Vol. 27A, P-3.128

Favez J.-Y., Lister J.B., Muellhaupt Ph., Srinivasan B., Villone F., *"Improving tokamak vertical position control in the presence of power supply voltage saturation"*, Proc. 30th EPS Conference on Controlled Fusion and Plasma Physics, St Petersbourg, Russia, July 2003, ECA Vol. 27A, P-3.125

Garbet X., Mantica P., Weisen H., Zabolotsky A., Garzotti L., Nordman H., Valovic M., *"Theoretical investigation of anomalous particle pinch and comparison with JET experimental results"*, Proc. 30th EPS Conference on Controlled Fusion and Plasma Physics, St Petersbourg, Russia, July 2003, ECA Vol. 27A, P-2.87

Isaev M., Cooper W.A., Watanabe K.Y., Nakajima N., *"SPBSC-terpsichore bootstrap current benchmark for the low collisionality regime"*, Proc. 30th EPS Conference on Controlled Fusion and Plasma Physics, St Petersbourg, Russia, July 2003, ECA Vol. 27A, P-4.9

Karpushov A.N., Coda S., Duval B.P., *"Observation of suprathermal ions in the TCV during ECH and ECCD"*, Proc. 30th EPS Conference on Controlled Fusion and Plasma Physics, St Petersbourg, Russia, July 2003, ECA Vol. 27A, P-3.123

Khayrutdinov R.R., Lister J.B., Dokouka V., Duval B.P., Favez J.-Y., Lukash V.E., Raju D., *"An open architecture version of the DINA 1.5 simulation code"*, Proc. 30th EPS Conference on Controlled Fusion and Plasma Physics, St Petersbourg, Russia, July 2003, ECA Vol. 27A, P-3.163

Lipschultz B., Andrew P., Coad J., et al., Pitts R.A., *"A study of JET SOL radial transport based on particle balance"*, Proc. 30th EPS Conference on Controlled Fusion and Plasma Physics, St Petersbourg, Russia, July 2003, ECA Vol. 27A, P-3.197

Lukash V.E., Lister J.B., Dokouka V., Khayrutdinov R.R., Camenen Y., Coda S., Favez J.-Y., Pochelon A., Sauter O., *"Simulation of TCV equilibrium evolution using the DINA code"*, Proc. 30th EPS Conference on Controlled Fusion and Plasma Physics, St Petersbourg, Russia, July 2003, ECA Vol. 27A, P-3.124

Mantsinen M.J., et al., Sauter O., *"Application of ICRF waves in tokamaks beyond heating"*, 30th EPS Conference on Controlled Fusion and Plasma Physics, St Petersbourg, Russia, July 2003 (invited talk)

Martynov A.A., Medvedev S.Yu., Villard L., *"Tokamak equilibria with negative core current density"*, Proc. 30th EPS Conference on Controlled Fusion and Plasma Physics, St Petersbourg, Russia, July 2003, ECA Vol. 27A, P-2.115

Medvedev S.Yu., Degeling A., Martin Y., Sauter O., Villard L., *"Edge kink/ballooning mode stability in TCV"*, Proc. 30th EPS Conference on Controlled Fusion and Plasma Physics, St Petersbourg, Russia, July 2003, ECA Vol. 27A, P-3.129

Nelson-Melby E., Alberti S., Goodman T., Henderson M., Nikkola P., *"A comparison of weakly and fully relativistic electron cyclotron wave damping in the presence of high energy electrons"*, Proc. 30th EPS Conference on Controlled Fusion and Plasma Physics, St Petersbourg, Russia, July 2003, ECA Vol. 27A, P-3.210

Nikkola P., Alberti S., Coda S., Goodman T.P., Harvey R.W., Nelson-Melby E., Sauter O., *"Fokker-Planck simulations of X3 EC wave absorption experiments in the TCV tokamak"*, Proc. 15th Topical Conference on Radio Frequency Power in Plasmas, Moran, Wyoming, USA, May 2003, AIP Conference Proceedings 687, Editor: Gary Forest, University of Wisconsin, Madison, WI, USA, AIP conference proceedings series, ISBN 0-7354-0158-6

Pitts R.A., Duran I., Erents S.K., Horacek J., Matthews G.F., and JET-EFDA Contributors, *"Retarding field analyser measurements in the JET plasma boundary"*, Proc. 30th EPS Conference on Controlled Fusion and Plasma Physics, St Petersbourg, Russia, July 2003, ECA Vol. 27A, P-2.84

Pochelon A., Aberti S., Angioni C., Arnoux G., Behn R., Blanchard P., Camenen Y., Coda S., Condrea I., Goodman T.P., Graves J., Henderson M.A., Hogge J.-P., Nelson-Melby E., Nikkola P., Porte L., Sauter O., Scarabosio A., Tran M.Q., Zhuang G., TCV Team, *"Physics Studies with ECH/ECCD in the TCV tokamak"*, Proc. 15th Topical Conference on Radio Frequency Power in Plasmas, Moran, Wyoming, USA, May 2003, AIP Conference Proceedings 687, Editor: Cary Forest, University of Wisconsin, Madison, WI, USA, AIP conference proceedings series, ISBN 0-7354-0158-6 (invited paper)

Podesta M., Fasoli A., Labit B., McGrath M., Mueller S., Poli F.M., *"First experimental results from the new toroidal device TORPEX"*, Proc. 30th EPS Conference on Controlled Fusion and Plasma Physics, St Petersbourg, Russia, July 2003, ECA Vol. 27A, P-4.16

Shafranov V.D., Cooper W.A., Isaev M.Yu., Mikhailov M.I., Nuehrenberg J., Samitov M.A., Skovoroda A.A., Subbotin A.A., Zille R., *"Optimized poloidal pseudosymmetry for toroidal systems"*, Proc. 30th EPS Conference on Controlled Fusion and Plasma Physics, St Petersbourg, Russia, July 2003, ECA Vol. 27A, P-4.17

Snipes J.A., Schmittdiel D.A., Fasoli A., Burke W., Granetz R.S., *"Initial active MHD spectroscopy results on Alcator C-Mod"*, Proc. 30th EPS Conference on Controlled Fusion and Plasma Physics, St Petersbourg, Russia, July 2003, ECA Vol. 27A, P-4.93

Subbotin A.A., Cooper W.A., Mikhailov M.I., Nuehrenberg J., Samitov M.A., Shafranov V.D., Zille R., *"Elimination of the bootstrap current factor in stellarators with poloidally closed contours of the magnetic field strength"*, Proc. 30th EPS Conference on Controlled Fusion and Plasma Physics, St Petersbourg, Russia, July 2003, ECA Vol. 27A, P-4.16

Testa D., Fasoli A., Jaun A., Mantsinen M., Beaumont P., *"Alfvén wave stability and fast ion distributions in ITER relevant scenarios"*, Proc. 30th EPS Conference on Controlled Fusion and Plasma Physics, St Petersbourg, Russia, July 2003, ECA Vol. 27A, P-3.141

Valovic M., et al., Sauter O., *"Density peaking in ELMy H-mode in JET"*, 30th EPS Conference on Controlled Fusion and Plasma Physics, St Petersbourg, Russia, July 2003, ECA Vol. 27A, P-1.105

Weisen H., Zabolotsky A., TCV Team, *"Observation and modelling of the anomalous particle pinch in TCV"*, Proc. 30th EPS Conference on Controlled Fusion and Plasma Physics, St Petersbourg, Russia, July 2003, ECA Vol. 27A, P-3.126

Zhuang G., Behn R., Sauter O., Nikkola P., *"Influence of non-Maxwellian velocity distributions during ECCD on electron temperature measurements by Thomson scattering"*, Proc. 30th EPS Conference on Controlled Fusion and Plasma Physics, St Petersbourg, Russia, July 2003, ECA Vol. 27A, P-2.59

American Physical Society (APS)

Buttery R.J., et al., Sauter O., *"Cross-machine NTM physics scalings"*, Oral presentation at the 45th APS Division of Plasma Physics Meeting 2003, Albuquerque, New Mexico, Bull. of the American Physical Society, Octobre 2003, Vol. 48(7), LO1.5

Fasoli A., Labit B., McGrath M., Mueller S., Podesta M., Poli F.M., *"The toroidal plasma experiment TORPEX for basic turbulence and transport studies"*, 45th Annual APS Division of Plasma Physics Meeting 2003, Albuquerque, New Mexico, USA, October 2003, Bull. of the American Physical Society, Octobre 2003, Vol. 48(7), FP1.124

Klimanov I., Alberti S., Blanchard P., Coda S., Fasoli A., Zhuang G., *"Reconstruction of the electron distribution function during ECCD and magnetic reconnection events"*, 45th Annual APS Division of Plasma Physics Meeting 2003, Albuquerque, New Mexico, USA, October 2003, Bull. of the American Physical Society, Octobre 2003, Vol. 48(7), BP1,16

La Haye R.J., et al., Sauter O., *"Progress on the Physics of the Neoclassical Tearing mode and its control in DIII-D"*, Oral presentation at the 45th APS Division of Plasma Physics Meeting 2003, Albuquerque, New Mexico, Bull. of the American Physical Society, Octobre 2003, Vol. 48(7), GO1.5

Mueller S., Fasoli A., Labit B., McGrath M., Podesta M., Poli F.M., *"Optimization, Modeling and Diagnostics Development in the TORPEX device"*, 45th Annual APS Division of Plasma Physics Meeting 2003, Albuquerque, New Mexico, USA, October 2003, Bull. of the American Physical Society, Octobre 2003, Vol. 48(7), FP1.126

Nave M.F.F., Coda S., Graves J., et al., Pitts R.A., Sauter O., and JET-EFDA contributors, *"Sawtooth studies in JET with reversed B"*, 45th Annual APS Division of Plasma Physics Meeting 2003, Albuquerque, New Mexico, USA, October 2003

Nave M.F.F., et al., Sauter O., *"Core and edge MHD studies in JET reversed B experiments"*, Oral presentation at the 45th APS Division of Plasma Physics Meeting 2003, Albuquerque, New Mexico, Bull. of the American Physical Society, Octobre 2003, Vol. 48(7), RP1.37

Pitts R.A., JET-EFDA contributors, *"Edge and divertor physics during reversed toroidal field operation in JET"*, 45th Annual APS Division of Plasma Physics Meeting

2003, Albuquerque, New Mexico, USA, October 2003, Bull. of the American Physical Society, Octobre 2003, Vol. 48(7), LO1.3

Poli F.M., Fasoli A., Labit B., McGrath M., Mueller S., Podesta M., *"Analysis of electrostatic fluctuations on the TORPEX plasma",* 45th Annual APS Division of Plasma Physics Meeting 2003, Albuquerque, New Mexico, USA, October 2003, Bull. of the American Physical Society, Octobre 2003, Vol. 48(7), FP1.125

Porte L., Alberti S., Arnoux G., Goodman R.P., Henderson M.A., Hogge J.P., Nelson-Melby E., Tran M.Q., *"High Power, third harmonic, top launch X-mode heating in TCV using 118GHz gyrotrons",* 45th Annual APS Division of Plasma Physics Meeting 2003, Albuquerque, New Mexico, USA, October 2003, Bull. of the American Physical Society, Octobre 2003, Vol. 48(7), RP1.62

Pinsker R.I., Luce T.C., Petty C.C., et al. Sauter O., *"DIII-D experiments on the effects of localized electron cyclotron heating and current drive on sawteeth",* Annual APS Division of Plasma Physics Meeting 2003, Albuquerque, New Mexico, USA, Octobre 2003, Bull. of the American Physical Society, Octobre 2003, Vol. 48(7), GO1.4

Turnbull A.D., Lao L.L., Cooper W.A., Garabedian P., Ku L.P., Zarnstorff M.C., *"Equilibrium and stability for compact stellarators",* Annual APS Division of Plasma Physics Meeting 2003, Albuquerque, New Mexico, USA, October 2003, Bull. of the American Physical Society, Octobre 2003, Vol. 48(7), QP1.33

Société Suisse de Physique (SSP)

Gindrat M., Dorier J.-L., Hollenstein Ch., Barbezat G., *"Characterisation of low pressure plasma jets by electrostatic probes",* Réunion Annuelle de la Société Suisse de Physique, Bâle, Suisse, Mars 2003, Bull. SPG/SSP 20, 231, 57 (2003)

Grognuz J., *"Electron Bernstein wave heating of hot plasma",* Réunion Annuelle de la Société Suisse de Physique, Bâle, Suisse, Mars 2003, Bull. SPG/SSP 20, 232, 58 (2003)

Mueller S., Fasoli A., Chavan R., Fasel D., Joye B., Labit B., Llobet X., Marmillod P., McGrath M., Perez A., Podesta M., Poli F.M., Tran M.Q., *The TORPEX toroidal plasma experiment for basic transport studies",* Réunion Annuelle de la Société Suisse de Physique, Bâle, Suisse, Mars 2003, Bull. SPG/SSP 20, 233, 59 (2003)

Popovich P., Cooper A.W., Villard L., *"Full-wave code for electromagnetic wave propagation in 3D plasmas",* Réunion Annuelle de la Société Suisse de Physique, Bâle, Suisse, Mars 2003, Bull. SPG/SSP 20, 234, 59 (2003)

B.2 Participation in other conferences in 2003

Alberti S., Arnoux G., Blanchard P., Camenen Y., Coda S., Goodman T.P., Henderson M., Hogge J.P., Moret J.-M., Nelson-Melby E., Nikkola P., Pochelon A., Porte L., Sauter O., Tran M.Q., and the TCV Team, *"ECRH and ECCD physics in the TCV tokamak",* IAEA Technical Meeting on ECRH Physics and Technology for ITER (F1-TM-26015), Kloster Seeon, Germany, July 2003

Alberti S., Fasel D., Goodman T., Henderson M., Hogge J.P., Tran M.Q., Yovchev I., Piosczyk B. et al., FZK, Arnold A.et al., Univ. Karlsruhe, Barrieu D. et al., Thalès, Dumbrajs O., TEKES, Wagner D., IPP, Garching, *"A 2 MW, CW,*

170 GHz coaxial cavity gyrotron for ITER", IAEA Technical Meeting on ECRH Physics and Technology for ITER (F1-TM-26015), Kloster Seeon, Germany, July 2003

Angelino P., Bottino A., Ganesh R., Vaclavik J., Villard L., *"E x B effects in global linear electromagnetic microinstabilities"*, 10th European Fusion Theory Conference, Helsinki, Finland, September 2003

Anghel A., Bruzzone P., *"Jordi, test facility for measurement of contact resistance in full-size conductor terminations"*, MT-18 Conference, Morioka, Japan, October 20-24, 2003

Arnoux G., Alberti S., Nelson-Melby E., Porte L., Blanchard P., Hogge J.P., and the TCV Team, *"Top-launch X3 ECH and its use as an electron energy diagnostic on the TCV Tokamak"*, IAEA Technical Meeting on ECRH Physics and Technology for ITER (F1-TM-26015), Kloster Seeon, Germany, July 2003

Ballutaud J., Hollenstein Ch., Howling A.A., Sansonnens L., Schmidt H., Schmitt J.P.M., *"Consequences of non-uniform RF plasma potential in large-area capacitive reactors"*, 16th International Symposium on Plasma Chemistry, Taormina, Italy, June 2003

Baluc N., Spaetig P., Tavassoli A-A.F., Alamo A., Bedel L., Forest L., Gentzbittel J-M., Rensman J-W., Lancha A-M., Fernandes P., Filaccioni G., Mergia K., Papastakouidis K., Diegele E., Lindau R., Schmitt T., Petersen C., Alves E., *"Materials design data for reduced activation martensitic steel type EUROFER"*, 11th Int. Conference on Fusion Reactor Materials, Kyoto, Japan, December 2003

Bonade R., Spaetig P., Victoria M., Yamamoto T., Odette G.R., *"Tensile and fracture properties of ferritic and martensitic iron-chromium-cabon model alloys"*, 11th Int. Conference on Fusion Reactor Materials, Kyoto, Japan, December 2003

Bottino A., Allfrey S., Angelino P., Sauter O., Villard L., Vaclavik J., *"Electrostatic microinstabilities in high confinement and internal transport barrier discharges"*, 2003 International Sherwood Fusion Theory Conference, Corpus Christi, Texas, USA, April2003

Bottura L., Bruzzone P., Marinucci C., *"Analysis of current redistribution in a CICC under transient heat pulses"*, Cryogenic Engineering Conference, Int. Cryogenic Materials Conference, Anchorage, Alaska, USA, September 2003

Brunetti M., Grandgirard V., Sauter O., Villard L., Vaclavik J., *"Nonlinear global simulations of electrostatic drift-kinetic ITG modes using a semi-Lagrangian code"*, 10th European Fusion Theory Conference, Helsinki, Finland, September 2003

Bruzzone P., *"The index n of the current-voltage curve, in the characterization and specificatin of technical superconductors"*, Topical ICMC '03 " The Voltage Current Relation", University of Twente, The Netherlands, May 2003

Bruzzone P., Pasztor G., *"Ic(B,T,strain) characterization of a Nb3Sn internal tin strand with enhanced specifications for use in fusion conductors"*, Cryogenic Engineering Conference, Int. Cryogenic Materials Conference, Anchorage, Alaska, USA, September 2003

Bruzzone P., Stepanov B., Wesche R., *"Coupling currents loss results from five NbTi CICC with layout variations"*, Cryogenic Engineering Conference, Int. Cryogenic Materials Conference, Anchorage, Alaska, USA, September 2003

Camenen Y., Pochelon A., Ryter F., Coda S., *"Electron heat transport studies under intense EC heating in TCV"*, IAEA Technical Meeting on ECRH Physics and Technology for ITER (F1-TM-26015), Kloster Seeon, Germany, July 2003

Campitelli E., Spaetig P., Hoffelner W., Victoria M., *"On the strength measurement of zircaloy cladding tube with non-standard tests"*, Int. Conference on the Strength of Metals and Alloys 13 (ICSMA 13), Budapast, Hungary, August 2003

Ciazynski D., Zani L., Ciotti M., et al., Huber S., Stepanov B., *"Test results of the first 50kA NbTi full size sample for ITER"*, EUCAS-2003 Conference, Sorrento, Italy, September 2003

Cooper W.A., Narushima Y., Watanabe K.Y., Yamazaki K., Suzuki C., Okamura S., *"Analysis of the MHD instability driving mechanims in 3D heliotron and quasi-axisymmetric systems"*, 13th Int. Toki Conference on Plasma Physics and Controlled NuclearFusion, Progress in Plasma Theory and Understanding of Fusion Plasmas, Toki, Japan, December 2003

Descoeudres A., Hollenstein Ch., Demellayer R., Waelder G., Beltrami I., *"Application of plasma emission spectrosocpy to the electrical discharge during EDM"*, TopNano Annual Meeting and Nano Conference, St-Gallen, Switzerland, 9-11 September 2003

Dorier J.-L., Jodoin B., Gindrat M., Blais A., Hollenstein C., Barbezat G., *"A novel approach to interpret enthalpy probe measurements in low pressure supersonic plasma jets"*, 16th International Symposium on Plasma Chemistry, Taormina, Italy, June 2003

Fasoli A., Egedal J., *"Dynamical plasma response to driven magnetic reconnection in the laboratory"*, 8th Easter Plasma Meeting on Basic and Fusion Plasma Physics, Turin, Italy, 22-25 April 2003 (Invited talk)

Fasoli A., Testa D., Way M., Walton R., Saunders S., Riccardo V., Titus P., Snipes J., Boswell C., Villard L., *"The new Alfvén wave active excitation system at JET"*, 8th IAEA Technical Meeting on Energetic Particles in Magnetic Confinement Systems, San Diego, USA, October 2003

Favez J.-Y., Lister J.B., Bonvin D., Muellhaupt Ph., Srinivasan B., *"Enhancing tokamak control given power supply voltage saturation"*, IX Int. Conference on Accelerator and Large Experimental Physics Control Systems, Gyeongju, Korea, October 2003

Ganesh R., Angelino P., Vaclavik J., Villard L., presented by Bottino A., *"A full radius gyro-kinetic stability analysis for large aspect ration high-β tokamaks: role of B//"*, 2003 International Sherwood Fusion Theory Conference, Corpus Christi, Texas, USA, April2003

Ganesh R., Angelino P., Villard L., Vaclavik J., *"A full radius gyro-kinetic stability analysis for large aspect ratio high-β tokamaks"*, 10th European Fusion Theory Conference, Helsinki, Finland, September 2003

Gislon P., Ciotti M., Spadoni M., et al., Stepanov B., *"ITER poloidal field-full size joint sample: DC tests results"*, EUCAS-2003 Conference, Sorrento, Italy, September 2003

Giunchi G., Raineri S., Wesche R., Bruzzone P., *"The voltage-current relations for MgB2 obtained by reactive liquid infiltration"*, Topical ICMC '03 " The Voltage Current Relation", University of Twente, The Netherlands, May 2003

Goodman T.P., Henderson M.A., *"Experience in multibeam alignment in TCV"*, IAEA Technical Meeting on ECRH Physics and Technology for ITER (F1-TM-26015), Kloster Seeon, Germany, July 2003

Graves J.P., *"The stabilising role of asymmetric energetic passing ion populations in negative-ion-base NBI sawtoothing discharges"*, 10th European Fusion Theory Conference, Helsinki, Finland, September 2003

Heller R., Aized D., Akhmetov A., et al., Wesche R., *"Design and fabrication of a 70kA current lead using Ag/Au stabilized Bi-2223 tapes as a demonstrator for the ITER TF-coil system"*, MT-18 Conference, Morioka, Japan, October 20-24, 2003

Henderson M.A., Behn R., Bottino A., Camenen Y., Coda S., Condrea I., Duval B.P., Goodman T.P., Karpushov A., Martin Y., Martynov An., Moret J.-M., Nikkola P., Pochelon A., Porte L., Sauter O., Scarabosio A., Weisen H., Zhuang G., and, The TCV Team, *"Creation and control of eITBs in stable plasma conditions on TCV"*, 9th IAEA Technical Meeting on H-mode Physics and Transport Barriers, San Diego, CA, USA, September 2003

Isaev M. Yu, Okamura S., Cooper W.A., *"The effect of reduced Pfirsch-Schlter current on the ideal MHD stability ans alpha particle confinement in 2-period compact configurations"*, 13th Int. Toki Conference, Japan, 2003

Labit B., Podesta M., Mller S., Fasoli A., McGrath M., Poli F.M., *"Torpex, a new toroidal plasma experiment for basic transport studies"*, 8th Easter Meeting, Turin, Italy, 23-25 April 2003

Leguey T., Baluc N., Jansen F., Victoria M., *"Characterization of hydrogen barrier coatings for titanium-base alloys"*, 10th Int. Conference on Fusion Reactor Materials, Baden-Baden, Germany, October 2001

Lister J.B., *"The evolution of feedback control in tokamaks"*, IX Int. Conference on Accelerator and Large Experimental Physics Control Systems, Gyeongju, Korea, October 2003

Lister J.B., Andreani R., Bartlett D., Bruhns H., Campbell D., Pamela J., Tran M.Q., Wagner F., Watkins M., *"Present status of European magnetic fusion research"*, Conference of the Japan Society of Plasma Science and Nuclear Fusion Research, Mito, Japan, November 2003 (invited paper)

Lister J.B., Duval B.P., Fredian T.J., Greenwald M., Llobet X., Saint-Laurent F., Spears W., Stillerman J.A., *"The ITER project and its data handling requirements"*, Invited paper at the IX Int. Conference on Accelerator and Large Experimental Physics Control Systems, Gyeongju, Korea, October 2003

Lister J.B., Favez J.Y., Bonvin D., Muellhaupt P., Srinivasan B., *"Enhancing tokamak control when power supply voltages saturate"*, Conference of the Japan Society of Plasma Science and Nuclear Fusion Research, Mito, Japan, November 2003

Marinucci C., Bottura L., Bruzzone P., Mitchell N., Stepanov B., Wesche R., *"Analysis and interpretation of Tcs tests of the ITER toroidal field conductor insert"*, MT-18 Conference, Morioka, Japan, October 20-24, 2003

Marmy P., *"In-beam mechanical testing of CuCrZr"*, 11th Int. Conference on Fusion Reactor Materials, Kyoto, Japan, December 2003

Martin Y.R., and, The TCV Team, *"Characteristics of L-mode to H-mode transitions in ohmic TCV plasmas"*, 9th IAEA Technical Meeting on H-mode Physics and Transport Barriers, San Diego, CA, USA, September 2003

Martynov An., Sauter O., *"Ideal stability of reversed shear plasmas in the TCV tokamak"*, 10th European Fusion Theory Conference, Helsinki, Finland, September 2003

McGrath M.A., Fasoli A., Labit B., Mller S., Podesta M., Poli F.M., CRPP Team, *"TORPEX - A new TORoidal Plasma EXperiment for basic plasma physics"*, 2003 Joint US-European Transport Force Meeting, Madison, Wisconsin, US, April 2003

Nita N., Baluc N., Victoria M., *"Thermal creep properties of EUROFER and ODS-EUROFER"*, 11th Int. Conference on Fusion Reactor Materials, Kyoto, Japan, December 2003

Pasztor G., Bruzzone P., *"Test results for Nb3Sn internal Sn strands for fusion conductors"*, Cryogenic Engineering Conference, Int. Cryogenic Materials Conference, Anchorage, Alaska, USA, September 2003

Pasztor G., Bruzzone P., Anghel A., Stepanov B., *"An alternative CICC design aimed at understanding critical performance issues in Nb3Sn conductors for ITER"*, MT-18 Conference, Morioka, Japan, October 20-24, 2003

Peacock A.T., Barabash V., Daenner W., Linke J., Lorenzetto P., Marmy P., Merola M., Singh B., Taehtinen S., van der Laan J., Wu C., *"Overview of recent European materials R&D for ITER"*, 11th Int. Conference on Fusion Reactor Materials, Kyoto, Japan, December 2003

Pedrozzi M., Gloor W., Anghel A., et al., *"First operational results of the 3rd harmonic superconducting cavities in SLS and ELETTRA"*, 2003 Particle Accelerator Conference, Portland, US, May 2003

Refke A., Barbezat G., Dorier J.-L., Gindrat M., Hollenstein Ch., *"Characterization of LPPS processes under various spray conditions for potential applications"*, Int. Thermal Spray Conference 2003, Orlando, USA, May 2003

Sansonnens L., Schmitt J.P.M., Howling A.A., Ballutaud J., Schmidt H., Hollenstein Ch., *"Challenges in RF plasma disposition on square-meter substrates"*, Invited paper at the 14th Int. Colloquium on "Plasma Processes", Juan-Les-Pins, Antibes, France, June/July 2003

Sauter O., *"On NTM onset and marginal β limits and consequences for ITER predictions"*, 10th European Fusion Theory Conference, Helsinki, Finland, September 2003

Schaeublin R., Baluc N., Victoria M., *"Irradiation induced behavior in ODS steels based on EUROER97"*, 11th Int. Conference on Fusion Reactor Materials, Kyoto, Japan, December 2003

Schaeublin R., Caturla M.J., Yao Z., Victoria M., *"Temperature dependence of the irradiation induced microstructure in Cu: experiments and simulations"*, 11th Int. Conference on Fusion Reactor Materials, Kyoto, Japan, December 2003

Schaeublin R., Eldrup M., Singh B., Kohlbrecher J., Spaetig P., Victoria M., *"Identification of Cavities in EUROFER97 irradiated at low dose"*, 11th Int. Conference on Fusion Reactor Materials, Kyoto, Japan, December 2003

Schaeublin R., Leguey T., Nita N., Bonade R., Baluc N., Victoria M., *"Microstructure and mechanical properties of a new ODS steel based on EUROFER97"*, 11th Int. Conference on Fusion Reactor Materials, Kyoto, Japan, December 2003

Spaetig P., Baluc N., Schaeublin R., Kohlbrecher J., Victoria M., *"SANS and TEM investigations of proton-irradiated martensitic steels",* 11th Int. Conference on Fusion Reactor Materials, Kyoto, Japan, December 2003

Spaetig P., Bonade R., Victoria M., *"Plastic flow of ferritic and martensitic model alloys",* Int. Conférence on the Strength of Metals and Alloys 13 (ICSMA 13), Budapast, Hungary, August 2003

Testa D., Fasoli A., Bigi M., Borba D., DeBenedetti M., Fu G., Jaun A., Mantsinen M., Sharapov S., Zonca F., JET-EFDA contributors, *"Alfvén modes stability and wave-particle interaction on the JET tokamak",* 8th IAEA Technical Meeting on Energetic Particles in Magnetic Confinement Systems, San Diego, USA, October 2003

Villard L., Allfrey S.J., Bottino A., Sauter O., *"An improved scheme for global nonlinear gyrokinetic simulations in curved magnetic configurations",* 10th European Fusion Theory Conference, Helsinki, Finland, September 2003

Wesche R., Anghel A., Bruzzone P., Stepanov B., *"Sudden take-off in large NbTi conductors: not a stability issue",* Cryogenic Engineering Conference, Int. Cryogenic Materials Conference, Anchorage, Alaska, USA, September 2003

Wesche R., Anghel A., Stepanov B., Bruzzone P., *"DC performance of subsize NbTi cable-in-conduct conductors",* MT-18 Conference, Morioka, Japan, october 20-24, 2003

Wesche R., Stepanov B., Anghel A., Huber S., Pastzor G., Vogel M., Bruzzone P., *"Self-field effect in NbTi Subsize cable-in-conduit conductors",* Topical ICMC '03 "The Voltage Current Relation", Enschede, The Netherlands, May 2003

Wesche R., Stepanov B., Anghel A., Huber S., Pasztor G., Vogel M., Bruzzone P., *"Self-field effects in NbTi subsize cable-in-conduit conductors",* ICMC '03 "The Voltage Current Relation", Enschede, The Netherlands, May 2003

Xin Gao, Hollenstein Ch., Schwaller M., Mathieu H.-J., *"Plasma surface modified polystyrene biochip for enhanced biological coupling",* 16th International Symposium on Plasma Chemistry, Taormina, Italy, June 2003

Yao Z., Schaeublin R., Caturla M.J., Victoria M., *"The accumulation of irradiation induced defects in pure Ni single crystal",* 11th Int. Conference on Fusion Reactor Materials, Kyoto, Japan, December 2003

Yao Z., Schaeublin R., Victoria M., *"The temperature dependence of the deformation in post irradiation Cu single crystal",* 11th Int. Conference on Fusion Reactor Materials, Kyoto, Japan, December 2003

Zanino R., Bagnasco M., Bruzzone P., Ciotti M., Gislon P., Savoldi Richard L., *"Analysis of thermal-hydraulic effects in the testing of the ITER poloidal field full size joint sample",* Cryogenic Engineering Conference, Int. Cryogenic Materials Conference, Anchorage, Alaska, USA, September 2003

B.3 Seminars presented at the CRPP in 2003

Dr. C. Angioni, IPP-Garching, Germany, *"Particle transport modelling of AUG H-mode plasmas: anomalous pinch, density peaking and collisionality"*

Dr. R. Singh, Inst. For Plasma Research, Gandhinagar, India, *"Non-linear feature of the electron temperature gradient mode and electron thermal transport"*

L. Abrardi, Politecnico di Torino, Italy, *"Transport properties in a non-equilibrium multi-temperature mixture of gases"*

M. Wisse, Laser Centre and Dept. of Physical Chemistry, Vrije Univ. Amsterdam, The Netherlands, *"Erosion and deposition in JET"*

Dr. H. Shidara, Graduate School of Energy Science, Kyoto Univ., Japan, *"70GHz electron cyclotron resonance heating system for Heliotron J"*

Prof. P. Bochsler, Physikalisches Inst., Univ. Bern, Switzerland, *"Plasma diagnostics with minor ions in the solar wind"*

J. Grognuz, CRPP-EPFL, *"Electron Bernstein wave heating of hot plasmas"*

A. Zabolotsky, CRPP-EPFL, *"Observation and empirical modelling of the anomalous particle pinch in TCV"*

Dr. P. Blanchard, CRPP-EPFL, *"High field side measurements of non-thermal electron cyclotron emission on TCV plasmas with ECH and ECCD"*

Dr. K.K. Kirov, IPP-Garching, Germany, *"ECRH power deposition studies in ASDEX Upgrade"*

B. Lüthi, Univ. Bern, Switzerland, *"Angular scattering in thin carbon foils"*

Dr. P. Bosshard, CRPP-EPFL, *"Ion confinement in the TCV tokamak measured by charge exchange recombination spectroscopy"*

Dr. H. Issler, President NAGRA (National Cooperative for the Disposal of Radioactive Waste), Switzerland, *"Challenges and problematics of radioactive waste disposal"*

T.S. Santosh Kumar, Inst. For Plasma Research, Gandhinagar, India, *"Plasma diffusion across multipole magnetic fields"*

Dr. E. Scavino, CRPP-EPFL, *"Transport of laser-ablated impurities in TCV"*

Ch. Schlatter, CRPP-EPFL, *"AXUV sur T-10"*

Prof. A. Fasoli, CRPP-EPFL, *"The new active MHD antenna system for JET enhancements"*

Dr. P.V. Savrukhin, Politecnico di Torino, Italy, *"Generation of suprathermal electrons during magnetic reconnection at the sawtooth instability and disruptions in tokamaks"*

Dr. E. Nelson-Melby, CRPP-EPFL, *"Fully relativistic electron cyclotron wave damping in the presence of high energy electrons"*

Dr. D. Testa, CRPP-EPFL, *"Alfvén eigenmodes and fast particles studies on JET"*

E. Fable, Politecnico di Torino, Italy, *"Driven magnetic reconnection in liquid metals"*

F. Bruetsch, ETH-Zürich, *"Solar thermal hydrogen production"*

Prof. A. Fasoli, CRPP-EPFL, *"Basic plasma phenomena in fusion plasmas"*

Dr. J. Marian, Graduate Aeronautical Lab., CALTECH, Pasadena, U.S.A., *"Computer modelling of deformation processes in metal at high strain rates"*

Dr. M. Samaras, Paul-Scherrer-Institute, NUM/ASQ, Villigen, Switzerland, *"Modelling radiation damage in nanocrystalline materials"*

Dr. D. Testa, CRPP-EPFL, *"Alfvén modes stability and wave-particle interaction on the JET tokamak"*

A. Mueck, IPP-Garching, Germany, *"Sawtooth tailoring and soft X-ray diagnostic on ASDEX-Upgrade"*

C. Michael, Australian National University, Canberra, Australia, *"Studies of the ion energy balance and distribution function in RF discharges in the H-1 Heliac using a coherence imaging camera"*

A. Ramar, Indian Institute of Technology Madras, Chennai India, *"Influence of grain refiner additions on the shape memory behaviour of Cu-Al-Ni alloys"*

B. McMillan, Australian National University, Canberra, Australia, *"Resistive MHD stability analysis in stellarators using the code Spector 3D"*

J.Gr. Pagonakis, National Technical University of Athens, Greece, *"ARIADNE, a 3D code for gyrotron beam tunnel simulation"*

Dr. O. Sauter, CRPP-EPFL, *"On NTM onset and marginal β limits and consequences for ITER predictions"*

Dr. G. Manfredi, Lab. de Physique des milieux Ionisés et Applications, CNRS et Univ. Henri Poincaré, Nancy, France, *"Kinetic simulations of ion temperature measurements from retarding field analyzers"*

W.-C. Mueller, IPP-Garching, Germany, *"Numerically studying the inherent properties of magnetohydrodynamic turbulence"*

Dr. Y. Sarazin, DRFC, CEA-Cadarache, France, *"Turbulent transport in the scrape-off layer: theory and numerical results"*

Dr. J.P. Graves & J.Horacek, CRPP-EPFL, *"Electrostatic turbulence in the TCV edge: Experiment and Theory"*

Dr. A. Garg, Inst. For Plasma Research, Gandhinagar, India, *"VME based real time data acquisition and control"*

Dr. J. Sanchez, CIEMAT, Madrid, Spain, *"Presentation of the TJ-II heavy ion beam probe (HIBP)"*

Dr. Y.L. Chiu, LEM/CNRS/ONERA, Chatillon, France, *"The role of the prismatic loops in microstructure evolution and twin-transformed Lattice defects"*

Dr. P. Ricci, Los Alamos Nationl Lab., Los Alamos, NM, USA, *"Kinetic simulations of collisionless magnetic reconnection"*

C. Zucca, Univ. of Genova, Italy, *"Turbulent generation of large-scale structures in non-uniform magnetized plasmas"*

B.4 Other external presentations in 2003

Alberti S., *"Fusion nucléaire une source d'nergie compatible avec un dveloppement durable",* Rotary Club St.-Sulpice, Switzerland, February 2003

Alberti S., *"Reproduire le soleil sur terre: la fusion nucléaire dans un tokamak",* Associations Astronomiques de la Cte (ASTRAC), Morges, Switzerland, May 2003

Alberti S., *"Reproduire le soleil sur terre: la fusion nucléaire dans un tokamak",* Société d'animation de la commune d'Ecublens, Ecublens, Switzerland, September 2003

Ballutaud J., A.A. Howling, Hollenstein Ch., *"Progess of the CTI project: Study of the deposition of amorphous silicon for solar cell production",* CTI Meeting held at CRPP-EPF Lausanne, Switzerland, February 2003

Ballutaud J., A.A. Howling, Hollenstein Ch., *"Progess of the CTI project: Study of the deposition of amorphous silicon for solar cell production",* CTI Meeting held at UNAXIS, Trübbach, Switzerland, July 2003

Baluc N., *"Effects of irradiation on the mechanical properties and microstructure of nanostructured materials",* Third Swiss-Japanese Joint Seminar on Advanced Microscopy for Nanotechnology, Switzerland, Arosa, 2003

Baluc N., *"De l'aéronautique à la fusion thermonucléaire",* Séminaire en l'honneur des Profs Benoit et Martin, EPFL, Lausanne, Switzerland, 2003

Baluc N., *"Resistance to radiation damage of nanostructured materials",* International Congress on Materials Science and Nanotechnolgoies, Brussels, Belgium, 2003

Baluc N., *"Les quasicristaux et leurs applications potentielles" (invited talk),* Séminaire INFOMAT: Neuchâtel, Switzerland (2003)

Bottino A., *"Stability analysis of ITB plasmas in AUG and JET (preliminary)*", seminar given at EFDA-JET Task Force T meeting, EFDA-CSU-Culham, Culham, U.K., April 2003

Bottino A., and the, CRPP Theory Group, General Atomics, San Diego, CA, University of California at Irvine, Irvine, CA, USA, May 2003

Condrea I., *"Fusion research projects on TCV",* Faculty of Physics, University of Iasi, Romania, 24 April 2003

Degeling A., *"The search for determinism in ELM dynamics on TCV and ASDEX Upgrade",* Max-Planck-Institut fuer Plasmaphysik, Garching, Germany, March 2003

Descoeudres A., Hollenstein Ch., *"Progress of the TopNano project on EDM plasma",* CTI meeting held at CRPP-EPF Lausanne, Switzerland, March 2003

Descoeudres A., Hollenstein Ch., *Annual review meeting of the TopNano EDM project: "Optical emission spectroscopy of EDM plasma",* CTI meeting held at the University of Bern, Switzerland, October 2003

Fasoli A., *"Basic Plasma Phenomena in Fusion Plasmas",* Institut de Physique de l'Energie et des Particules (IPEP), CRPP-EPFL, September 2003

Fasoli A., *"New AE antennas for JET" and "Wave-particle interaction studies for burning plasma physics on JET",* Plasma Science and Fusion Center, MIT, Boston, MA, USA, 2003

Fasoli A., *"The new MHD active antenna system",* EFDA-CSU Culham, 2003

Fasoli A., *"Tokamak operational limits and instabilities",* EU Science and Technology Advisory Committee Meeting, Brussels

Hollenstein Ch., *"Progress of the TopNano project on EDM plasma",* CTI meeting held at CRPP-EPF Lausanne, Switzerland, 29 August 2003

Labit B., *"Transport de chaleur électroniquedans les tokamaks par simulation numrique directe d'une turbulence de petite chelle"*, CEA Cadarache, France, January 2003

Lister J.B., *"The future of energy production. Could controlled fusion be a coal- and fission free option?",* CERN, Meyrin, Switzerland, April 2003

Lister J.B., *"Modelling of vertical position control in MAST",* UKAEA Fusion Association, Culham, Angleterre, May 2003

Martin Y., *"La fusion contrôlée, une énergie pour le futur",* Cycle de conférence sur l'Energie: Perspectives sur la recherche en énergie, organisé par la SVSN (Société Vaudoise des Sciences Naturelles) et l'AVCP (Association Vaudoise des Chercheurs en Physique), EPFL, Lausanne, Novembre 2003

Paris P.J., *"Consommations et ressources énergétiques ... une option: la fusion",* Congrès EUROGEM 2003, Martigny, May 2003

Paris P.J., *"Fusion energy: the appealing joker",* Korea Fusion Industry and Technology Association, Daejeon, Korea, August 2003

Paris P.J., *"Fusion energy: ITER, the way",* China Institute of Atomic energy, Beijing, PRC, August/September 2003

Paris P.J., *"Rêve énergétique: la fusion",* Club RAVEL, Lausanne, March 2003

Paris P.J., *"Energy: a challenge for the 21st century; Fusion: a joker?",* Rutherford Appleton Lab., UK, June 2003

Paris P.J., *"De l'énergie d'aujourd'hui à celle de demain: la fusion",* Club ATOUT, Lausanne, July 2003

Paris P.J., *"Le 21ème siècle sera celui de l'énergie",* Club 50, Genève, September 2003

Popovitch P., *"Full Wave Propagation Code in 3D Plasmas",* General Atomics, San Diego, USA, University of Wisconsin, Madison, Princeton Plasma Physics Laboratory, Princeton, Columbia University New York, USA, November 2003

Sauter O., *"NTM avoidance, sawtooth control and real time control,* TF S1 Meeting, JET-EFDA, April 2003

Sauter O., *"Effects of EC on sawteeth on TCV and implementation of model in transport codes",* General Atomics, San Diego, CA, USA, June 2003

Schaeublin R., *"Computational tools for the link between simulation and experiment" & "Diffraction: to the resolution limits and beyond",* Centre d'Etude de l'Energie Nucléaire, SCK-CEN, Mol, Belgium

Schaeublin R., *"TEM imaging of crystal nano defects",* ETH Hoenggerberg, Zuerich, October 2003

Schmidt H., Hollenstein Ch., Howling A.A., Sansonnens L., *"Progess of the HDS project",* CTI meeting held at CRPP-EPF Lausanne, Switzerland, April 2003

Schmidt H., Hollenstein Ch., Howling A.A., Sansonnens L., *"Progess of the HDS project",* CTI meeting held at UNAXIS Trübbach, Switzerland, September 2003

Schmidt H., Hollenstein Ch., Howling A.A., Sansonnens L., *"Progess of the HDS project",* CTI meeting held at CRPP-EPF Lausanne, Switzerland, December 2003

Tran M.Q., *"Sur la terre comme au ciel: l'exploitation de l'énergie de fusion",* Office Fédérale de l'Education et de la Science, January 2003

Tran M.Q., *"Energy research in the Faculty of Basic Sciences",* Ecole Polytechnique Fédérale de Lausanne, Energy, A Challenge for Mankind, Part of the EPFL 150th Anniversary Celebrations, May, 2003

Tran M.Q., *"The roadmap towards fusion energy",* Paul Scherrer Institut, Villigen, September 2003

Weisen H., *"Shear dependence of density peaking in JET",* Task Force Meeting, EFDA-JET, Abingdon, UK, October 2003

Zabolostky A., *"Observation and empirical modelling of the anomalous particle pinch in TCV",* EFDA-JET Task Force T meeting, EFDA-CSU, Culham, UK, March 2003

B.5 Other external activities organised by the CRPP in 2003

International workshop on "15 Months of NbTi CICC results in SULTAN", Gstaad, Switzerland, 22-24 January 2003

This 3-day workshop brought together over 30 scientists from Europe, America, Russia and Asia. It consisted of oral presentations and discussion sessions about the progress in NbTi cable-in-counduit conductor development and testing, focusing on the ITER PF conductors. Topics such as AC loss behavior, non uniform current distribution, *n*-index of voltage-current law, transient field stability, quench behavior, sudden take-off, comparison of DC and strand performance, thermal hydraulic simulations, etc. were presented and discussed. In a special session on Nb3Sn, the ongoing R&D project at CRPP and a review of the ITER conductor design were presented.

APPENDIX C External activities of CRPP Staff during 2003

C.1 National and international committees and ad-hoc groups

MEMBERSHIP

K. Appert	Member of the International Scientific Committee 18th International Conference on the Numerical Simulation of Plasmas, 7-10 September 2003, Cape Cod, Massachusetts
N. Baluc	Scientific and Technical Advisory Committee, Euratom Symposium on Fusion Technology Organising Committee IEA Annex II Executive Committee Task Coordinator of the Subproject entitled 'Radiation Resistant Materials' within the EXTREMAT integrated project (IP) of the 6th European Framework Program. Task Coordinator of the EURATOM Task TTMS-003 “Compatibility of Steels with Hydrogen and Liquids, within the Tritium Breeding and Materials Programme of EFDA”
P. Bruzzone	International Magnet Technology Conference Organising Committee EFDA, Magnet Expert Group
J-L. Dorier	31st EPS Conference Programme Committee, London 2004
A. Fasoli	Scientific and Technical Advisory Committee, Euratom ASDEX Programme Committee, Germany Programme Committee of the Turin Easter Plasma Conference International Tokamak Physics Activities: Steady-State Operation and Energetic Particles Topical Group Program Committee of 8th IAEA Technical Meeting on Energetic Particles in Magnetic Confinement Systems, 2003
Ch. Hollenstein	"Conseil scientifique du Département Science pour l'Ingénieur du CNRS" Scientific council of the Institute of Surface Modifications at Leibzig (Wissenschaftsgemeinschaft Gottfried Wilhlem Leibniz) Expert for a "Sonderforschungsbereich-Projekt" of the Deutschen Forschungsgemeinschaft.
J.B. Lister	International Tokamak Physics Activities: MHD, Disruption and Control Topical Group EPS-13, Bern 2005, International Core Programme Committee 31st EPS Conference Programme Committee, London 2004 International Scientific Advisory Committee for ICALEPCS 2005 (Geneva)
C. Marinucci	CHATS, Scientific Programme Committee
R.A. Pitts	International Tokamak Physics Activities: Diagnostics Topical Group 30th EPS Conference Programme Committee
O.Sauter	Scientific Committee of the 10th European Fusion Theory Conference
R. Schäublin	Member of the board of the Swiss Society for optics and microscopy
M.Q. Tran	Electron Cyclotron Wave Task Area Leader Chairman of the Electron cyclotron Wave-Coordinating Committee Consultative Committee for the Euratom Specific Research and Training Programme in the field of Nuclear Energy, Fusion (CCE-FU) CCE-FU Special Working Group on "Possible joint implementation of ITER"

	EFDA* Steering Committee Scientific and Technical Advisory Committee, Euratom Chairman of the Ad-hoc Group for the Monitoring of the project W7-X Chairman of the Review Panel on Fusion, Helmoltz Gemeinschaft, Germany Member of the Review panel on nuclear Safety, Helmoltz Gemeinschaft, Germany Standing Committee of the International Symposium on Fusion Nuclear Technology Scientific Committee of the IAEA Technical Meeting on ECRH Physics and Technology for ITER Scientific Committee of the IAEA 3rd TCM on Steady State Operation of magnetic fusion devices
M. Victoria	Chairman, Executive Committee IEA Fusion Material Agreements Chairman, IEA Modeling and Experimental Validation Collaboration International Advisory Committee fo the Int. Conf. On Fusion Reactor Materials EFDA Task Coordinator on Modelling
L. Villard	Scientific and Technical Advisory Committee, Euratom "Conseil Scientifique du Département de Recherche sur la Fusion Contrôlée" – CEA, France Chairman, Ad-Hoc Group for the assessement of an application for a Cost-Sharing Action by the University of Ljubljana.
H. Weisen	International Advisory Board of the IPP Prague, Czech Republic

PARTICIPATION

B. Duval	Remote Participation Users Group, EFDA-JET
C. Marinucci	ITER TFMC Test and Analysis Group
Y.R. Martin	International Tokamak Physics Activity: Confinement Database and Modelling Topical Group
R.A. Pitts	International Tokamak Physics Activity: SOL and Divertor Topical Group
O. Sauter	International Tokamak Physics Activity: MHD, Disruption and Control Topical Group

C.2 Editorial and society boards

S. Alberti	Committee of the Swiss Physical Society, Responsible for Applied Physics
Ch. Hollenstein	Vice President of the Swiss Vacuum Society Committee "Union Radio-Scientifique Internationale" Editorial Board of Plasma Chemistry and Plasma Processing
J.B. Lister	Vice President of the European Physical Society Plasma Physics Division Editorial Board of Plasma Physics and Controlled Fusion
Y.R. Martin	Chairman of the Association Vaudoise des Chercheurs en Physique
P.J. Paris	Fusion Expo Consortium Committee EFDA Information Network "Fédération Romande de l'Energie" Committee

* EFDA: European Fusion Development Agreement

	Chairman of the "International Association of Specialists in Energy" (AISEN) Council of the "Chambre Franco-Suisse du Commerce et de l'Industrie"
L. Sansonnens	Committee of the Swiss Physical Society, Responsible for Applied Physics
M.Q. Tran	Board of Editors of Nuclear Fusion
M. Victoria	Invited Editor, J. Nucl. Materials

C.3 EPFL committees and commissions

N. Baluc	Commission Ecole Doctorale en Science et Génie des Matériaux
J-L. Dorier	Commission du Doctorat de la Section de Physique, FSB-EPFL
A. Fasoli	Commission d'Enseignement de la Section de Physique, FSB-EPFL
Ch. Guillemin	Assemblée d'Ecole, EPFL
J-Ph. Hogge	Commission du Doctorat de la Section de Physique, FSB-EPFL
B.Marlétaz	Conseil de la Faculté des Sciences de Base, EPFL
O. Sauter	Commission d'Informatique, FSB-EPFL
M.Q. Tran	Président de l'Assemblée d'Ecole (until October 2003) Commission du Doctorat de la Section de Physique, FSB-EPFL
L. Villard	Commission d'Enseignement de la Section de Physique, FSB-EPFL Délégué à la "Commission Scientifique du 3ème Cycle de la Physique en Suisse Romande"

APPENDIX D Lausanne Reports (LRP)

(see CRPP archives at http://crppwww.epfl.ch/archives)

Allfrey S., Hatzky R., *"A revised delta f algorithm for nonlinear PIC simulation"*, LRP 749/03

Angioni C., Goodman T.P., Henderson M.A., Sauter O., *"Effects of localised electron heating and current drive on the sawtooth period"*, LRP 761/03

Ballutaud J., Bucher C., Hollenstein Ch., Howling A.A., Kroll U., Benagli S., Shah A., Buechel A., *"Plasma deposition of p-i-n devices in a single-chamber larger area PECVC reactor: Reduction of the Boron cross-contamination"*, LRP 776/03

Bosshard P., *"Confinement ionique dans le tokamak TCV mesur par spectroscopie d'change de charge (thse EPFL No. 2723(2003))"*, LRP 750/03

Degeling A.W., Martin Y.R., Lister J.B., Villard L., Dokouka V.N., Lukash V.E., Khayrutdinov R.R., *"Magnetic triggering of ELMs in TCV"*, LRP 753/03

Delachaux T., *"Etude d'un procd de nitruration de la Zircone Ttragonale massive assist par un plasma arc haut courant continu"*, LRP 767/03

Descoeudres A., Sansonnens L., Hollenstein Ch., *"Attachment-induced ionization instability in electronegative capacitive RF discharges"*, LRP 751/03

EPS Participants, *"Papers presented at the 30th EPS Conference on Plasma Physics and Controlled Fusion, St Petersbourg, Russia, July 2003"*, LRP 766/03

Falchetto G.L., Vaclavik J., Villard L., *"Global-Gyrokinetic Study of Finite β Effects on Linear Microinstabilities"*, LRP 752/03

Favez J.-Y., Mullhaupt Ph., Srinivasan B., Lister J.B., Bonvin D., *"Improving the region of attraction of ITER in the presence of actuator saturation"*, LRP 754/03

Furno I., Weisen H., Zabolotsky A., and TCV Team, *"Particle convection in TCV - two papers"*, LRP 760/03

Ganesh R., Angelino P., Vaclavik J., Villard L., *"A full radius gyrokinetic stability analysis for large aspect ratio finite- β tokamaks"*, LRP 772/03

Graves J., *"Influence of asymmetric energetic ion distributions on Sawtooth stabilization"*, LRP 770/03

Graves J.P., Sauter O., Gorelenkov N.N., *"The internal kink mode in an anisotropic flowing plasma with application to modelling neutral beam injected sawtoothing discharges"*, LRP 745/03

Henderson M.A., Alberti S., Angioni C., Arnoux G., Behn R., Blanchard P., Bosshard P., Camenen Y., Coda S., Condrea I, Goodman T.P., Hofmann F., Hogge J.-Ph., Karpushov A., Manini A., Martynov An., Moret J.-M., Nikkola P., Nelson-Melby E., Pochelon A., Porte L., Sauter O., Ahmed S.M., Andrebe Y., Appert K., Chavan R., Degeling A., Duval B.P., Etienne P., Fasel D., Fasoli A.,, Favez J.-Y., Furno I., Horacek J., Isoz P., Joye B., Klimanov I., Lavanchy P., Lister J.B., Llobet X., Magnin J.-C., Marletaz B., Marmillod P., Martin Y., Mayor J.-M., Mlynar J., Paris P.J., Perez A., Peysson Y., Pitts R.A., Raju D., Reimerdes H., Scarabosio A., Scavino E., Seo s.H., Siravo U., Sushkov A., Tonetti G., Tran M.Q., Weisen H., Wischmeier M. ZabolotskyA., Yhuang G., *"Recent results from the EC heated plasmas in the TCV tokamak"*, LRP 747/03

IAEA Kloster Seeon Participants, *"Papers presented at the IAEA Technical Meeting on ECRH Physics and Technology for ITER, Kloster Seeon, Germany, July 2003"*, LRP 768/03

IAEA TCM Participants, *"Papers presented at the 9th IAEA Technical Meeting on H-mode Physics and Transport Barriers, San Diego, USA, September 2003"*, LRP 779/03

Isaev M. Yu., Okamura S., Cooper W.A., *"High β quasi-axisymmetric configuration with small Pfirsch-Schlueter current"*, LRP 756/03

ISPC16 participants, *"Papers presented at the 16th Int. Symposium on Plasma Chemistry, Taormina, Italy, 22-27 June 2003"*, LRP 759/03

Klinger L., Vos J.B., Appert K., *"Gradient evaluation on non-orthogonal meshes for the application of a plasma torch"*, LRP 748/03

Klinger L., Vos J.B., Appert K., *"High-resolution CFD simulation of a plasma torch in 3 dimensions"*, LRP 762/03

Marinucci C., *"Analysis and interpretation of Tcs measurements of the TFCI experiment (EFDA Task TM.005.G1-Magnet_M12, deliverable #7)"*, LRP 775/03

Marmy P., *"In-beam mechanical testing of CuCrZr "*, LRP 764/03

Marmy P., Luppo M., Hegedus F., Bruetsch M., Kopajtic Z., Krois M., *"The effect of hydrogen on the fracture toughness of the titanium alloys Ti6A14V and Ti5A12.5Sn before and after neutron irradiation (EFDA TASK TWO-T429/01: Titanium Alloys Irradiation Testing - Extension)"*, LRP 778/03

Martynov A., Medvedev S.Yu., Villard L., *"Tokamak equilibria with reversed current density "*, LRP 755/03

Moret J.-M., Buehlmann F., Tonetti G., *"Fast single loop diamagnetic measurements on the TCV tokamak"*, LRP 757/03

Pitts R.A., Alberti S., Blanchard P., Horacek J., Reimerdes H., Stangeby P.C., *"ELM driven divertor target currents on TCV"*, LRP 744/03

Pitts R.A., Chavan R., Erents S.K., Kaveney G., Matthews G.F., Neill G., Vince J.E., and JET-EFDA workprogramme contributors, Duran I., *"A retarding field energy analyser for the JET plasma boundary"*, LRP 765/03

Raju D., Sauter O., Lister J.B., *"Study of nonlinear mode coupling during neoclassical tearing modes using bispectrum analysis"*, LRP 746/03

Refke A., Barbezat G., Dorier J.-L., Gindrat M., Hollenstein Ch., *"Characterization of LPPS processes under various spray conditions for potential applications"*, LRP 743/03

RF-2003 Participants, *"Papers presented at the 15th Topical Conference on Radio Frequency Power in Plasmas, Moran, Wyoming, USA, May 2003"*, LRP 769/03

Scavino E., *"Transport of laser-ablated impurities in the TCV tokamak"*, LRP 758/03

Scavino E., Bakos J.S., Dux R., Weisen H., and TCV Team, *"Effects of plasma shape on laser blow-off injected impurity transport in TCV"*, LRP 774/03

Schmidt H., Sansonnens L., Howling A.A., Hollenstein Ch., Elyaakoubi M., Schmitt J.P.M., *"Plasma uniformity experiments using lens-shaped electrodes in a large area VHF reactor"*, LRP 773/03

Siegrist M.R., Hawkes N., Weisen H., *"Feasibility of an MSE system on the TCV tokamak"*, LRP 777/03

Stellarator Workshop Participants, *"Papers presented at the 14th Int. Stellarator Workshop, Greifswald, Germany, September 2003"*, LRP 771/03

Villard L., Allfrey S.J., Bottino A., Brunetti M., Falchetto G.L., Grandgirard V., Hatzky R., Nuehrenberg J., Peeters A.G., Sauter O., Sorge S., Vaclavik J., *"Full radius linear and nonlinear gyrokinetic simulations for tokamaks and stellarators: Zonal flows, applied E x B flows, trapped electrons and finite β "*, LRP 763/03

APPENDIX E The basis of controlled fusion

E.1 Fusion as a sustainable energy source

Research into controlled fusion aims to demonstrate that it is a valid option for generating power in the long term future in an environmentally, politically and economically acceptable way. Controlled fusion is a process in which light nuclei fuse together to form heavier ones: during this process a very large amount of energy is released. For a fusion reactor it is planned to use the two isotopes of hydrogen: deuterium (D) and tritium (T), which fuse together much more readily than any other combination of light nuclei according to the following reaction:

$$D^2 + T^3 \rightarrow He^4 + n + 17.6MeV$$

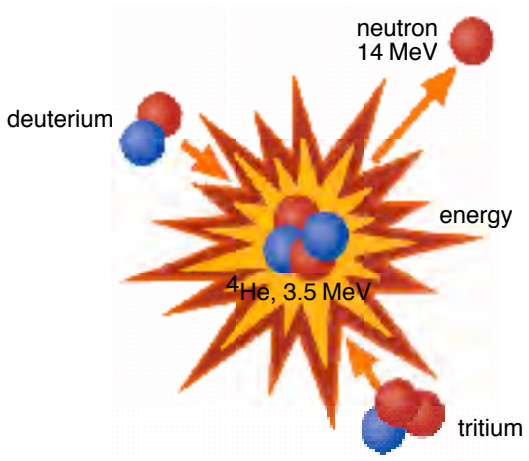

Fig. E.1 *Schematic of a fusion reaction between deuterium and tritium nuclei. The products are 3.5MeV ^4He, the common isotope of helium, and a 14MeV free neutron.*

The end products are helium and neutrons (n). The total energy liberated by fusing one gram of a 50:50% mixture of deuterium and tritium is 94000kWh, which is 10 million times more than from the same mass of oil. 80% of this energy is carried by the neutrons with an energy of 14MeV while the remaining 20% is carried by the helium nucleus. All this energy eventually becomes heat to be stored or converted by conventional means into electricity.

The temperature at which fusion reactions start to become significant are above a few tens of millions of degrees. For the D-T reaction, the optimal temperature is of the order of 70-200 million degrees. At such temperatures the D-T fuel is in the plasma state.

Deuterium is very abundant on the earth and can be extracted from water (0.034g/l). Tritium does not occur naturally, since its half-life is only 12.3 years, but it can be regenerated from lithium using the neutrons produced by the D-T fusion reactions. The two isotopes of natural lithium contribute to this breeding of tritium according to the reactions:

$$Li^6 + n \rightarrow He^4 + T^3 + 4.8MeV$$

$$Li^7 + n \rightarrow He^4 + T^3 + n - 2.5MeV$$

The relative abundance of the two lithium isotopes Li^6 and Li^7 are 7.4% and 92.6%, respectively. The known geological resources of lithium both in the earth and in the sea water are large enough to provide energy in an unlimited time.

E.2 Attractiveness of fusion as an energy source

The inherent advantages of fusion as an energy source are:

- The fuels are plentiful and their costs are negligible because of the enormous energy yield of the reaction;
- The end product of the reaction is helium, an inert gas;
- No chain reaction is possible; at any time only a very small amount of fuel is in the reacting chamber and any malfunction would cause an immediate drop of temperature and the reaction would stop;
- No after-heat problem can lead to thermal runaway;
- None of the materials required by a fusion power plant are subject to the provisions of the non-proliferation treaties.

Its further potential advantages are:

- Radioactivity of the reactor structure, caused by neutrons, can be minimised by careful selection of low-activation materials resulting in a manageable quantity of long lived radioactive waste;
- The release of tritium in normal operation can be kept to a very low level. The inventory of tritium in the breeding section of the reactor and on the site can be sufficiently small so that the worst possible accident could not lead to a harmful release to the environment requiring evacuation of the nearby population.

APPENDIX F Glossary

The following is a general purpose glossary for the field of controlled fusion and plasma physics.

Additional heating: Usually with reference to a plasma which is initially heated by a toroidal current induced in the plasma (ohmic heating), additional heating designates other means of heating a plasma (absorption of electromagnetic waves or of injected fast neutral particles).

Advanced Tokamak Scenarios: Tokamaks normally generate natural profiles of plasma current and plasma pressure. Using external non-inductive current drive and local control of the current and pressure profiles can allow access to enhanced regimes and even steady state operation, generally referred to as Advanced Tokamak Scenarios.

ALCATOR C-MOD: High field, high density tokamak at MIT (USA) with an elongated, diverted plasma.

Alfvén gap modes: The toroidal nature of tokamak plasmas produces gaps in the otherwise continuous spectrum of Alfvén waves, populated by discrete, weakly damped Alfvén gap modes. Under certain conditions these modes can be destabilised by resonant energy transfer from energetic particles, e.g. α-particles from fusion reactions.

Alfvén waves: A fundamental plasma wave, which is primarily magneto-hydrodynamic in character with an oscillation of the magnetic field and, in some cases, plasma pressure. In tokamaks, these waves are typically strongly damped. See also fast Alfvén wave.

Alfvén velocity: The velocity of propagation of Alfvén waves in the direction of the magnetic field; it is proportional to the magnetic field strength, and inversely proportional to the square root of the mass density.

alpha particle, or α-particle He^4: The nucleus of the helium atom, composed of two protons and two neutrons, is one of the two products of the DT fusion reaction (the other one is a neutron). The α-particles, being electrically charged, are trapped by the magnetic confinement field and therefore can release their energy to the plasma contrary to the neutrons which escape from the plasma and transfer their energy in the blanket surrounding the plasma core. The plasma heating which is provided by these α-particles as they slow down due to collisions is essential for achieving ignition.

Alternative lines: Magnetic confinement development other than the tokamak.

Analytic/Computational modelling: Analytic: algebraic solution of basic equations. Computational: numerical solution of basic equations.

Anomalous transport: Measured heat and particle loss is anomalously large compared with collisional theory of heat transport in toroidal plasmas.

ASDEX-Upgrade: Medium-sized Tokamak at Garching (Association Euratom-IPP, Germany) with an elongated, diverted plasma.

Aspect ratio: The ratio between the large radius and the small radius of a torus.

Auxiliary heating: See additional heating.

Ballooning instability: A local instability which can develop in the tokamak when the plasma pressure exceeds a critical value; it therefore constrains the maximum β that can be achieved. It is analogous to the unstable bulge which develops on an over-inflated tyre.

Beta (β): Ratio of plasma pressure to magnetic field pressure. One of the figures of merit for magnetic confinement: the magnitude of the magnetic field pressure determine the cost of the field coil that generates it; since fusion reactivity increases with the square of the plasma pressure, a high value of ß indicates good performance. The highest values achieved in tokamaks reach 40% (START).

Beta-normalised (β_N): The ratio of plasma current (in MA) to the product of minor radius (in m) and magnetic field (in T) characterises the limit to the achievable β imposed by ideal MHD. β -normalised is the ratio of β (as a percentage) to the above ideal MHD parameter. Generally β_N ~3 should be achievable, but techniques for obtaining higher values have been observed experimentally.

Blanket: A structure containing lithium or lithium compounds surrounding the plasma core of a fusion reactor. Its functions are to breed tritium, via lithium-neutron reactions, and to absorb most of

the fusion energy to be used for electricity generation.

Bootstrap current: Theory developed in 1970 predicted that a toroidal electric current will flow in a tokamak which is fuelled by energy and particle sources that replace diffusive losses. This diffusion driven "Bootstrap current", which is proportional to β and flows even in the absence of an applied voltage, could be used to provide the poloidal magnetic field: hence the concept of a Bootstrap tokamak, which has no toroidal voltage. A Bootstrap current consistent with theory was observed many years later on JET and TFTR; it now plays a role in optimising advanced tokamaks.

Breakeven: The fusion performance of a power plant is denoted by Q, which is the ratio of the power released by fusion reactions to that used to heat the plasma. As a convention, scientific breakeven corresponds to Q=1 and ignition to Q=infinity. A fusion power plant would operate at Q~50.

Breeding ratio: The number of tritium atoms produced in the blanket of a fusion power station per tritium nucleus burned in the fusion plasma.

Burn: The fusion process of consuming DT fuel in a reactor, releasing energy.

CCE-FU: The Consultative Committee for the Euratom Specific Research and Training Programme in the field of Nuclear Energy, Fusion. Formerly the CCFP.

CEA: Commissariat à l'Energie Atomique, France. Partner in the Association EURATOM-CEA which operates the TORE SUPRA tokamak.

CFI: Committee on Fusion-Industry.

Charge exchange measurement: Measures the plasma ion temperature. Neutral atoms in the plasma (for example from a neutral beam) donate electrons to hot plasma ions, which are thereby neutralised. These hot atoms are no longer confined by the magnetic field and leave the plasma. Their energy is measured by a neutral particle analyser.

CIEMAT: Centro de Investigaciones Energéticas Medioambientales y Tecnológicas, Spain. Partner in the Association EURATOM-CIEMAT. Operates the flexible heliac stellarator TJ-II.

Classical transport: Collisions between the individual particles of a plasma allow them to move across the magnetic field. Theories which describe this mechanism are called "classical" (or "neo-classical" when additional effects due to the toroidal geometry are included). The measured heat and particle transport is usually higher than predicted by these theories.

Collisionality: Non-dimensional parameter, which is the inverse ratio of the mean free path of plasma particles between collisions to a characteristic length of the magnetic field configuration.

Compact torus: Class of closed magnetic configurations in which no material elements (coils, conductors or walls) need to link through the bore of the plasma torus. Thus the vessel of compact tori can be spherical or cylindrical.

COMPASS: COMPact ASSembly, a tokamak for studies of plasma stability, at Culham, UK (Association EURATOM-UKAEA). Originally with circular vessel (COMPASS-C), now with D-shaped vessel (COMPASS-D).

Confinement time: In a fusion plasma neither particles nor energy are perfectly confined. Particle confinement time is the time during which the particles, on average, stay confined. The energy confinement time, which is usually shorter than the particle confinement time, is defined in steady state as the ratio of the plasma energy content to the total power input to the plasma and is a measure of how fast a plasma would cool if there were no heating.

CRPP: Centre de Recherches en Physique des Plasmas. Fusion laboratories of the Association EURATOM-Swiss Confederation at the Ecole Polytechnique Fédérale de Lausanne and the Paul-Scherrer Institute, Villigen (CRPP-Fusion Technology).

Current drive (non-inductive): In a tokamak, plasma current can be driven inductively, with the toroidal plasma acting as a secondary winding of a transformer whose primary coil is at the central column of the device. Continuous current cannot be driven by transformer action. 'Non-inductive' current drive methods are applied either by injecting particles with directed momentum into the plasma or by accelerating electrons by electromagnetic waves so that they carry the current. Also being applied to control instabilities and to optimise confinement by modifying the current profile. The bootstrap effect also drives current.

Current profile (current distribution): The distribution of current density across the minor radius of the plasma.

Current ramp-up (down): The increase (decrease) of plasma current either at the start of operation or during operation.

Cyclotron frequency: Charged particles in a magnetic field have a natural frequency of gyration in the plane perpendicular to the magnetic field - the cyclotron frequency. For electrons in a tokamak, the cyclotron frequency is typically a few tens of GHz (28 GHz per Tesla), and for ions, a few tens of MHz (7.5 MHz per Tesla for deuterium).

Cylindrical approximation: An approximation to the true tokamak geometry in which the torus is straightened, so that the toroidal direction becomes the cylinder axis. There are two directions of symmetry: along the axis (the 'toroidal' direction) and about the axis (the 'poloidal' direction).

DCU: Dublin City University, Ireland. Partner in the Association EURATOM-DCU.

DEMO: Demonstration Reactor (the first device in the European fusion strategy intended to produce significant amounts of electricity).

Deuterium: A stable isotope of hydrogen, whose nucleus contains one proton and one neutron. In heavy water, normal hydrogen is replaced by deuterium. Sea water contains, on average, 34g deuterium per m^3. Deuterium plasmas are used routinely in present-day experiments; in a fusion power plant the plasma will consist of a mixture of deuterium and tritium which fuse more readily then two deuterium nuclei.

DG Research (DG RTD): The Directorate-General of the European Commission, Brussels, responsible for Research and Development**.** Formerly DG XII.

Diagnostic: Apparatus used for measuring one or more plasma quantities (temperature, density, current, etc.).

Diffusion, thermal (or particle): The random flow of heat (or particles) in the presence of a thermal (or density) gradient.

DIII-D: The largest operating US tokamak, run by General Atomics, San Diego. It has a flexible configuration and studies core and divertor physics with intense additional heating.

D-He^3: Deuterium-^{3}Helium: A potential fuel for fusion with low release of neutrons, but which would require a much higher fusion triple product ($n\tau$) than DT to reach ignition. ^{3}Helium is an isotope of helium which is not available in appreciable quantities on Earth.

Disruption, Disruptive instability: A complex phenomenon involving MHD instability which results in a rapid release of energy to the wall and strong electromechanical forces in a tokamak. Plasma control may be lost, triggering a VDE (q.v.). This phenomenon places a limit on the maximum density, pressure and current in a tokamak.

Distribution function: Describes both the space and velocity distribution of plasma particles.

Divertor: A magnetic field configuration with a separatrix, affecting the edge of the confinement region, designed to remove heat and particles from the plasma, i.e. divert impurities and helium ash to divertor plates in a target chamber. Alternative to using a limiter to define the plasma edge.

Double null: See Single/double null divertors.

Drift kinetic theory: Kinetic theory which describes plasma processes which have spatial scales much greater than the particle Larmor radii.

Drift orbits: Particle motion is tied to straight magnetic field lines. However, electric fields and gradients of the magnetic field give an additional drift perpendicular to the magnetic field creating drift surfaces displaced from the magnetic surfaces.

Driven current: Plasma current produced by a means external to the plasma, inductively or non-inductively.

Driver: In inertial confinement fusion, the laser or particle beam system used to compress a target pellet.

DTE: The deuterium-tritium experiment at JET which in 1997 set new records for fusion power production. Followed the Preliminary Tritium Experiment of 1991.

ECCD: Electron Cyclotron Current Drive. Non-inductive current drive technique using directed electron cyclotron resonance waves.

ECE: Electron Cyclotron Emission. Radiation emitted by electrons as a result of their cyclotron motion around magnetic field lines. Used to measure electron temperature.

ECH: Electron-Cyclotron Heating. Radio wave heating near the resonance frequency (or its multiple) of the electron gyration in a magnetic field. In present and future machines ECH is at typically 60-170 GHz, depending on the magnetic field strength in a machine.

EFDA: European Fusion Development Agreement. The new organisational framework of the EU fusion activities on the exploitation of the JET Facilities, international collaboration (including ITER) and supporting technology. EFDA replaces the NET agreement.

EFET: European Fusion Engineering & Technology: a fusion technology oriented European Economic Interest Grouping.

Electron temperature: A measure of electron thermal energy in units of degrees or electron volts (1 eV ~ 10^4 degrees Kelvin).

ELM: Edge localised mode. An instability which occurs in short periodic bursts during the H-mode in divertor tokamaks. It modulates and enhances the energy and particle transport at the plasma edge. These transient heat and particle losses could be damaging in a reactor.

ENEA: Ente per le Nuove Tecnologie, l'Energia e l'Ambiente, Italy. Partner in the Association EURATOM-ENEA.

Energetic particle: In terms of energy, the particles in a plasma can be divided into two classes. The more numerous thermal particles are characterised by a temperature typically in the range 1-30 keV for modern tokamaks. The less numerous class of energetic particles has significantly higher energy up to several MeV. Energetic particles can be created by electric fields, fusion reactions, neutral beam injection or RF heating.

Error fields: The magnetic coils of a tokamak are designed to give the desired magnetic field configuration. The finite number of coils and imperfections in their construction lead to unwanted deviations from this configuration known as error fields. These could lead to disruptions and are of particular concern for larger tokamaks.

EXTRAP T-II: External Trap II, a medium-sized reversed field pinch (RFP) at the Royal Institute of Technology, Stockholm (Association EURATOM-NFR), built for RFP transport and shell stabilisation studies in support of RFX.

EURATOM: European Atomic Energy Community.

Faraday rotation: The rotation of the plane of polarisation of light passing through a magnetised plasma.

Fast Alfvén wave: The fast Alfvén wave exists over a broad frequency spectrum, from the ion cyclotron range of frequencies (ICRF) where its character is electromagnetic, down to magnetohydrodynamic frequencies. Its velocity is comparable to the Alfvén velocity. The fast Alfvén wave is used routinely for high-power (~20MW) ICRF heating on JET, as it is efficiently absorbed in the plasma by the mechanism of ion cyclotron resonance. Although usually stable in tokamaks, the wave can be excited by energetic ion populations.

Fast wave current drive: Current drive produced by a fast wave. The wave can penetrate the plasma more easily than a lower hybrid wave.

Feedback: Use of measurements of plasma parameters to control the parameters, shape or profiles of the plasma to obtain desired conditions.

Field lines, Flux surfaces: Imaginary lines marking the direction of a force field. In a tokamak these define a set of nested toroidal surfaces, to which particles are approximately constrained, known as flux surfaces.

Field reversed configuration: A compact torus with a strongly elongated plasma. The plasma is contained in a cylindrical vessel inside a straight solenoid. The confining magnetic field usually has only a poloidal component. Not to be confused with reversed field pinch.

FIR: Far infra-red (e.g. wavelength ~ 0.2 to 1mm). FIR lasers are used to measure the magnetic field and plasma density.

"**Fishbones**": Rapid bursts of MHD activity sometimes observed when neutral beam heating is used in tokamaks (fishbone refers to the shape of the bursts in oscillating magnetic field when plotted as a function of time).

First wall: The first material boundary that surrounds the plasma. Today, the first wall in all machines is protected by low-Z materials (such as carbon tiles, boron or beryllium coating).

Flat-top current: Constant current during quasi-stationary operating conditions.

Fokker-Planck Code: A computer code to calculate the velocity distribution of plasma particles allowing for collisional relaxation and plasma heating. Calculates distribution functions (q.v.).

FOM: Stichting voor Fundamenteel Onderzoek der Materie (Foundation for basic investigations of matter), The Netherlands. Partner in the Association EURATOM-FOM.

FPC: The Fusion Physics Committee, a sub-committee of the CCE-FU which reports to it principally on the physics aspects of the programme. Formerly the Programme Committee (PC).

FTC: The Fusion Technology Committee, a sub-committee of the CCE-FU which reports to it principally on strategic issues.

FTU: Frascati Tokamak Upgrade, a high density, high current tokamak at Frascati, Italy (Association EURATOM-ENEA).

Fusion triple product: Product of (ion) density, (ion) temperature and energy confinement time. A measure of the proximity to break-even and ignition.

Fusion product: The product of a fusion reaction, for example an α-particle or neutron in a deuterium-tritium plasma.

Fusion reactivity: Fusion reaction rate. For present typical tokamak conditions, it increases with the square of the density and the ion temperature of the plasma.

Full wave theory: Wave theory which includes complete accounting of wave energy (transmitted, reflected and absorbed, including energy transferred to other waves) for studying RF heating.

FZK: Forschungszentrum Karlsruhe, Germany. Partner in the Association EURATOM-FZK, active in fusion technology and, with the development of gyrotrons, in plasma engineering.

FZJ: Forschungszentrum Jülich GmbH, Germany. Partner in the Association EURATOM-FZJ, operating the tokamak TEXTOR.

GSI: Gesellschaft fuer Schwerionenforschung, Darmstadt, Germany. Studying heavy-ion physics, and driver physics with possible application for inertial confinement fusion.

Gyro-kinetic theory: Version of kinetic theory in which the Larmor radius is not assumed to be small. An essential theory for investigating fine-scale instabilities which might be responsible for driving turbulence, which may in turn be responsible for anomalous transport.

Gyrotron: Device used for generating high power microwaves in the electron cyclotron range of frequencies (50 - 200 GHz). This UHF wave is mostly used to heat the plasma at the electron cyclotron resonance frequency. It also could be used to diagnose the plasma.

Heliac: Stellarator configuration with a central toroidal coil around which the plasma column is wound helically. Because of its high capability of investigating a wide range of stellarator configurations, it is used for TJ-II.

Helias: Optimised stellarator configuration, used with modular coils for Wendelstein VII-X (Germany) and SHEILA (Australia).

H-mode: A High confinement regime that has been observed in tokamak plasmas. It develops when a tokamak plasma is heated above a characteristic power threshold, which increases with density, magnetic field and machine size. It is characterised by a sharp temperature gradient near the edge (resulting in an edge "temperature pedestal"), ELMs and typically a doubling of the energy confinement time compared to the normal "L" regime. Today, a variety of high confinement modes have been identified in divertor and in limiter configurations (e.g. the I-mode), which, in part, have been obtained by special tailoring of the radial plasma current profile.

H-transition (or L-to-H transition): Transition into the H-regime from the L-regime, usually quite sudden, at a certain threshold power of additional heating and specific plasma parameters.

Halo currents: See Vertical Displacement Event.

Helicity injection: The helicity of a toroidal plasma is related to a linkage of toroidal and poloidal magnetic fluxes, and is approximately conserved throughout a discharge. If additional helicity can be injected, the plasma current could be sustained or even increased.

Helium ash: Fusion reactions in a deuterium-tritium plasma produce energetic α-particles (helium nuclei), which heat the plasma as they slow down. Once this has happened, the α-particles have no further use: they constitute helium ash,

which dilutes the fuel and must be removed to maintain a burning plasma.

High beta (β): Condition in which the plasma energy is a significant fraction of the energy in the magnetic field. An alternative measure is the ratio between the plasma energy and the energy in the poloidal magnetic field, the poloidal β.

High field ECH launch: Electron cyclotron waves can be launched from the inside of the plasma torus. This allows higher density plasma to be heated.

Hydrogen: The lightest element; the nucleus consists of only one proton, the atomic shell of one electron. Isotopes of hydrogen, with one or two additional neutrons in the nucleus, are deuterium and tritium respectively.

IAEA: International Atomic Energy Agency (of the United Nations), Vienna, Austria. The ITER-EDA is undertaken under the auspices of the IAEA.

ICE: Ion Cyclotron Emission. Observed in JET and TFTR as a suprathermal signal, apparently driven by collective instability of energetic ion populations such as fusion products and injected beam ions.

ICF: Inertial Confinement Fusion. Intense beams of laser light or light or heavy ion beams are used to compress very rapidly and heat tiny target pellets of fusion fuel to initiate fusion burn in the centre. Sufficient fusion reactions must occur in the very short time before the fuel expands under its own pressure. The inertia of the pellet's own mass determines the time scale during which fusion reactions occur, hence the name inertial confinement.

ICRH: Ion Cyclotron Resonance Heating by launching waves into the plasma in the range of the ion cyclotron frequency (radio frequency, typically at several tens of MHz).

ICRF: Ion Cyclotron Resonance Frequencies.

Ideal: In the context of MHD, 'ideal' implies that the magnetic field and the plasma always move together. For this to occur, the electrical resistivity of the plasma must be negligible.

Ideal internal kink modes: An MHD instability of the central region of a tokamak. This, or its close relative the resistive internal kink mode, may be involved in the Sawtooth disruptions which occur in most Tokamaks.

IEA: International Energy Agency (of the OECD), Paris, France. Implementing agreements for international collaboration on specific topics in fusion have been set up in the frame of the IEA.

Ignition condition: Condition for self-sustaining fusion reactions: heat provided by fusion α-particles replaces the total heat losses. External sources of plasma heating are no longer necessary and the fusion reaction is self-sustaining. Ignition is not required for energy gain in a power station. Retaining a level of external heating or current drive will be required to control the plasma pressure and current profiles, to optimise the performance, leading to a so-called "driven burn".

Impurities: Ions, other than the basic plasma ion species, which are unwanted as they lose energy by radiation and dilute the plasma.

Impurity screening: The prevention of impurities from entering the plasma.

Internal kink: A type of MHD instability that can occur within the central region of the plasma (where $q < 1$) reducing the peak temperature and density.

Internal Reconnection Event (IRE): An instability which breaks magnetic field lines and reconnects them with a different topology to reduce the system to a lower energy state - associated with the operating limits of spherical tokamaks.

Ion Bernstein wave: A wave which only exists in a hot plasma and is supported by the ions. It propagates at right angles to the magnetic field, when it is undamped, at harmonics of the ion cyclotron frequency. There is also an electron Bernstein wave which propagates at harmonics of the electron cyclotron frequency.

Ion Cyclotron Current Drive (ICCD): Non-inductive current drive using ICRH.

Ion Cyclotron Resonance Heating (ICRH) / Ion Cyclotron Resonance Frequencies (ICRF): Additional heating method using RF waves at frequencies (~ 20-50 MHz) matching the frequency at which ions gyrate around the magnetic field lines.

IPP: Max-Planck-Institut fuer Plasmaphysik, Garching, Germany. Partner in the Association EURATOM-IPP, operating the tokamak ASDEX-Upgrade and the stellarator Wendelstein VII-AS. Also has sites in Berlin and in Greifswald, where the construction of the large superconducting stellarator Wendelstein VII-X is in progress.

IR: Infra Red part of the electromagnetic spectrum.

IRE: Internal Reconnection Event.

IST: Instituto Superior Técnico, Portugal. Partner in the Association EURATOM-IST.

ISTTOK: Tokamak, for study of non-inductive current drive, at the Instituto Superior Técnico (IST), Lisbon, Portugal.

ITER: International Thermonuclear Experimental Reactor (the next step as a collaboration between EURATOM, Japan, the Russian Federation and originally the USA, under the auspices of the IAEA). After a conceptual design phase - CDA (1988-1990), and engineering design activities (ITER-EDA, 1992-2001), now under the Coordinated Technical Activities (CTA). TAC, Technical Advisory Committee. See also Next Step.

JAEC: Japan Atomic Energy Commission, Tokyo, Japan.

JAERI: Japan Atomic Energy Research Institute. Headquarters in Tokyo, Japan.

JET: Joint European Torus. The largest tokamak in the world, sited at Abingdon, UK. Operated as a Joint Undertaking (JET Joint Undertaking), until the end of 1999. The scientific exploitation of the JET facilities is now guaranteed by the Euratom fusion Associations within the EFDA framework. The operation of the facility is the responsibility of the Association Euratom-UKAEA.

JT-60U: Japanese tokamak at Naka. The largest Japanese tokamak and second largest operating experiment after JET, but not designed for use with D-T fuel.

keV: Kilo-electronvolt. Energy which an electron acquires passing a voltage difference of 1000 volts. Also used to measure the temperature of a plasma (1 keV corresponds to 11.8 million degrees Kelvin).

Kinetic instability: Oscillation which is unstable as a result of the energy distribution of ions or electrons.

Kinetic theory: A detailed mathematical model of a plasma in which trajectories of electrons and ions are described. More complex than fluid and two-fluid theories, it is necessary in the study of RF heating and some instabilities, particularly when energetic particles are involved.

L-H transition: Change from L regime to H regime (usually quite sudden).

L-mode: As opposed to the H mode. Regime with degradation of confinement, in additionally heated plasmas, with respect to plasmas heated ohmically by the plasma current.

Langmuir probe: Electrical probe inserted into the edge of a plasma for measurements of density, temperature and electric potential.

Larmor radius: Radius of the gyratory motion of particles around magnetic field lines.

Large scale ideal modes: A large scale mode has a wavelength which is a significant fraction of the plasma dimensions and assumes ideal MHD.

Laser ablation: Use of lasers to produce a sudden influx of impurities into the plasma from a solid surface.

Last closed flux surface: The boundary separating those magnetic field lines that intersect the wall (open lines) from the magnetic field lines that never intersect the wall (closed lines).

Lawson criterion: The value of the confinement time multiplied by the ion density (at the required temperature) which must be exceeded in a fusion reactor to reach ignition.

Limiter: A material surface within the tokamak vessel which defines the edge of the plasma and thus avoids contact between the plasma and the vessel. A pumped limiter can also be used to remove heat and particles and is an alternative exhaust system to the divertor.

LLNL: Lawrence Livermore National Laboratory, Livermore, USA.

Locked modes: MHD modes that cease rotating (though they can still grow).

Low-activation materials: Materials which do not develop high, long-lived radioactivity under neutron irradiation.

Low aspect ratio: Low ratio of major to minor radius of the torus.

Lower hybrid current drive (LHCD): Non-inductive current drive using lower hybrid waves.

Lower hybrid heating (LHRH): Plasma heating by radio frequency waves at the "lower hybrid" resonance frequency in the plasma. Typical frequencies are a few GHz.

Lower hybrid (LH) wave: A plasma wave of frequency between the ion and electron cyclotron frequencies. It has a component

of electric field parallel to the magnetic field, so it can accelerate electrons moving along the field lines.

Magnetic axis: The magnetic surfaces of a tokamak form a series of nested tori. The central 'torus' defines the magnetic axis.

Magnetic Confinement Fusion (MCF): Confinement and thermal insulation of a plasma within the reactor core volume by the action of magnetic fields. In toroidal magnetic confinement, usually both toroidal and poloidal components of the magnetic field are needed (the field lines are threaded like the filaments of a cable which is bent into a ring).

Magnetic islands: Islands in the magnetic field structure caused either by externally applied fields or internally by unstable current or pressure gradients. See tearing magnetic islands.

Magnetic surfaces (flux surfaces): In toroidal magnetic confinement, the magnetic field lines lie on nested toroidal surfaces. The plasma pressure, but not the amplitude of the magnetic field, is a constant on each magnetic surface.

Magneto-acoustic cyclotron instability: This instability results from an exchange of energy between the fast Alfvén wave (or magneto-acoustic wave) and an ion Bernstein wave which has a source of free energy through the presence of a population of energetic (non-thermal) ions, e.g. fusion products. The instability occurs for propagation perpendicular to the equilibrium magnetic field.

Major radius: The distance from the tokamak symmetry axis to the plasma centre.

Marfe: A localised and radiating thermal instability sometimes observed near the edge of tokamak plasmas.

Marginal Stability: Close to the transition from stability to instability.

MAST: Mega Amp Spherical Tokamak at Culham (Association EURATOM-UKAEA), twice as big as START. Began operation in 1999.

MeV: Mega-electronvolt, unit for nuclear energies. Energy which an electron acquires passing a voltage difference of 1 million volts.

MHD (Magnetohydrodynamics): A mathematical description of the plasma and magnetic field, which treats the plasma as an electrically conducting fluid. Often used to describe the bulk, relatively large-scale, properties of a plasma.

MHD instabilities: Unstable distortions of the shape of the plasma/magnetic field system.

Microinstabilities: Instabilities with characteristic wave-lengths similar to the ion Larmor radii, rather than to the tokamak dimensions. These are thought to be responsible for the fine scale turbulence in tokamaks, and hence anomalous transport.

Minor radius: Half the small diameter of the tyre-shaped toroid.

Mirnov coils: Pick-up coils at the edge of the plasma for measuring the time variation of magnetic fields arising from instabilities.

Mirror: A linear magnetic confinement concept with a weaker magnetic field in a central region and with strong fields at both ends which reflect contained particles by the mirror effect. Some variants exist to increase the magnetic field in all directions from the centre or to improve the closure of the bottlenecks. The Tandem Mirror confinement concept also involves electrostatic fields.

MIT: Massachusetts Institute of Technology, Boston, USA. Operates the high-field divertor tokamak ALCATOR C-MOD.

Mode: A resonant wave or oscillation in a plasma. Also used as a synonym for an operating regime.

Mode number: Characterises the wavelength of a mode.

Monte Carlo code: A statistical technique used in numerical calculations where events may occur many times, each with a certain probability.

Motional Start Effect (MSE): The measurement of shifts and splitting of spectral lines emitted from particles moving in a local electric field. This can be interpreted to give the local magnetic field inside the tokamak if the particle velocity is known, and is a major diagnostic on some tokamaks to deduce the current profile.

MPQ: Max-Planck-Institut fuer Quantenoptik, Garching, Germany. Active, within its programme, in ICF (laser fusion) related physics. Partially supported by Euratom, for a "keep in touch activity" in ICF.

Negative ion beam: To produce neutral beams, negative ions (obtained by the addition of electrons to neutral atoms) are accelerated and then neutralised before entering the plasma. The efficiency of creating neutral beams from positive ions is too low at the beam energy required for a fusion power station, of the order of 1 MeV.

Neo-classical theory: Classical collisional plasma transport theory, corrected for toroidal effects. The neoclassical theory predicts the existence of the bootstrap current.

Neo-classical tearing mode: The magnetic island produced by a tearing mode perturbs the bootstrap current which further amplifies the island and degrades confinement or leads to a disruption.

NET: Next European Torus, a design for the Next Step which had been prepared by the NET team (located at the Association EURATOM- IPP in Garching) and which has largely influenced the ITER design. The European ITER contributions in physics and technology were organised by the NET team, until its replacement by EFDA in 1999.

Neural network: A computer algorithm that uses incoming data to derive plasma parameters, having previously been "trained" on a series of examples of a non-linear input-output mapping.

Neutrons: Neutral particles in the nucleus. Products of Deuterium-Tritium and other fusion reactions.

Neutral beams: Since charged particles cannot easily penetrate the magnetic confinement fields of the plasma, high energy beams of neutral atoms are injected into the plasma for fuelling, heating and current drive. Within the plasma, the atoms of the beam are ionized and are then confined.

Neutron multiplier: The fusion of deuterium and tritium consumes one tritium nucleus per reaction, producing one neutron. Since in the blanket of a power station not every neutron reacts with lithium to produce a new tritium atom, a neutron multiplying element may be used in the blanket to enhance the tritium production so as to make the power station self-sufficient in tritium supply.

Next Step: The next experimental device in the strategy of the European Fusion Programme. Presently pursued via the ITER EDA, with a European activity as a fall-back option. The generic name for an experimental reactor with a long pulse burning plasma at high fusion gain.

NFR: Naturvetenskapliga Forskningsrädet (Natural Science Council), Sweden. Partner in the Association EURATOM-NFR.

NIFS: National Institute for Fusion Science, Nagoya, Japan.

NRIM: National Research Institute for Metals, Sakura-mura, Japan.

Non-inductive heating and current drive: See additional heating and current drive.

NSTX: Spherical tokamak at Princeton, USA. A similar size to MAST, but of different design. Started operation in 1999.

Ohmic heating (OH): The resistive heating resulting from a current flowing within the plasma corresponding to the heating of a wire by a current flowing through it. Ohmic heating in a tokamak is insufficient to reach thermonuclear temperatures since, contrary to a wire, the resistance of a plasma decreases strongly with increasing temperature, thus making Ohmic heating weak at high temperatures.

ORNL: Oak Ridge National Laboratory, USA.

Operating limits: See tokamak operating boundaries.

Optimised shear: Adjusting the current profile to optimise tokamak.

PbLi: Eutectic lithium-lead alloy considered for use as blanket breeding material.

Peeling mode: An edge MHD instability which exists when the current density at the plasma edge is non-zero. It may be associated with ELMs.

Pellet: In inertial confinement concepts, the fuel is contained in tiny spheres, called pellets, which are compressed by laser or particle beams. In magnetic fusion, pellets of frozen hydrogen, deuterium, tritium, accelerated up to several kilometres per second, are used to refuel the plasma and to obtain very high densities.

PIREX: Proton Irradiation Experiment, material test facility (Association Euratom-Switzerland, CRPP-FT, PSI, Villigen, CH).

Plasma: State of matter above a few thousand degrees where atoms are broken into their constituents, ions and electrons, thereby creating an electrically conducting medium. Plasmas can therefore interact strongly with electric and magnetic fields.

Plasma confinement: Retention of plasma energy or particles within a given region, including the heat and particle losses from the plasma.

Plasma parameters: Physical quantities which characterise the plasma and which must be measured experimentally, such as current, density, temperature, confinement time, β.

Plasma pressure: Proportional to the product of plasma density and temperature. There is an electron and an ion pressure and the plasma pressure is the sum of the two. In magnetic confinement devices, this pressure is counterbalanced by magnetic pressure.

Plasma shape: Describes the plasma vertical cross-section, circular, elongated, D-shape, diverted, single null, double null.

Polarimetry: Measurement of the rotation of the plane of polarisation of light passing through a magnetically confined plasma; used to measure the local magnetic field and thus the safety factor (see Faraday rotation).

Poloidal field: Component of the magnetic field perpendicular to the toroidal direction and the major radius. The poloidal field is essential for confinement and is generated in a tokamak by the plasma current and the external coils.

Power threshold: The L-H transition and improved performance regimes related to reversed shear occur when the power exceeds a certain threshold value - the power threshold.

PPPL: Princeton Plasma Physics Laboratory, New Jersey, USA.

Preliminary Tritium Experiment (PTE): Three plasma discharges on JET, November 1991, into which a significant amount of tritium was injected for the first time in a tokamak. The power liberated from fusion reactions (~ 2MW for ~ 2 seconds) was in accordance with expectations. Followed by the more ambitious DTE in 1997.

Profile: Variation of plasma parameters with minor radius.

Profile control: Controlling the profiles of pressure, density or current, in order to control instabilities.

PSI: Paul-Scherrer-Institut, Villigen, Switzerland, active, in muon physics among others fields. The Association EURATOM-Swiss Confederation has their fusion technology activities working in superconductor and materials technology located at Villigen.

Pumped divertor: Divertor field lines directed into a pumped chamber surrounding the target plate.

q, q_{95}: See Safety factor.

Q: Ratio of fusion power to total additional heating power. At $Q=\infty$, no external power is required and the plasma is said to be ignited. A power station should operate with $Q\sim50$ to be economical.

Radial electric field: Arises when there is a charge imbalance in the plasma.

Radio frequency (RF) heating: Heating with waves in the radiofrequency range at resonance frequencies of the plasma (see ECH, ICRH, LHH).

Reflectometry: Use of reflected microwaves to measure plasma density.

Relaxation: The evolution of a plasma to a lower energy state.

Resistive ballooning modes: A class of ballooning mode which would be stable in the absence of resistivity, but can be unstable in its presence. Related to tearing modes, but topologically different.

Resistive instability: Instability due to diffusion and rearrangement of magnetic field lines. When the plasma resistivity is small, these instabilities have a slow growth rate.

Resistivity: The tendency to resist the flow of electric current, thereby dissipating energy. Plasmas are very good conductors of electric current, so that their resistivity can often be neglected. In this case, 'ideal' magnetohydrodynamics may be applied.

Resonant ions/electrons: Resonance occurs when one of the characteristic frequencies of particle motion in the plasma (for example, the cyclotron frequency) matches the frequency of some applied perturbation (for example, an RF wave).

Resonant magnetic perturbation (RMP): An externally applied magnetic perturbation matched to the spatial structure and optionally the frequency and phase of an instability.

Reverse Field Pinch (RFP): A toroidal magnetic confinement device, similar to a tokamak, in which the poloidal and toroidal fields are of comparable magnitude. Capable of higher plasma current and pressure for a given external magnetic field.

They require a conducting shell close to the plasma for stabilisation.

Reverse (magnetic) shear: In a tokamak the current density is usually greatest at the magnetic axis, in which case the safety factor increases from the centre to the edge of the plasma. Using non-inductive current drive and/or the bootstrap current the current density can be made to increase away from the centre. In this "reverse shear" case, the safety factor has a minimum away from the plasma centre. Using reverse or low shear ("optimised shear") some tokamaks, notably DIII-D and TFTR in the US and more recently JT-60U in Japan and JET, have shown greatly improved plasma performance. Reverse shear is an attractive option for advanced tokamak scenarios.

RF: Radio-Frequency.

RFX: Reversed Field pinch Experiment at CNR-Padova, Italy (Association EURATOM-ENEA).

RISØ: Forskningscenter Risø, Denmark. Partner in the Association EURATOM-RISØ.

Rotational transform: Measure of the ratio of poloidal to toroidal flux defining the pitch of the helical field lines. The q-value of the tokamak is proportional to the reciprocal of the rotational transform.

RTP: Rijnhuizen Tokamak PETULA, for study of transport in a plasma, at Nieuwegein (Rijnhuizen), the Netherlands (Association EURATOM-FOM). Ceased operation in 1998, the activities of the Association being transferred to TEXTOR, as part of the Tri-lateral Euregio Cluster.

Runaway electron: An electron with a very high energy has a decreasing probability of colliding with another charged particle and of losing its energy. Such a particle then gains more and more energy in the electric field of a tokamak, reaching 10's of MeV.

Safety factor: Number of turns the helical magnetic field lines in a tokamak make round the major circumference for each turn round the minor circumference, denoted q. Has no connection with the ordinary sense of "safety" other than q=1 surfaces are ideally unstable. For diverted plasmas q goes to infinity at the separatrix, so instead q_{95} is used to describe the safety factor near the edge, which is the safety factor of the plasma surface which contains 95% of the poloidal flux.

Sawtooth: A cyclically recurring instability which causes an energy loss from the central region of tokamak discharges. The temperature periodically falls abruptly, then slowly recovers. The jagged trace produced by plotting temperature against time gives the instability its name.

Sawtooth crash: The rapid collapse of the central temperature in a tokamak during a sawtooth cycle.

Scaling laws: Empirical or theoretical expressions for how various plasma phenomena (eg confinement, power threshold, etc) vary with tokamak parameters. They are particularly used for predicting the performance of future tokamaks.

Scrape-off-layer (SOL): The residual plasma between the "edge" of the plasma (defined by the limiter radius or the separatrix) and the tokamak vessel wall.

Semi-empirical: A theoretical approach in which the behaviour of some key quantities is deduced from experiment, rather than a priori.

SEAFP: The Safety and Environmental Assessment of Fusion Power is an extensive study conducted by several teams in the associated laboratories, NET, industry and the JRC, published in June 1995.

SEAL: The Safety and Environmental Assessment of Fusion Power Long-term is a programme, launched in 1995, being undertaken for the European Commission in the framework of the Fusion Programme.

Separatrix: Magnetic surface at which the rotational transform vanishes and the safety factor becomes infinite.

Shear: The safety factor usually varies from magnetic surface to magnetic surface across the plasma cross-section; this variation is measured by the non-dimensional quantity called "shear". Also refers to the variation of plasma flow (flow shear). If the type of shear is not specified, it usually means magnetic shear.

Single/double null: Points of zero poloidal magnetic field where the separatrix crosses itself are the X-points or nulls. Usually sited above and/or below the plasma. Tokamak divertor configurations have either one or two nulls.

Single fluid model: The set of equations which represent a plasma as a magnetised, electrically conducting fluid with the usual fluid properties of viscosity, thermal conductivity, etc. The possibility of distinct

behaviour of electrons and ions (i.e. 2 "fluids") is excluded.

Small aspect ratio: Same as Low aspect ratio.

Spectroscopy: The detection and analysis of the spectrum of radiation emitted by a plasma. This can yield information about temperatures, impurities, rotation, using different parts of the electromagnetic spectrum (IR, visible, VUV, XUV, etc.)

Spherical tokamak (ST): A very low aspect ratio tokamak - it appears almost spherical, though topologically it remains a torus with a centre column. The spherical tokamak is being further investigated, with a larger experiment, MAST.

Spheromak: A spherical plasma in which comparable toroidal and poloidal currents flow. The toroidal current is not driven by transformer action.

Stability theory: The theory of how small perturbations to a system evolve in time. Spontaneous growth is due to instability. Instabilities can saturate at some small amplitude, in which case they may degrade confinement, or grow uncontrollably, in which case the equilibrium is lost leading to a disruption.

START: Small Tight Aspect Ratio Tokamak, a "spherical" tokamak with a very small aspect ratio at the Association EURATOM-UKAEA (Culham). This very fat ring-shaped configuration showed experimentally a lesser tendency to disruptions and is efficient in its use of magnetic energy. Ceased operation in 1998, replaced by MAST.

Start-up assist: Assisting plasma formation to cross a range of plasma temperature at which impurities radiate strongly, with the aim of minimising the start-up delay and transformer requirements, usually using ECH.

STC: Scientific and Technical Committee, advisory committee set up by the EURATOM Treaty, competent for nuclear programmes.

Steady state power plant: A continuously (as opposed to cyclically) operated power plant.

Stellarator: Closed configuration having the shape of a three-dimensionally distorted ring in which the plasma is confined principally by an externally generated magnetic field (produced by non-planar coils outside the plasma vessel). The coils can be arranged in a modular fashion. Stellarators do not need a transformer; they need an additional heating system for the plasma start-up. Due to the fact that no toroidal plasma current is needed to maintain the confinement configuration, they naturally provide steady state operation.

SULTAN: Supra Leiter Test ANlage. Large Superconductor Test Facility, CRPP at PSI Villigen, Switzerland (Association EURATOM-Swiss Confederation).

Super Alfvénic velocity: A velocity greater than the Alfvén velocity. In a tokamak, only energetic particles have super Alfvénic velocities; because they satisfy this condition, they may resonantly transfer their energy to magnetohydrodynamic modes, which may grow as a result (eg TAE modes).

Superthermal radiation: Electromagnetic radiation produced by energetic particles, as opposed to thermal particles.

Survey spectrometer: An instrument which gives information concerning the radiated spectrum over a large range of frequencies.

TAE modes: Toroidal Alfvén Eigenmodes. One class of Alfvén gap modes.

Target plates: See Divertor.

TCV: "Tokamak à Configuration Variable", for study of elongated and strongly shaped plasmas, at Lausanne, Switzerland (Association EURATOM-Swiss Confédération).

TEKES: Technology Centre Finland. Partner in the Association EURATOM-TEKES.

Tearing magnetic islands: The disturbance caused by a tearing mode which alters the topology of the confining magnetic field and causes transfer of heat across the affected region.

Tearing mode: A class of resistive MHD instability which has been predicted theoretically in tokamaks and positively identified in experiments.

Temperature pedestal: In an H-mode discharge there is a region of steep temperature gradient at the plasma edge. The temperature at the top of this steep gradient region is the temperature pedestal.

Tesla: Unit of magnetic field strength (more exactly the magnetic induction). $1T = 1Vs/m^2 = 10{,}000Gauss$.

TEXTOR: Torus Experiment for Technology Oriented Research. Tokamak at Jülich, Germany (Association EURATOM-FZJ). Refurbished and upgraded, in 1994, as TEXTOR-94.

TFTR: "Tokamak Fusion Test Reactor" at Princeton, the largest US device with a major campaign using deuterium-tritium fuel from 1993 - 1997. Ceased operation in March 1997.

Thermal cycling: Successive heating and cooling of materials can lead to cracks or rupture, particularly at boundaries between materials that expand at different rates.

Thermal particles: As a result of collisional energy exchange, the energy of most plasma particles falls within a Maxwellian distribution which is described by a single temperature (typically 1-30keV for tokamaks). These are the thermal particles, as distinct from energetic particles which lie outside the thermal distribution.

Thomson scattering diagnostic: Diagnostic to measure temperature and density by detecting laser light scattered and Doppler shifted by the thermal plasma electrons.

Tight aspect ratio: Same as Low aspect ratio.

TJ-II: A heliac stellarator at Madrid, Spain (Association EURATOM-CIEMAT). (TJ-IU was a torsatron at CIEMAT, built and operated in preparation for TJ-II).

Tokamak: Magnetic configuration with the shape of a torus. The plasma is stabilised by a strong toroidal magnetic field. The poloidal component of the magnetic field is produced by an electrical current flowing toroidally in the plasma. This current is induced via transformer action and, for steady state, must be maintained by non-inductive current drive and by self-generation of bootstrap current inside the plasma.

Tokamak operating boundaries: The set of plasma parameters, beyond which it is impossible to operate a tokamak. Careful choice of plasma cross-sectional shapes and current and pressure profiles can increase the operating regime.

TORE SUPRA: Large tokamak with superconducting toroidal magnetic field coils and a circular plasma cross-section at the Association EURATOM-CEA in Cadarache, France.

Toroidal Alfvén Eigenmodes: See TAE modes.

Toroidal field: The component of the magnetic field along the major circumference of the torus. The largest magnetic field component in a tokamak.

Toroidal stability: Stability analysis taking account of effects due to the toroidal geometry. These are sometimes neglected to identify possible instabilities, but must usually be included for accurate predictions of stability boundaries.

Toroidal turbulence code: A turbulence code which includes effects due to the toroidal geometry.

TOSKA: Large facility testing for superconductors (Association EURATOM-FZK, Karlsruhe, Germany).

Transformer drive: The use of a transformer action to produce plasma current.

Transport: The processes by which particles and energy move across magnetic surfaces.

Transport barrier: In certain operational scenarios (e.g. the H-mode or ITB-mode) a region of low transport exists giving rise to a steep local pressure gradient. Such a region is referred to as a transport barrier.

Transport scaling: The magnitude of heat transport may be expressed, empirically or theoretically, in terms of a simple functional dependence on a few plasma parameters. This allows us to model how the heat transport varies (scales) in response to changes in the value of these parameters.

Trapped particles: The outside (large major radius) of a tokamak plasma has a lower magnetic field than the inside. Particles with low velocity parallel to the magnetic field compared with the velocity perpendicular to the magnetic field may not enter the higher field (inside) region and become trapped on the outside. They are not free to circulate toroidally but instead bounce back and forth, performing so-called banana orbits.

Tri-lateral Euregio Cluster (TEC): A collaboration between the Associations Euratom-FZJ, -FOM and –Etat Belge, to exploit the TEXTOR tokamak at FZJ, Julich, Germany.

Tritium: An isotope of hydrogen, whose nucleus consists of one proton and two neutrons. Tritium does not occur naturally, because it is unstable to radioactive decay

with a half-life of 12.3 years. Due to its rapid decay, tritium is almost absent on earth. For a fusion reactor, tritium will be produced in the breeding blanket surrounding the core of a fusion power station. Special tritium-handling technology is required whenever the use of deuterium-tritium plasmas is contemplated and has been developed on TFTR and JET.

Tritium inventory: The amount of tritium contained in a fusion power station or in a specified part of it.

Turbulence: Randomly fluctuating, as opposed to coherent, wave action. For example, the turbulent water beneath a waterfall can only be described in terms of its averaged properties, such as the scale and duration of fluctuations; whereas a more systematic description can be given to waves on the surface of a still pond.

Turbulent transport: Anomalous heat transport associated with plasma turbulence.

Two-fluid model and multi-fluid model: The extended set of equations which represent a plasma as interpenetrating and interacting fluids of electrons and ions, impurity ions etc.

UKAEA: United Kingdom Atomic Energy Authority. Partner in the Association EURATOM-UKAEA which operates the tokamak COMPASS-D and the spherical tokamak MAST. Also charged with the operation of the JET facilities under EFDA.

Vertical Displacement Event (VDE): An event which arises when control of the plasma is lost and the plasma moves vertically. It can lead to a "halo current" in components which surround the plasma resulting in large, potentially damaging, forces on these components. The forces are much larger in larger tokamaks and are therefore a particular concern for JET and ITER.

VUV: The "Vacuum Ultra Violet" range of the electromagnetic spectrum.

Warm plasma refuelling: Fuelling of plasma using medium energy particles or particle clusters.

WEC: World Energy Council.

WENDELSTEIN VII-AS: Advanced stellarator, in operation at Garching, Germany (Association EURATOM-IPP).

WENDELSTEIN VII-X: Large advanced superconducting stellarator, optimised to produce a reactor-relevant plasma configuration, designed at Garching. Construction in progress at Greifswald, Germany (Association EURATOM-IPP) with first operation scheduled for 2006.

X-point: See single/double null.

XUV: The "Extreme Ultra Violet" range of the electromagnetic spectrum. Shorter wavelengths than VUV.

Acknowledgement: This glossary was adapted from the "Glossary of fusion terms" by UKAEA Culham, UK, and from the glossary of "Fusion programme evaluation", 1996, EUR 17521, European Commission.

APPENDIX G Sources of Financial Support

The work carried out at the CRPP and presented in this annual report was financed from several sources. The major financial support is derived from the Ecole Polytechnique Fédérale de Lausanne (EPFL), EURATOM, the Paul Scherrer Institute (PSI), which hosts the supraconductivity and materials science activities, and the Swiss National Science Foundation. Other public and private organisations which contributed funding for our research in 2003 include, in alphabetical order: Balzers Tribology, Charmilles SA, the Swiss Commission pour la Technologie et l'Innovation (CTI), Fischer-Connectors, the Swiss Office Fédéral de l'Education et de la Science (OFES), Sulzer Metco AG, Tetra Pak SA and Unaxis Balzers.

The CRPP is the Host of a Euratom Fellowship, Dr. M. McGrath entitled *"Nonlinear structures in turbulent transport plasmas and methods of control".*

The Fonds National Suisse de la Recherche Scientifique provides a grant during this period for *"Basic plasma physics for fusion energy research"*, which partly finances TORPEX and the CRPP-JET collaboration on Alfven waves and fast particles. Prof. A. Fasoli is supported by this grant as "Professeur Boursier du Fonds National".